

GEOLOGICA ULTRAIECTINA

Mededelingen van de
Faculteit Aardwetenschappen der
Rijksuniversiteit te Utrecht

No. 91

Pillared Clays

**Preparation and Characterization of clay
minerals and Aluminum-Based Pillaring
Agents**

J. T. Kloprogge

GEOLOGICA ULTRAIECTINA

Mededelingen van de
Faculteit Aardwetenschappen der
Rijksuniversiteit te Utrecht

No. 91

Pillared Clays

**Preparation and Characterization of clay
minerals and Aluminum-Based Pillaring
Agents**

CIP-GEGEVENS KONINKLIJK BIBIOTHEEK, DEN HAAG

Kloprogge, Jacob Teunis

Pillared Clays: preparation and characterization of clay minerals and aluminum-based pillaring agents / Jacob Teunis Kloprogge. - [Utrecht : Faculteit Aardwetenschappen der Rijksuniversiteit Utrecht]. - (Geologica Ultraiectina, ISSN 0072-1026 ; no. 91 Proefschrift Rijksuniversiteit Utrecht - Met samenvatting in het Nederlands.
ISBN 90-71577-45-7
Trefw.:klei / mineralen.

PILLARED CLAYS

**PREPARATION AND CHARACTERIZATION OF CLAY MINERALS
AND ALUMINUM-BASED PILLARING AGENTS**

GEPILAARDE KLEIEN

**BEREIDING EN KARAKTERISERING VAN KLEI MINERALEN EN OP
ALUMINIUM GEBASEERDE PILAAR VLOEISTOFFEN**

(MET EEN SAMENVATTING IN HET NEDERLANDS)

PROEFSCHRIFT

TER VERKRIJGING VAN DE GRAAD VAN DOCTOR
AAN DE RIJKSUNIVERSITEIT TE UTRECHT
OP GEZAG VAN DE RECTOR MAGNIFICUS, PROF. DR. J.A. VAN GINKEL,
INGEVOLGE HET BESLUIT VAN HET COLLEGE VAN DEKANEN
IN HET OPENBAAR TE VERDEDIGEN OP DONDERDAG
15 OKTOBER 1992 DES NAMIDDAGS OM 12.45 UUR

DOOR

JACOB TEUNIS KLOPROGGE
GEBOREN OP 19 FEBRUARI 1965, TE ZOETERMEER

PROMOTORES: PROF. IR. J.W. GEUS
PROF. DR. R.D. SCHUILING
COPROMOTOR: DR. J.B.H. JANSEN

Aan mijn ouders
Aan Marloes

The gods had condemned Sisyphus to ceaselessly rolling a rock to the top of a mountain, whence the stone would fall back of its own weight. They had thought with some reason that there is no more dreadful punishment than futile and hopeless labour.

...Each atom of that stone, each mineral flake of that night-filled mountain, in itself forms a world. The struggle itself towards the heights is enough to fill a man's heart. One must imagine Sisyphus happy.

From: *The myth of Sisyphus* (Camus)

VOORWOORD

Hier aan het begin van mijn proefschrift wil ik graag al die mensen bedanken die hebben bijgedragen aan het tot stand komen ervan. Om te beginnen wil ik hier vooral mijn ouders bedanken voor al hun steun, interesse en hulp gedurende mijn studie en promotie. Papa, mama, jullie waren mijn grote steun en toeverlaat in al die jaren. Dat geldt natuurlijk ook voor Marloes, die me er soms echt doorheen heeft gesleept.

Een hele grote constructieve, vaak ook kritische, bijdrage werd geleverd door mijn co-promotor Dr. J. Ben H. Jansen. Ben, enorm bedankt voor jouw enthousiaste inzet en steun. Ik heb veel van je geleerd de afgelopen vijf jaar.

Verder wil ik mijn promotores Prof. Ir. Geus en Prof. Dr. Schuiling bedanken voor de nuttige, en ook gezellige, discussies en intensieve review van mijn manuscripten.

Er is echter nog iemand die ik speciaal wil bedanken, namelijk Ad van der Eerden. Niet alleen voor zijn hulp in het HPT laboratorium, maar ook voor zijn steun en vriendschap de afgelopen jaren. Ik hoop dat dat nog lang zo zal blijven. Ad, ik ben blij dat ik jou zo goed heb mogen leren kennen. Je was voor mij een haast onmisbare steunpilaar deze jaren.

Veel aangename uren heb ik doorgebracht in gezelschap van mijn collega-promovendi: Diederik Visser, Mark Titulaer, Paul Buining, Jan van Beek, Ronald Bakker, Peter Dirken, Gerko Lieftink en Roland Vogels, vaak aangevuld met Vian Govers en Nellie Slaats. Ik zal het gezellige geklets tussen de middag in de kantine nog missen.

Verder wil ik alle mensen in het instituut bedanken die hebben bijgedragen aan het tot stand komen van dit proefschrift, te weten: Tony van der Gon - Netscher, Vian Govers, Christina Strom, Cees Woensdregt, Nellie Slaats, Ton Zalm, Paul Anten, Tilly Bouten, René Poorter, Ineke Kalt, de medewerkers van de bibliotheek en AV dienst.

Ook van de faculteit Scheikunde hebben diverse mensen hun bijdrage geleverd: Fred Broersma, Jos van Dillen, Piet Elberse, Rikki van Zelst.

Het NMR werk werd tot een goed einde gebracht door de enthousiaste steun van Don Seykens voor het vloeistof werk en in Nijmegen voor het vaste stof werk van Gerda Nachtegaal en Arno Kentgens.

Niet onvermeld mag blijven de stageperiode die ik heb doorgebracht bij op de afdeling CGP/2 van het Koninklijke/Shell Laboratorium in Amsterdam. Johan Breukelaar, bedankt voor jouw begeleiding gedurende deze stage. Verder wil ik graag Andre de Winter bedanken, die in Amsterdam een beetje de rol speelde van een tweede Ad van der Eerden. Verder iedereen op deze afdeling bedankt, die ervoor hebben gezorgd dat ik er een fijne tijd heb gehad.

Een belangrijk deel van mijn proefschrift is tot stand gekomen door twee bijvak studenten: Roland Vogels, nu mijn collega en opvolger in dit project, en Ernst Booij. Jongens, hartstikke bedankt voor jullie uitstekende werk.

Zoals bij alle proefschriften, ging het ook hier op het laatst niet van een leien dakje. Computers zijn een personificatie van de wet van behoud van ellende. Twee mensen, Ad en mijn moeder, wil ik hier nogmaals apart bedanken voor hun hulp bij het herstellen van de aangerichte schade.

Marloes, bedankt voor je geduld en steun gedurende vooral dit laatste moeilijke jaar.

CONTENTS

Voorwoord	vii
Contents	ix
Chapter I Introduction	1
1.1 Smectites	2
1.2 Synthesis of smectites	4
1.2.1 Compositional series	4
1.2.2 Dioctahedral smectites	7
1.2.2.1 Beidellite	7
1.2.2.2 Nontronite and other ferric smectites	8
1.2.3 Trioctahedral smectites	9
1.2.3.1 Saponite	10
1.2.3.2 Hectorite and Stevensite	12
1.3 Pillared clays	14
1.3.1 Al pillared clays	15
1.3.2 Other metal pillared clays	19
1.4 Catalysis by pillared clays	21
1.5 Scope of this thesis	24
Chapter II Hydrothermal synthesis of Na-beidellite	39
2.1 Introduction	39
2.2 Starting materials and experimental methods	40
2.3 Results	41
2.3.1 Influence of temperature and pressure	41
2.3.2 Gel composition	41
2.3.3 Characterization	41
2.3.4 Influence of F	47
2.4 Conclusions	48
Chapter III Characterization of synthetic Na-beidellite	51
3.1 Introduction	51
3.2 Experimental and analytical techniques	52
3.3 Results	54
3.4 Discussion	62
Chapter IV Synthesis field of Na-beidellite in terms of temperature, water pressure and sodium activity	69
4.1 Introduction	69
4.2 Experimental and analytical techniques	70
4.3 Results	71
4.4 Discussion	76
4.5 Conclusions	82

Chapter V The interlayer collapse during dehydration of synthetic Na _{0.7} -beidellite: a ²³ Na solid-state magic-angle spinning NMR study	87
5.1 Introduction	87
5.2 Experimental methods	89
5.2.1 Samples	89
5.2.2 Analytical techniques	89
5.3 Results	90
5.4 Discussion	95
5.5 Conclusion	100
Chapter VI Low temperature synthesis of ammonium-saponites from gels with variable ammonium concentration and water content	107
6.1 Introduction	107
6.2 Experimental methods	108
6.3 Results	114
6.4 Discussion	125
6.4.1 Saponite crystallinity	125
6.4.2 Saponite chemistry	126
6.4.3 Crystallization model	127
Chapter VII Solid-state nuclear magnetic resonance spectroscopy on synthetic ammonium-saponites; aluminum on the interlayer	133
7.1 Introduction	133
7.2 Experimental section	135
7.2.1 Saponite synthesis	135
7.2.2 Solid-state NMR	136
7.3 Results and Discussion	137
Chapter VIII Hydrothermal crystallization of ammonium-saponite at 200°C and autogeneous water pressure	145
8.1 Introduction	145
8.2 Experimental methods	146
8.2.1 Saponite synthesis	146
8.2.2 Analytical techniques	148
8.3 Results	151
8.4 Discussion	158
8.5 Conclusions	161
Chapter IX Characterization of Mg-saponites synthesized with gels containing small amounts of Na ⁺ , K ⁺ , Rb ⁺ , Ca ²⁺ , Ba ²⁺ or Ce ⁴⁺	165
9.1 Introduction	165
9.2 Experimental method	166

9.3 Results	168
9.4 Discussion	172
Chapter X An ^{27}Al nuclear magnetic resonance study on the optimalization of the development of the Al13 polymer	177
10.1 Introduction	177
10.2 Experimental method	178
10.3 Results	179
10.4 Discussion	187
10.4.1 Reference chemical shift	187
10.4.2 Relation between OH/Al molar ratio and the chemical shift and linewidth	187
10.4.3 Quadrupole relaxation	188
10.4.4 Relation between OH/Al molar ratio and Al13 concentration	189
10.4.5 Alkalis solution injection and mixing conditions	190
10.4.6 Aging	191
10.5 Conclusions	192
Chapter XI Temperature influence on the Al13 complex in partially neutralized aluminum solutions: an ^{27}Al nuclear magnetic resonance study	197
11.1 Introduction	197
11.2 Experimental	199
11.3 Results	200
11.4 Discussion	204
11.5 Conclusions	207
Chapter XII Aluminum monomer line-broadening as evidence for the existence of $[\text{AlOH}]^{2+}$ and $[\text{Al}(\text{OH})_2]^+$ during forced hydrolysis: an ^{27}Al nuclear magnetic resonance study	213
12.1 Introduction	213
12.2 Experimental	214
12.3 Results	215
12.4 Discussion	217
12.5 Conclusions	221
Chapter XIII The effects of concentration and hydrolysis on the oligomerization and polymerization of Al(III) as evident from the ^{27}Al NMR chemical shifts and linewidths	225
13.1 Introduction	225
13.2 Experimental	226
13.3 Results	227
13.3.1 Al hydrolysis products	227

13.3.2 Chemical shift and linewidth	231
13.4 Discussion	233
13.4.1 Changes in the fractions of the different Al species	233
13.4.2 Resonance changes	234
13.5 Conclusions	237
Chapter XIV The tridecamer aluminum complex as an appropriate precursor for fibrous boehmite: an ^{27}Al NMR study on the partial hydrolysis of aluminum <i>sec</i> -butoxide	241
14.1 Introduction	241
14.2 Experimental methods	242
14.2.1 Preparation of the acidified Al alcoxide solutions	242
14.2.2 Analytical techniques	243
14.3 Results	244
14.3.1 Colloids	244
14.3.2 ^{27}Al NMR	245
14.3.3 Aging at 20°C	246
14.3.4 Aging at 90°C	247
14.3.5 Solutions prepared between 20 and 90°C	249
14.3.6 Heating in the NMR apparatus	250
14.4 Discussion	251
14.5 Conclusions	254
Chapter XV Thermal stability of basic aluminum sulfate	259
15.1 Introduction	259
15.2 Experimental techniques	260
15.2.1 The tridecamer solution	260
15.2.2 Basic aluminum sulfate	261
15.3 Results	262
15.3.1 Preparation	262
15.3.2 Characterization	262
15.3.3 Thermal stability	268
15.4 Discussion	270
Chapter XVI One- and two-dimensional ^{27}Al MAS NMR study of basic aluminum sulfate	277
16.1 Introduction	277
16.2 Theoretical background	278
16.3 Experimental	279
16.4 Results	281
16.4.1 Second order quadrupole induced shift	281
16.4.2 2D nutation NMR	282
16.4.3 Computer simulation	284
16.5 Discussion	284
16.6 Conclusions	286

Chapter XVII	The effect of thermal treatment on the properties of hydroxy-Al and hydroxy-Ga pillared montmorillonite and beidellite	291
17.1	Introduction	291
17.2	Experimental	293
17.2.1	Starting clays	293
17.2.2	Pillaring agents	294
17.2.3	Pillaring process	294
17.2.4	Characterization of the pillaring agents and pillared clays	295
17.3	Results	297
17.3.1	Pillaring agents	297
17.3.2	Al-pillared montmorillonite and beidellite	297
17.3.3	Ga-pillared montmorillonite	310
17.4	Discussion	312
Chapter XVIII	Catalytic activity of nickel sulfide catalysts supported on Al-pillared montmorillonite for thiophene hydrodesulfurisation	325
18.1	Introduction	325
18.2	Experimental	327
18.2.1	Starting clays	327
18.2.2	Pillaring agent	327
18.2.3	Pillaring process and characterization of the pillared clay	327
18.2.4	Catalytic preparation	328
18.2.5	Activity measurement	328
18.3	Results and Discussion	328
18.4	Conclusions	334
Chapter XIX	Concluding remarks	339
	Summary	344
	Samenvatting	346
	Curriculum vitae	349

Chapter II has been published in *Geologie en Mijnbouw* **69** (1990) 351-357. Co-authors: A. M. J. van der Eerden, J. B. H. Jansen and J. W. Geus.

Chapter III has been published in *Clays and Clay Minerals* **38** (1990) 409-414. Co-authors: J. B. H. Jansen and J. W. Geus.

Chapter IV has been accepted for publication (with revisions) in *Clays and Clay Minerals*. Co-authors: A. M. J. van der Eerden, J. B. H. Jansen, J. W. Geus and R. D. Schuiling.

Chapter V has been submitted to *Clays and Clay Minerals*. Co-authors: J. B. H. Jansen, R. D. Schuiling and J. W. Geus.

Chapter VI has been accepted for publication (with revisions) in *Clays and Clay Minerals*. Co-authors: J. Breukelaar, J. B. H. Jansen and J. W. Geus.

Chapter X has been published in *Journal of Non-Crystalline Solids* **142** (1992) 94-102. Co-authors: D. Seykens, J. B. H. Jansen and J. W. Geus.

Chapter XI has been published in *Journal of Non-Crystalline Solids* **142** (1992) 87-93. Co-authors: D. Seykens, J. W. Geus and J. B. H. Jansen.

Chapter XII has been accepted for publication (with revisions) in *Journal of Non-Crystalline Solids*. Co-authors: D. Seykens, J. B. H. Jansen and J. W. Geus.

Chapter XIV has been accepted for publication (with revisions) in *Journal of Non-Crystalline Solids*. Co-authors: R. J. M. J. Vogels (first author), P. Buining, D. Seykens, J. B. H. Jansen and J. W. Geus.

Chapter XV is in press *Thermochimica Acta* (1992). Co-authors: J. W. Geus, J. B. H. Jansen and D. Seykens.

CHAPTER I

INTRODUCTION

The use of clay for mainly clay figures, pottery and ceramics was already known by primitive people about 25.000 years ago (Shaikh and Wik, 1986). Today clay is an important material with a large variety of applications in ceramics, oil drilling, and the metal and paper industry. Clay is furthermore used as adsorbent, decoloration agents, ion exchanger, and molecular sieve catalyst (Fowden et al., 1984). For the application as molecular sieve catalyst a group of expandable clays known as smectites is employed. The word smectite is derived from the Greek word *smectos*, *σμηγμα*, which means soap.

Pillared smectites are clays of a high permanent porosity obtained by separating the clay sheets by a molecular prop or pillaring agent. These pillaring agents can be organic, organometallic, or inorganic complexes, preferably of a high positive charge. With evenly distributed pillars a two-dimensional channel system results with micropores comparable to those of zeolites. Large pillaring agents can establish channels wider than those of molecular sieves; clays with wide channels can be utilized in hydrocracking of larger hydrocarbons that cannot penetrate into the pore system of zeolites. Other requisites for clays to be used instead of zeolite catalysts are small and rigid clay sheets, negligible adsorption of the pillaring agent at the external surface, and pillaring of essentially all clay sheets. Special pillared clays have chemical bonds between the pillars and the oxygen at the surface of the sheets. In the literature clays with these chemical bonds are known as cross-linked smectites.

This chapter will first provide a background on the structure and synthesis of smectites, which is followed by a discussion of various smectites pillared by metal ions, and the use of pillared smectites in catalytic reactions. Finally, the scope of this thesis will be outlined.

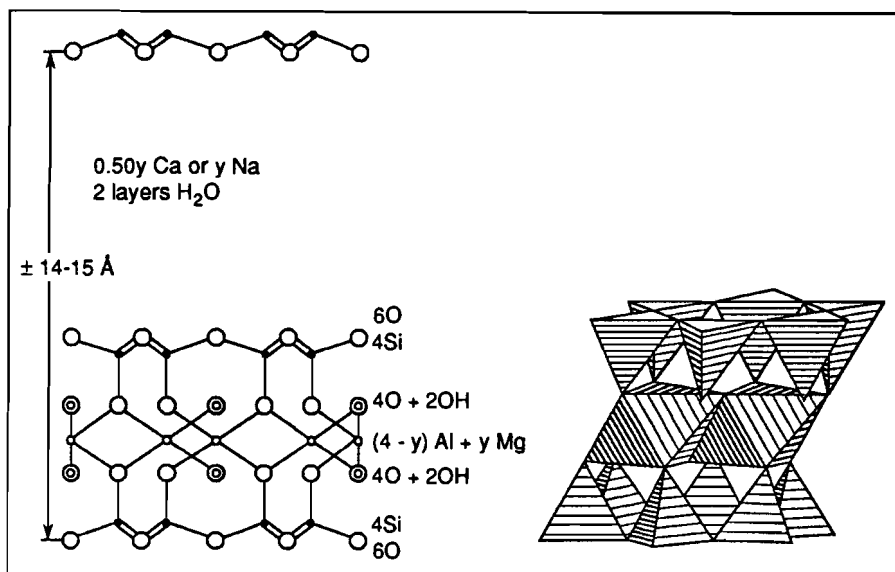


Figure 1.1 Schematic structure of a smectite.

1.1 SMECTITES

Smectites are phyllosilicates or layer silicates having a layer lattice structure in which two-dimensional oxoanions are separated by layers of hydrated cations. The oxygen atoms define upper and lower sheets enclosing tetrahedral sites, and a central sheet having the brucite or gibbsite structure enclosing octahedral sites (Fig. 1.1). Smectites having two tetrahedral sheets around the central octahedral sheet are known as 2:1 phyllosilicates. Kaolinite, on the other hand, has one tetrahedral and one octahedral sheet (1:1 phyllosilicate).

A further designation can be made based on the type and location of the cations in the oxygen framework. In one unit cell composed of twenty oxygen atoms and four hydroxyl groups, there are eight tetrahedral and six octahedral sites. A smectite is dioctahedral if two-thirds of the octahedral sites are occupied by trivalent cations, and trioctahedral if all octahedral sites are filled with bivalent cations. Table 1.1 summarizes the most common smectites and their idealized structural formulas. For comparison, kaolinite, a dioctahedral 1:1 clay, chrysotile,

Introduction

a trioctahedral 1:1 clay, and the micas phlogopite and paragonite are included. Micas, though no smectites, have identical 2:1 phyllosilicate oxygen frameworks.

In talc and pyrophyllite all tetrahedral sites are filled with Si^{4+} and the octahedral sites either completely by Mg^{2+} or for 2/3 by Al^{3+} , respectively. The electrically neutral sheets are bonded together by relatively weak dipolar and Van der Waals forces (Giese, 1975). In contrast, smectite layers have a positive charge deficiency resulting from the following isomorphous substitutions, viz., (i) Si^{4+} by Al^{3+} at tetrahedral sites, and (ii) Al^{3+} by Mg^{2+} , or (iii) Mg^{2+} by Li^+ (or a vacancy) at octahedral sites. The charge deficiency is balanced by hydrated interlayer cations, such as, Na^+ , K^+ , or Ca^{2+} .

The charge deficiency of smectites is intermediate between that of micas and that of pyrophyllite and talc. Differences in the charge of the layers, the origin of the charge deficiency, and the interlayer cations result in different physical and chemical properties, such as, thermal stability and swelling behavior (Fig. 1.2). The

Table 1.1 Classification of hydrous phyllosilicates

Layer type	Interlayer	Layer charge	Species	formula
1:1	none or H ₂ O only	≈ 0	kaolinite	$\text{Al}_4\text{Si}_4\text{O}_{10}(\text{OH})_8$
			chrysotile	$\text{Mg}_6\text{Si}_4\text{O}_{10}(\text{OH})_8$
2:1	none	≈ 0	pyrophyllite	$\text{Al}_4\text{Si}_6\text{O}_{20}(\text{OH})_4$
			talc	$\text{Mg}_6\text{Si}_8\text{O}_{20}(\text{OH})_4$
hydrated exchangeable cations		0.4-1.2	montmorillonite	$\text{M}_{x/n}^{n+}[\text{Al}_{4-x}\text{Mg}_x][\text{Si}_8]\text{O}_{20}(\text{OH})_4 \cdot n\text{H}_2\text{O}$
			beidellite	$\text{M}_{x/n}^{n+}[\text{Al}_4][\text{Si}_{8-x}\text{Al}_x]\text{O}_{20}(\text{OH})_4 \cdot n\text{H}_2\text{O}$
			nontronite	$\text{M}_{x/n}^{n+}[\text{Fe}_4][\text{Si}_{8-x}\text{Al}_x]\text{O}_{20}(\text{OH})_4 \cdot n\text{H}_2\text{O}$
		1.2-1.8	saponite	$\text{M}_{x/n}^{n+}[\text{Mg}_6][\text{Si}_{8-x}\text{Al}_x]\text{O}_{20}(\text{OH})_4 \cdot n\text{H}_2\text{O}$
			(F-)hectorite	$\text{M}_{x/n}^{n+}[\text{Mg}_{6-x}\text{Li}_x][\text{Si}_8]\text{O}_{20}(\text{OH},\text{F})_4 \cdot n\text{H}_2\text{O}$
			vermiculite	$[\text{Mg},\text{Ca}]_{x/2}^{2+}[\text{Al}_{4-x}\text{Mg}_x][\text{Si}_8]\text{O}_{20}(\text{OH})_4 \cdot 8\text{H}_2\text{O}$
non-hydrated cations	1.0-2.0	paragonite	$[\text{Mg},\text{Ca}]_{x/2}^{2+}[\text{Mg}_6][\text{Si}_{8-x}\text{Al}_x]\text{O}_{20}(\text{OH})_4 \cdot n\text{H}_2\text{O}$	
		phlogopite	$\text{Na}_2[\text{Al}_4][\text{Si}_6\text{Al}_2]\text{O}_{20}(\text{OH})_4$ $\text{K}_2[\text{Mg},\text{Fe}]_6[\text{Si}_6\text{Al}_2]\text{O}_{20}(\text{OH},\text{F})_4$	

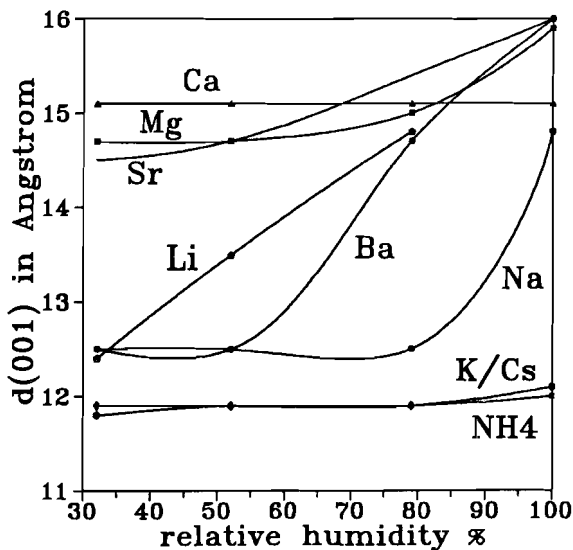


Figure 1.2 Swelling behavior of smectites as function of relative humidity (after Brindley and Brown, 1980)

layer charge of an octahedrally substituted smectite (e.g., montmorillonite) is distributed over the complete oxygen framework, whereas tetrahedral substitution (as, e.g., with beidellite) leads to a more localized charge distribution, and the last smectites tend to a higher three-dimensional order (Brindley, 1980; Suquet et al., 1975).

1.2 SYNTHESIS OF SMECTITES

1.2.1 Compositional series

The main incentive for using synthetic smectites is that several interesting clay minerals are not available in sufficient quantities in their natural form (e.g., beidellite) or have an unreliable quality, and exhibit a large variation in impurity content (Kloprogge et al., 1990). Smectites have been synthesized using various starting materials, such as, gels, oxides, glasses, and fine powders of minerals and rocks, to study processes of hydrothermal alteration, stability fields, and compositional limits.

Introduction

Early studies mainly concerned the possible variation in cation exchange capacities (CEC) of single phase smectites prepared from gels in montmorillonite-beidellite and saponite-beidellite compositional ranges under various conditions of pressure and temperature (Roy and Roy, 1952, 1955; Sand et al., 1953, 1957; Roy and Sand, 1956). The results of these studies did not provide conclusive evidence of the variability of the CEC. Koizumi and Roy (1959) stated that the phases obtained in the early studies were not demonstrated to be homogeneous and completely crystalline. To provide more reliable evidence they prepared two series of gels in the beidellite and saponite compositional region by mixing Ludox silica sol with a solution of the nitrates of Al^{3+} or Mg^{2+} and NaOH, drying the resulting mixtures, and firing at 500°C . The gels resulting from addition of water to the above solids were reacted at a water pressure of 1000 atmosphere (approximately 1 kbar) and at temperatures ranging from 200° to 850°C . Single phase beidellite and saponite with CEC values varying with the starting composition resulted at temperatures from 260° to 450°C . The results of this study and that of Roy and Sand (1956) suggested the possibility to control the nature and the extent of the isomorphous substitutions. Harward and Brindley (1965), therefore, conducted experiments with gel compositions in the beidellite range to achieve tetrahedral, and in the montmorillonite range to achieve octahedral substitution. Their results showed that isomorphous substitution is only possible within a relatively small composition range and that differences in the CEC values may be attributed to the occurrence of other phases as the composition of the gel is thus modified to raise the extent of substitution. Nowadays, the results obtained with beidellite can be explained by the Al-O-Al avoidance rule (Loewenstein, 1954), and the theory concerning a homogeneous dispersion of charges (Herrero et al., 1985, 1987).

Koizumi and Roy (1959) reported the formation of mixed layer smectites from sodium-rich compositions. Iiyama and Roy (1963) have attempted to systematize the preparation of mixed layer phases and to obtain information about their stability. They used gels with compositions along the join talc - Na-saponite - Na-

phlogopite. At 1 kbar and within the temperature range between 450° and 575°C, they found randomly stacked phases, whereas at higher pressures regularly interstratified mixed layer phases, generally 1:1, phases were observed.

The study on the maximum hydrothermal stability of montmorillonites by Ames and Sand (1958) showed that the highest stability is found when all possible cations positions in the layer are occupied, i.e., with trioctahedral smectites, when an optimum tetrahedral or octahedral substitution is provided, and when the resulting layer charge is compensated by exchangeable cations other than H⁺. They thus observed a maximum stability of only 480°C for beidellite and montmorillonite (dioctahedral smectites) and 750°C for saponite and hectorite (trioctahedral smectites). A marked decrease in the stability temperature was observed when the substitution deviated from the optimum level.

Eberl and Hower (1977) have hydrothermally treated beidellite glasses prepared by the Ludox gel method (Luth and Ingamells, 1965) at temperatures below 300°C. After run times of 92 and 259 days the authors obtained a reaction series containing products varying from 100% expandable Na-beidellite to randomly interstratified mixed layer paragonite-beidellite plus kaolinite and quartz. Above 300°C, however, Na-beidellite reacted to form Na-rectorite, together with pyrophyllite and quartz or feldspar. Na-rectorite is a regularly interstratified paragonite-beidellite. Starting from glasses Yamada et al. (1991a) have recently synthesized smectites in the compositional range montmorillonite-beidellite at a pressure of 1 kbar. With initial compositions ranging from that corresponding to 100% montmorillonite to that corresponding to 78% montmorillonite and 22% beidellite, they obtained single phase montmorillonite at temperatures below 375°C. Initial composition corresponding to the range from 78% montmorillonite and 22% beidellite to 100% beidellite led at temperatures below 400°C to beidellite. An initial composition corresponding to 50% montmorillonite and 50% beidellite, however, resulted in a mixed layer phase of regularly interstratified montmorillonite-beidellite at temperatures below 400°C. Above 450°C they found Na-rectorite. Klopogge et al. (1992)(chapter IV) were not able to observe this

mixed layer phase in their products after the comparatively short run time of 7 days.

1.2.2. Dioctahedral Smectites

1.2.2.1 Beidellite

Plee et al. (1987) and Schutz et al. (1987) have prepared synthetic Na-beidellite of a composition $\text{Na}_{0.7}\text{Al}_{4.7}\text{Si}_{7.3}\text{O}_{20}(\text{OH})_4 \cdot n\text{H}_2\text{O}$. Since this clay mineral only has tetrahedral substitutions, they used it to prepare Al-pillared beidellite. The above synthetic Na-beidellite resulted in a more ordered pillar distribution and a much stronger acidity than displayed by pillared montmorillonite prepared under similar conditions. Plee et al. (1987) prepared a gel according to the method of Luth and Ingamells (1965). The gel was placed in a gold capsule together with a 0.01 N NaOH solution and hydrothermally treated for 10 days at 340°C and 600 bars, resulting in single phase beidellite with a CEC of 100 meq/100 g. Schutz et al. (1987) treated 200 mg gel plus 640 ml 0.1 M NaOH in a 1 liter autoclave for 5 days at 320°C and 130 bars, yielding more than 90 % beidellite. The CEC was determined to be 94 meq/100 g. These CEC values are higher than that of 70 meq/100 g measured by Klopogge et al. (1990). The lower value may be attributed to the collapse of some part of the interlayer space (Plee et al., 1987).

Since water is an essential constituent of smectites, Yamada et al. (1991) have investigated the role of water in the formation of beidellite by varying the water/solid (glass $\text{Na}_{0.66}\text{Al}_{4.66}\text{Si}_{7.34}\text{O}_{22}$) ratio at synthesis temperatures between 250° and 450°C at 1 kbar using run-times of 7 days. Between 300° and 400°C they observed only beidellite as crystalline phase, while at 250°C beidellite is accompanied by kaolinite and amorphous material. At 450°C a dioctahedral smectite with octahedral charge, cristobalite and quartz, both SiO_2 phases, are observed besides beidellite. At higher water/solid ratios Na-rectorite is formed instead of beidellite.

Several patents (Granquist, 1966; Capell and Granquist, 1966, Jaffe, 74) describe synthesis procedures for 2:1 layer silicates having the beidellite structure and substitution of Al and Si by metal cations, such as, Cr, Mn, Co, Ga, Rh, Sc, Ni, Cu, Zn, and Ge, to improve the catalytic characteristics. Although these materials do not contain any montmorillonite, but have the beidellite structure, they are known as synthetic mica-montmorillonite (SMM). The reason for this designation is that the materials are thought to be randomly interstratified phases containing alternating expandable beidellite layers and nonexpandable mica layers. Based on an improvement of the procedure of Granquist (1966), Gaaf et al. (1983), Robschlager et al. (1984), and van Santen et al. (1985) synthesized pure beidellite and Ni substituted beidellite, which they mentioned to be identical to SMM. In 1985 Heinerman patented the improved procedure, involving the use of commercial amorphous silica-alumina as a starting material and minimum quantities of water.

1.2.2.2 Nontronite and other ferric smectites

Harder (1976, 1978), Decarreau and Bonnin (1986), and Decarreau et al. (1987) performed the main experiments on the low-temperature synthesis of iron bearing smectites. Caillère et al. (1953,1955) obtained nontronite and iron-saponite by aging mixed dilute solutions of silica, ferrous or ferric chlorides, magnesium and aluminum salts at 100°C and at pH-levels between 8.5 and 9.5. In these clays the octahedral sites were partly occupied by either Mg^{2+} or Fe^{2+} . Elevated temperature nontronite syntheses were reported earlier by Ewell and Insley (1935). These authors kept mixtures of silica gel and ferric oxide at 350°C and 167 atmosphere for 6 days. Hamilton and Furtwängler (1951) kept dilute solutions of Na_2SiO_3 in $FeCl_3$ at high temperatures.

The nontronite synthesis described by Harder (1976) under reducing conditions is largely analogous to the procedure he used for other trioctahedral smectites (Harder, 1972; 1977), in which the brucite, $Mg(OH)_2$, or gibbsite, $Al(OH)_3$,

Introduction

template is replaced by $\text{Fe}(\text{OH})_2$. Addition of sodium dithionite or hydrazinium dichloride established the reducing conditions. Iron was added as $\text{Fe}(\text{III})\text{SO}_4$ and precipitated as $\text{Fe}(\text{II})$ hydroxide. A suspension containing 1 % of the solid was aged up to 15 days at 3° and at 20°C. The presence of Fe^{2+} and Mg^{2+} was required for the formation of octahedral sheets containing Al^{3+} and Fe^{3+} . At high Si/Fe ratios nontronite and lempbergite, the di- $\text{Fe}(\text{III})$ and tri- $\text{Fe}(\text{II})$ three-layer octahedral silicates were formed. Lower Si/Fe ratios resulted in the formation of the two-layer silicates greenalite and chamosite (Harder, 1976).

Decarreau and Bonnin (1986) and Decarreau et al. (1987) synthesized ferric smectites according to a procedure similar to that described for hectorite and stevensite (Decarreau, 1980). The procedure involves aging of freshly prepared coprecipitated gels of silica and $\text{Fe}(\text{II})$ sulphate under initially reducing conditions at 75°C for 15 days or for 1 month, at 100°C for 1 month, or at 150°C for 12 days. Upon oxidation of the $\text{Fe}(\text{II})$ the smectite crystallization is accelerated. Intermediate dissolution according to the reaction: $[\text{Fe}(\text{II})_{3-x}]$ -smectite + $\text{H}_2\text{O} \rightleftharpoons [\text{Fe}(\text{III})_{2-x}]$ -smectite + $\text{FeOOH} + 3\text{H}^+ + 3\text{e}^-$, does not proceed. As a result all the iron ions remain at the octahedral sites of the sheets. Only very small amounts of cryptocrystalline iron hydroxide or oxide were intergrown with the smectite. Mössbauer spectroscopy could only detect the iron (hydr)oxide species. The structural formula was suggested to be $\text{Na}_{0.05}\text{Fe}(\text{III})_{1.95}\text{Si}_4\text{O}_{10}(\text{OH})_2$. Under oxidizing conditions only Decarreau et al. (1987) were able to synthesize a ferric smectite at 100° and 150°C with a composition of $\text{Ca}_{0.26}\text{Fe}(\text{III})_{1.83}\text{Si}_4\text{O}_{10}(\text{OH})_2$. This smectite was considered to be a "defect" nontronite with the octahedral vacancies generating the layer charge.

1.2.3 Trioctahedral smectites

Saponites and hectorites are the main authigenic clay minerals widespread in nature formed by the alteration of oceanic and continental basalts and other basic volcanic rocks at low temperatures and pressures. Low temperature synthesis will therefore yield fundamental data to understand these geological processes.

Synthesis of saponite and hectorite at temperatures that are very low as compared to the relatively high temperatures (above 300°C) required for the synthesis of beidellite, is also important for the industrial application of synthetic clays as starting material for pillared clays. Expensive equipment for hydrothermal synthesis is not involved.

The low-temperature (3° to 60°C) synthesis of Harder (1972, 1977) was based on coprecipitation of SiO_2 and $\text{Al}^{3+}/\text{Mg}^{2+}$ hydroxides. The $\text{Al}^{3+}/\text{Mg}^{2+}$ hydroxides should develop two-dimensional sheet having the brucite, $\text{Mg}(\text{OH})_2$, or the gibbsite, $\text{Al}(\text{OH})_3$, structure, which were assumed to act as templates for the condensation of silica. The silica concentration had to be very low, in the range 10 to 100 ppm SiO_2 , to prevent polymerization of the monomers of the silicic acid solution. The silica-to-metal hydroxide ratio in the precipitate had to be similar to that of the desired smectite. Harder (1972) was unable to determine whether his reaction products contained single phase smectites or mixtures of smectites and X-ray amorphous phases. He therefore could not assess neither the exact composition nor the substitutions established in the smectite samples prepared. The main disadvantage of Harder's procedure is the very low silica concentration required, which inhibits production of large quantities of smectites.

Decarreau (1980, 1985) developed another fairly simple procedure. This author synthesized trioctahedral smectites at low temperatures by mixing stoichiometric amounts of sodium metasilicate (Na_2SiO_3) and metal salts (e.g., Mg, Al, Fe, Co, Ni, Zn) into solution of an appropriate acid. The resulting silicometallic precipitate contained small smectite nuclei, the crystallinity of which improved upon aging in the aqueous suspension at temperatures below 100°C. This procedure exhibits some important advantages over Harder's method (1972, 1977). Decarreau's procedure provides a better control of the homogeneity of the smectites, it is easily reproducible, and can produce large quantities of homogeneous smectites.

1.2.3.1 Saponite

The major problem encountered in the synthesis of saponite is that in addition to the tetrahedral substitution $\text{Si}^{4+} \Leftrightarrow \text{Al}^{3+}$, substitutions, such as, $3\text{Mg}^{2+} \Leftrightarrow 2 \text{Al}^{3+} +$ vacancy, or $\text{Mg}^{2+} \Leftrightarrow \text{Al}^{3+}$ at octahedral sites can proceed, as well as incorporation of Mg^{2+} and/or Al^{3+} at the interlayer positions. The different substitutions prevent control of the composition and the layer charge of the composites during a synthesis as will be demonstrated in chapters VI to X.

In 1974/1975 Hickson patented a procedure to synthesize a trioctahedral clay of the saponite type, which can be used as a component of a hydroconversion catalyst. The procedure comprises hydrothermal crystallization at a pH level between approximately 9 and 10 and at temperatures between 300° and 350°C for about 4 hours from aqueous slurries of hydrous silica sol, aluminum hydroxide and magnesium hydroxide, and ammonium hydroxide or ammonium fluoride. XRD indicated the presence of a clay structure of the saponite type with a basal reflection d_{001} of 11.5 to 14 Å, which expands to 18 Å upon treatment with glycol and a d_{060} of 1.52 Å.

Almost simultaneously with Decarreau (1980), Brat and Rajan (1980) reported the synthesis of saponite using a rather similar gel prepared by dissolving sodium silicate and sodium aluminate in HCl. In contrast to Decarreau, Brat and Rajan obtained the saponite by boiling the gel in a solution of $\text{Mg}(\text{CH}_3\text{COO})_2$ for 45 days, and thus not using hydrothermal conditions. Later on Decarreau (1985) also mentioned the use of sodium aluminate as Al source. The saponite he obtained had a considerable adsorption capacity and could be effectively used in the disposal of liquid radioactive waste containing Cs or Sr.

In the seventies Suquet et al. (1977) started to synthesize saponites according to a method similar to that of Hamilton and Henderson (1968). Boojj (1992) had considerable difficulties with this method, due to the formation of the olivine forsterite, Mg_2SiO_4 . Forsterite formation proceeded during the calcination performed to remove the nitrates from the gel. Suquet et al. (1977, 1981a) did not reported the formation of forsterite, probably, because the calcination procedure

(600°C during 24 hours) used by these authors was not sufficiently severe to start crystallization. Suquet et al. (1981a,b) varied the composition of the saponite and, subsequently, the extent of tetrahedral and octahedral Al substitutions. According to the general formula $\text{Na}_x(\text{Mg}_{3-q}\text{Al}_q)(\text{Si}_{4-s}\text{Al}_s\text{O}_{10}(\text{OH})_2$, the layer charge x , being $s-q$, ranged from 0.33 to 1.00, assuming a one-to-one substitution of $\text{Mg}^{2+} \Leftrightarrow \text{Al}^{3+}$. This substitution resulted in a positively charged octahedral layer, instead of the zero-charged substitution of $3\text{Mg}^{2+} \Leftrightarrow 2\text{Al}^{3+} + 1$ vacancy, which is usual in micas. Based on this substitution, for which no evidence was presented in their papers, Suquet et al. extensively studied the influence of the layer charge, the tetrahedral and octahedral substitution, and the amount of interlayer water on the following crystallographic parameters, viz., the b -axis and the basal spacing d_{001} (Suquet et al., 1981a,b), and on the interaction with the interlayer cation (Suquet et al., 1982). By means of mineral chemistry and, especially, by ^{27}Al and ^{29}Si NMR, Klopogge et al. (1992) have shown that Al^{3+} substitutions cannot be controlled only by the gel composition, and that Mg^{2+} and Al^{3+} may even be accommodated in the interlayer (see Chapter VI and VII).

Urabe et al. (1989) have shown that the use of Ni as octahedral cation instead of Mg results in a saponite, which works very efficiently as a catalyst for the selective dimerization of ethene. These authors carried out the synthesis by hydrothermally treating an aqueous Na-Ni-Si-Al gel of a Ni:Si:Al ratio of 8.13:9.36:1 (which leads to a small excess of nickel as compared to the stoichiometric composition) at 280°C and saturated water vapour pressure (approximately 65 bar) for 2 hours.

1.2.3.2 *Hectorite and Stevensite*

Trioctahedral (Mg) smectites with octahedral layer charges caused by either Li substitution (hectorite) or vacancies (stevensite) are closely related. Often Li substitution and vacancies are present together in the same octahedral sheet. Hectorite suspensions display a high viscosity and transparency as well as other attractive rheologic properties, which renders hectorite a very valuable clay mineral

Introduction

for industrial applications. A number of different procedures has therefore been developed to synthesize hectorite in large volumes (Güven, 1988).

Granquist and Pollack (1960) synthesized hectorite by hydrothermal treatment of an aqueous slurry containing approximately 10 % freshly precipitated $\text{Mg}(\text{OH})_2$, silica gel, and various amounts of NaOH and/or LiOH or LiF. The synthesis conditions used by these authors ranged from reflux temperature and atmospheric pressure to 300°C and approximately 1200 psi (approximately 83 bar). LiF was found to accelerate the crystallization of hectorite. The observations of Baird et al. (1971, 1973), based on the same synthesis procedures, suggest that crystallization proceeds by condensation of silica monomers onto previously formed brucite sheets, confirming Harder's assumption (1972).

A commercial synthetic hectorite from Laporte Industries Limited, known by the trade name Laponite, has both vacancies and Li substitutions. Neumann and Sampson (1970) reported a composition of $\text{Na}_{0.30}(\text{Mg}_{2.55}\text{Li}_{0.30}\text{vac}_{0.15})\text{Si}_4\text{O}_{9.70}(\text{OH})_{2.30}$. The layer charge is apparently reduced by the presence of silanol (Si-OH) groups. Two patents are describing the basics of the synthesis (Neumann, 1971, 1972), which comprises the formation of an aqueous slurry from water soluble Mg-salts, sodium silicate, sodium carbonate or hydroxide, and lithium fluoride. This slurry is hydrothermally treated by boiling at reflux temperature under atmospheric pressure for 10 to 20 hours (Neumann, 1971). A year later (Neumann, 1972) an improvement of the procedure was described in a patent application. The main difference is the hydrothermal treatment in an autoclave at 150 to 700 psi (10 to 50 bar) and 185° to 265°C for at most 8 hours. Prolonged treatment results in further crystallization, which affects the rheological properties adversely.

Torii and Iwasaki (1986, 1987) published a method which differs from that of Laporte Industries Ltd. in that homogeneous slurries of the desired hectorite composition are utilized. The slurries were prepared by dissolving MgCl_2 in a solution of sodium silicate and nitric acid, followed by precipitation with ammonia, washing, and addition of NaOH and LiOH. The resulting slurries were

hydrothermally treated at 125° to 300°C at autogeneous water vapor pressures for 1 to 24 hours.

Orlemann (1972) used naturel pure talc as a starting material, which was calcined between 760° and 980°C together with Li_2CO_3 . The resulting solid is hydrothermally treated together with an aqueous solution of sodium silicate and carbonate for 8 to 16 hours at 185°C and at the corresponding water vapor pressure (11 bar). The main advantages of Orlemann's procedure are the use of a relatively cheap and readily available source of a reactant material of high purity, talc, and the less complicated and time consuming series of process steps.

Barrer and Jones (1970) have described a widely used method to synthesize fluorhectorite (i.e., hectorite without structural hydroxyl groups). In this procedure reagent grade chemicals, such as, pure silica, MgO, MgF_2 , LiF, and Na_2CO_3 are reacted in the solid state at 800°C within 24 hours or as a melt at 850°C within 2 hours.

1.3 PILLARED CLAYS

In 1955 Barrer and McLeod (1955) demonstrated the concept of intercalation of clays by organic compounds. However, organic and organometallic intercalating or pillaring agents decompose at relatively modest temperatures causing the pillared clay structure to collapse. Nowadays, these types of pillared clays are industrially used as gelling agents, thickeners, and fillers (Schoonheydt, 1991).

The escalation of the oil prices in 1973 confronted the oil industry with the problem how to maximize the processing of crude oil, especially the heavy fractions to gasoline components. A strong impulse was thus given to the development of catalysts with relative large pore sizes, able to deal with larger molecules than molecular sieves, and a good thermal and hydrothermal stability. The oil crisis thus resulted in a renewed interest in the concept of pillared clays. The use of inorganic hydrated polyoxocations as pillaring agents provided thermally

stable pillared clays with high surface areas (200 to 500 m²/g). Upon calcination the hydrated polyoxocations dehydrate and dehydroxylate, and react to fixed metal oxide pillars (Fig. 1.3). Brindley and Sempels (1977), Lahav et al. (1978), Vaughan and Lussier (1980), and Vaughan et al. (1979, 1981) were the first to report independently on the intercalation with Al polyoxocations, resulting in a basal spacing of 17 to 18 Å and thermal stabilities up to 500°C.

1.3.1 Al pillared clays

Until now most of the research on pillared clays has been focussed on the Al-13 polyoxocation as a pillaring agent. Solutions containing this complex are prepared through forced hydrolysis by either addition of a base to AlCl₃ or Al(NO₃)₃ solutions up to an OH/Al molar ratio of 2.5 (Kloprogge et al., 1992; Ch. X) or by dissolving Al powder in AlCl₃. The last type of solution is known as chlorohydrate or chlorhydrol and is commercially available (e.g., Reheis Chemical Company). ²⁷Al NMR (Akitt et al., 1972; Bottero et al., 1980; Bertsch et al., 1986a,b) and small angle X-ray scattering (Rausch and Bale, 1964; Bottero et al., 1982) have proven that the complex is most probably the tridecamer [AlO₄Al₁₂(OH)₂₄(H₂O)₁₂]⁷⁺, a Keggin structure previously described in the solid state of basic aluminum sulphate by Johansson (1960).

Pinnanavaia et al. (1984) demonstrated that the procedure according to which a flocculated pillared clay is dried largely determines the apparent pore size of pillared

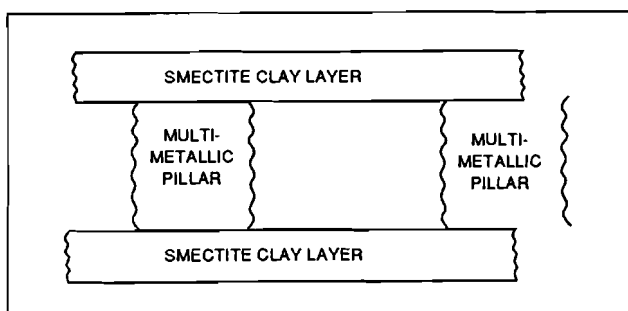


Figure 1.3 Schematic representation of a pillared clay (after Vaughan et al., 1981)

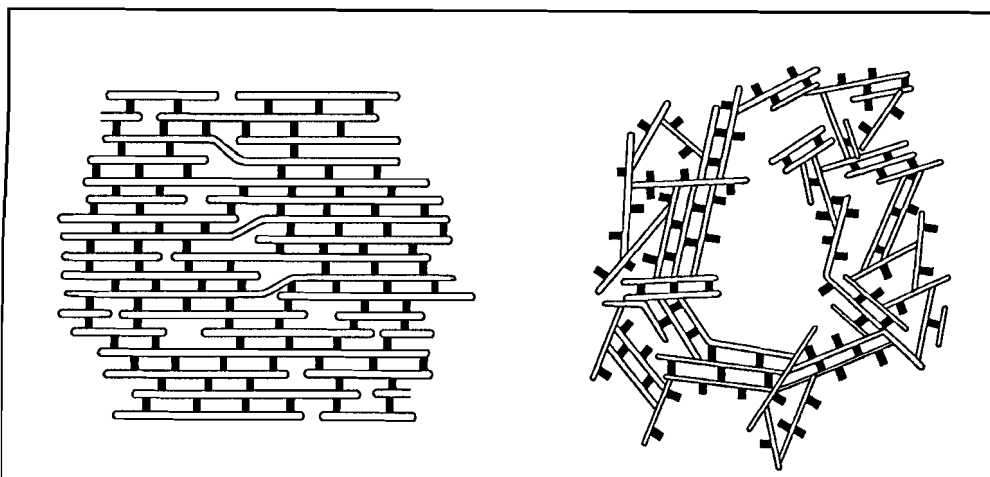


Figure 1.4 Schematic representation of (left) a lamellar aggregation and (right) an aggregation resembling a house of cards (after Occelli et al., 1987)

products. In flocculated clays both face-to-face (lamellar) and delaminated (edge-to-face and edge-to-edge) layers occur, the delaminated structures resembling a house of cards (Fig. 1.4). The structure established after flocculation is more or less preserved during freeze drying, which leads to macropores, while air drying results in a reorganization of the delaminated aggregates to face-to-face aggregation. Occelli et al. (1987) observed the house of cards structure directly with the transmission electron microscope.

The amount of Al bound in the interlayer per unit cell varies only within a small range (2.78 to 3.07) and shows no correlation with the charge of the layer. The absence of a correlation suggests a more or less uniform monolayer of hydrated Al polyoxocations to be present in the interlayer. The charge balance is achieved through hydrolysis of the pillaring agents (Pinnavaia et al., 1984). Accordingly, pillaring results in an effective reduction of the initial CEC of the starting clay (Keren, 1986).

Shabtai et al. (1984) pillared La^{3+} - and Ce^{3+} -exchanged hectorites with the Al polyoxocation, since acidic (H^+ , La^{3+} , Ce^{3+}) pillared clays exhibit a high catalytic cracking activity. Pillared fluor-hectorite exhibited higher surface areas (300 to 380

Introduction

m^2/g), larger basal spacings (between 18.2 and 20 Å), and a higher thermal stability as compared to pillared hectorite (220 - 280 m^2/g , 17 to 18 Å).

Plee et al. (1985) have used ^{27}Al and ^{29}Si solid state nuclear magnetic resonance techniques to study the thermal transformation of the pillars and their linkage with the clay sheets. The ^{27}Al spectra of beidellite revealed a decrease in the Al^{IV} resonance intensity tailing towards lower shifts. A shoulder was present at 56.5 ppm, which could be related to the more negative shift observed for the $\text{Si}(1\text{Al})$ resonance in the ^{29}Si spectra. A model was proposed in which linking of the pillar to the tetrahedral sheet induced an inversion of an Al tetrahedron of the tetrahedral sheet (Fig. 1.5). This would lead to new $\text{Si-O-Al}^{\text{IV}}$ linkages, in which the negative charge is exposed in the interlayer space. Such a linkage should induce a larger number of stronger acid sites, which is indeed observed for pillared beidellite.

No reaction between pillar and tetrahedral sheet was observed for smectites

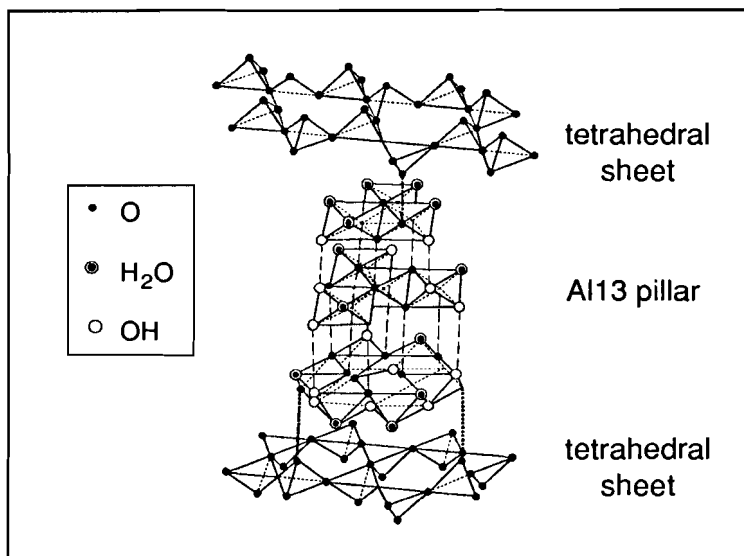


Figure 1.5 Schematic structure of a pillar linked to three inverted Al tetrahedra of two tetrahedral layers (after Plee et al., 1985)

without tetrahedral substitutions (hectorite, montmorillonite). In contrast to the findings of Plee et al. (1985), Pinnavaia et al. (1985) observed that pillared fluor-hectorite does undergo structural transformations upon thermal treatment. They concluded that the structural fluor causes the Si-O bands to be more labile, which promotes coupling with the pillar. They moreover concluded that the composition of the layer cannot be ruled out as a factor determining the activity of the layer. Schutz et al. (1987) and Plee et al. (1987) used synthetic beidellite to produce pillared clays. As compared to pillared montmorillonite, beidellite has a more ordered distribution of pillars in the interlayer space of the clay. Infrared spectroscopy using pyridine as a probe molecule revealed the presence of both Lewis and Brønsted acid sites (Schutz et al., 1987).

Depending on the drying conditions Kodama and Singh (1988) and Singh and Kodama (1988) obtained three different types of Al pillared montmorillonites. Extremely dry conditions led to a phase exhibiting a basal spacing of 18.8 Å. An intermediate phase was formed under ambient conditions. Both phases transformed to a phase displaying a basal spacing of 28 Å upon aging. The phase of a basal spacing of 18.8 Å converted to the phase of a basal spacing of 28 Å upon thermal treatment at 700°C. The phase of a basal spacing of 28 Å is a relatively regular interstratified structure of non-expanding layers of a spacing of 9.6 Å and expandable layers of a spacing of 18.8 Å in a ratio of 0.46:0.54.

Al pillared clays of a specific pillar density can be obtained by controlling the CEC of the starting clay. Suzuki et al. (1988) and Suzuki and Mori (1989) used partial ion exchange of Na⁺ for Ni²⁺ to achieve decreased CEC values. Upon calcination at 400°C about 75 % of the Ni²⁺ initially taken up can no longer be exchanged and the CEC is, consequently, effectively reduced. The reduction is determined by the initial Ni²⁺ to Na⁺ ratio in the starting clay.

Another method was published by Figueras et al. (1990), who used competitive ion exchange of the Al polyoxocation and NH₄⁺. The result was an increased homogeneity of the pillared montmorillonite and a higher acidity as compared to usually pillared montmorillonite. An analogously increased homogeneity and sharp

Introduction

pore size distribution (25 to 30 Å) were also achieved by ion exchange of the Al polyoxocation in the presence of polyvinyl alcohol, which does not affect the ion exchange itself (Suzuki et al., 1988; Suzuki and Mori, 1990).

Malla and Komarneni (1990) studied the adsorption of water by Al pillared montmorillonite. The shape of the isotherm, which neither fits the BET nor the Langmuir equation, is attributed to the unique pore size and hydrophobicity of pillared montmorillonite. The hydrophobicity developed on calcination is due to migration of protons, released from the pillars, from the interlayer spaces to the octahedral sheets. When the clay is treated with NH_3 the protons migrate again to the interlayer space and, subsequently, react to NH_4^+ . Exchange of NH_4^+ by Ca^{2+} causes the clay to become hydrophilic, which is reflected in the shape of the water adsorption isotherm, the heat of sorption of water, and the total adsorption capacity.

Recently, two studies have been conducted on pillaring interstratified clays. Sterte (1990) used interstratified illite/smectite, containing 30 to 60 % smectite, as starting material. The uptake of Al polyoxocations and the surface area were proportional to the fraction of smectite layers. Occelli (1990) pillared rectorite, an interstratified clay containing non-expandable mica type layers and expandable beidellite type layers. This resulting material was thermally stable up to 800°C and remained unaffected even after a steam treatment at 760°C for five hours. Pyridine adsorption showed the presence of both Lewis and Brønsted acid sites.

McCauley (1988) and Sterte (1990, 1991) prepared thermally very stable pillared clays with large basal plane spacings of approximately 28 Å. They used hydrothermally treated or refluxed solutions containing the Al polyoxocation and cerium or lanthanum chloride. The presence of cerium or lanthanum seemed to promote polymerization of the Al polyoxocation. They were not able to assess the structure of the thus formed polyoxocations. Although the interlayer spacing is twice that of a normal Al pillared clay, chemical analyses of the pillared clays indicate the presence of smaller amounts of Al and Ce or La than expected with a mere polymerization of the original Al polyoxocation.

1.3.2 Other metal pillared clays

Although the Al polyoxocation is by far the most studied pillaring agent in both the scientific and the patent literature, other metal polyoxocations have been investigated too. The most stable pillared clays are obtained by using Zr and Ti as pillaring cations. A good review has been presented in a special issue of *Catalysis Today* (1988), devoted to the preparation and characterization of pillaring agents and pillared clays.

Zr polyoxocations of the type $[\text{Zr}_4(\text{OH})_{16-n}(\text{H}_2\text{O})_{n+8}]^{n+}$ have been formed by dissolution and aging of zirconyl chloride, $\text{ZrOCl}_2 \cdot 8\text{H}_2\text{O}$ (Yamanaka and Brindley, 1979; Bartley and Burch, 1985; Ocelli and Finseth, 1986; Bartley, 1988). Not only aging, but also the concentration and the pH affect the extent of polymerization. Addition of bases, such as, NaOH, accelerates the polymerization and increases the stability of the Zr pillared clays (Fanfan-Torres et al., 1990). Controlled polymerization offers the possibility to prepare pillared clays of different interlayer distances and surface areas (Bartley, 1988).

Cr polyoxocations were prepared by base hydrolysis analogous to that of Al polyoxocations (Brindley and Yamanaka, 1979; Hopkins et al., 1984; Carr, 1985; Pinnavaia et al., 1985). Pinnavaia et al. (1985), and Tzou and Pinnavaia (1988) showed that increasing the hydrolysis temperature from 25 °C, as used by Brindley and Yamanaka (1979), to 95 °C results in larger polymers, giving pillared clays with basal plane spacings near 27 Å instead of 17 Å. Moini et al. (1990) found that the pillared clay with the 27 Å basal plane spacing is far more reactive in the dehydrogenation of benzene than the clay with the 17 Å basal plane spacing.

Yamanaka et al. (1980) prepared Bi-pillared clays similarly as described for Zr and Cr pillared clays. Although Bi-pillared clays exhibit basal plane spacings of 16 Å, they have surface areas lower than 80 m²/g. Sterte (1986) reported on Ti-pillared clays prepared by ion exchange of Ti polyoxocations formed by partial hydrolysis of TiCl_4 in HCl. These pillared clays were stable to 700 °C and had surface areas of 200 to 350 m²/g, growing with decreasing HCl concentration.

Introduction

Yamanaka and Brindley (1978) and Brindley and Kao (1980) prepared Ni- and Mg-pillared clays by in situ hydrolysis of $\text{Ni}(\text{NO}_3)_2$ and $\text{Mg}(\text{NO}_3)_2$. This procedure is useful for the preparation of polyoxocations which cannot be formed in aqueous solutions, due to the precipitation of the metal hydroxide. Fe(III) pillared clays can be prepared in various ways by intercalation with (i) hydroxy Fe(III) polycations, (ii) phenantroline-Fe(II) cations, or (iii) trinuclear Fe(III) acetato cations (Yamanaka et al., 1984; Doff et al., 1988; Yamanaka and Hattori, 1988; Warburton, 1988; Martin-Luengo et al., 1989) followed by in situ conversion to an oxide pillar.

Endo et al. (1980) prepared very stable SiO_2 pillared clays by in situ hydrolysis of tris (acetylacetonato)silicon cations. Unfortunately, the interlayer distances were relatively small (basal plane spacings between 9.6 and 12.6 Å). Endo et al. (1980) and Pinnavaia et al. (1983) observed basal spacings of 16.7 Å for $\text{Si}(\text{acac})_3^+$ intercalated montmorillonites. Hydrolysis leads to a decrease of the basal spacing to values between 12.1 and 12.6 Å. The same results were found by the in situ reaction of clays solvated with acetylacetone with SiCl_4 in either benzene or benzaldehyde. Lewis et al. (1985) proposed an alternative approach utilizing organosilicon compounds as intercalating agents. The organic compounds are decomposed upon calcination, converting the pillar to the corresponding oxide.

Two additional types of pillared clays are obtained by intercalation of mixed-metal complexes, such as Fe/Al (Lee et al., 1989, Bergaya et al., 1990) or Al/Zr (Occelli and Finseth, 1986), and of monometallic complexes on which a second cation is grafted, e.g., Si on the Al polyoxocation (Sterte and Shabtai, 1987). A completely new procedure to prepare pillared clays is the direct intercalation of metal oxide sols of, for example, SiO_2 or Al_2O_3 . These sols must necessarily consist of stable particles of nanometer or subnanometer dimensions having a positive charge on their surface. Pinnavaia (1989) reported the successful intercalation of tubular imogolite, $\text{Al}_4\text{Si}_2\text{O}_6(\text{OH})_8$

1.4 CATALYSIS BY PILLARED CLAYS

The pillaring of clays increases the accessibility of reactant molecules to the catalytic sites at the interlayer positions, resulting in a potentially high catalytic activity. Simultaneously, the interlayer and interpillar distances provide shape-selectivity. Shape-selectivity arises either from the fact that some reactants and reaction products do not fit into the pores of a catalyst or from controlling the rates of diffusion of reactants, reaction intermediates, and products. Most catalytic reactions using pillared clays as catalysts are based on the mild acidic properties of the catalyst.

Pillared clays have both Brönsted and Lewis acid sites. The Lewis acidity of pillared clays is comparable or even stronger than that of zeolite Y. The Brönsted acidity seems to be associated with the liberation of protons during dehydroxylation of the pillars. The Brönsted acidity decreases significantly with thermal treatment at increasing temperatures, either by dehydroxylation of the surface of the sheets, or by migration of protons from the interlayer space into the octahedral sheets, which has been observed in H-montmorillonite (Russel and Fraser, 1971; Yariv and Heller-Kallai, 1973). High-temperature treatment of pillared montmorillonites has shown that the amount of both the Brönsted and the Lewis sites decreases, which supports the second explanation

Table 1.2 summarizes some acid catalyzed reactions on pillared clays. Cracking reactions on pillared clays are mainly determined by the Brönsted acidity. At temperatures above 400°C the conversion quickly drops, due to the loss of hydroxyl groups and Brönsted acid sites, which causes pillared clays to be unsuitable as commercial cracking catalysts in present day processes. At low temperatures the cracking activity is comparable to the high activity of zeolites, but the selectivity for coke formation is higher (Vaughan et al., 1979, 1981).

The selectivity for disproportionation of trimethylbenzene has been shown to be positively affected by increasing the ratio of the Lewis-to-Brönsted acid sites. Catalyst deactivation of pillared clays in disproportionation reactions can be

Table 1.2 Examples of acid catalyzed reactions on pillared clays.

reaction	reactant	reference
cracking	cumene	Ming-Yuan et al. (1988)
	<i>n</i> -paraffin	Ming-Yuan et al. (1988)
	isopropylinaphthalene	Shabtai et al. (1980)
	dodecahydrotriphenyle	Shabtai et al. (1980)
disproportionation	trimethylbenzene	Ming-Yuan et al. (1988) Kikuchi and Matsuda (1988)
alkylation	<i>m</i> -xylene	Mori and Suzuki (1989)
	toluene/ethylene	Occelli et al. (1985)
	toluene/methanol	Urabe et al. (1986)
	trimethylbenzene/ methanol	Matsuda et al. (1986)
methanol conversion	benzene/olefins	Ming-Yuan et al. (1988) Occelli et al. (1984) Burch and Warburton (1986)

prevented by loading the clay with small amounts of Pt or Pd and using hydrogen as a carrier gas. Increasing the Brønsted acidity favors the activity for isomerization reactions (Kikuchi and Matsuda, 1988).

One of the important catalytic processes based on shape selectivity is the production of *p*-xylene by alkylation of toluene with methanol. The selectivity of Al pillared clays in this reaction is surprisingly higher than that of the zeolite ZSM-5 (Urabe et al., 1986). The production of *p*-Ethyltoluene by ethylation of toluene involves a larger molecule than *p*-xylene and is, therefore, more shape-selective controlled. The high selectivity of pillared clays is thought to be the result of their moderate acidity resulting in a decrease in secondary isomerization of the primary product (Kikuchi and Matsuda, 1988).

Zr and Al pillared clays are active catalysts for methanol conversion to hydrocarbons. The selectivity of Zr pillared clays for the formation of C₂-C₄ olefins is higher than that of Al pillared clays. The higher selectivity is caused by the narrower interlayer distance of the Zr pillared clay, retarding the conversion of olefins to aromatic hydrocarbons. Burch and Warburton (1986) found that Zr pillared clays of a low surface area had a higher catalytic activity than those of a high surface area. The lower activity is attributed to the increasing number of pillars that presumably shield or block the acid sites.

Bifunctional catalytic reactions for which pillared clays have been used comprise hydrocracking and hydro-isomerization. The fact that the pores of pillared clays can be significantly wider than those of zeolites suggests the use of pillared clays for processing the larger molecules present in heavier feed stocks. However, the low thermal stability of pillared clays has prevented their utilization in fluid catalyst cracking, where regeneration of the catalyst is carried out at high temperatures. Occelli and Rennard (1988) obtained an excellent catalyst for hydrocracking of vacuum gas oil by using pillared clays as support for Ni-Mo in a composite catalysts promoted with 30 % zeolite. No excessive coke formation proceeded as the catalytic activity increased with the reaction temperature. The coke formation may be suppressed by interaction of Lewis acid sites and the hydrogen carrier gas. Poncelet and Schutz (1986) published an example of hydroisomerization. For the hydroisomerization of *n*-heptane Pt-loaded pillared beidellite showed an activity comparable to that of zeolites, whereas the selectivity was superior to that zeolites. The high selectivity was attributed to the moderate acidity of the pillared beidellite.

1.5 SCOPE OF THIS THESIS

The scope of this thesis is fourfold:

- i) to synthesize and extensively characterize the smectites Na-beidellite and NH_4 -saponite, which will be used as starting materials for pillaring and to study the synthesis conditions in terms of pressure, temperature, run-time, and chemistry.
- ii) to study the forced hydrolysis of aluminum nitrate by base addition, to optimize the Al polyoxocation yield in the pillaring solutions, and to obtain information about the stability of the Al polyoxocation on aging and heat treatment.
- iii) to prepare and characterize the pillaring process of the synthetic smectites by Al polyoxocations and to study the linkages formed between the pillaring agent and the clay sheets during calcination.
- iv) to perform, in cooperation with the Technical University Eindhoven, some catalytic test reactions using the Al pillared smectites as catalyst.

Chapters II to V deal with Na-beidellite, and chapter VI to IX with ammonium- and magnesium-saponite. Chapters X to XVI are concerned with the hydrolysis of Al^{3+} and the characterization of the resulting species. Chapter XVII discusses the pillaring of synthetic beidellite and natural montmorillonite, while chapter XVIII describes the catalytic reaction of thiophene over the pillared clays prepared in this study.

Chapter II and III thus discuss the hydrothermal synthesis and the characterization of Na-beidellite, while the conditions of temperature, water pressure, and sodium activity under which Na-beidellite can be synthesized are investigated in chapter IV. In chapter V solid-state magic-angle spinning ^{23}Na NMR is used to study the interlayer collapse during dehydration of synthetic Na-beidellite.

The low-temperature synthesis of ammonium-saponites is considered in chapter VI, while solid-state ^{27}Al combined with ^{29}Si NMR provide evidence for the

presence of Al at the interlayer sites in chapter VII. In Chapter VIII a crystallization model is developed based on the hydrothermal synthesis of ammonium-saponite with increasing periods of time. Chapter IX deals with the synthesis of Mg-saponites using gels containing different competing cations.

Since the preparation of Al pillaring agents is highly important in the pillaring of clay minerals, much work has been devoted to the study of the reactions of Al^{3+} . Chapter X to XV are dealing with NMR studies of the aqueous chemistry of Al^{3+} . Chapters X to XIII concentrate on the formation of monomeric and oligomeric Al^{3+} species during hydrolysis. The aging of the tridecameric Al complex in partly hydrolyzed Al-sec-butoxide solutions and the reaction to fibrous boehmite are considered in chapter XIV. Chapter XV and XVI deal with the thermal stability and NMR properties of basic Al sulfate.

Pillaring of synthetic beidellite and natural montmorillonite is described in chapter XVII and the catalytic conversion of thiophene over pillared clays in chapter XVIII. Finally chapter XIX summarizes the results obtained in this study.

REFERENCES

- Akitt, J. W., Greenwood, N. N., Kandelwahl, B. L. and Lester, G. D. (1972) ^{27}Al nuclear magnetic resonance studies of the hydrolysis and polymerisation of the hexa-aquo-aluminum(III) cation: *J. Chem. Soc. Dalton Trans.* **1972**, 604-610.
- Ames, L. L. and Sand, L. B. (1958) Factors effecting maximum hydrothermal stability in montmorillonites: *Amer. Mineral.* **43**, 641-648.
- Baird, T., Cairns-Smith, A. G. and MacKenzie, D. W. (1973) An electron microscopic study of magnesium smectite synthesis: *Clay Minerals* **18**, 17-26.
- Baird, T., Cairns-Smith, A. G., MacKenzie, D. W. and Snell, D. (1971) Electron microscope studies on synthetic hectorite: *Clay Minerals* **9**, 250-252.
- Barrer, R. M. and Jones, D. L. (1970) Chemistry of soil minerals. Part VII. Synthesis and properties of fluorhectorites: *J. Chem. Soc. A.* **1970**, 1531-1537.
- Barrer, R. M. and McLeod, D. M. (1955) Activation of montmorillonite by ion exchange and sorption complexes of tetraalkylammonium montmorillonites: *Trans. Faraday Soc.* **51**, 1290-1300.
- Bartley, G. J. J. (1988) Zirconium pillared clays: *Catal. Today* **2**, 233-241.
- Bartley, G. J. J. and Burch, R. (1985) Zr-containing pillared interlayer clays. Part III. Influence of method of preparation on the thermal and hydrothermal stability: *Appl. Catal.* **19**, 175-185.
- Bergaya, F., Hassoun, N., Gatinéau, L. and Barrault, J. (1990) Mixed Al-Fe pillared laponites: preparation, characterization and catalytic properties in syngas conversion: in *Scientific bases for the preparation of heterogeneous catalysts, 5th Int. Symp. Louvain-La-Neuve (Belgium)*, preprint, **1990**, 141-148.
- Bertsch, P. M., Thomas, G. W. and Barnhisel, R. I. (1986a) Characterization of hydroxy-aluminum solutions by aluminum-27 nuclear magnetic resonance spectroscopy: *Soil Sci. Soc. Amer. J.* **55**, 825-830.

- Bertsch, P. M., Layton, W. J. and Barnhisel, R. I. (1986b) Speciation of hydroxy-aluminum solutions by wet chemical and aluminum-27 NMR methods: *Soil Sci. Soc. Amer. J.* **50**, 1449-1454.
- Booij, E. (1992) M.Sc. Thesis, University of Utrecht.
- Bottero, J. Y., Cases, J. M., Fiessinger, F. and Poirier, J. E. (1980) Studies of the hydrolyzed aluminum chloride solutions. 1. Nature of aluminum species and composition of aqueous solutions: *J. Phys. Chem.* **84**, 2933-2939.
- Bottero, J. Y., Tchoubar, D., Cases, J. M. and Fiessinger, F. (1982) Investigation of the hydrolysis of aqueous solutions of aluminum chloride. 2. Nature and structure by small angle X-ray scattering: *J. Phys. Chem.* **86**, 3667-3673.
- Brat, S. and Rajan, N. S. S. (1981) Synthetic magnesium aluminosilicates in radioactive waste treatment: *Indian J. Chem.* **20A**, 311-312.
- Brindley, G. W. (1980) Order and disorder in clay mineral structures: in *Crystal Structures of Clay Minerals and Their X-ray Identification*, G. W. Brindley and G. Brown, eds., Mineralogical Society, London, Chapter 2.
- Brindley, G. W. and Brown, G., eds., (1980) *Crystal Structures of Clay Minerals and Their X-ray Identification*, Mineralogical Society, London.
- Brindley, G. W. and Kao, C.-C. (1980) Formation, compositions and properties of hydroxy-Al- and hydroxy-Mg-montmorillonite: *Clays & Clay Minerals* **28**, 435-443.
- Brindley, G. W. and Sempels, R. E. (1977) Preparation and properties of some hydroxy-aluminium beidellites: *Clay Minerals* **12**, 229-237.
- Brindley, G. W. and Yamanaka, S. (1979) A study of hydroxy-chromium montmorillonites and the form of the hydroxy-chromium polymers: *Amer. Mineral.* **64**, 830-835.
- Burch, R. (ed.)(1988) Pillared Clays: *Catal. Today* **2**, 185-368.
- Burch, R. and Warburton, C. I. (1986) Zr-containing pillared interlayer clays I. Preparation and structural characterisation: *J. Catal.* **97**, 503-510.

Introduction

- Burch, R. and Warburton, C. I. (1986) Zr-containing pillared interlayer clays II. Catalytic activity for the conversion of methanol into hydrocarbons: *J. Catal.* **97**, 511-515.
- Caillère, S., Henin, S. and Esquevin, J. (1953) Synthèses à basse température de phyllites ferrifères: *C.R. Acad. Sci. Paris* **239**, 1535-1537.
- Caillère, S., Henin, S. and Esquevin, J. (1955) Synthèses à basse température de quelques minéraux ferrifères (silicates et oxydes): *Bull. Soc. Fr. Miner. Crist.* **79**, 408-421.
- Capell, R. G. and Granquist, W. T. (1966) *U.S. Patent 3,252,889*.
- Carr, R. M. (1985) Hydration states of interlamellar chromium ions in montmorillonite: *Clays & Clay Minerals* **33**, 357-361.
- Decarreau, A. (1980) Cristallogène expérimentale des smectites magnésiennes: hectorite, stévensite: *Bull. Minéral.* **103**, 579-590.
- Decarreau, A. (1985) Partitioning of divalent transition elements between octahedral sheets of trioctahedral smectites and water: *Geochim. Cosmochim. Acta* **49**, 1537-1544.
- Decarreau, A. and Bonnin, D. (1986) Synthesis and crystallogenesis at low temperature of Fe(III)-smectites by evolution of coprecipitated gels: experiments in partially reducing conditions: *Clay Minerals* **21**, 861-877.
- Decarreau, A., Bonnin, D., Badaut-Trauth, D., Couty, R. and Kaiser, P. (1987) Synthesis and crystallogenesis of ferric smectite by evolution of Si-Fe coprecipitates in oxidizing conditions: *Clay Minerals* **22**, 207-223.
- Doff, D. H., Gangas, N. H. J., Allan, J. E. M. and Coey, J. M. D. (1988) Preparation and characterization of iron oxide pillared montmorillonite: *Clay Minerals* **23**, 367-377.
- Eberl, D. and Hower, J. (1977) The hydrothermal transformation of sodium and potassium smectite into mixed-layer clay: *Clays & Clay Minerals* **25**, 215-227.
- Endo, T., Mortland, M. M. and Pinnavaia, T. J. (1980) Intercalation of silica in smectite: *Clays & Clay Minerals* **28**, 105-110.

- Fanfan-Torres, E. M., Dedecker, O. and Grange, P. (1990) Zirconium pillared clays. Influence of basic polymerization of the precursors on their structure and stability: in *Scientific bases for the preparation of heterogeneous catalysts, 5th Int. Symp. Louvain-La-Neuve (Belgium)*, preprint, 1990, 469-475.
- Figueras, F, Klapyta, Z., Massiani, P., Mountassir, Z., Tichit, D. and Fajula, F. (1990) Use of competitive ion exchange for intercalation of montmorillonite with hydroxy-aluminum species: *Clays & Clay Minerals* **38**, 257-264.
- Fowden, L., Barrer, R. M. and Tinker, P. B. (eds.)(1984) *Clay Minerals: their Structure, Behaviour and Use*, The Royal Society, London.
- Gaaf, J., van Santen, R. A., Knoester, A. and van Wingerden, B. (1983) Synthesis and catalytic properties of pillared Nickel substituted mica montmorillonite clays: *J. Chem. Soc. Commun.* **1983**, 655-657.
- Giese, R. F., Jr. (1975) Interlayer bonding in talc and pyrophyllite: *Clays & Clay Minerals* **23**, 165-166.
- Granquist, W. T. (1966) *U.S. Patent 3,252,757*.
- Granquist, W. T. (1974) *U.S. Patent 3,852,405*.
- Granquist, W. T. and Pollack, S. S. (1960) A study of the synthesis of hectorite: *Clays & Clay Minerals* **8**, 150-169.
- Güven, N. (1988) Smectites: in *Hydrous Phyllosilicates (exclusive of micas)*, S. W. Bailey, ed., Mineral. Soc. Amer. Reviews Mineral. **19**, 497-559.
- Harder, H. (1972) The role of magnesium in the formation of smectite minerals: *Chem. Geol.* **10**, 31-39.
- Harder, H. (1976) Nontronite synthesis at low temperatures: *Chem. Geol.* **18**, 169-180
- Harder, H. (1977) Clay mineral formation under lateritic weathering conditions: *Clay Minerals* **12**, 281-288.
- Harder, H. (1978) Synthesis of iron layer silicate minerals under natural conditions: *Clays & Clay Minerals* **26**, 65-72.

Introduction

- Harward, M. E. and Brindley, G. W. (1965) Swelling properties of synthetic smectites in relation to lattice substitutions: *Clays & Clay Minerals* **6**, 209-222.
- Heinerman, J. J. L. (1985) *U.S. Patent 4,511,752*.
- Herrero, C. P., Sanz, J. and Serratos, J. M. (1985) Tetrahedral cation ordering in layer silicates by ^{29}Si NMR spectroscopy: *Solid State Commun.* **53**, 151-154.
- Herrero, C. P., Gregorkiewitz, M., Sanz, J. and Serratos, J. M. (1987) ^{29}Si MAS-NMR spectroscopy of mica-type silicates: observed and predicted distribution of tetrahedral Al-Si: *Phys. Chem. Minerals* **15**, 84-90.
- Hickson, D. A. (1974) *U.S. Patent 3,844,979*.
- Hickson, D. A. (1975) *U.S. Patent 3,887,454*.
- Hickson, D. A. (1975) *U.S. Patent 3,892,655*.
- Hopkins, P. D. (1984) *U.S. Patent 4,452,910*.
- Iiyama, J. T. and Roy, R. (1963) Controlled synthesis of heteropolytypic (mixed layer) clay minerals: *Clays & Clay Minerals* **10**, 4-22.
- Jaffe, J. (1974) *U.S. Patent 3,803,026*.
- Johansson, G. (1960) On the crystal structure of some basic aluminum salts: *Acta Chem. Scand.* **14**, 771-773.
- Keren, R. (1986) Reduction of the cation-exchange capacity of montmorillonite by take-up of hydroxy-Al polymers: *Clays & Clay Minerals* **34**, 534-538.
- Kikuchi, E. and Matsuda, T. (1988) Shape selective acid catalysis by pillared clays *Catal. Today* **2**, 297-307.
- Kloprogge, J. T., van der Eerden, A. M. J., Jansen, J. B. H. and Geus, J. W. (1990) Hydrothermal synthesis of Na-beidellite. *Geologie & Mijnbouw* **69**, 351-357.
- Kloprogge, J. T., Jansen, J. B. H. and Geus, J. W. (1990) Characterization of synthetic Na-beidellite: *Clays & Clay Minerals* **38**, 409-414.
- Kloprogge, J. T., van der Eerden, A. M. J., Jansen, J. B. H. and Geus, J. W. (1992) Synthesis field of Na-beidellite in terms of temperature, water-pressure and sodium activity: *this thesis* Ch. IV.

- Kloprogge, J. T., Seykens, D., Jansen, J. B. H. and Geus, J. W. (1992) A ^{27}Al nuclear magnetic resonance study on the optimization of the development of the Al13 polymer: *J. Non-Cryst. Solids* **142**, 94-102.
- Kodama, H. and Singh, S. S. (1989) Polynuclear hydroxyaluminum-montmorillonite complexes: formation of 18.8 Å and 28 Å pillared structures: *Solid State Ionics* **32/33**, 363-372.
- Koizumi, M. and Roy, R. (1959) Synthetic montmorillonoids with variable exchange capacity: *Amer. Mineral.* **44**, 788-805.
- Lahav, N., Shani, U. and Shabtai, J. (1978) Cross-linked smectites. I. Synthesis and properties of hydroxy-aluminum montmorillonite: *Clays & Clay Minerals* **26**, 107-115.
- Lee, W. Y., Raythatha, R. H. and Tatarchuk, B. J. (1989) Pillared-clay catalysts containing mixed-metal complexes: *J. Catal.* **115**, 159-179.
- Lewis, R. M., Ott, K. C. and van Santen, R. A. (1985) *U.S. Patent* **4,510,257**.
- Loewenstein, W. (1954) The distribution of aluminum in the tetrahedra of silicates and aluminates: *Amer. Mineral.* **39**, 92-96.
- Luth, W. C. and Ingamells, C. O. (1965) Gel preparation of starting materials for hydrothermal experimentation: *Clays & Clay Minerals* **25**, 215-227.
- Malla, P. B. and Komarneni, S. (1990) Synthesis of highly microporous and hydrophilic alumina-pillared montmorillonite: water-sorption properties: *Clays & Clay Minerals* **38**, 363-372.
- Martin-Luengo, M. A. , Martins-Carvalho, H., Ladriere, J. and Grange, P. (1989) Fe(III)-pillared montmorillonites: preparation and characterization: *Clay Minerals* **24**, 495-504.
- McCauley, J. R. (1988) *U.S. Patent* **4,818,737**.
- Ming-Yuan, H., Zhonghui, L and Enze, M. (1988) Acidic and hydrocarbon catalytic properties of pillared clays: *Catal. Today* **2**, 321-338.
- Moini, A., Brewer, T. D., Tzou, M.-S., Landau, S. D., Teo, B.-K. and Pinnavaia, T.J. (1990) Catalytic properties of chromia-pillared montmorillonite and preliminary

Introduction

- study results: in *Spectroscopic characterization of minerals and their surfaces*, Amer. Chem. Soc., 455-467.
- Mori, T. and Suzuki, K. (1989) Shape selective property of alumina-pillared montmorillonite with different lateral distances in m-xylene conversion: *Chem. Letters* **1989**, 2165-2168.
- Neumann, B. S. (1971) *U.S. Patent 3,586,478*.
- Neumann, B. S. (1972) *U.S. Patent 3,671,190*.
- Neumann, B. S. and Sansom, K. G. (1970) The formation of stable sols from laponite, a synthetic hectorite-like clay: *Clay Minerals* **8**, 389-404.
- Occelli, M. L. (1990) Thermal stability, acidity and cracking properties of pillared rectorite catalysts: in *Scientific bases for the preparation of heterogeneous catalysts, 5th Int. Symp. Louvain-La-Neuve (Belgium)*, preprint, **1990**, 99-111.
- Occelli, M. L. and Finseth, D. H. (1986) Preparation and characterization of pillared hectorite catalysts: *J. Catal.* **99**, 316-326.
- Occelli, M. L., Innes, R. A., Hwu, S. S. and Hightower, J. W. (1985) Sorption and catalysis on sodium-montmorillonite interlayered with aluminum oxide clusters: *Appl. Catal.* **14**, 69-82.
- Occelli, M. L., Perulekar, V. N. and Hightower, J. W. (1984) Sorption of normal paraffins in a pillared clay mineral: *Proc. Int. Congr. Catal. 8th*, Berlin, **4**, 725-733.
- Occelli, M. L. and Rennard, R. J. (1984) *Prep., Amer. Chem. Soc., Div. Fuel Chem.* **29**,3.
- Occelli, M. L. and Rennard, R. J. (1988) Hydrotreating catalysts containing pillared clays: *Catal. Today* **2**, 309-320.
- Occelli, M. L., Senders, J. V. and Lynch, J. (1987) TEM analysis of pillared and delaminated hectorite catalysts: *J. Catal.* **107**, 557-565.
- Orlemann, J. K. (1972) *U.S. Patent 3,666,407*.
- Pinnavaia, T. J. (1989) Poster presentation at the 9th Int. Clay Conf., Strasbourg, France.

- Pinnavaia, T. J., Landau, S. D., Tzou, M.-S., Johnson, I. D. and Lipsicas, M. (1985) Layer cross-linking in pillared clays: *J. Amer. Chem. Soc.* **107**, 7222-7224.
- Pinnavaia, T. J., Mortland, M. M. and Endo, T. (1983) *U.S. Patent* 4,367,163.
- Pinnavaia, T. J., Tzou, M.-S., Landau, S. D. and Raythatha, R. H. (1984) On the pillaring and delamination of smectite clay catalysts by polyoxo cation of aluminum: *J. Mol. Catal.* **27**, 195-212.
- Pinnavaia, T. J., Tzou, M.-S. and Landau, S. D. (1985) New chromia pillared clay catalysts: *J. Amer. Chem. Soc.* **107**, 4783-3785.
- Plee, D., Borg, F., Gataineau, L. and Fripiat, J. J. (1985) High-resolution solid-state ^{27}Al and ^{29}Si nuclear magnetic resonance study of pillared clays: *J. Amer. Chem. Soc.* **107**, 2362-2369.
- Plee, D., Gataineau, L. and Fripiat, J. J. (1987) Pillaring processes with and without tetrahedral substitution: *Clays & Clay Minerals* **35**, 81-88.
- Poncelet, G. and Schutz, A. (1986) Pillared montmorillonite and beidellite. Acidic and catalytic properties: in *Chemical reactions in organic and inorganic systems*, R. Setton, ed., NATO ASI Series **C165**, D. Reidel Publishing Company, Dordrecht, 165-178.
- Robschlagel, K. H. W., Emeis, C. A. and van Santen, R. A. (1984) On the hydroisomerisation activity of nickel-substituted mica montmorillonite: *J. Catal.* **86**, 1-8.
- Roy, D. M. and Roy, R. (1952) Studies in the system $\text{MgO-Al}_2\text{O}_3\text{-SiO}_2\text{-H}_2\text{O}$: *Bull. Geol. Soc. Amer.* **63**, 1293 (abstract).
- Roy, D. M. and Roy, R. (1955) Synthesis and stability of minerals in the system $\text{MgO-Al}_2\text{O}_3\text{-SiO}_2\text{-H}_2\text{O}$: *Amer. Mineral.* **40**, 147-178.
- Roy, R. and Sand, L. B. (1956) A note on some properties of synthetic montmorillonites: *Amer. Mineral.* **41**, 505-509.
- Russel, J. D. and Fraser, A. R. (1971) I.R. spectroscopic evidence for interaction between hydronium ions and lattice OH groups in montmorillonite: *Clays & Clay Minerals*, **19**, 55-59.

Introduction

- Sand, L. B., Roy, R. and Osborn, E. F. (1953) Stability relations of some minerals in the system $\text{Na}_2\text{O}-\text{Al}_2\text{O}_3-\text{SiO}_2-\text{H}_2\text{O}$: *Bull. Geol. Soc. Amer.* **64**, 1469-1470 (abstract).
- Sand, L. B., Roy, R. and Osborn, E. F. (1953) Stability relations of some minerals in the $\text{Na}_2\text{O}-\text{Al}_2\text{O}_3-\text{SiO}_2-\text{H}_2\text{O}$ system: *Econ. Geol.* **52**, 169-179.
- van Santen, R. A., Röbschläger, K.-H. W. and Emeis, C. A. (1985) The hydroisomerisation activity of nickel-substituted mica montmorillonite clay: in *Solid State Chemistry in Catalysis*, R. K. Grasselli and J. F. Brazdil, eds., ACS Symp. Series **279**, Amer. Chem. Soc., Washington, D.C., 275-291.
- Schoonheydt, R. A. (1991) Clays: from two to three dimensions: in *Introduction to Zeolite Science and Practice*, H. van Bekkum, E. M. Flanigen and J. C. Jansen, eds., Studies in Surface Science and Catalysis **58**, Elsevier, Amsterdam, 201-239.
- Schutz, A., Stone, W. E. E., Poncelet, G. and Fripiat, J. J. (1987) Preparation and characterization of bidimensional zeolitic structures obtained from synthetic beidellite and hydroxy-aluminum solutions: *Clays & Clay Minerals* **35**, 251-261.
- Shabtai, J., Lazar, R. and Oblad, A. G. (1980) Acidic forms of cross-linked smectites - a novel type of cracking catalysts: *Proc. Int. Congr. Catal. 7th*, Kodansha Elsevier, Tokyo, 828-840.
- Shabtai, J., Rosell, M. and Tokarz, M. (1984) Cross-linked smectites. III. Synthesis and properties of hydroxy-aluminum hectorites and fluorhectorites: *Clays & Clay Minerals* **32**, 99-107.
- Shaikh, N. A. and Wik, N.-G., eds. (1986) *Clay Minerals - Modern Society*, Nordic Society for Clay Research, Uppsala.
- Singh, S. S. and Kodama, H. (1988) Reactions of polynuclear hydroxyaluminum cations with montmorillonite and the formation of a 28-Å pillared complex: *Clays & Clay Minerals* **36**, 397-402.
- Sterte, J. (1986) Synthesis and properties of titanium oxide cross-linked montmorillonite: *Clays & Clay Minerals* **34**, 658-664.

- Sterte, J. (1990) Preparation and properties of pillared interstratified illite/smectite: *Clays & Clay Minerals* **38**, 609-616.
- Sterte, J. (1990) Preparation and properties of large-pore RE/Al-pillared montmorillonite, a comparison of RE-cations: in *Scientific bases for the preparation of heterogeneous catalysts, 5th Int. Symp. Louvain-La-Neuve (Belgium)*, preprint, 112-122.
- Sterte, J. (1991) Preparation and properties of large-pore La-Al-pillared montmorillonite: *Clays & Clay Minerals* **39**, 167-173.
- Sterte, J. and Shabtai, J. (1987) Cross-linked smectites. V. Synthesis and properties of hydroxy-silicoaluminum montmorillonites and fluorhectorites: *Clays & Clay Minerals* **35**, 429-439.
- Suquet, H., De La Calle, C. and Pezerat, H. (1975) Swelling and structural organization of saponite: *Clays & Clay minerals* **23**, 1-9.
- Suquet, H., Iiyama, J. T., Kodama, H. and Pezerat, H. (1977) Synthesis and swelling properties of saponites with increasing layer charge: *Clays & Clay Minerals* **25**, 231-242.
- Suquet, H., Malard, C., Copin, E. and Pezerat, H. (1981) Variation du parametre b et de la distance basale d_{001} dans une serie de saponites a charge croissante: I. etats hydrates: *Clay Minerals* **16**, 53-67.
- Suquet, H., Malard, C., Copin, E. and Pezerat, H. (1981) Variation du parametre b et de la distance basale d_{001} dans une serie de saponites a charge croissante: II. etats 'zero couche': *Clay Minerals* **16**, 181-193.
- Suquet, H., Prost, R. and Pezerat, H. (1982) Etude par spectroscopie infrarouge et diffraction X des interactions eau-cation-feuillet dans les phases a 14.6, 12.2 et 10.1 Å d'une saponite-Li de synthese: *Clay Minerals* **17**, 231-241.
- Suzuki, K. and Mori, T. (1989) Synthesis of alumina-pillared clay with desired pillar population using Na-montmorillonite having controlled cation exchange capacity: *J. Chem. Soc., Chem. Commun.* **1989**, 7-8.
- Suzuki, K., Horio, M. and Mori, T. (1988) Preparation of alumina-pillared montmorillonite with desired pillar population: *Mat. Res. Bull.* **23**, 1711-1718.

Introduction

- Suzuki, K., Mori, T., Kawase, K., Sakami, H. and Iida, S. (1988) Unique pore structure formed in montmorillonite in the presence of polyvinyl alcohol and aluminium chlorohydroxide: *J. Chem. Soc., Chem. Commun.* **1988**, 122-123.
- Suzuki, K., Mori, T., Kawase, K., Sakami, H. and Iida, S. (1988) Preparation of delaminated clay having a narrow micropore distribution in the presence of hydroxyaluminum cations and polyvinyl alcohol: *Clays & Clay Minerals* **36**, 147-152.
- Torii, K. and Iwasaki, T. (1986) Synthesis of new trioctahedral Mg-Smectite: *Chemistry Letters*, **1986**, 2021-2024.
- Torii, K. and Iwasaki, T. (1987) Synthesis of hectorite. *Clay Sci.* **7**, 1-16.
- Tzou, M.-S. and Pinnavaia, T. J. (1988) Chromia pillared clays: *Catal. Today* **2**, 243-359.
- Urabe, K., Koga, M. and Izumi, Y. (1989) Synthetic Ni-substituted saponite as a catalyst for selective dimerization of ethene: *J. Chem. Soc., Chem. Commun.* **1989**, 807-808.
- Urabe, K., Sakurai, H. and Izumi, Y. (1986) Pillared synthetic saponite as an efficient alkylation catalyst: *J. Chem. Soc., Chem. Commun.* **1986**, 1074-1076.
- Vaughan, D. E. W., Lussier, R. J. (1980) Preparation of molecular sieves based on pillared interlayered clays: in *Proc. 5th Int. Conf. Zeolites, Naples, 1980*, L. V. C. Rees, ed., Heyden, London, 94-101.
- Vaughan, D. E. W., Lussier, R. J. and Magee, J. S. (1979) *U.S. Patent 4,176,090*.
- Vaughan, D. E. W., Lussier, R. J. and Magee, J. S. (1981) *U.S. Patent 4,248,739*.
- Vaughan, D. E. W., Lussier, R. J. and Magee, J. S. (1981) *U.S. Patent 4,271,043*.
- Warburton, C. I. (1988) Preparation and catalytic properties of iron oxide and iron sulphide pillared clays: *Catal. Today* **2**, 271-280.
- Yamada, H., Nakazawa, H., Yoshioka, K. and Fujita, T. (1991a) Smectites in the montmorillonite-beidellite series: *Clay Minerals* **26**, 359-369.

- Yamada, H., Yoshioka, K. and Nakazawa, H. (1991b) Hydrothermal synthesis of beidellite from aluminosilicate glass by varying water/solid ratio: *Mineral. J.* **15**, 300-308.
- Yamanaka, S. and Brindley, G. W. (1978) hydroxy-nickel interlayering in montmorillonite by titration method: *Clays & Clay Minerals* **26**, 21-24.
- Yamanaka, S. and Brindley, G. W. (1979) High surface area solids obtained by reaction of montmorillonite with zirconyl chloride: *Clays & Clay Minerals* **27**, 119-124.
- Yamanaka, S. and Hattori, M. (1988) Iron oxide pillared clay: *Catal. Today* **2**, 261-270.
- Yamanaka, S., Doi, T., Sako, S. and Hattori, M. (1984) High surface area solids obtained by intercalation of iron oxide pillars in montmorillonite: *Mat. Res. Bull.* **19**, 161-168.
- Yamanaka, S., Yamashita, G. and Hattori, M. (1980) Reaction of hydroxy-bismuth polycations with montmorillonite: *Clays & Clay Minerals* **28**, 281-284.
- Yariv, S. and Heller-Kallai, L. (1973) I.R. evidence for migration of protons in H- and organo-montmorillonites: *Clays & Clay Minerals* **21**, 199-200.

CHAPTER II

HYDROTHERMAL SYNTHESIS OF Na-BEIDELLITE

ABSTRACT

Na-beidellite was hydrothermally synthesized using various starting materials at a range of P-T conditions. The best crystallized Na-beidellite was carefully investigated with XRD, SEM, TGA, MAS-NMR and IR-spectroscopy. Cell parameters are: $a = 5.18 \pm 0.005 \text{ \AA}$; $b = 8.96 \pm 0.008 \text{ \AA}$; $c = 12.54 \pm 0.011 \text{ \AA}$; $V = 581.9 \pm 0.5 \text{ \AA}^3$. Indexing is based on an orthorhombic cell. ^{29}Si MAS-NMR reveal three peak positions: -92.7 ppm (Si-0Al); -88.4 ppm (Si-1Al); -82.3 ppm (Si-2Al), indicating an Al^{IV}/Si ratio of 0.106 per unit cell. The presence of small amounts of F in the hydrothermal fluid causes a significant increase in crystallinity. Na-beidellite is the only crystalline product applying a starting gel of composition $\text{Na}_{0.7}\text{Al}_{4.7}\text{Si}_{7.3}\text{O}_{22}$. A $\text{Na}_{1.0}\text{Al}_{5.0}\text{Si}_{7.0}\text{O}_{22}$ gel results in Na-beidellite + paragonite and gels with higher Na content produce only paragonite.

2.1 INTRODUCTION

The name Beidellite was given by Larsen and Wherry (1925) to a clay specimen from Beidell, Colorado, which they had earlier described as leverrierite (Larsen and Wherry, 1917). Nowadays Beidellite is defined as a dioctahedral Al-smectite (Ross and Hendricks, 1945; Weir and Greene-Kelly, 1962) with the formula $(0.5\text{Ca}, \text{Na}, \text{K})_p(\text{Al}^{\text{VI}})_4\text{Si}_{8-p}(\text{Al}^{\text{IV}})_p\text{O}_{20}(\text{OH})_4 \cdot n\text{H}_2\text{O}$. Natural Beidellite exhibit an average layer charge (p) of 0.66, which represent the amount of Al^{IV}.

Smectites have received much attention due to their swelling behaviour in water and the possibility to form pillared clays with organic and inorganic complexes (Loeppert et al., 1979; Plee et al., 1987; Sterte and Shabtai, 1987; Klopogge et al., 1990). These pillared clays can be used as molecular sieve and catalyst in e.g. oil cracking reactions, comparable with the use of synthetic zeolites. However, natural smectites exhibit unreliable quality and large variation in impurity content. Therefore, hydrothermal synthesis has been attempted in recent years (Torii and Iwasaki, 1986; 1987; Plee et al., 1987; Schutz et al., 1987).

In this paper we present results on the hydrothermal synthesis of Na-beidellite

with composition $\text{Na}_{0.7}\text{Al}_{4.7}\text{Si}_{7.3}\text{O}_{20}(\text{OH})_4 \cdot n\text{H}_2\text{O}$ under a variety of conditions. The best crystallized samples were selected for characterization with XRD, IR, TGA, DTA, SEM and Magic Angle Spinning Nuclear Magnetic Resonance (MAS-NMR).

2.2 STARTING MATERIALS AND EXPERIMENTAL METHODS

As starting material a Na-Al-Si gel with the required composition was prepared according to the method of Hamilton and Henderson (1968). The chemicals are listed in Table 2.1 The experiments were carried out in goldcapsules of 30 mm length and 2.4 mm internal diameter, placed in Tuttle-type, externally heated, cold-seal pressure vessels (Tuttle, 1949) as described in detail by Bos et al. (1987) and Klopogge et al. (1990).

X-ray powder diffraction patterns were recorded on a Philips PW 1050/25 diffractometer using $\text{CuK}\alpha$ radiation. Infrared absorption spectra were scanned on powdered samples in KBr tablets (1 wt% sample) with a Perkin Elmer 580 IR spectrophotometer. The morphology of the products was investigated with a Cambridge S150 scanning electron microscope. Thermogravimetric analyses were made on a Dupont 1090 Thermal Analyzer. Chemical analyses were made on a

Table 2.1 List of used chemicals.

Na_2CO_3	Merck no. 6392
$\text{Al}(\text{NO}_3)_3 \cdot 9\text{H}_2\text{O}$	Merck no. 1063
TEOS $\text{Si}(\text{OC}_2\text{H}_5)_4$	Merck-Schuchardt no. 800658
Ethanol	Nedalco C.V.
NaOH	Merck no. 6498
NaF	Merck no. 6449
H_2O	double distilled

JEOL JXA-8600 electron microprobe. ^{27}Al and ^{29}Si MAS-NMR spectra were recorded on a Bruker WM500 (11.7 Tesla) at the Department of Physical Chemistry, Faculty of Science, University of Nijmegen. Chemical shifts are reported in ppm relative to $[\text{Al}(\text{H}_2\text{O})_6]^{3+}$ for ^{27}Al and to tetramethylsilane (Me_4Si) for ^{29}Si .

2.3 RESULTS AND DISCUSSION

2.3.1 Influence of temperature and pressure

The experimental results under different conditions are summarized in **Table 2.2**. Variation in temperature indicates roughly four fields. At 250°C kaolinite is the only clay mineral formed, accompanied by a minor amount of quartz. The 300°C run represents a transition zone between the kaolinite and beidellite fields. At 350°C and 400°C beidellite is the predominant crystalline product. Higher temperature runs yielded beidellite accompanied by metastable SiO_2 in the form of cristobalite. In the beidellite field pressure can be as low as 200 bar without any change in crystallization. A more detailed investigation of the pressure/temperature influence on the stability of beidellite is in progress (Ch. IV).

2.3.2 Gel composition

The layer charge of beidellite can vary between 0.4 and 1.2. Run E598 started with a gel, that would be expected to give a beidellite with a layer charge of 1.0. However, the result of this run consists of amorphous material and a mixture of beidellite and low crystalline paragonite, $\text{Na}_{2.0}\text{Al}_6\text{Si}_6\text{O}_{20}(\text{OH})_4$. The beidellite must have a lower layer charge than 1.0. Unfortunately the two minerals could not be separated mechanically for chemical analyses. Higher Na contents ($\text{Na}_{1.5}\text{Al}_{5.5}\text{Si}_{6.5}\text{O}_{22}$ and $\text{Na}_{2.0}\text{Al}_{8.0}\text{Si}_{8.0}\text{O}_{22}$) resulted in the crystallization of only paragonite.

2.3.3 Characterization

The beidellite of run E432 was extensively investigated. The product of this run exhibited small flakes of beidellite of approximately 30 μm together and

Table 2.2 Selected experimental results.

Run nr.	T (°C)	P (bar)	Run time (days)	Gel nr. ¹	Solution	Crystalline phases produced ²
E520	250	1000	7	1	H ₂ O	Kaol + minor Qtz
E549	300	1000	7	1	H ₂ O	Beid + Kaol + minor Qtz
E432	350	1000	10	1	H ₂ O	Beid
E444	400	1000	10	1	NaOH ³	Beid + minor Qtz
E544	450	1000	7	1	H ₂ O	Beid + Crist + minor Qtz
E427	350	500	10	1	H ₂ O	Beid
E498	350	400	15	1	H ₂ O	Beid
E499	350	300	15	1	H ₂ O	Beid
E500	350	200	15	1	H ₂ O	Beid
E452	350	1000	10	1	NaF/NaOH 0.2 ³	Beid
E453	350	1000	10	1	NaF/NaOH 1.0 ³	Beid
E454	350	1000	10	1	NaF ³	Beid
E598	350	1000	7	2	H ₂ O	Beid + Par
E583	350	1000	7	3	H ₂ O	Par
E584	350	1000	7	4	H ₂ O	Par

¹ Gel 1 = Na_{0.7}Al_{4.7}Si_{7.3}O₂₂
 2 = Na_{1.0}Al_{5.0}Si_{7.0}O₂₂
 3 = Na_{1.5}Al_{5.5}Si_{6.5}O₂₂
 4 = Na_{2.0}Al_{6.0}Si_{6.0}O₂₂

² Kaol = Kaolinite, Qtz = Quartz, Beid = Na-beidellite, Par = Paragonite.

³ 0.01 Mol/l Na⁺.

approximately 10 wt% unreacted amorphous material (Fig. 2.1). The XRD pattern (Table 2.3) is comparable with that of natural beidellite from Unterrupsroth (Nadeau et al., 1985). Cell parameters were calculated with a least squares refinement program on 7 reflections; computer calculated reflections are consistent with that of beidellite. The structural formula of the synthetic beidellite, based on microprobe analyses, is Na_{0.81}Al_{4.7}Si_{7.3}O₂₀(OH)₄, which is in agreement with the gel composition

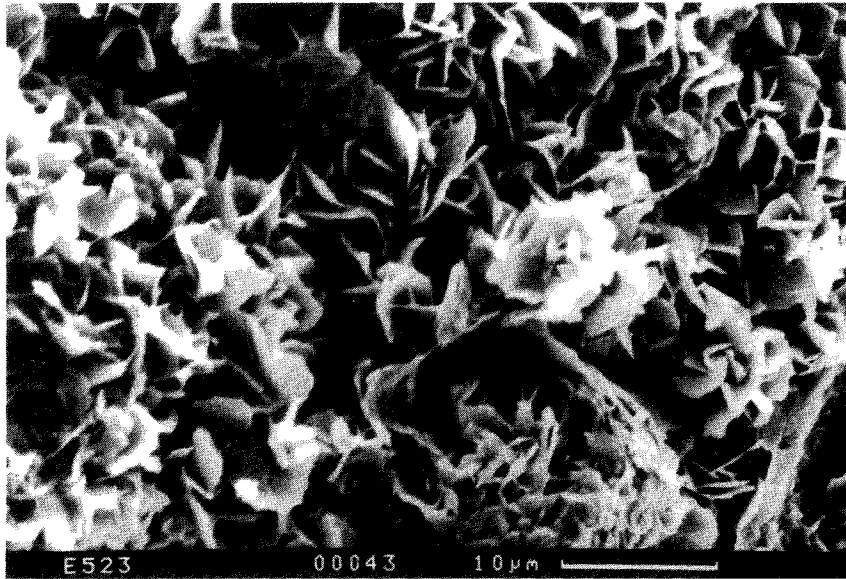


Figure 2.1 Scanning electron microscope (SEM) photograph of Na-beidellite flakes.

Table 2.3 X-ray pattern of synthetic Na-beidellite

hk + 00l	d(calc)	d(obs)	I/I _o	cell parameters
001	12.54	12.56	100	orthorhombic
002	6.27	6.25	30	
02, 11	4.48	4.45	90	a(Å) = 5.18 ± 0.005
004	3.14	3.13	40	b(Å) = 8.96 ± 0.008
20, 13	2.59	2.56	45	c(Å) = 12.54 ± 0.011
24	1.679	1.68	20	V(Å ³) = 581.9 ± 0.5
33	1.495	1.49	35	
06	1.493			

$\text{Na}_{0.7}\text{Al}_{4.7}\text{Si}_{7.3}\text{O}_{22}$, except for the sodium that was apparently evaporized during the microprobe analyses (Table 2.4). The Al substitution in the tetrahedral layer based on the analytical data is 0.7 Al per unit cell. This substitution can be established in situ from MAS-NMR spectra (Fig. 2.2). The ^{27}Al NMR spectrum reveal that most Al is in octahedral coordination (3.9 ppm) and a small amount in tetrahedral coordination (69.9 ppm). Due to the differences in peak width and side band structure it is not possible to make a quantitative assessment by simply comparing peak heights. These problems are not encountered with ^{29}Si NMR, so the ratio $\text{Al}^{\text{IV}}/\text{Si}$ can be calculated from the formula (Sanz and Serratosa, 1984; Nadeau et al., 1985)

$$2\text{Si}^2 + (\text{Si}^1 - 4\text{Si}^2)/3$$

$$\text{Si}^0 + \text{Si}^1 + \text{Si}^2$$

where Si^0 , Si^1 and Si^2 represent the intensity of the NMR peaks for Si atoms with zero (-92.7 ppm), one (-88.4 ppm) and two Al (-82.3 ppm). The ratio $\text{Si}^0:\text{Si}^1:\text{Si}^2$ is around 42:20:7 predicting an Al substitution of 0.76 per unit cell, which, within instrumental accuracy, is similar with the analytical data. The peak positions agree with those reported by Diddams et al. (1984) for synthetic beidellite and by Nadeau et al. (1985) for natural beidellite (Table 2.5).

Table 2.4 Chemical analysis (by microprobe) and structural formula

	wt%	formula based on 22 O	
SiO_2	56.76	tetrahedral Si	7.30
Al_2O_3	30.96	Al	0.70
Na_2O	2.44*		
LOI	9.65	octahedral Al	4.00
total	99.81		
		interlayer Na	0.61*
		CEC (meq/100 gr)	68

* low, due to evaporation during analyses.

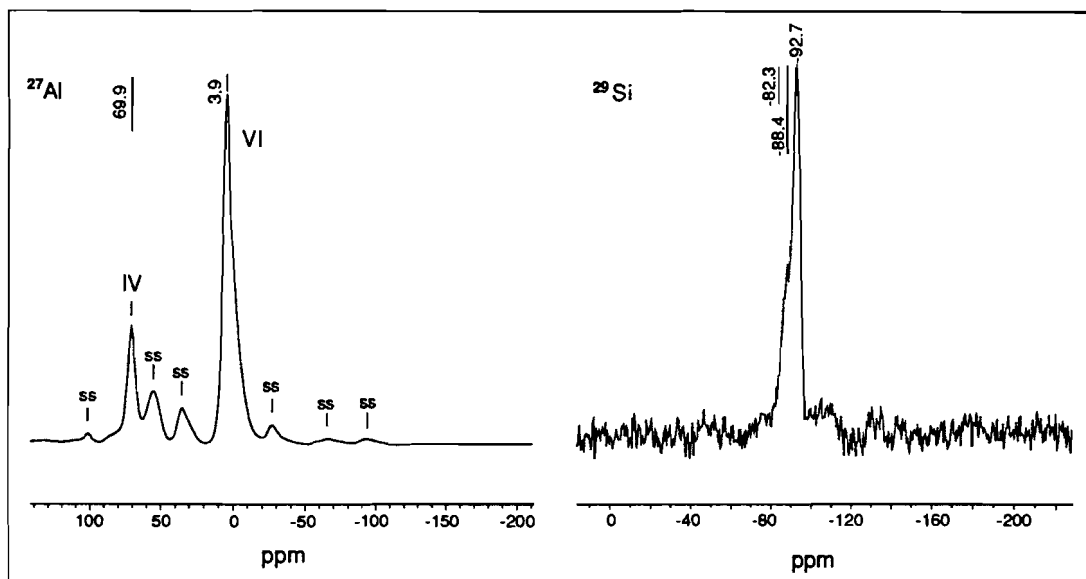


Figure 2.2 11.7 T ^{27}Al and ^{29}Si MAS-NMR spectra of synthetic Na-beidellite.

Table 2.5 ^{27}Al and ^{29}Si NMR peak positions (chemical shift δ in ppm) for synthetic and natural beidellite.

	^{27}Al		^{29}Si		
	Al^{IV}	Al^{VI}	Si-0Al	Si-1Al	Si-2Al
Nadeau et al. (1985)	69.2	2.34	-92.6	-87.7	-83.2 ¹
natural beidellite	69.1	2.46	-92.3	-87.3	-82.5 ²
Diddams et al. (1984)	± 70	± 5	-93	-88	
synthetic beidellite					
Plee et al. (1985)	69.3	3.0	-95.2	-90.2	-85.6
synthetic beidellite					
This study	69.9	3.9	-92.7	-88.4	-82.3
synthetic beidellite					

¹ size fraction < 1.4 μm

² size fraction > 3.0 μm

The TGA show two major steps of weight loss (Fig. 2.3). Below 100°C approximately 10 % adsorped water is lost, equivalent with 5 mole water per unit cell, after correction for amorphous material. Between 600° and 700°C 3.6 % water is lost by dehydroxylation, corresponding with 4.3 % based on dry weight. Ideal beidellite should loose 4.9 %, equivalent with 2 mole H₂O. The discrepancy of 0.6 % is equivalent with 12.5 % unreacted, amorphous material, in agreement with the approximation based on SEM photographs.

A typical IR spectrum is displayed in Figure 2.4. The IR-vibrations are consistent with the data of van der Marel and Beutelspacher (1976). Band positions in the region 4000-1200 cm⁻¹ are dominated by OH stretching vibrations. In the region below 1200 cm⁻¹ SiO and AlOH bending vibrations are visible. The vibrations at 3445 and 1635 cm⁻¹ belong to adsorped H₂O.

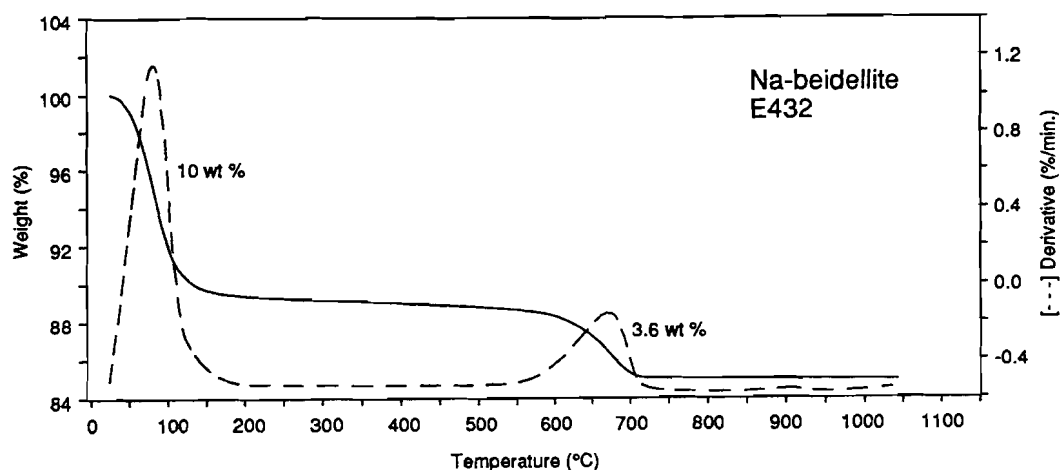


Figure 2.3 TGA (solid line) and DTG (dashed line) plot of Na-beidellite.

Hydrothermal synthesis of Na-beidellite

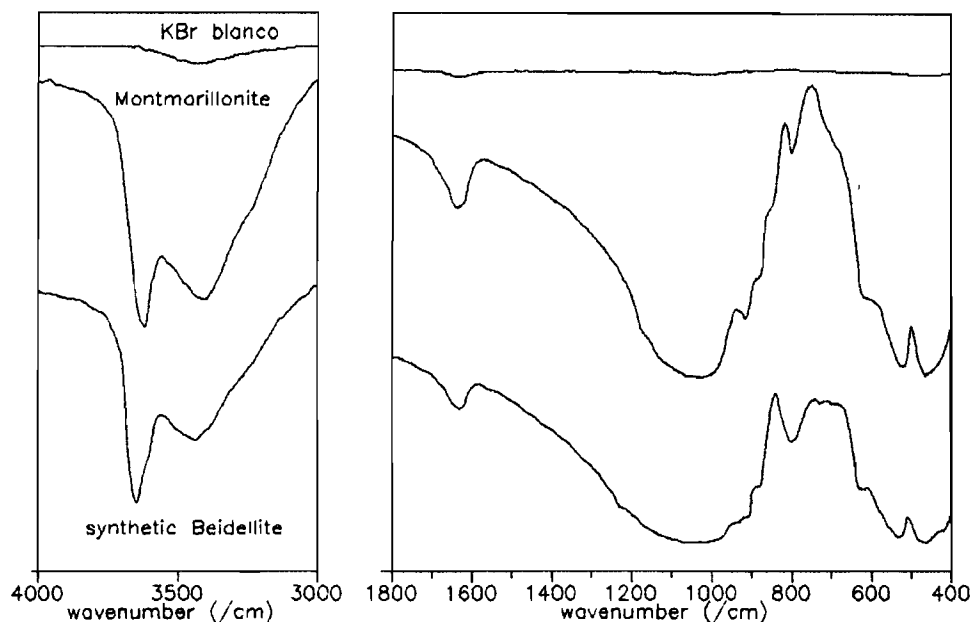


Figure 2.4 IR-spectrum of synthetic Na-beidellite. An IR-spectrum of natural montmorillonite is drawn for reference. A spectrum of a KBr blanco is displayed at the top of the figure.

2.3.4 Influence of F

The presence of small amounts of NaF in combination with NaOH in the hydrothermal fluid has a marked influence on the crystallinity of the beidellite (Fig. 2.5). In the runs with mixtures of NaF-NaOH in solution the crystallinity is strongly increased. Pure NaF solution produced very badly crystallized Na-beidellite. The IR spectra exhibit less adsorption on the AlOH bending vibrations at 935, 881 and 800 cm^{-1} . TGA reveals a weight loss due to dehydroxylation of 2.2 wt%. This indicates that the beidellite crystallinity increases when a part of the OH is replaced by F. These results are in agreement with the data presented by Torii and Iwasaki (1986) for trioctahedral Mg-smectite. The replacement of OH by F has no effect on the swelling behaviour of the Na-beidellite. It is possible that the pressure and temperature needed for beidellite synthesis can be decreased when an optimum amount of F is added to the hydrothermal fluid.

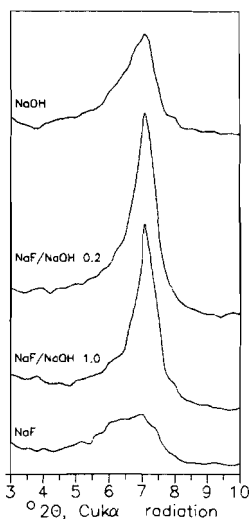


Figure 2.5 Partial XRD-pattern of the 001 reflection displaying the influence of NaF on the beidellite crystallinity.

2.4 CONCLUSIONS

1. Beidellite is synthesized at temperatures in the range of 350°C to 400°C and pressures down to 200 bar.
2. Hydrothermal treatment of a gel with an amount of Na, corresponding with a beidellite with a theoretical layer charge of 1.0 and more, results in the crystallization of paragonite instead of beidellite at 350°C and 1000 bar.
3. Characterization of beidellite with MAS-NMR quantified Al^{IV} substitution in the tetrahedral Si-layer. Al^{IV} substitution was 0.76 per unit cell, which is in sufficient agreement with the value of 0.70 based on microprobe analysis.
4. The presence of a small amount of F in the hydrothermal fluid during Na-beidellite synthesis increases the crystallinity of beidellite, without effecting its swelling behaviour.

ACKNOWLEDGMENTS

The authors wish to thank H. M. V. C. Govers for the X-ray powder diffraction patterns, T. Zalm for the TGA and DTA curves, R. P. E. Poorter for the microprobe analyses and J. Pieters for help with the electron microscopy. G. Nachtegaal is specially thanked for the technical assistance at the SON HF-NMR facility at Nijmegen.

REFERENCES

- Bos, A., de Haas, G. J. L. M., Voncken, J. H. L., van der Eerden, A. M. J. and Jansen, J. B. H. (1987) Hydrothermal synthesis of ammonium phlogopite: *Geol. Mijnbouw* **66**, 251-258.
- Diddams, P. A., Thomas, J. M., Jones, W., Ballantine, J. A. and Purnell, J. H. (1984) Synthesis, characterization and catalytic activity of Beidellite-Montmorillonite layered silicates and their pillared analogues: *J. Chem. Soc. Chem. Commun.* **1984**, 1340-1342.
- Hamilton, D. L. and Henderson, C. M. B. (1968) Preparation of silicate compositions by a gelling method: *Mineral. Mag.* **36**, 832-838.
- Klopprogge, J. T., Jansen, J. B. H. and Geus, J. W. (1990) Characterization of synthetic Na-beidellite: *Clays & Clay Minerals* **38**, 409-414.
- Larsen, E. S. and Wherry, E. T. (1917) Leverrierite from Colorado: *J. Wash. Acad. Sci.* **7**, 208-217.
- Larsen, E. S. and Wherry, E. T. (1925) Beidellite, a new mineral name: *J. Wash. Acad. Sci.* **15**, 465-466.
- Loeppert, R. H., Mortland, M. M. and Pinnavaia, T. J. (1979) Synthesis and properties of heat-stable expanded smectite and vermiculite: *Clays & Clay Minerals* **27**, 201-208.
- van der Marel, H. W. and Beutelspacher, H. (1976) *Atlas of infrared spectroscopy*

- of clay minerals and their admixtures*: Elsevier, Amsterdam, 396 pp.
- Nadeau, P. H., Farmer, V. C., McHardy, W. J. and Bain, D. C. (1985) Compositional variations of the Unterrupsroth beidellite: *Amer. Mineral.* **70**, 1004-1010.
- Plee, D., Borg, F., Gatineau, L. and Fripiat, J. J. (1985) High-resolution solid-state ^{27}Al and ^{29}Si nuclear magnetic resonance study of pillared clays: *J. Amer. Chem. Soc.* **107**, 2362-2369.
- Plee, D., Gatineau, L. and Fripiat, J. J. (1987) Pillaring processes of smectites with and without tetrahedral substitution : *Clays & Clay Minerals* **35**, 81-88.
- Ross, C. S. and Hendricks, S. B. (1945) Minerals of the Montmorillonite group: *U.S. Geol. Surv. Prof. Paper* **205-B**.
- Sanz, J. and Serratos, J. M. (1984) ^{29}Si and ^{27}Al high-resolution MAS-NMR spectra of phyllosilicates: *J. Amer. Chem. Soc.* **106**, 4790-4793.
- Schutz, A., Stone, W. E. E., Poncelet, G. and Fripiat, J. J. (1987) Preparation and characterization of bidimensional zeolitic structures obtained from synthetic beidellite and hydroxy-aluminum solutions: *Clays & Clay Minerals* **35**, 251-261.
- Sterte, J. and Shabtai, J. (1987) Cross-linked smectites. V. Synthesis and properties of hydroxy-silicoaluminum montmorillonites and fluorhectorites: *Clays & Clay Minerals* **35**, 429-439.
- Torii, K. and Iwasaki, T. (1986) Synthesis of new trioctahedral Mg-smectite: *Chem. Letters* **1986**, 2021-2024.
- Torii, K. and Iwasaki, T. (1987) Synthesis of hectorite: *Clay Sci.* **7**, 1-16.
- Tuttle, O. F. (1949) Two pressure vessels for silicate-water studies: *Geol. Soc. Amer. Bull.* **60**, 1727-1729.
- Weir, A. H. and Greene-Kelly, R. (1962) Beidellite: *Amer. Mineral.* **47**, 137-146.

CHAPTER III

CHARACTERIZATION OF SYNTHETIC Na-BEIDELLITE

ABSTRACT

Na-beidellite, a member of the smectite group, was grown hydrothermally from a gel of composition $0.35\text{Na}_2\text{O}\cdot 2.35\text{Al}_2\text{O}_3\cdot 7.3\text{SiO}_2$ in NaOH solutions at a pH between 7.5 and 13.5, a pressure of 1 kbar, and a temperature of 350°C. The synthetic Na-beidellite was characterized by means of scanning electron microscopy, X-ray powder diffraction, infrared spectroscopy, electron microprobe, inductively coupled plasma-atomic emission spectroscopy and thermogravimetric analysis. The unit-cell parameters of the orthorhombic cell are: $a = 5.18$, $b = 8.96$, and $c = 12.54 \text{ \AA}$. The cation exchange capacity was determined to be 70 meq/100 g. A maximum of 40 wt. % water was present and reversibly lost by heating to about 55°C. The loss of water caused a decrease of the basal spacing to 9.98 Å. At temperatures $\leq 600^\circ\text{C}$, the Na-beidellite started to dehydroxylate, reaching its maximum in the range $600^\circ - 630^\circ\text{C}$. At 1100°C the remaining solid recrystallized to $\text{Al}_6\text{Si}_2\text{O}_{13}$ (mullite) and SiO_2 (cristobalite).

3.1 INTRODUCTION

Cation exchange, swelling in water, and incorporation of organic and inorganic complexes to produce pillared clays, have been studied to investigate the technical utilization of natural clays (Loeppert et al., 1979; Breen et al., 1985; Goh and Huang, 1986; Plee et al., 1987; Schutz et al., 1987; Sterte and Shabtai, 1987; Olivera et al., 1988). The high costs of recovering the smectites, which usually have an unreliable quality and a large variation in impurity content, cause the industrial demand for natural smectites in these applications to be limited (Torii and Iwasaki, 1987).

To avoid the problems inherent to the use of natural raw materials, hydrothermal synthesis of pure smectites has been attempted (Tsunashima et al., 1975; De Kimpe, 1976; Torii and Iwasaki, 1986; Torii and Iwasaki, 1987; Plee et al., 1987; Schutz et al., 1987).

The structural formula for beidellite can be written as $(0.5\text{Ca,Na,K,0.5Mg})_p\text{Al}_4\text{Si}_{8-p}\text{Al}_p\text{O}_{20}(\text{OH})_4 \cdot n\text{H}_2\text{O}$. Natural beidellite has an average layer charge of 0.66, although theoretically values ranges from 0.4 to 1.2. Plee et al. (1987) and Schutz et al. (1987) synthesized under basic conditions (0.01 M resp. 0.1 M NaOH) Na-beidellite as starting material for pillaring processes. However, they do not present a characterization of their beidellite. The aim of the present study was to synthesize Na- beidellite in less basic solutions from a gel of composition $\text{Na}_{0.7}\text{Al}_{4.7}\text{Si}_{7.3}\text{O}_{22} \cdot n\text{H}_2\text{O}$ following the procedure of Hamilton and Henderson (1968) and to characterize the synthetic Na-beidellite. This clay was used to synthesize beidellite cross-linked with metal-hydroxide polymers having a Keggin structure.

3.2 EXPERIMENTAL AND ANALYTICAL TECHNIQUES

As starting material a gel of anhydrous composition $0.35\text{Na}_2\text{O} \cdot 0.2 \cdot 35\text{Al}_2\text{O}_3 \cdot 7.3\text{SiO}_2$ was prepared according to the procedure of Hamilton and Henderson (1968). The chemicals used in the preparation of the gel were $\text{Al}(\text{NO}_3)_3 \cdot 9\text{H}_2\text{O}$ (Merck no. 1063), Na_2CO_3 (Merck no. 6392) and tetraethyl orthosilicate (Merck - Schuchardt no. 800658). Fifty milligrams of the gel (containing 7.3% water) together with 70 μl of NaOH solution (10^{-6} , 10^{-5} or 10^{-4} M) were placed into a gold capsule welded at one end. The capsule was closed by arc-welding, while its main body was constantly cooled in an ice-water bath. All capsules were checked for leakage before the experiment.

The synthesis was carried out in a Tuttle-type, externally heated, cold-seal pressure vessel (Tuttle, 1949) using argon as the pressure medium. Experiments were made at 350°C and at total pressures of 0.5 and 1.0 kbar (Table 3.1). Temperature was measured by a chromel-alumel thermocouple, which is considered to be accurate within 5°C. Pressure was read from a Bourdon-type pressure gauge having an accuracy of 10 bar. After quenching the pressure vessels

Table 3.1 Experimental runs at 350°C.

Run	P (kbar)	Time (days)	pH	Starting solution	Product
E414-1	1.0	5	12	Na ₂ CO ₃ ¹ + H ₂ O	beid + qtz
E414-2	1.0	5	13.5	Na ₂ CO ₃ ¹ + NaOH	beid + qtz
E415-1	1.0	5	8	NaOH	beid + qtz
E415-2	1.0	5	9	NaOH	beid + qtz
E426	1.0	5	10	NaOH	beid + qtz
E427	0.5	10	10	NaOH	beid + qtz
E432	1.0	10	7.8	H ₂ O	beid
E448 ²	1.0	20	10	NaOH	beid + qtz
E476	1.0	20	10	NaOH	beid + qtz

¹ = solid Na₂CO₃.

² = used for heating experiment at 1150°C.

beid = Na-beidellite; qtz = quartz.

with compressed cold air, the capsules were reweighed to check for leakage.

The morphology of the products obtained were investigated with a Cambridge S150 and M600 scanning electron microscopes (SEM) equipped with an energy dispersive X-ray (EDX) analyzer. X-ray powder diffraction (XRD) patterns were recorded with a Philips PW 1050/25 diffractometer using CuK α radiation. Unit-cell dimensions were calculated using the least square refinement computer program Unitcellc (Strom, 1976). Infrared (IR) absorption spectra were obtained on powdered samples in KBr tablets (sample concentration = 1 wt. %) using a Perkin Elmer 580 IR spectrophotometer. The solid product was analyzed thermogravimetrically using a Dupont 1090 Thermal Analyzer at heating rates of 10°, 1°, and 0.2°C/min. Differential thermal analyses were made at a heating rate of 10°C/min. Chemical analyses were made using a JEOL JXA-8600 electron microprobe. The CEC was measured on a sample dried overnight at 120°C. The

sample was exchanged with 1 M KCl solution. After centrifugation the solution was analyzed for Na using inductively coupled plasma-atomic emission spectroscopy.

3.3 RESULTS

SEM showed the hydrothermal products to consist of flakes exhibiting mainly (001) faces (Fig. 3.1a). The (100), (010), and (110) faces were exceptionally well developed on crystals of run E426 (Fig. 3.1b). Also, small aggregates were noted, which consisted mainly of anhedral material and some quartz. The presence of quartz was confirmed by XRD. In Figure 3.2b, the EDX analyses of a small quartz particle (A) and of a large flake (B), presumably Na-beidellite, are represented. The flake yielded a relative low Na content, probably due to diffusion of Na during exposure to the electron beam (van der Pluijm et al., 1988).

Microprobe analyses gave a composition of 56.76% SiO₂, 30.96% Al₂O₃, 2.44% Na₂O and 9.84% H₂O, corresponding to Na_{0.61}Al_{4.70}Si_{7.32}O₂₀(OH)₄. Here, also a relative low Na content was observed, probably due to diffusion of Na. The hydrothermal solution after synthesis contained 157 ppm Na, 188 ppm Al, and 1833 ppm Si. The cation exchange capacity of the solid was determined to be 70 meq/100 g.

The hkl values of the synthetic Na-beidellite were indexed mainly according to Weir and Greene-Kelly (1962), except for the 001, 002, and 004 reflections. Good agreement between the calculated and observed values was observed, as long as the 024 reflection was changed into 004 (Table 3.2). The unit-cell parameters based on the revised indices are compared with data for Na-beidellite from Brindley and Brown (1980) and for Ca-beidellite from Weir and Greene-Kelly (1962) in Table 3.3. The Na-beidellite expanded to d(001) = 16.48 Å with ethylene glycol at room temperature, which is comparable with the value of 16.7 Å given by Brindley and Brown for natural beidellite. A Li-saturated sample with glycerol and

Characterization of synthetic Na-beidellite

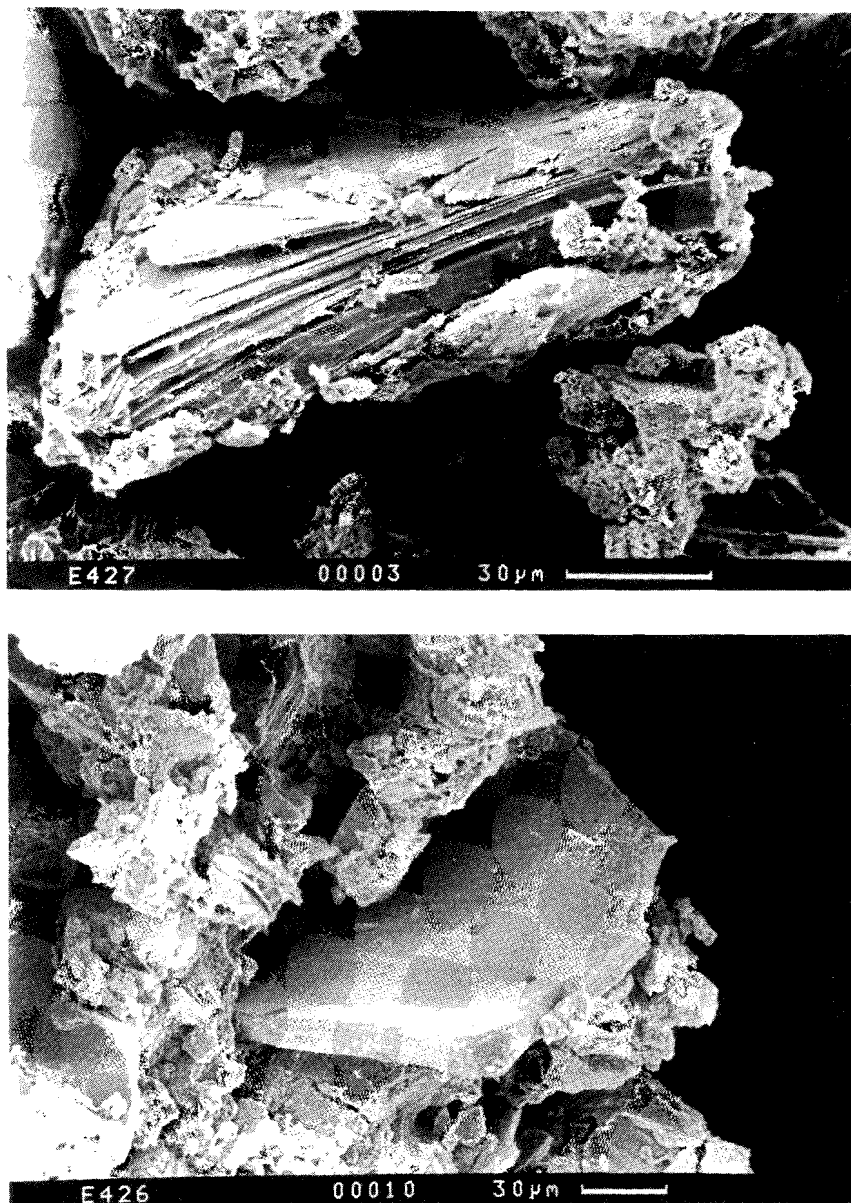


Figure 3.1 Scanning electron micrographs of (a, upper) Na-beidellite crystal synthesized at 350°C and 500 bar (run E427); (b, lower) Na-beidellite crystal synthesized at 350°C and 1 kbar (run E426).

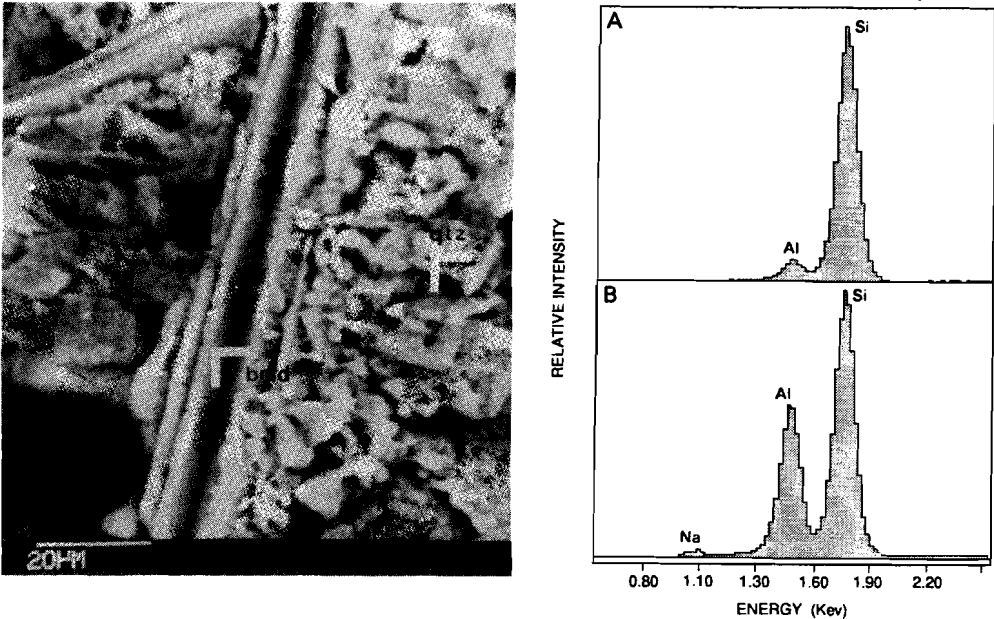


Figure 3.2 Scanning electron micrograph of (a) small particle formed from the excess SiO_2 (arrow indicates position of the energy-dispersive X-ray analyses A and B) (run E448); (b) energy-dispersive X-ray analysis of (A) quartz-bearing particle and (B) Na-beidellite (Table 3.2).

heated overnight at 300°C (Hofmann-Klemen and Greene-Kelly test) resulted in a basal spacing of 17.67 \AA , confirming that the product was Na-beidellite. Heating the product to 55°C caused a gradual decrease in $d(001)$ from 12.54 \AA to 9.98 \AA and a proportional decrease in $d(002)$, due to the loss of interlayer water. The 004 reflection decreased in intensity and was replaced by the 003 reflection.

As is apparent from Figure 3.3, the starting solution influenced the degree of crystallinity of the product Na-beidellite. The optimum crystallinity was obtained at pHs of 9 and 10; however, whether the degree of crystallinity was influenced by only the pH or by the Na concentration is not known. The two small peaks in Figure 3.3 at $d = 4.26$ and 3.34 \AA are the 100 and 101 reflections of a trace of quartz.

Characterization of synthetic Na-beidellite

Table 3.2 X-ray powder diffraction data for hydrothermally synthesized Na-beidellite (run E415-2).

d(obs) ¹	d(calc) ¹	I/I ₀ ¹	hk + 00l ¹	d(calc) ²	I ²	hkl ²
12.44	12.54	100	001			
6.19	6.27	5	002 ³			
4.43	4.48	75	02,11	4.48	10	020, 110
	4.22			4.35		021
				3.56	10	023
3.12	3.14	55	004 ⁴	3.15	2	024 ⁴
2.59	2.59	15	20,13	2.59	-	200, 130
2.54	2.54	20		2.56	8	201
				2.48	10	202
1.670	1.679	5	24	1.687	6	241
				1.664	8	242
1.490	1.495	15	33	1.495	10	060, 330
	1.493		06			

¹ Na-beidellite from run E415-2.

² Brown (1961); Weir and Greene-Kelly (1962).

³ 002 not given by Brown (1961), Weir and Greene-Kelly (1962).

⁴ 004 instead of 024 as given by Weir and Greene-Kelly (1962).

Table 3.3 Unit-cell parameters (Å) of hydrothermally synthesized Na-beidellite (run E415-2), based on an orthorhombic unit-cell.

	a	b	c
This study	5.18 ± 0.0044	8.96 ± 0.0076	12.54 ± 0.0106
Weir & Greene-Kelly (1962), Brown (1961) ¹	5.179	8.970	17.57
Brindley and Brown (1980)	-----	-----	12.5

¹ sample Ca-saturated and glycerol expanded

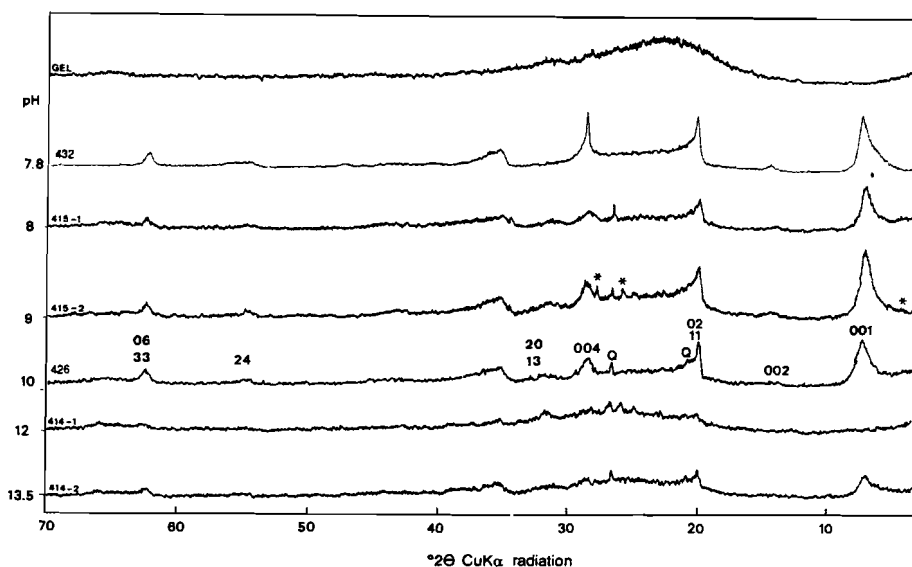


Figure 3.3 X-ray powder diffraction patterns of beidellite formed at different pHs. For comparison, the pattern of the gel is also given. Q = two strongest lines of quartz; * = three strongest lines of $\text{SiO}_2\text{-X}_2$, an intermediate phase in the crystallization of quartz from amorphous silica in alkaline media (Mitsyuk et al., 1976).

The IR spectra of the starting gel, the Na-beidellite synthesized in run E415-3, and a natural Na-montmorillonite from Clay Spur, Wyoming, are shown in Figure 3.4. The absorption maxima of the synthetic and natural Na-beidellite (van der Marel and Beutelspacher, 1976) are listed in Table 3.4. The maxima for the synthetic Na-beidellite are shifted by about 2% towards higher wavenumbers compared with natural beidellite (van der Marel and Beutelspacher, 1976). The very small shoulders at 1200 and 460 cm^{-1} are probably due to the trace of quartz.

TGA and DTA plots depicting dehydration and dehydroxylation processes are shown in Figure 3.5. The results presented below are based on a heating rate of $0.2^\circ\text{C}/\text{min}$. During heating to 55°C , 40 wt. % of absorbed water was lost. The DTA curve showed a strong endothermic maximum. The weight loss due to dehydration ranged from 30% to 40% after 14 days drying in air before the measurement.

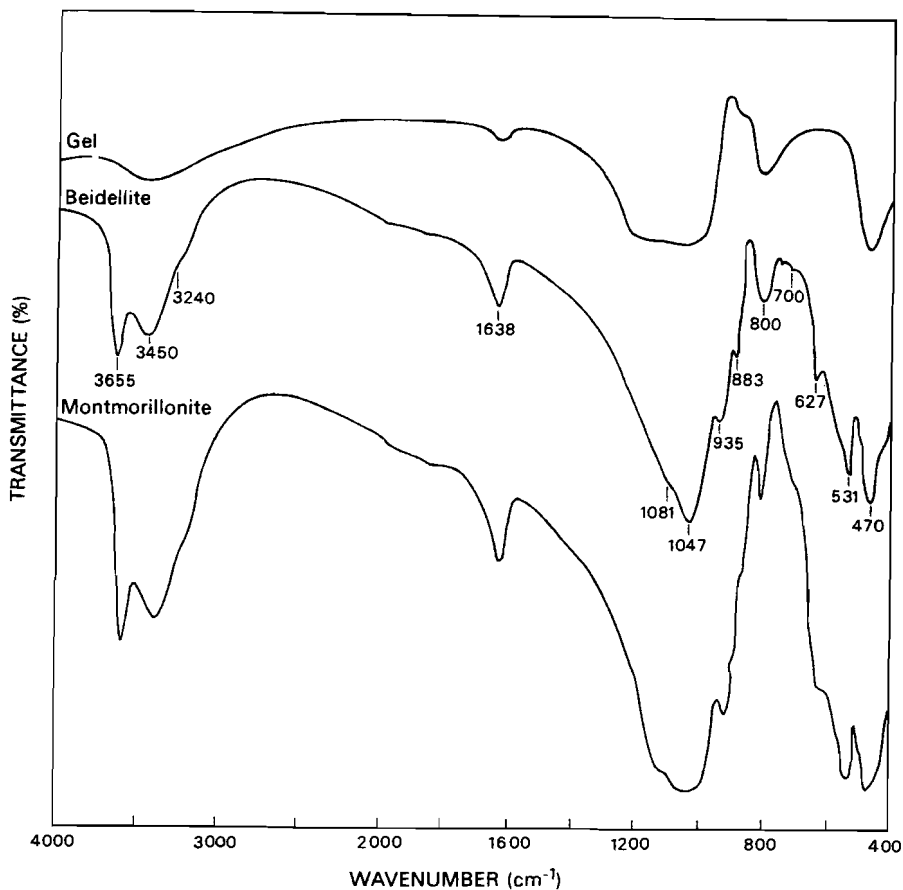


Figure 3.4 Infrared spectrum of Na-beidellite (run E415-3). Spectra of gel and natural Na-montmorillonite are included as references.

In the range 55° to 600°C the sample gradually lost 2.5% weight (3.4% based on water-free Na-beidellite). This loss is attributed to the removal of interlayer water and to the dehydroxylation, which began at about 400°C. Mackenzie (1970) and Gerard and Herbillon (1983) proposed an overlap of dehydroxylation and the last part of the dehydration between 150° and 600°C. Another possibility is that the weight loss was derived partially from unreacted noncrystalline material.

Table 3.4 Infrared absorption maxima (cm^{-1}) of hydrothermally synthesized Na-beidellite (run E415-3) and natural beidellite.

This study	van der Marel and Beutelspacher (1976)	Stubican and Roy (1961); Farmer (1974)
3655 strong	3625	Al--O-H stretching
3450 strong	3420 - 3415	H-O-H stretching
3240 weak (shoulder)	3220	H-O-H stretching
1638 medium	1625	H-O-H bending
1081 weak (shoulder)	1100 - 1098	Si-O stretching
1047 strong	1030 - 1028	Si-O-Si stretching
935 medium	914	Al--O-H bending
883 medium	875	Al--O-H bending
800 medium	796	Al--O-H bending
700 weak	698 - 693	Si-O-Al bending
627 weak	640 - 622	Al-O-H bending
531 strong	530 - 520	Si-O-Al bending
470 strong	471 - 467	Si-O bending
440 weak (shoulder)	419	Si-O bending

Between 600° and 630°C the dehydroxylation reached a maximum, and the sample lost 2.0% weight (2.6% based on water-free Na-beidellite).

Theoretically, the complete dehydroxylation of Na-beidellite involves the production of two moles of H_2O and corresponds to a weight loss of 4.9%. The experimental weight loss between 55° and 630°C was about 6.0%, however, which is more than the theoretical value for dehydroxylation.

TGA experiments at relatively slow heating rates showed lower temperatures of dehydration and dehydroxylation (Fig. 3.5). At a heating rate of $0.2^{\circ}\text{C}/\text{min}$ most of the water was lost $<55^{\circ}\text{C}$, instead of 130°C at $10^{\circ}\text{C}/\text{min}$. The maximum dehydroxylation was at 600° - 630°C at $0.2^{\circ}\text{C}/\text{min}$, vs. 630° - 740°C at a

Characterization of synthetic Na-beidellite

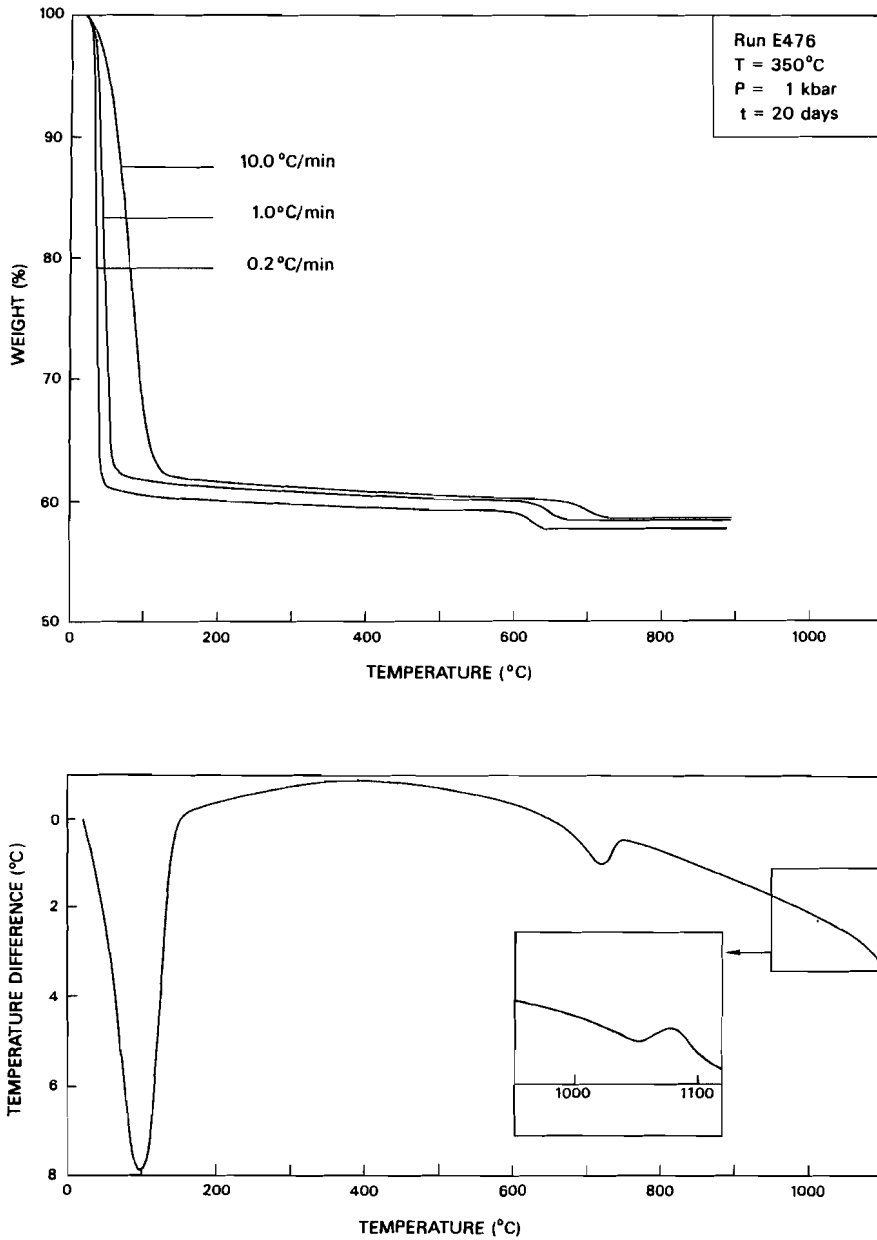


Figure 3.5 Thermogravimetric analyses (heating rate = 10°, 1°, and 0.2°C/min) and differential thermal analysis (10°C/min) of Na-beidellite (run E476).

heating rate of 10°C/min. At temperatures > 630°C no further weight loss of H₂O was observed.

The small S-shaped endothermic-exothermic peak system at 1045° - 1095°C (Fig. 3.5, DTA curve) was probably due to the breakdown of the anhydrous beidellite to a X-ray-amorphous material from which the new phases mullite and cristobalite crystallized.

3.4 DISCUSSION

In all experiments the synthesis of Na-beidellite was successful (Table 3.1). The degree of crystallinity apparently depended on pressure, temperature, the length of time at the hydrothermal conditions and, the pH or NaOH concentration of the starting solution (unpublished results in this laboratory). The most highly crystallized Na-beidellite was synthesized at 350°C, 1 kbar, 5 days, and a pH of 10 of the starting solution. Plee et al. (1987) and Schutz et al. (1987) produced Na-beidellite at pressures of 600 and 130 bar, but provided no information on crystallinity or morphology. The CEC value of 70 meq/100 g is low compared with the expected CEC of 97 meq/100 g for Na-beidellite having a composition of Na_{0.7}Al_{4.7}Si_{7.3}O₂₀(OH)₄.xH₂O, probably because the CEC was determined on a mixture of Na-beidellite and unreacted material, which could not be separated from each other.

XRD yielded a basal spacing of 12.54 Å, which is consistent with the theoretical value of 12.50 Å (Weir and Greene-Kelly, 1962; Brindley and Brown, 1980). Indexing based on the calculated lattice parameters revealed that an 024 index for the peak at 3.15 Å reported by Weir and Greene-Kelly (1962) is incorrect. An assignment of 004 is more consistent with the other reflections. The indexing given here is in accord with the data given by Nadeau et al. (1985) for the Unterrupsroth beidellite.

The decrease in basal spacing from 12.54 at 25°C to 9.98 Å at 55°C and the corresponding weight loss in the TGA experiment demonstrate a loss of absorbed water. Na-beidellite having a basal spacing of 9.98 Å should contain a maximum of 1.1% water in the interlayer, next to the Na ions, as evidenced by the fact that between 55° and 630°C, 6% water was lost, which can not be ascribed to the loss of hydroxyl groups alone. Realistically, some water was probably absorbed by the unreacted noncrystalline material. The microprobe analyses indicate a water content of 9.84% (adsorbed water plus hydroxyl groups), which is much less than the TGA results, thereby supporting the possibility that some water was absorbed by the unreacted starting material. At temperatures > 600°C 2.2% weight was lost. This bipartitional dehydroxylation probably took place, because the hydroxyl groups in the Al octahedral layer of beidellite are not equivalent, inasmuch as 8.8%, based on microprobe analyses, (9.6% based on ²⁹Si MAS- NMR, see Ch. 2) of the Si in the Si tetrahedral layer has been substituted by Al. This substitution may have distorted the hexagonal rings of tetrahedra and the Al octahedra.

Slow heating rates during the TGA led to low temperatures of dehydration and dehydroxylation. These processes were probably controlled by diffusion. A standard heating rate of 10°C/min is normally used for weight loss determinations, but not for the determination of decomposition temperatures, if diffusion plays an important role.

The presence of quartz in the products of runs having NaOH solution as the reaction medium indicate that the kinetics of dissolution of silica in basic conditions was too rapid compared with the formation of beidellite. For the liquid/solid ratio used in these experiments sursaturation of silica should have occurred, and the silica should have segregated as quartz. In pure water, the dissolution of silica would have been slower, thereby avoiding sursaturation in silica and yielding no quartz.

The two peaks at 1045° and 1095°C in the DTA curve (Fig. 3.5) are probably due to the breakdown of the anhydrous Na-beidellite to a noncrystalline phase,

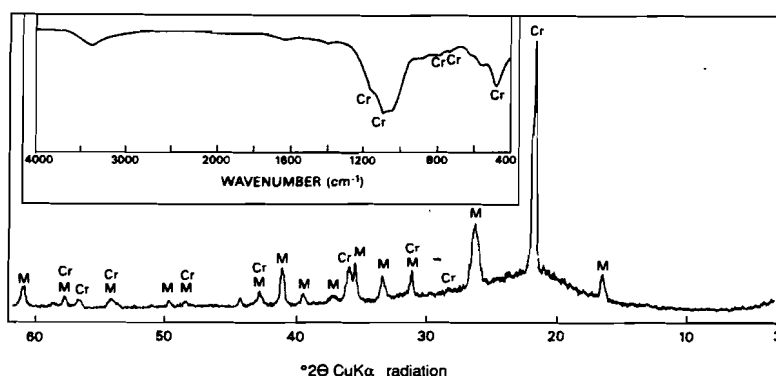


Figure 3.6 X-ray powder diffraction pattern and infrared spectrum of the products of run E448 after heating at 1150°C. C = cristobalite; M = mullite.

from which new phases crystallized (Grim and Bradley, 1940; Bradley and Grim, 1951; Greene-Kelly, 1957). XRD of the product of run E448 heated for 18 hr at 1150°C revealed the presence of mullite and cristobalite (see Fig. 3.6).

ACKNOWLEDGMENTS

The authors thank A. M. J. van der Eerden for his advice and help in the HPT laboratory of the Institute for Earth Sciences, H. M. V. C. Govers for the XRD patterns, T. Zalm for the TGA and DTA curves, C. Strom for help with the unit-cell refinements, R. P. E. Poorter for the microprobe analyses, P. Anten for the ICP analyses, and J. Pieters for help with the electron microscopy. We also thank R. D. Schuiling, D. Visser, and M. K. Titulaer for critical reviewing the manuscript.

REFERENCES

- Bradley, W. F. and Grim, R. E. (1951) High temperature thermal effects of clay and related materials: *Amer. Mineral.* **36**, 182-201.
- Breen, C., Adams, J. M., and Riekel, C. (1985) Review of the diffusion of water and pyridine in the interlayer space of montmorillonite: Relevance to kinetics of catalytic reactions in clays: *Clays & Clay Minerals* **33**, 275-284.
- Brindley, G. W. and Brown, G., eds. (1980) *Crystal Structures of Clay Minerals and their X-ray Identification*: Mineralogical Society London, 495 pp.
- Brown, G., ed. (1961) *The X-ray Identification and Crystal Structures of Clay Minerals*: Mineralogical Society London, 544 pp.
- De Kimpe, C. R. (1976) Formation of phyllosilicates and zeolites from pure silica-alumina gels: *Clays & Clay Minerals* **24**, 200-207.
- Farmer, V. C. (1974) The layer silicates: in *The Infrared Spectra of Minerals*: Mineralogical Society London, 331-363.
- Gerard, P. and Herbillon, A. J. (1983) Infrared studies of Ni-bearing clay minerals of the kerolite-pimelite series: *Clays & Clay Minerals* **31**, 143-151.
- Goh, T. B. and Huang, P. M. (1986) Influence of citric and tannic acids on hydroxy-Al interlayering in montmorillonite: *Clays & Clay Minerals* **34**, 37-44.
- Greene-Kelly, R. (1957) The montmorillonite minerals (smectites): in *The Differential Thermal Investigation of Clays*, R. C. Mackenzie, ed., Mineralogical Society London, 140-164.
- Grim, R. E. and Bradley, W. F. (1940) Effect of heat on illite and montmorillonite: *J. Amer. Ceram. Soc.* **23**, 242-248.
- Hamilton, D. L. and Henderson, C. M. B. (1968) The preparation of silicate compositions by a gelling method: *Mineral. Mag.* **36**, 832-838.
- Loeppert, R. H., Mortland, M. M., and Pinnavaia, T. J. (1979) Synthesis and properties of heat-stable expanded smectite and vermiculite: *Clays & Clay Minerals* **27**, 201-208.

- Mackenzie, R. C. (1970) Simple phyllosilicates based on gibbsite-like and brucite-like sheets: in *Differential Thermal Analysis*, Vol. 1, R. C. Mackenzie, ed., Academic Press, London, 775 pp.
- van der Marel, H. W. and Beutelspacher, H. (1976) *Atlas of Infrared Spectroscopy of Clay Minerals and their Admixtures*: Elsevier, Amsterdam, 396 pp.
- Mitsyuk, B. A., Gorotskaya, L. I. and Rastrenko, A. I. (1976) The nature and properties of the new varieties of silica: *Geochem. Int.* **13**, 101-111.
- Nadeau, P. H., Farmer, V. C., McHardy, W. J. and Bain, D. C. (1985) Compositional variations of the Unterrupsthal beidellite: *Amer. Mineral.* **70**, 1004-1010.
- Olivera, P., Rodriguez-Castellon, E., and Rodriguez-Garcia, A. (1988) Uptake of Lanthanides by vermiculite: *Clays & Clay Minerals* **36**, 68-72.
- Plee, D., Gatinneau, L., and Fripiat, J. J. (1987) Pillaring processes of smectites with and without tetrahedral substitution: *Clays & Clay Minerals* **35**, 81-88.
- van der Pluijm, B. A., Lee, J. H., and Peacor, D. R. (1988) Analytical electron microscopy and the problem of potassium diffusion: *Clays & Clay Minerals* **36**, 498-504.
- Schutz, A., Stone, W. E. E., Poncelet, G., and Fripiat, J. J. (1987) Preparation and characterization of bidimensional zeolitic structures obtained from synthetic beidellite and hydroxy-aluminum solutions: *Clays & Clay Minerals* **35**, 251-261.
- Sterte, J. and Shabtai, J. (1987) Cross-linked smectites. V. Synthesis and properties of hydroxy-silicoaluminum montmorillonites and fluorhectorites: *Clays & Clay Minerals* **35**, 429-439.
- Stubican, V. and Roy, R. (1961) A new approach to assignment of infra-red absorption bands in layer-structure silicates: *Z. Kristallogr.* **115**, 200-214.
- Strom, C. (1976) *Unitcellc, an interactive APL program for computing cell constants*: Geol. Mineral. Institute, State University of Leiden, Leiden, The Netherlands.

Characterization of synthetic Na-beidellite

Torii, K. and Iwasaki, T. (1986) Synthesis of new trioctahedral Mg-smectite: *Chem. Letters*, 2021-2024.

Torii, K and Iwasaki, T. (1987) Synthesis of hectorite: *Clay Sci.* **7**, 1-16.

Tsunashima, A., Konamura, F., Veda, S., Koizumi, M., and Matsushita, T. (1975) Hydrothermal synthesis of amino acid-montmorillonites and ammonium micas: *Clays & Clay Minerals* **23**, 115-118.

Tuttle, O. F. (1949) Two pressure vessels for silicate-water studies: *Geol. Soc. Amer. Bull.* **60**, 1727-1729.

Weir, A. H. and Greene-Kelly, R. (1962) Beidellite: *Amer. Mineral.* **47**, 137-146.

CHAPTER IV

SYNTHESIS FIELD OF NA-BEIDELLITE IN TERMS OF TEMPERATURE, WATER PRESSURE AND SODIUM ACTIVITY

ABSTRACT

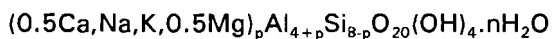
In the chemical system $\text{Na}_2\text{O}-\text{Al}_2\text{O}_3-\text{SiO}_2-\text{H}_2\text{O}$ the stability field of Na-beidellite is presented as a function of pressure, temperature, and Na- and Si-activity. $\text{Na}_{0.7}$ -beidellite is hydrothermally synthesized using a stoichiometric gel composition in the temperature range from 275° to 475°C and at pressures from 0.2 to 5 kbar. Below 275°C kaolinite is the only crystalline phase and above about 500°C paragonite and quartz develop instead of beidellite. An optimum yield of 95 % of the $\text{Na}_{0.7}$ -beidellite is obtained at 400°C and 1 kbar after 20 days. Gels with a Na-content lower than 0.3 do not produce beidellite. They yield kaolinite below 325°C and pyrophyllite above 325°C. With gels of a Na-content of 1.5 the Na-beidellite field shifts to a minimum between temperatures of 275° and 200°C. This offers the possibility to synthesize beidellite at low temperatures. The beidellite synthesized from $\text{Na}_{1.0}$ -gel seems to get a $\text{Na}_{1.35}$ composition and those from $\text{Na}_{1.5}$ - and $\text{Na}_{2.0}$ -gels a $\text{Na}_{1.8}$ composition.

4.1 INTRODUCTION

The hydrothermal synthesis of smectites has become important because of their high chemical purity and the possibility to selectively vary the smectite structure (Torii and Iwasaki, 1986; 1987; Plee et al., 1987; Schutz et al., 1987; Kloprogge et al., 1990a,b). Also the systematic incorporation of specific organic and inorganic complexes, generating pillared clays with an aimed range of basal and lateral spacings has stimulated the interest in the smectite synthesis (Lahav et al., 1978; Breen et al., 1985; Pinnavaia et al., 1985; Sterte, 1986; Sterte and Shabtai, 1987; Singh and Kodama, 1988). The pillared clays may be used simultaneously as molecular sieves and catalysts, e.g., in oil cracking reactions involving large organic

molecules (Barrer, 1978; Ocelli, 1983; 1987; Rupert et al., 1987; Welters, pers. comm.).

Beidellite is a dioctahedral member of the smectite group and can be described by the general formula



(Kloprogge et al., 1990a). In natural beidellites p -values can vary between 0.4 and 1.2, with an average p -value of 0.66. At this value Al exhibits a completely homogeneous random distribution over the tetrahedral sites and, therefore, it represents the most stable composition.

The first aim of this study is to locate the synthesis field of Na-beidellite from a gel with composition $\text{Na}_{0.7}\text{Al}_{4.7}\text{Si}_{7.3}\text{O}_{20}(\text{OH})_4 \cdot n\text{H}_2\text{O}$ ($p = 0.7$), in terms of temperature, pressure and time in order to produce optimum yields in experiments at low temperature and pressure conditions within a short period of time. The second purpose is to investigate the variation of the Na-content of the beidellite with compositions of the starting gels ranging from pyrophyllite $\text{Al}_4\text{Si}_8\text{O}_{20}(\text{OH})_4$ ($p = 0.0$) to paragonite $\text{Na}_2\text{Al}_6\text{Si}_6\text{O}_{20}(\text{OH})_4$ ($p = 2.0$) and to establish the influence of temperature at a fixed pressure of 1 kbar on the synthesis field of Na-beidellite.

4.2 EXPERIMENTAL AND ANALYTICAL TECHNIQUES

The starting materials for the Na-beidellite syntheses were gels prepared according to the procedure of Hamilton and Henderson (1968). The chemicals for the gel preparation were $\text{Al}(\text{NO}_3)_3 \cdot 9\text{H}_2\text{O}$ (Merck no. 1063), Na_2CO_3 (Merck no. 6392), and T.E.O.S. (Merck-Schuchardt no. 800658). Experimental charges were prepared according to Kloprogge et al. (1990a). Experiments were carried out in a Tuttle-type, externally heated cold-seal pressure vessel (Tuttle, 1949).

X-ray powder diffraction patterns were recorded with a Philips PW 1050/25 diffractometer using $\text{CuK}\alpha$ radiation. Beidellite identification was based on the d_{hkl} values of natural Ca-saturated beidellite determined by Weir and Green-Kelly (1962) and on the d_{hkl} values of synthetic Na-beidellite determined by Kloprogge et al.

(1990a,b). The morphology of the products has been investigated with a Cambridge S150 scanning electron microscope. Infrared spectra were measured on powdered samples in KBr tablets (concentration 1 wt%) with a Perkin Elmer 580 IR spectrophotometer. Chemical analyses were made using a JEOL JXA-8600 electron microprobe.

4.3 RESULTS

The synthesis conditions of beidellite and the development of other phases produced are summarized in a P-T diagram (Fig. 4.1). At temperatures below 300°C kaolinite and quartz are the predominant crystalline phases. All experiments

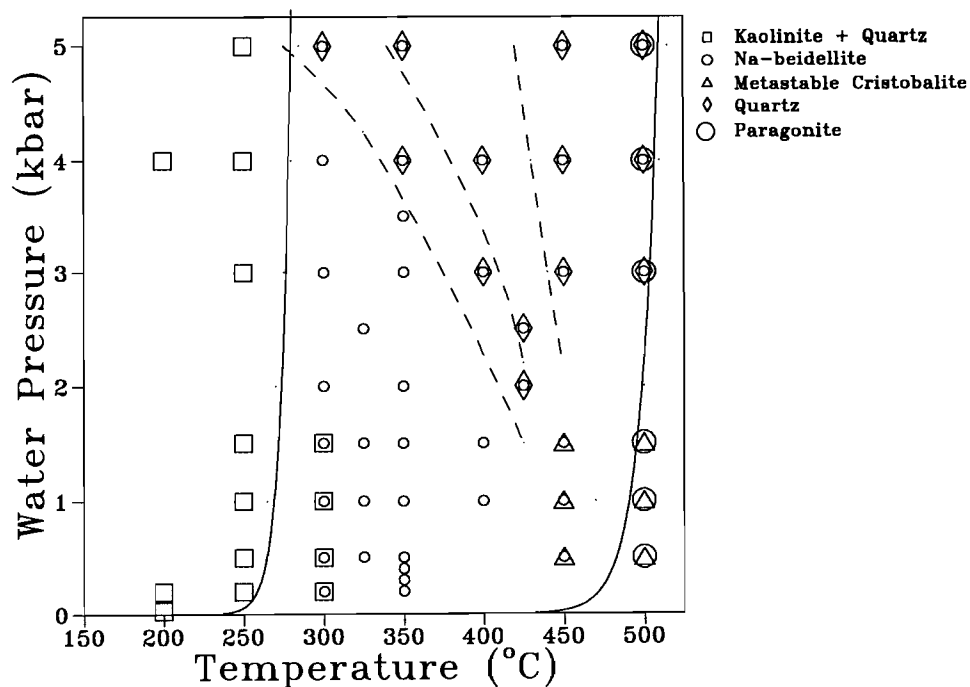


Figure 4.1 Experimental results on the Na-beidellite synthesis field from a gel with composition $\text{Na}_{0.7}\text{Al}_{4.7}\text{Si}_{7.3}\text{O}_{22} \cdot x\text{H}_2\text{O}$. Note the presence of SiO_2 phases, including metastable cristobalite. Dashed lines represent increasing amounts of SiO_2 with increasing temperature.

producing kaolinite and quartz yield a considerable amount (20 to 50 %) of amorphous material. A small transition zone to the beidellite field seems to exist around 300°C due to the sluggish reaction kinetics of kaolinite to Na-beidellite, as evidenced by the disappearance of kaolinite when higher heating rates were used (approximately 30°C/ min). The zone with beidellite, kaolinite, quartz and amorphous material disappears at water pressures above 2 kbar. Na-beidellite is the main crystalline phase in the temperature range 275° - 475°C. 5 to 20 % amorphous material is still present in Na-beidellite-rich yields. At 450°C Na-beidellite is accompanied by cristobalite at pressures <2 kbar and over a wider

Table 4.1 Microprobe analyses of beidellite and amorphous material from selected runs and for the beidellite the structural formula based on 22 O.

a) runs with gel composition $p = 0.7$

Run E.	542	427	543	549	554	641	593
T (°C)	300	350	450	300	400	300	300
P kbar	0.5	0.5	0.5	1.5	1.5	2.0	4.0
SiO ₂	55.99	56.76	56.56	59.39	59.45	60.69	59.90
Al ₂ O ₃	30.29	30.96	29.10	31.89	31.82	30.53	29.84
Na ₂ O	0.89	2.44	1.59	0.88	1.36	0.41	1.11
total	87.17	90.16	87.25	92.16	92.63	91.63	90.85
Si	7.33	7.30	7.47	7.35	7.36	7.53	7.56
Al ^{IV}	0.67	0.70	0.53	0.65	0.64	0.47	0.44
Al ^{VI}	4.00	4.00	4.00	4.00	4.00	4.00	4.00
Na	0.23	0.61	0.41	0.21	0.33	0.10	0.27
sum	12.23	12.61	12.41	12.21	12.33	12.10	12.27
n [#]	3	10	3	14	13	8	15
mean p [§]	0.61	0.71	0.53	0.60	0.63	0.45	0.47
s.d.	0.25	0.13	0.29	0.21	0.11	0.13	0.11

temperature range and pressures ≥ 2 kbar by quartz. The amount of quartz increases mainly with the synthesis temperature and less clearly with the pressure. At 500°C paragonite is formed as the phyllosilicate phase. At pressures ≥ 2 kbar still some beidellite is present again together with traces of quartz.

Calculations based on the microprobe analyses (Table 4.1a), reveal only a small variation in the composition of the beidellite with p-values between 0.5 and 0.7 at pressures below 2 kbar independent of the temperature. At higher pressures a somewhat lower p-value of approximately 0.45 is observed. The Na analyses are consequently much lower than expected from the Si and Al analyses, presumably due to evaporation of Na during exposure to the electron beam in the microprobe (van der Pluijm et al., 1988; Klopogge et al., 1990a).

Table 4.1b microprobe analyses of amorphous material

Run E.	542	542	543	543	549	549	554
T (°C)	300	300	450	450	300	300	400
P kbar	0.5	0.5	0.5	0.5	1.5	1.5	1.5
SiO ₂	73.25	64.96	84.31	72.44	67.84	65.19	64.67
Al ₂ O ₃	24.39	29.81	12.29	21.30	31.57	31.04	33.31
Na ₂ O	bd	1.84	0.24	1.78	0.88	1.33	0.55
total	97.64	96.61	96.84	95.52	100.29	97.56	98.53
Run E.	554	641	641	593	593		
T (°C)	400	300	300	300	300		
P kbar	1.5	2.0	2.0	4.0	4.0		
SiO ₂	59.45	71.42	51.49	71.32	68.47		
Al ₂ O ₃	31.93	28.05	27.92	21.81	26.04		
Na ₂ O	4.04	0.42	16.51	0.51	1.57		
total	95.42	99.89	95.92	93.64	96.08		

Table 4.1c microprobe analyses from runs at constant pressure of 1 kbar.

Run E.	694	716-2	711-2	712-1	711-3	712-2
Na _x	1.0	1.5	1.5	1.5	2.0	2.0
T(°C)	300	200	225	325	225	275
SiO ₂	50.25	51.77	41.90	42.47	42.59	43.99
Al ₂ O ₃	34.77	38.78	35.38	35.80	35.39	36.12
Na ₂ O	3.41	6.73	6.19	7.18	6.63	6.57
total	88.43	97.28	83.47	85.45	84.61	86.68
Si	6.61	6.37	6.01	6.02	6.06	6.10
Al ^{IV}	1.39	1.63	1.99	1.98	1.94	1.90
Al ^{VI}	4.00	4.00	4.00	4.00	4.00	4.00
Na	0.87	1.61	1.72	1.97	1.83	1.77
sum	12.87	13.61	13.72	13.97	13.83	13.77
n [#]	11	7	6	11	9	8
mean p [‡]	1.39	1.68	1.87	1.91	1.92	1.89
s.d.	0.08	0.05	0.17	0.08	0.04	0.10

[#] number of analyses

[‡] average of n analyses, s.d. = standard deviation

bd below detection limit

Beidellite forms rather big flakes of a diameter up to 100 μm and a thickness of approximately 15 to 20 μm . No other crystal faces than (001) have been observed. Most flakes show a package of platelets separated by small open spaces (Fig. 4.2a). This is in contrast with kaolinite, which exhibits massive flakes of a diameter up to 75 μm and a thickness of approximately 5 μm (Fig. 4.2b). In all samples variable amounts of amorphous material can be recognized as massive fragments of a variable composition as evidenced by the microprobe analyses (Table 4.1b).

The crystallization of Na-beidellite proceeds rather fast at 350°C and 1 kbar. After one day already 15 % Na-beidellite is produced. A maximum of 85 % is

Synthesis field of Na-beidellite in terms of temperature, water pressure and sodium activity

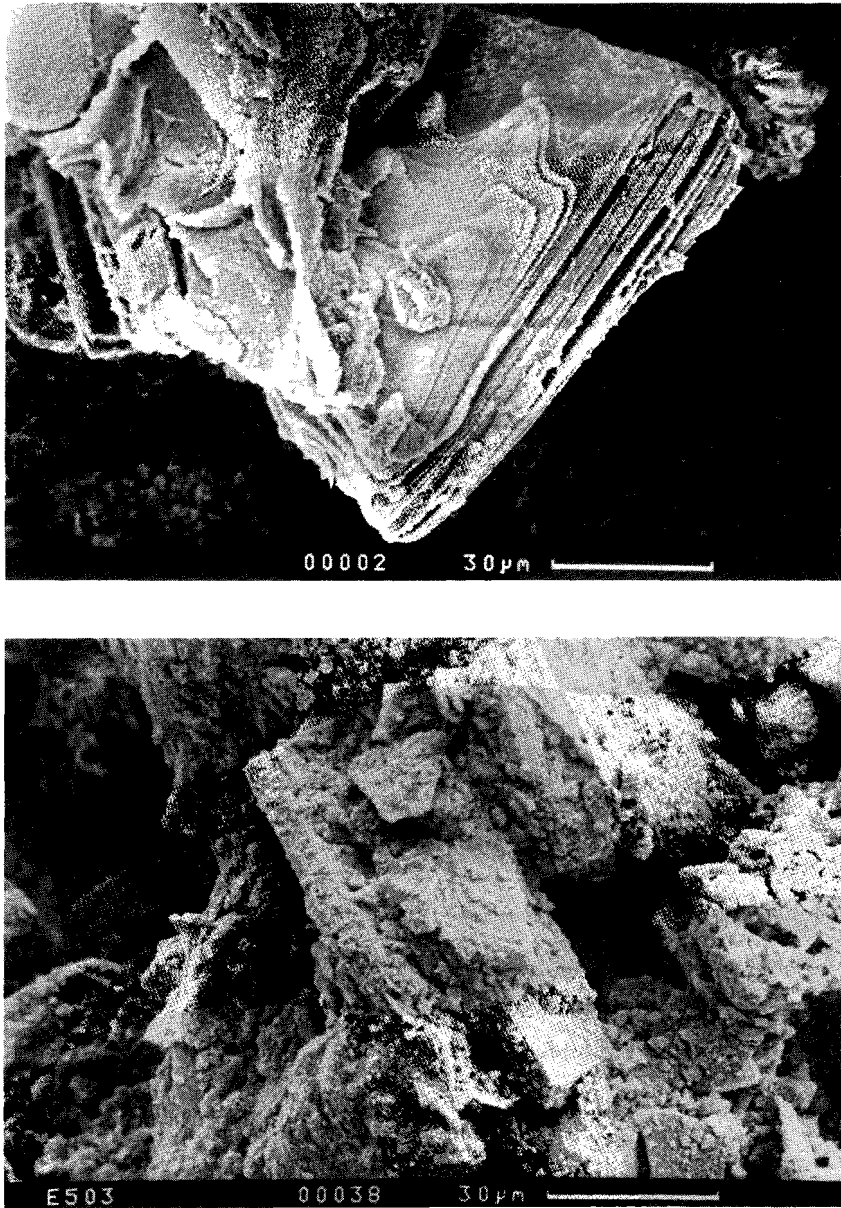


Figure 4.2 Scanning electron microscope photographs a) Na-beidellite from run E427 (upper) and b) kaolinite from run E503 (lower). Note specks of quartz and spheres of amorphous material.

reached after 14 days (Fig. 4.3). A synthesis temperature of 400°C accelerates the crystallization and increases the maximum yield to 95 % within 20 days. A longer run time does not significantly improve the Na-beidellite yield for the applied gel composition.

The synthesis field in relation to the gel composition is illustrated in a T-gelcomposition diagram at 1 kbar (Fig. 4.4), in which the relative Na-content represents p in the formula $\text{Na}_p\text{Al}_{4+p}\text{Si}_{8-p}\text{O}_{20}(\text{OH})_4$. The formation of Na-beidellite is dependent on both the temperature and the gel composition. Amorphous material of a variable composition is produced at temperatures below 200°C. In the composition range where $p < 0.4$, kaolinite and quartz is formed below 325°C, while above 325°C pyrophyllite is produced. Above 300°C and at a Na-content of 0.7 and lower pyrophyllite is formed instead of paragonite. At $p = 0.7$ beidellite exhibits a maximum stability ranging from 450°C to 275°C. For $p = 1.0$ some bayerite is formed at 225°C as a crystalline phase. Increasing the Na-content to 1.5 results in a significant lowering of the Na-beidellite stability field to temperatures between 300°C and 175°C. The actual sodium content of the beidellite made from a gel of a composition of $p = 1.5$, is significantly higher than expected from the gel composition and increases with the temperature from $p = 1.63$ to 1.91 (Table 4.1c). The beidellite formed from a gel with a paragonite composition, $p = 2.0$, has a composition with p around 1.9.

Microprobe analyses (Table 4.1b), based on Si and Al, reveal the compositions of the beidellite, formed from gels with p - values of 1.0 and higher, to cluster around p -values of approximately 1.4 and 1.8 at a pressure of 1 kbar. Increasing the synthesis temperature results in a small increase in p -value.

4.4 DISCUSSION

Between 0.2 and 2 kbar the temperature conditions for the $\text{Na}_{0.7}$ -beidellite synthesis do not significantly depend on pressure, which agrees with the results of Sand et al. (1957). They observed the stability field to shift less than 25°C to

Synthesis field of Na-beidellite in terms of temperature, water pressure and sodium activity

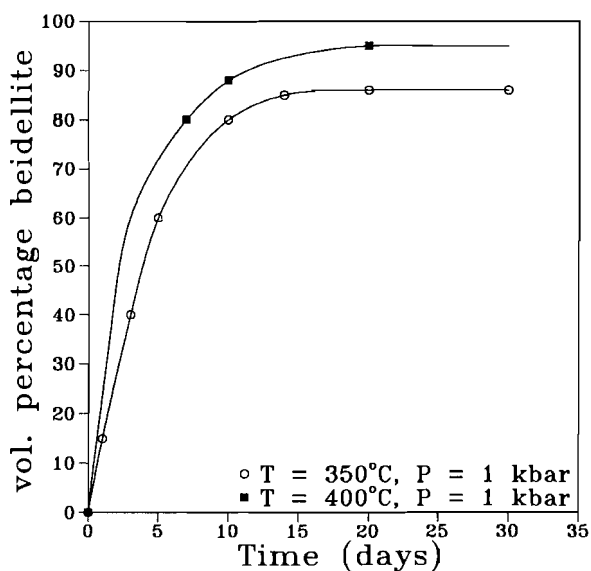


Figure 4.3 Beidellite yield in vol% estimated from SEM photographs as a function of the synthesis time at 350°C and 400°C at 1 kbar.

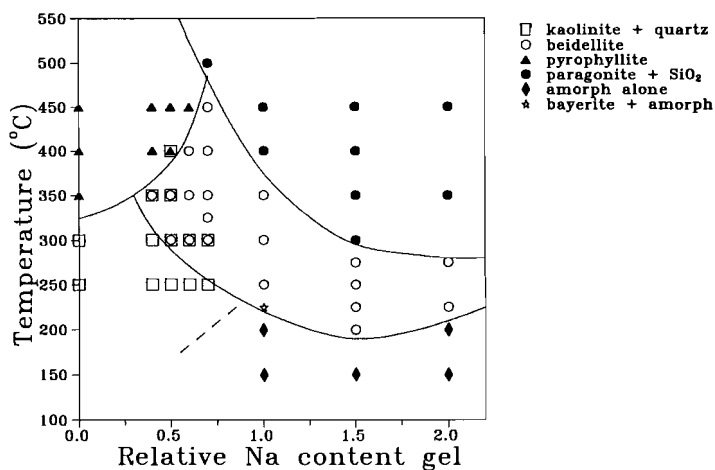


Figure 4.4 Experimental results at a constant pressure of 1 kbar of the synthesis field of Na-beidellite as a function of temperature and gel composition. The beidellite composition is variable. The presence of amorphous material or SiO_2 phase is not indicated.

higher temperatures in a similar pressure range. The conditions of 320°C/130 bar and 340°C/600bar, which are applied for the synthesis of beidellite from a gel with composition $\text{Na}_{0.91}\text{Al}_{4.91}\text{Si}_{7.09}\text{O}_{20}(\text{OH})_4$ (Schutz et al., 1987; Plee et al., 1987), are within the field of pure beidellite. Eberl and Hower (1977) synthesized fully expandable $\text{Na}_{0.66}$ -beidellite together with some quartz between 392° and 445°C at 2 kbar, which fits within our results. They found a 75-90 % expandable mixed-layer phase consisting of beidellite- and some paragonite-like layers, and kaolinite between 260° and 350°C, where we observed pure beidellite. In our experiments the presence of small amounts of paragonite-like layers in the beidellite can not be completely ruled out, as no ethylene glycol test could be carried out on the very small quantities of runproducts. However, neither microprobe analyses nor XRD give any indication of the presence of paragonite-like layers in the beidellite.

The upper temperature limit of 470°C (Ames and Sand, 1958) and of 480°C (Sand et al., 1957) for a $\text{Na}_{0.66}$ -beidellite at a pressure of 1 kbar is comparable with our upper temperature limit of between 450°C and 500°C for the formation of $\text{Na}_{0.7}$ -beidellite. The composition corresponding to $p = 0.66$ is thought to represent the optimum substitution of aluminum for silicon at the tetrahedral sites (Ames and Sand, 1958). The distribution of Al over the tetrahedral layer is basically governed by the Al-O-Al avoidance rule (Loewenstein, 1954). The principle of the HDC (Homogenous Dispersion of Charges) (Herrero et al., 1985, 1987) adds to the Loewenstein rule the fact that each hexameric ring in the tetrahedral sheet must contain a number of Al atoms as close as possible to the average Al/Si ratio corresponding to the composition. This results in probabilities H_0 and H_1 of 50 % for both hexameric rings with zero and one Al for $\text{Na}_{0.66}$ -beidellite, supporting the suggestion of Ames and Sand (1958). Our experiments with sodium contents $p > 0.7$ in the starting gel result in a lowering of both the upper and the lower temperature limit of the beidellite synthesis field. The HDC theory indicates that at higher sodium contents the aluminum distribution over the tetrahedral layer becomes less homogeneous, caused by the formation of hexameric rings with an unequal distribution of one and two aluminum atoms per ring substituted. A

homogeneous distribution of one and two aluminum atoms per hexameric ring is theoretically present when p has a value of 1.35. Two aluminum atoms in each ring (H_2 100%) results in a paragonite composition with $p = 2$. Both distributions result in the formation of rather stable phyllosilicates. The microprobe analyses of beidellites formed from gels with p -values of one and higher (Table 4.1c) indicate that the system tends to form beidellite with average p -values of 1.4 and 1.9, approximating the above mentioned homogeneous distributions (Fig. 4.5).

Examination of experiments with increasing synthesis temperatures at a constant pressure and gel composition in Figure 4.1 reveal a succession of minerals with increasing sodium content: kaolinite and quartz, beidellite, beidellite and SiO_2 , and paragonite and quartz. The chemical potential of Na, μ_{Na} , increases with the synthesis temperature. Velde (1985) has observed the sequence: kaolinite and quartz, via beidellite, paragonite to finally zeolite. This sequence agrees well with our results. The rather constant composition of the beidellite demonstrates that the quartz crystallized from unreacted amorphous material. At high temperatures the

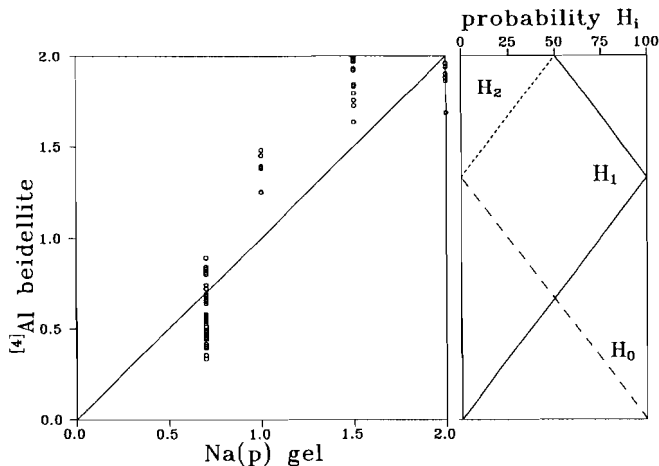
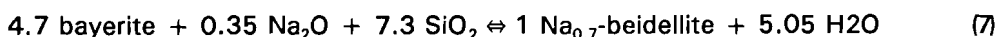
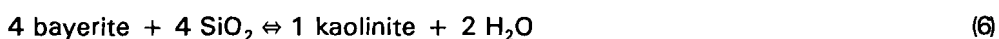
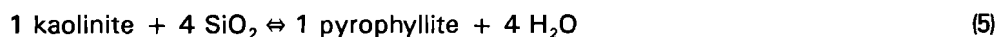
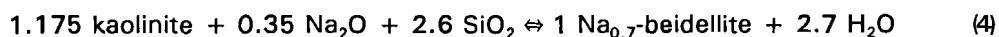
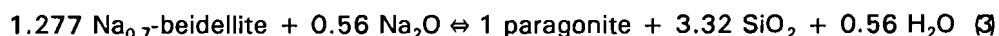
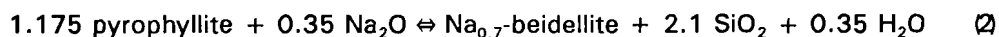
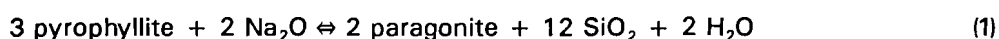


Figure 4.5 ^{14}Al content of the beidellite as function of the starting gel composition and the probabilities H_i , i representing the number of ^{14}Al per hexameric Si ring, as predicted by the HDC theory (Herrero et al. 1985; 1987).

dissolution of silica which is rapid as compared to the formation of beidellite causes supersaturation of silica and, therefore, the formation of quartz. At low temperatures the dissolution of silica is slow, thereby avoiding supersaturation and precipitation of a SiO₂ polymorph.

The temperature-composition diagram (Fig. 4.4) exhibits a minimum in both lower and upper temperature limit at $p = 1.5$. Although these temperature limits are comparable with the results of Koizumi and Roy (1959) in the p -range below 1.34, they still found an expandable phase together with a mica or chlorite like phase above the upper temperature limit, where we observe only paragonite. The existence of a minimum in the lower temperature limit offers the possibility to synthesize large quantities of Na_{1.35}-beidellite already at 200°C at pressures < 150 bar in simple Teflon coated autoclaves. At these industrially viable conditions it is possible to avoid the rather expensive synthesis procedures at high pressure using gold capsules and high-pressure equipment as used in this study.

Using a geometric method to construct phase diagrams, Schreinemakers analysis, $\mu - \mu$ diagrams are constructed (Fig. 4.6), considering one of the components H₂O, Al₂O₃ or SiO₂ as inert. Based on Figure 4.4 reactions between bayerite (Al(OH)₃), kaolinite (Al₄Si₄O₁₀[OH]₈), pyrophyllite (Al₄Si₈O₂₀[OH]₄), paragonite (Na₂Al₆Si₈O₂₀[OH]₄), Na_{0.7}-beidellite (Na_{0.7}Al_{4.7}Si_{7.3}O₂₀[OH]₄) and quartz/cristobalite (SiO₂) can be written, considering Al₂O₃ to be inert:



The reaction between kaolinite and paragonite cannot be observed in Figure 4.4 and turns out to be metastable. Changing the beidellite composition in the

Synthesis field of Na-beidellite in terms of temperature, water pressure and sodium activity

reactions (2) and (3) does not change the orientation of the phase boundaries with pyrophyllite and paragonite, although the positions do change. The boundaries between kaolinite and beidellite defined by reaction (4) and between bayerite and beidellite (7) become less steep upon increasing sodium content of the beidellite. For low $\mu_{\text{Na}_2\text{O}}$ and μ_{SiO_2} values this diagram is in good agreement with the $\mu(\text{K},\text{Na}) - \mu(\text{Si})$ diagram reported by Velde (1985) and the ion activity diagrams reported by Garrels (1984), although they report gibbsite ($\text{Al}[\text{OH}]_3$) instead of bayerite ($\alpha\text{-Al}[\text{OH}]_3$).

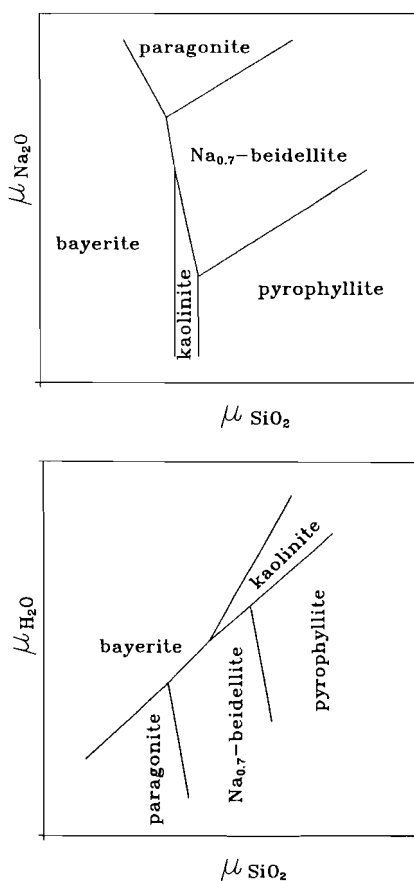


Figure 4.6 a) Sodium - silica activity diagram; b) water - silica activity diagram.

The phase boundary in the Na-free system between kaolinite and pyrophyllite at $P = 1$ kbar and T between 300° and 350°C agrees well with the experimental result of $325^\circ \pm 20^\circ\text{C}$ at 1 kbar reported by Thompson (1970) for reaction (5).

4.5 CONCLUSIONS

- 1) The synthesis field of $\text{Na}_{0.7}$ -beidellite is limited between the temperatures of 300°C and 450°C at pressures below 2 kbar. The beidellite has a rather constant composition of $p = 0.6 - 0.7$.
- 2) Below 300°C kaolinite is the only crystalline phase produced for a gel composition of $p = 0.7$.
- 3) At 500°C paragonite is the crystalline phyllosilicate instead of Na-beidellite, accompanied by quartz or metastable cristobalite.
- 4) At the high temperature and pressure side of the beidellite field quartz or metastable cristobalite additionally result.
- 5) The composition of the beidellite synthesized from gels with $p = 1.5$ and 2.0 is approximately $\text{Na}_{1.4}\text{Al}_{5.4}\text{Si}_{6.6}\text{O}_{20}(\text{OH})_4$ and $\text{Na}_{1.9}\text{Al}_{5.9}\text{Si}_{6.1}\text{O}_{20}(\text{OH})_4$.
- 6) At 1 kbar both the lower and upper temperature limit exhibit a minimum at 200° and 300°C starting with a gel with a composition of $p = 1.5$.
- 7) A maximum temperature of 450°C is observed at 1 kbar and a composition of $p = 0.7$, near the average natural composition.

ACKNOWLEDGMENTS

The authors thank H. M. V. C. Govers for the assistance with the X-ray powder diffraction patterns, R. P. E. Poorter and T. Bouten for the help with the electron microprobe, which is financially supported by NWO-WACOM. J. Pieters is thanked for the help with the electron microscopy. We also thank P. Buining, M. K. Titulaer and J. van Beek for critically reviewing this manuscript.

REFERENCES

- Ames, L.L. and Sand, L.B. (1958) Factors influencing maximum hydrothermal stability in montmorillonites: *Amer. Mineral.*, **43**, 641-648.
- Breen, C., Adams, J.M. and Riekkel, C. (1980) Review of the diffusion of water and pyridine in the interlayer space of montmorillonite: Relevance to kinetics of catalytic reactions in clays: *Clays & Clay Minerals*, **33**, 275-284.
- Eberl, D. and Hower, J. (1977) The hydrothermal transformation of sodium and potassium smectite into mixed-layer clay: *Clays & Clay Minerals*, **25**, 215-227.
- Gadsden, J.A. (1975) *Infrared spectra of minerals and related inorganic compounds*, Butterworth, London, 277 p.
- Garrels, R.M. (1984) Montmorillonite/illite stability diagrams: *Clays & Clay Minerals*, **32**, 161-166.
- Hamilton, D.L. and Henderson, C.M.B. (1968) The preparation of silicate compositions by a gelling method: *Mineral. Mag.*, **36**, 832-838.
- Herrero, C.P., Sanz, J. and Serratosa, J.M. (1985) Tetrahedral cation ordering in layer silicates by ^{29}Si NMR spectroscopy: *Solid State Commun.*, **53**, 151-154.
- Herrero, C.P., Gregorkiewitz, M., Sanz, J. and Serratosa, J.M. (1987) ^{29}Si MAS-NMR spectroscopy of mica-type silicates: observed and predicted distribution of tetrahedral Al-Si: *Phys. Chem. Minerals*, **15**, 84-90.
- Kloprogge, J.T., Jansen, J.B.H. and Geus, J.W. (1990a) Characterization of synthetic Na-beidellite: *Clays & Clay Minerals*, **38**, 409-414.
- Kloprogge, J.T., van der Eerden, A.M.J., Jansen, J.B.H. and Geus, J.W. (1990b) Hydrothermal synthesis of Na-beidellite: *Geologie & Mijnbouw*, **69**, 351-357.
- Koizumi, M. and Roy, R. (1959) Synthetic montmorillonoids with variable exchange capacity: *Amer. Mineral.*, **44**, 788-805.
- Lahav, N., Shani, U. and Shabtai, J. (1978) Cross linked smectites I. Synthesis and properties of hydroxy- aluminum-montmorillonite: *Clays & Clay Minerals*, **26**, 107-115.

- Loewenstein, W. (1954) The distribution of aluminium in the tetrahedra of silicates and aluminates: *Amer. Mineral.*, **39**, 92-96.
- van der Marel, H.W. and Beutelspacher, H. (1976) *Atlas of infrared spectroscopy of clay minerals and their admixtures*: Elsevier, Amsterdam, 396 p.
- Ocelli, M. (1983) Catalytic cracking with an interlayered clay. A two-dimensional molecular sieve: *Ind. Eng. Chem. Prod. Res. Dev.*, **22**, 553-559.
- Ocelli, M. (1987) Surface and catalytic properties of some pillared clays: in *Proceedings of the International Clay Conference, Denver, 1985*, L.G. Schultz, H. van Olphen and F. A. Mumpton (eds.), 319-323.
- Pinnavaia, T.J., Tzou, M.-S. and Landau, S.D. (1985) New chromia pillared clay catalysts: *J. Amer. Chem. Soc.*, **107**, 4783-4785.
- Plee, D., Gatineau, L. and Fripiat, J.J. (1987) Pillaring processes of smectites with and without tetrahedral substitution: *Clays & Clay Minerals*, **35**, 81-88.
- van der Pluijm, B.A., Lee, J.H. and Peacor, D.R. (1988) Analytical electron microscopy and the problem of potassium diffusion: *Clays & Clay Minerals*, **36**, 498-504.
- Rupert, J.P., Granquist, W.T. and Pinnavaia, T.J. (1987) Catalytic properties of clay minerals: in *Chemistry of Clays and Clay Minerals*, A.C.D. Newman, ed., Mineral. Soc., Longman Scientific & Technical, London, 275-318.
- Sand, L.B. and Crowley, M.S. (1956) Comparison of a natural bentonite with its synthetic analogue: *Nat. Res. Council Publ.*, **456**, 96-100.
- Sand, L.B., Roy, R. and Osborn, E.F. (1957) Stability relations of some minerals in the $\text{Na}_2\text{O}-\text{Al}_2\text{O}_3-\text{SiO}_2-\text{H}_2\text{O}$ system: *Econ. Geol.*, **52**, 169-179.
- Schutz, A., Stone, W.E.E., Poncelet, G. and Fripiat, J.J. (1987) Preparation and characterization of bidimensional zeolitic structures obtained from synthetic beidellite and hydroxy- aluminum solutions: *Clays & Clay Minerals*, **35**, 251-261.
- Singh, S.S. and Kodama, H. (1988) Reactions of polynuclear hydroxyaluminum cations with montmorillonite and the formation of a 28 Å pillared complex: *Clays & Clay Minerals*, **36**, 397-402.

- Sterte, J. (1986) Synthesis and properties of titanium oxide cross-linked montmorillonite: *Clays & Clay Minerals*, **34**, 658-664.
- Sterte, J. and Shabtai, J. (1987) Cross linked smectites V. Synthesis and properties of hydroxy-silicoaluminum montmorillonites and fluorhectorites: *Clays & Clay Minerals*, **35**, 429-439.
- Thompson, A.B. (1970) A note on the kaolinite-pyrophyllite equilibrium: *Amer. J. Sci.*, **268**, 454-458.
- Torii, K. and Iwasaki, T. (1986) Synthesis of new trioctahedral Mg-Smectite: *Chemistry Letters*, **1986**, 2021-2024.
- Torii, K. and Iwasaki, T. (1987) Synthesis of hectorite. *Clay Science* **7**, 1-16.
- Tuttle, O.F. (1949) Two pressure vessels for silicate-water studies: *Geol. Soc. Amer., Bull.*, **60**, 1727-1729.
- Velde, B. (1985) *Clay minerals. A physico-chemical explanation of their occurrence*, Developments in Sedimentology **40**. Elsevier, Amsterdam, 427 p.

CHAPTER V

THE INTERLAYER COLLAPSE DURING DEHYDRATION OF SYNTHETIC $\text{Na}_{0.7}\text{-BEIDELLITE}$: A ^{23}Na SOLID-STATE MAGIC-ANGLE SPINNING NMR STUDY

ABSTRACT

The dehydration and migration of the interlayer cation of the synthetic beidellite $\text{Na}_{0.7}\text{Al}_{4.7}\text{Si}_{7.3}\text{O}_{20}(\text{OH})_4 \cdot n\text{H}_2\text{O}$, are studied with solid-state ^{23}Na and ^{27}Al MAS-NMR, heating stage XRD, and thermogravimetric analyses (TGA, DTA). The ^{23}Na MAS-NMR of Na-beidellite at 25°C displays a chemical shift of 0.2 ppm, which indicates a configuration comparable with that of Na^+ in solution. Total dehydration proceeds reversibly in two temperature ranges. Four water molecules per Na^+ are gradually removed from 25° to 85°C. As a result, the basal spacing decreases from 12.54 Å to 9.98 Å and the Na^+ surrounded by the two remaining water molecules is relocated in the hexagonal cavities of the tetrahedral sheet. The chemical shift of 1.5 ppm exhibited after the first dehydration stage illustrates an increased influence of the tetrahedral sheet. The high local symmetry is maintained throughout the entire first dehydration stage. During the second dehydration, which proceeds in a narrow temperature range at approximately 400°C, the remaining two water molecules are removed reversibly without any change of the basal spacing.

5.1 INTRODUCTION

Smectites are important as minerals in geological hydrothermal systems. Properties, such as, compaction and plasticity, play a significant role in oil exploration. Last decade pillared smectites are increasingly studied for the possible use as catalysts and molecular sieves. The nature of the interlayer cation and its hydration shell largely determine properties, such as, swelling, cation exchange, and catalytic activity, e.g., in oil cracking reactions .

Dehydration reactions provide important information about the interlayer configuration. With the synthetic beidellite $\text{Na}_{0.7}\text{Al}_{4.7}\text{Si}_{7.3}\text{O}_{20}(\text{OH})_4 \cdot n\text{H}_2\text{O}$ Klopogge et al. (1990a) observed one main dehydration reaction proceeding below 55°C, followed by a slow but continuous dehydration up to approximately 400°C.

Experimental studies by Koster van Groos and Guggenheim (1984,1986,1987) have demonstrated that montmorillonite exhibits dehydration proceeding in two stages. The two dehydration steps were interpreted as dehydration of a voluminous, but weakly bonded outer hydration shell around the interlayer cation, and of a more strongly bonded inner hydration shell at approximately 140° to 150°C and 200° to 210°C, respectively.

Solid-state Magic-Angle Spinning Nuclear Magnetic Resonance (MAS-NMR) on zeolites and clays is a powerful technique to elucidate the structural environment of exchangeable cations, such as, ^7Li , ^{23}Na (Janssen et al., 1989a,b), ^{113}Cd (Bank et al., 1989), and ^{133}Cs (Chu et al., 1987; Kirkpatrick, 1988; Weiss et al., 1990a,b). ^{23}Na MAS-NMR has been applied to zeolites, sodium-feldspars

Table 5.1. Chemical composition, unit cell parameters and ^{27}Al and ^{29}Si MAS-NMR chemical shifts of the synthetic Na-beidellite (Kloprogge et al., 1990a,b).

chemistry		X-ray diffraction		solid-state MAS-NMR			
wt%	formula (22 O)	unit cell* parameters (Å)	^{27}Al $\delta(\text{ppm})$	I	^{29}Si $\delta(\text{ppm})$	I	
SiO_2	56.76	Si 7.3	a 5.18 ± 0.005	Al^{IV} 69.9	0.25	Si(OAl) -92.7	0.61
Al_2O_3	30.96	Al 4.7	b 8.96 ± 0.008	Al^{VI} 3.9	0.75	Si(1Al) -88.4	0.29
Na_2O	2.44	Na 0.6	c 12.54 ± 0.011			Si(2Al) -82.3	0.10
H_2O	9.65						

* orthorhombic cell (Kloprogge et al., 1990a)

(Kirkpatrick et al., 1985, Yang et al., 1986) and framework aluminosilicate glasses (Oestrike et al., 1987). Most of the structural information is gathered from the ²³Na chemical shifts and from the changes in the second order quadrupole interactions.

The purpose of present study is to elucidate the interlayer geometry of Na-beidellite during dehydration. Knowledge of the interlayer geometry as function of the extent of dehydration may provide insight in phenomena proceeding during pillaring of synthetic Na-beidellite. More particularly, information may be gained concerning the position of the pillars and the structural relation with the tetrahedral sheets of the clay. Therefore, ²³Na and ²⁷Al Magic Angle Spinning Nuclear Magnetic Resonance (MAS-NMR) is performed in experiments in which the Na-beidellite is heated to 105°C. For refinement of the interpretation the results are combined with Thermogravimetric (TGA) and Differential Thermal Analysis (DTA) up to 1100°C, and heating stage X-Ray Diffraction (HT-XRD) up to 400°C.

5.2 EXPERIMENTAL METHODS

5.2.1 Samples

Na-beidellite of a chemical composition of Na_{0.7}Al_{4.7}Si_{7.3}O₂₀(OH)₄.nH₂O is hydrothermally synthesized from a stoichiometric gel prepared according to the method of Hamilton and Henderson (1968). The synthesis is performed at 350°C and 1 kbar in a Tuttle-type, externally heated, cold-seal pressure vessel (Tuttle, 1949). Kloprogge et al. (1990a,b) have reported on the synthesis procedure and product characterization. The samples are dried overnight at 120°C and rehydrated in air of approximately 60 % relative humidity before the dehydration experiments. A short review of the relevant data is given in **Table 5.1**.

5.2.2 Analytical techniques

Thermogravimetric analyses (TGA, DTG) and differential thermal analyses (DTA) were performed on a Dupont 1090 analyzer, applying heating rates of 0.5°C/min and 10°C/min within a N₂ flow. Heating stage X-ray powder diffraction was carried out with a HT Guinier CuKα₁, Enraf Nonius FR553, focussing powder camera, applying a heating rate of 1°C/min. ²³Na and ²⁷Al MAS-NMR spectra were recorded on a Bruker WM500 (11.7 Tesla) at 132.258 MHz and 130.321 MHz, respectively, at the Department of Physical Chemistry, Faculty of Science, University of Nijmegen. The samples were spun at a frequency of approximately 3 kHz. Standard 256 Free Induction Decays (FIDs) were accumulated at a repetition time of 1 s. Chemical shifts are reported in ppm relative to a NaCl solution for ²³Na and to Al(H₂O)₆³⁺ for ²⁷Al.

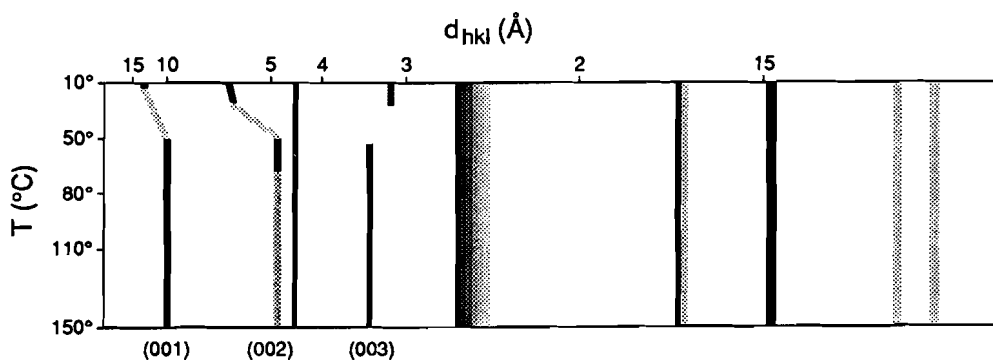


Figure 5.1 Heating stage X-ray powder diffraction pattern in the temperature range 20° to 150°C (Guinier film).

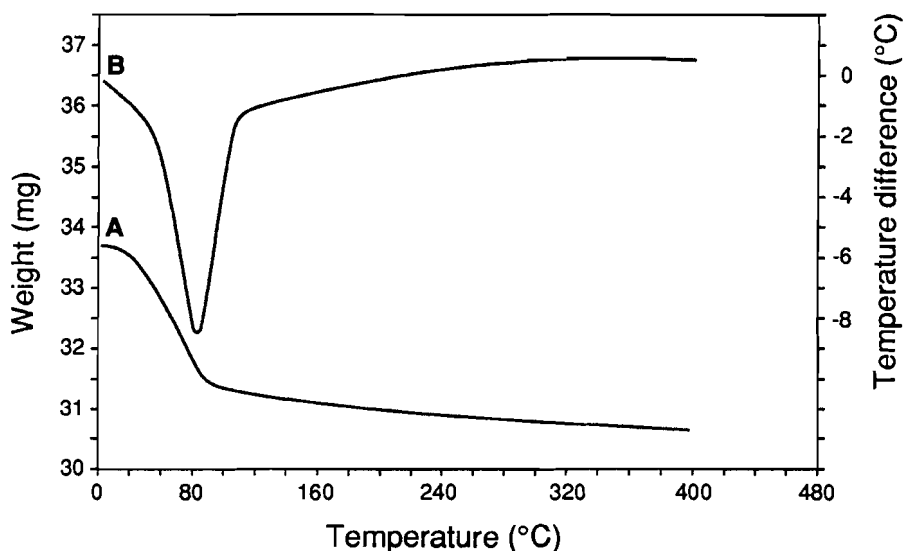


Figure 5.2 Thermogravimetric analysis of synthetic Na- beidellite: a) TGA, b) DTA.

5.3 RESULTS

HT-XRD reveals a collapse of the interlayer spacing in the temperature range of 20° to 54°C. The basal spacing d_{001} and the corresponding d_{002} decrease from 12.54 Å and 6.27 Å at 20°C to 9.98 Å and 4.99 Å at 54°C, respectively. The intensity of the (004) reflection decreases in this temperature interval and ultimately disappears, whereas the (003) reflection becomes stronger (Fig. 5.1). Up to 400°C the basal spacing remains constant.

The collapse of the interlayer spacing coincides with a strong weight loss of 6.6 % below 85°C as confirmed by TGA (Fig. 5.2), applying the same heating rate (0.5°C/min) as in the HT-XRD. Between 85° and 400°C an additional amount of

2.6 wt% water is gradually lost. The DTA exhibits one strong endothermic peak at 80°C (Fig. 5.2).

A water resorption experiment was performed in a TGA-balance after dehydration up to 400°C followed by cooling to 25°C and keeping the sample at 25°C for 1400 min. The Na-beidellite resorbs water until a constant weight is reached after 1300 min (Fig. 5.3). An amount of 2.16 moles water is adsorbed per mole Na-beidellite in air of a relative humidity of approximately 60 %. XRD of the resorbed Na-beidellite reveals a rapid recovery of the basal spacing to 12.44 Å after approximately 45 min.

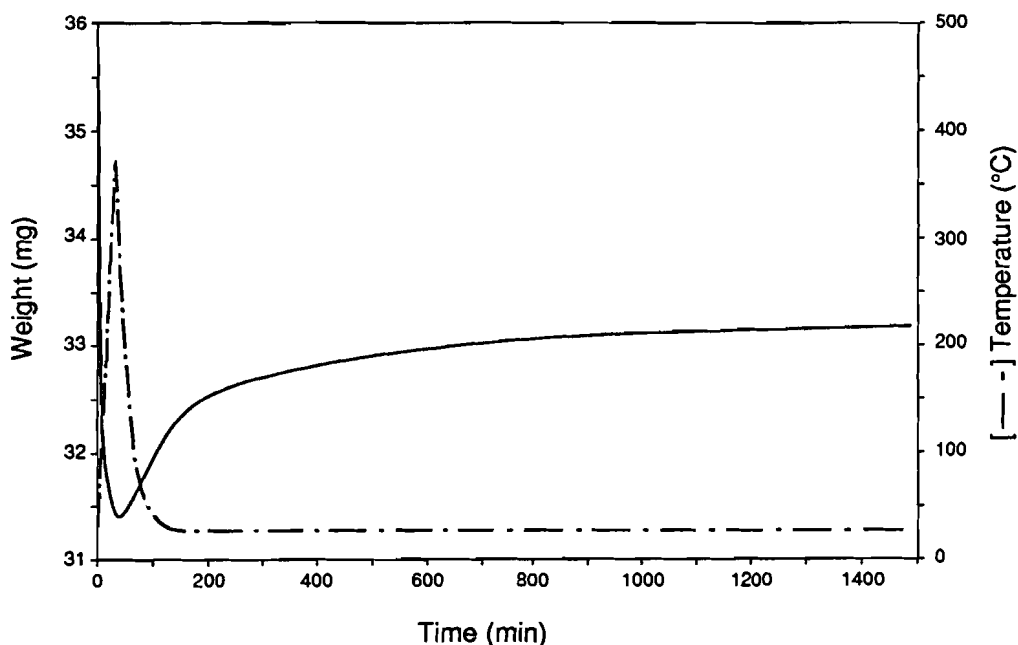


Figure 5.3 Resorption of water after dehydration up to 400°C and subsequent cooling to room temperature in a TGA plot of sample weight against time. The increase in weight represents 3 molecules H₂O per Na⁺.

The interlayer collapse during dehydration of synthetic Na_{0.7}-beidellite: a ²³Na solid-state magic-angle spinning NMR study

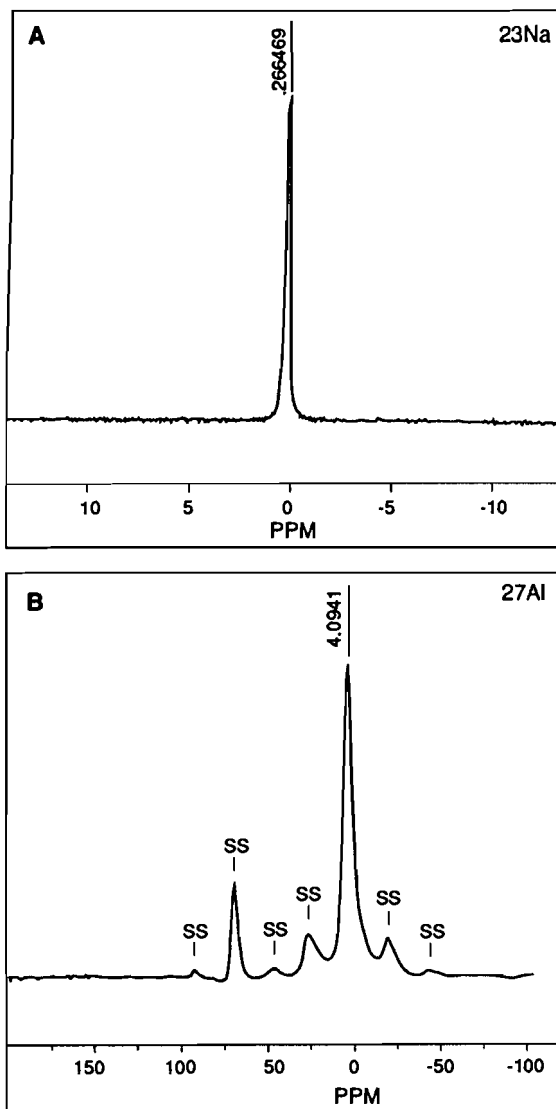


Figure 5.4 Solid-state MAS-NMR spectra of synthetic Na-beidellite: a) ²³Na and b) ²⁷Al. The asterisk signifies spinning sidebands.

Table 5.2. ^{23}Na and ^{27}Al MAS-NMR chemical shifts δ (ppm) and full width at half height FWHH (Hz) as function of dehydration temperature.

T(°C)	^{23}Na		$^{27}\text{Al}^{\text{IV}}$		$^{27}\text{Al}^{\text{VI}}$	
	δ	FWHH	δ	FWHH	δ	FWHH
25	0.266	33.6	69.9	488	3.9	895
45	0.632	30.5	69.9	488	3.9	827
65	0.899	25.4	69.9	488	3.9	786
85	1.223	24.4	69.9	488	3.9	732
105	1.555	20.3	69.9	488	3.9	692

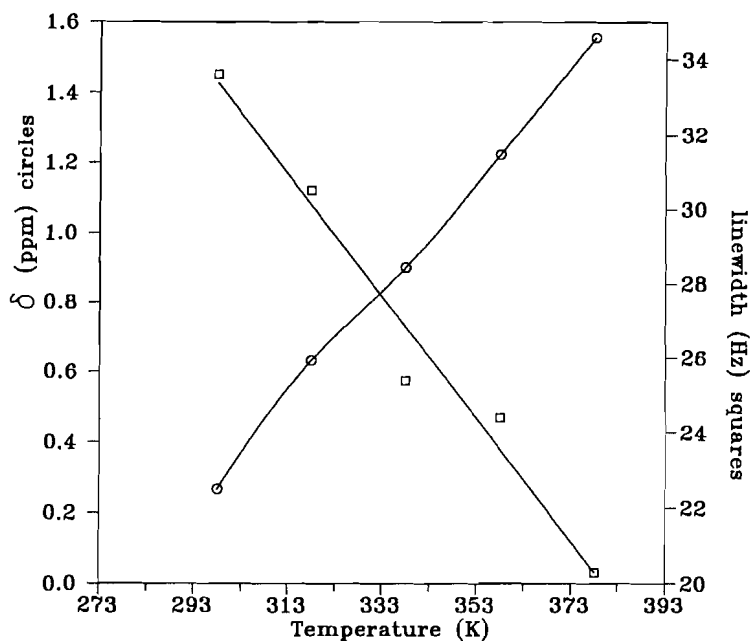


Figure 5.5 Chemical shift δ (open circles) and the linewidth at half height (FWHH)(solid squares) of ^{23}Na as function of the dehydration temperature.

²³Na MAS-NMR spectra of Na-beidellite exhibit one sharp resonance near 0 ppm (Fig. 5.4a). No doublets typical for relatively large second order quadrupole interactions are observed. Upon dehydration the chemical shift δ_{Na} , taken as the peak maximum, changes linearly from 0.27 ppm at 25 °C to 1.56 ppm at 105 °C (Fig. 5.5). The linewidth at half height (FWHH) decreases simultaneously from 33.6 to 20.3 Hz (Table 5.2).

In the ²⁷Al spectra two resonances are recognized with chemical shifts δ_{Al} of approximately 3.9 ppm and 69.9 ppm (Fig. 5.4b), representing Al^{VI} and Al^{IV}, respectively, in the Na-beidellite structure (Kloprogge et al., 1990a). The Al^{VI} resonance exhibits a right-side asymmetry. Dehydration has no influence on the chemical shifts of both Al^{IV} and Al^{VI}. The FWHH of the tetrahedral Al resonance remains constant, whereas that of the octahedral one decreases from 895 Hz at 25 °C to 692 Hz at 105 °C (Table 5.2).

5.4 DISCUSSION

The basal spacing of Na-beidellite of 12.54 Å indicates the presence of a monomolecular layer of water in the interlayer, in which each Na⁺ atom, surrounded by water molecules, is positioned very close to the center of the interlayer space (Kawano and Tomita, 1991) The decrease of the basal spacing to 9.98 Å during dehydration to 85 °C indicates the break up of the monomolecular layer. The TGA profile displays a major loss of 6.6 wt%, which is equivalent to 2.9 mole of water per mole of Na_{0.7}-beidellite, representing 4 molecules of water per atom Na⁺. Upon heating to 400 °C the dehydration of the Na-beidellite takes place at a constant basal spacing of 9.98 Å and slowly progresses to a total weight loss of 9.2 %, which is equivalent to 6 molecules of water per atom of Na⁺. Sodium surrounded by 6 water molecules is known to have an octahedral coordination which would result in the development of a two-layer hydrate of Na-beidellite

having a basal spacing of 14-15 Å. At the applied relative humidity of 60 % capillary condensation in the interaggregate and intraaggregate pores of the beidellite may well be initiated and account for some of the adsorbed water. This explains the basal spacing of 12.54 Å of a one-layer hydrate beidellite.

The synthetic Na-beidellite exhibits a continuous dehydration between 85° and 400°C, which, smoothly, changes into dehydroxylation above approximately 400°C (Kloprogge et al., 1990b). According to Koster van Groos and Guggenheim (1987) the second dehydration step of montmorillonite terminates at approximately 260°C. The difference in dehydration behaviour of beidellite and montmorillonite is attributed to a difference in the clay structures. Especially, the distribution of electrostatic charge will affect the configuration of the interlayer region. In montmorillonite the negative charge originates mainly from octahedral M^{2+} substitution for Al^{3+} and, therefore, relatively diffuse in the interlayer. In beidellite, on the other hand, the negative charge is due to tetrahedral Al^{3+} substitution for Si^{4+} . The negative charge thus is mainly located on the three basal oxygens of the Al^{3+} substituted tetrahedron, resulting in a strong localized interaction with the adjacent interlayer region.

The dimensions of the water molecules force the Na-beidellite to assume the original basal spacing immediately after the start of the water resorption. The amount of 2.16 moles of water per mole of $Na_{0.7}$ -beidellite, which is equivalent to 3 molecules water per atom Na^+ , is sufficient to retain a basal spacing of 12.44 Å. The dehydration experiments have shown that after the first dehydration stage the basal spacing is 9.98 Å with still two water molecules per atom Na^+ present, suggesting a reorganization of the geometry of the remaining interlayer water around the Na^+ . The uptake of one additional molecule of water per Na^+ is sufficient to restore the original geometry and, therefore, a basal spacing of 12.44 Å is restored.

The chemical shift of the ^{23}Na resonance at 25°C of the Na-beidellite is very close to that of Na^+ in solution, indicating a similar environment. The rapid motion of water molecules around the Na^+ causes an efficient relaxation, as previously

reported for ¹¹³Cd in montmorillonite (Bank et al., 1989). Therefore, a very short repetition delay of 0.15 s suffices to obtain the ²³Na MAS-NMR spectra. The change of the local environment due to the removal of 4 water molecules and the collapse of the interlayer space from approximately 3 Å to 0.5 Å upon dehydration seems to make the peak maxima more positive. It has to be kept in mind that exact interpretation of the observed differences in chemical shift is difficult due to the influence of the motionally averaged environment of the Na⁺. The chemical shift differences point to a steadily increasing influence of the tetrahedral sheet and especially the Al³⁺ substituted tetrahedra on the Na⁺ site. The sharp single resonance of ²³Na reflects a relatively small quadrupole coupling constant (QCC = e²qQ/h) and, therefore, a high local symmetry. Neglecting the influence of the motionally averaged environment, an approximate quadrupole coupling constant can be calculated from the measured linewidth at half height (FWHH), applying the formulae for the linewidth postulated by Akitt (1989) following the calculations of Kentgens et al. (1983):

$$\text{FWHH} = \frac{\nu_Q^2}{3\nu_0}$$

in which $\nu_Q = 3e^2qQ/h2I(2I-1)$ ($e^2qQ/h = \text{QCC}$ in kHz, ²³Na spin $I = 3/2$) and ν_0 is the Larmor frequency (in kHz). At 25 °C the quadrupole coupling constant is approximately 230 kHz. This value is only slightly higher than that of solid NaCl (approximately 117-135 kHz at 25 °C based on a FWHH of 3-4 ppm at 39.7 MHz, Meadows et al., 1982), which has a very high local symmetry with each Na⁺ in an octahedron of six Cl⁻, but lower than the QCC of NaNO₃ (≈ 300 kHz) or NaNO₂ (≈ 1.1 MHz, Engelhardt and Michel, 1987).

Modification of the local environment of the Na⁺ caused no changes in the ²⁷Al MAS-NMR chemical shifts for both Al^{IV} and Al^{VI} in the first dehydration interval.

Applying the same relation for the calculation of the quadrupole coupling constants of the Al^{IV} and Al^{VI} results in values of 2.9 MHz and 3.9 MHz, respectively. The value obtained for the octahedral resonance is rather questionable, because the asymmetry of the resonance may arise from several sites with the same coordination and similar chemical shift, but different quadrupole coupling constants and asymmetry parameters η . Woessner (1989) reported for natural beidellite from the Black Jack Mine, Idaho slightly greater linewidths, viz., 4.2 ppm (547 Hz) and 4.4 ppm (573 Hz) for tetrahedral ($\delta = 70.0$ ppm) and octahedral ($\delta = 3.1$ ppm) Al, respectively. Based on the formula (Kunwar et al., 1984):

$$\delta \text{ (ppm)} = -6 \times 10^3 (e^2qQ/h\nu_0)^2(1 + 1/3\eta^2),$$

in which η is the asymmetry parameter, Woessner (1989) calculated a SOQE (second order quadrupole effect), which is equal to $(e^2qQ/h)(1 + 1/3\eta^2)^{1/2}$, for the tetrahedral resonance of 2.54 MHz. The asymmetric octahedral resonance was described by a peak with $\eta = 0$ and QCC = 5.6 MHz and one with SOQE = 2.1 MHz. In general the SOQE for Al^{IV} increases with increasing tetrahedral substitution resulting from a tetrahedral sheet distortion (Ghose and Tsang, 1973). In comparison with the Black Jack beidellite the synthetic beidellite has a slightly lower tetrahedral Al substitution (Al^{IV}/Si = 0.151 and 0.096, respectively) and thus a lower SOQE is expected. Based on the QCC of 2.9 MHz and assuming $\eta = 0$, the SOQE is slightly higher than the value of 2.49 MHz observed by Woessner (1989). The difference in QCC may be caused by a poorer crystallinity of the synthetic Beidellite. The decreasing linewidths of the ²³Na and ²⁷Al resonances are caused by second order quadrupole effects due to heating in the NMR apparatus.

Upon dehydration small monovalent interlayer cations, such as Na⁺, can take up position in the hexagonal cavities close to the Al³⁺ substituted tetrahedra (Kawano and Tomita, 1991), forming chains parallel to the b-axis. The Na⁺ is thereby bonded to only one tetrahedral sheet. The alternate chain of hexagonal cavities is left vacant (Güven, 1988). The positioning of Na⁺ in the hexagonal cavities explains the high local symmetry and change in chemical shift observed by ²³Na MAS-NMR after the first dehydration step. It also agrees with the decrease

of the interlayer space to 0.5 Å, which is even smaller than the effective radius of Na⁺ (e.g. 0.99 Å for Na^{IV} and increases to 1.39 Å for Na^{XII} in chalcogenides and halides, Shannon, 1976). In paragonite, Na₂Al₆Si₆O₂₀(OH)₄, the sodium ions are similarly situated in the hexagonal cavities having an octahedral coordination with an average distance Na-O of 2.63 Å (Sidorenko et al., 1977a,b; Lin and Bailey, 1984). The dimensions of a water molecule combined with the relatively high dehydration temperature of the remaining two water molecules without any further decrease in basal spacing indicate that the water molecules are more strongly bonded to the tetrahedral layer and may be located in one or two hexagonal cavities. This is supported by the fact that the enthalpy per water molecule for the second dehydration step in montmorillonites is clearly higher than that of the first step (Koster van Groos and Guggenheim, 1987).

The ordering of the Na⁺ in chains due to the distribution of Al over the tetrahedral sheet following the Loewenstein avoidance rule (Loewenstein, 1954) has also implications for the distribution of pillaring complexes, such as, the tridecameric polymer Al₁₃, in pillared clays. The pillars are probably situated directly between two hexagonal rings from two adjacent tetrahedral sheets containing substituted Al, also resulting in a rather regular hexagonal distribution of the pillars. After calcination these pillars are presumably anchored to the apex oxygen of the inverted aluminum tetrahedra pointing out into the interlamellar space from the tetrahedral sheet, as suggested by Plee et al. (1985) based on ²⁷Al and ²⁹Si MAS-NMR.

5.5 CONCLUSION

The data consistently point to a model in which the Na^+ in Na- beidellite exhibits a behaviour comparable to that of Na^+ in solution with a rapid motion of the water molecules around the Na^+ , as evidenced by the rapid relaxation. The very high local symmetry is supported by the small QCC of 113 kHz. During the first step of the dehydration, which proceeds below 85°C , four of the six water molecules are easily removed, resulting in a decrease of the basal spacing from 12.54 \AA to 9.98 \AA . The total amount of 6 water molecules per Na^+ lost during dehydration and the observation of a basal spacing of a one-layer hydrate beidellite indicate that not only interlayer hydrate complexes are formed but also capillary condensation in the pores takes place. The remaining two water molecules and the Na^+ are relocated in chains of hexagonal cavities near the Al^{3+} substituted tetrahedra without further decrease of the basal spacing. The Na^+ is situated within the hexagonal cavity, because the remaining interlayer space of 0.5 \AA is smaller than the effective radius of the Na^+ ion. This relocation results in a slightly stronger bonding of the water molecules to the tetrahedral sheet as evidenced by the high dehydration temperature of 400°C .

ACKNOWLEDGMENT

The authors wish to thank H. M. V. C. Govers for the HT-XRD patterns, T. Zalm for the TGA, DTA and DSC curves. They are especially thankful to G. Nachtegaal for the technical assistance at the NWO-SON HF-NMR facility at Nijmegen. We also thank M. K. Titulaer, J. J. van Beek, P. J. Dirken, R. Vogels for critically reviewing the manuscript. N. Güven is especially thanked for his critical review and discussion of the modes of hydration of smectites.

REFERENCES

- Akitt, J. W. (1989) Multinuclear studies of aluminum compounds: *Progr. NMR Spectr.* **21**, 1-149.
- Bank, S., Bank, J., and Ellis, P. D. (1989) Solid-State ^{113}Cd nuclear magnetic resonance study of exchanged montmorillonite: *J. Phys. Chem.* **93**, 4847-4855.
- Chu, P. J., Gerstein, B. C., Nunan, J., and Klier, (1987) A study by solid-state NMR of ^{133}Cs and ^1H of a hydrated and dehydrated cesium mordenite: *J. Phys. Chem.* **91**, 3588-3592.
- Engelhardt, G., and Michel, D. (1987) *High-resolution solid-state NMR of silicates and zeolites*: Wiley, New York, 485 pp.
- Ghose, S., and Tsang, T. (1973) Structural dependence of quadrupole coupling constant e^2qQ/h for ^{27}Al and crystal field parameter D for Fe^{3+} in aluminosilicates: *Amer. Mineral.* **58**, 748-755.
- Güven, N. (1988) Smectites: in *Hydrous phyllosilicates*, S. W. Bailey, ed., Mineral. Soc. Amer. Rev. Mineralogy, **19**, 497-559.
- Hamilton, D. L., and Henderson, C. M. B. (1968) Preparation of silicate compositions by a gelling method: *Mineral. Mag.* **36**, 832-838.
- Janssen, R., Dols, P. P. M. A., Tijink, G. A. H., and Veeman, W. S. (1989a) High temperature NMR of zeolites: in *Zeolite Conference Amsterdam 1989*.
- Janssen, R., Tijink, G. A. H., Veeman, W. S., Maesen, T. L. M., and van Lent, J. F. (1989b) High temperature NMR study of zeolite Na-A: detection of a phase transition: *J. Phys. Chem.* **93**, 899-904.
- Kawano, M., and Tomita, K. (1991) X-ray powder diffraction studies on the rehydration properties of beidellite: *Clays & Clay Minerals* **39**, 77-83.
- Kentgens, A. P. M., Scholle, K. F. M. G. J., and Veeman, W. S. (1983) Effect of hydration on the local symmetry around aluminum in ZSM-5 zeolites studied by aluminum-27 nuclear magnetic resonance: *J. Phys. Chem.* **87**, 4357-4360.

- Kirkpatrick, R. J. (1988) MAS NMR spectroscopy of minerals and glasses: in *Spectroscopic Methods in Mineralogy and Geology*, F. C. Hawthorne ed., Mineral. Soc. Amer. Rev. Mineralogy **18**, 341-403.
- Kirkpatrick, R. J., Kinsey, R. A., Smith, K. A., Henderson, D. M., and Oldfield, E. (1985) High resolution solid-state sodium-23, aluminum-27, and silicon-29 nuclear magnetic resonance spectroscopic reconnaissance of alkali and plagioclase feldspars: *Amer. Mineral.* **70**, 106-123.
- Kloprogge, J. T., van der Eerden, A. M. J., Jansen, J. B. H., and Geus, J. W. (1990a) Hydrothermal synthesis of Na-beidellite: *Geologie en Mijnbouw* **69**, 351-357.
- Kloprogge, J. T., Jansen, J. B. H., and Geus, J. W. (1990b) Characterization of synthetic Na-beidellite: *Clays & Clay Minerals* **38**, 409-414.
- Koster van Groos, A. F., and Guggenheim, S. (1984) The effect of pressure on the dehydration reaction of interlayer water in Na-montmorillonite (SWy-1): *Amer. Mineral.* **69**, 872-879.
- Koster van Groos, A. F., and Guggenheim, S. (1986) Dehydration of K-exchanged montmorillonite at elevated temperatures and pressures: *Clays & Clay Minerals* **34**, 281-286.
- Koster van Groos, A. F., and Guggenheim, S. (1987) Dehydration of a Ca- and a Mg-exchanged montmorillonite (SWy-1) at elevated pressures: *Amer. Mineral.* **72**, 292-298.
- Kunwar, A. C., Thompson, A. R., Gutowsky, H. S., and Oldfield, E. (1984) Solid state aluminum-27 NMR studies of tridecameric Al-oxo-hydroxy clusters in basic aluminum selenate, sulfate, and the mineral zunyite: *J. Magn. Reson.* **60**, 467-472.
- Lin, C.-Yi, and Bailey, S. W. (1984) The crystal structure of paragonite-2M₁: *Amer. Mineral.* **69**, 122-127.
- Loewenstein, W. (1954) The distribution of aluminum in the tetrahedra of silicates and aluminates: *Amer. Mineral.* **57**, 1089-1108.

- Meadows, M. D., Smith, K. A., Kinsey, R. A., Rothgeb, T. M., Skarjune, R. P., and Oldfield, E. (1982) High-resolution solid-state NMR of quadrupolar nuclei: *Proc. Nat. Acad. Sci. USA* **79**, 1351-1355.
- Oestrike, R., Yang, W.-H., Kirkpatrick, R. J., Hervig, R. L., Navrotsky, A., and Montez, B. (1987) High resolution ^{23}Na , ^{27}Al , and ^{29}Si NMR spectroscopy of framework aluminosilicate glasses: *Geochim. Cosmochim. Acta* **51**, 2199-2209.
- Plee, D., Borg, F., Gatineau, L. and Fripiat, J. J. (1985) High-resolution solid-state ^{27}Al and ^{29}Si nuclear magnetic resonance study of pillared clays: *J. Am. Chem. Soc.* **107**, 2362-2369.
- Shannon, R. D. (1976) Revised effective ionic radii and systematic studies of interatomic distances in halides and chalcogenides: *Acta Crystallogr.* **A32**, 751-767.
- Sidorenko, O. V., Zvyagin, B. B., and Soboleva, S. V. (1977a) Refinement of the crystal structure of 2M₁ paragonite by the method of high-voltage electron diffraction: *Sov. Phys./Amer. Inst. Phys. Crystallography* **22**, 554-556 (translated from *Kristallografija* **22**, 971-975, 1977).
- Sidorenko, O. V., Zvyagin, B. B., and Soboleva, S. V. (1977b) The Crystal structure of 3T paragonite: *Sov. Phys./Amer. Inst. Phys. Crystallography* **22**, 557-560 (translated from *Kristallografija* **22**, 976-981, 1977).
- Tuttle, O. F. (1949) Two pressure vessels for silicate-water studies: *Geol. Soc. Amer. Bull.* **60**, 1727-1729.
- Weiss, C. A., Kirkpatrick, R. J., and Altaner, S. P. (1990a) The structural environment of cations adsorbed onto clays: ^{133}Cs variable-temperature MAS NMR spectroscopic study of hectorite: *Geochim. Cosmochim. Acta* **54**, 1655-1669.
- Weiss, C. A., Kirkpatrick, R. J., and Altaner, S. P. (1990b) Variations in interlayer cation sites of clay minerals as studied by ^{133}Cs MAS nuclear magnetic resonance spectroscopy: *Amer. Mineral.* **75**, 970-982.

The interlayer collapse during dehydration of synthetic Na_{0.7}-beidellite: a ²³Na solid-state magic-angle spinning NMR study

Woessner, D. E. (1989) Characterization of clay minerals by ²⁷Al nuclear magnetic resonance spectroscopy: *Amer. Mineral.* **74**, 203-215.

Yang, W.-H., Kirkpatrick, R. J., and Henderson, D. M. (1986) High resolution ²⁹Si, ²⁷Al, and ²³Na NMR spectroscopic study of Al-Si disordering in annealed albite and oligoclase: *Amer. Mineral.* **71**, 712-726.

CHAPTER VI

LOW TEMPERATURE SYNTHESIS OF AMMONIUM-SAPONITES FROM GELS WITH VARIABLE AMMONIUM CONCENTRATION AND WATER CONTENT

ABSTRACT

Ammonium-saponite is hydrothermally grown at temperatures below 300°C from a gel with an overall composition corresponding to $(\text{NH}_4)_{0.6}\text{Mg}_3\text{Si}_{3.4}\text{Al}_{0.6}\text{O}_{10}(\text{OH})_2$. The synthetic saponite and coexisting fluid are characterized by means of X-ray powder diffraction, X-ray fluorescence, Induced Coupled Plasma-Atomic Emission Spectroscopy, thermogravimetric analysis, transmission electron microscopy, CEC determination using an ammonia selective electrode, and pH measurement. A crystallization model is developed, in which crystallization starts with the growth of individual tetrahedral layers with an aluminum substitution controlled by the $\text{Al}^{\text{IV}}/\text{Al}^{\text{VI}}$ ratio in the gel and hydrothermal fluid, on which the octahedral Mg layers can grow. During the synthesis individual sheets stack to form thicker flakes, while also lateral growth takes place. Remaining Al^{VI} replaces partly ammonium as interlayer cation.

6.1 INTRODUCTION

During the last ten years the interest in the use of smectites as catalysts and molecular sieves has increased. Synthetic clays, such as, beidellite (Plee et al., 1987; Schutz et al., 1987, Klopogge et al., 1990a,b), hectorite, and fluorhectorite (Shabtai et al., 1984; Sterte and Shabtai, 1987; Torii and Iwasaki, 1987), are preferred to natural smectites, because of their high purity and their adjustable composition. However, the possibility to use synthetic saponites as catalysts or molecular sieves has so far not received much attention, although the saponites exhibit a higher (hydro)thermal stability than other smectites.

Only a few studies have been devoted to the synthesis of Na-saponites. Koizumi and Roy (1959) and Iiyama and Roy (1963) used a gel consisting of the nitrates of aluminum, magnesium and, sodium together with Ludox, a commercial colloidal

silica suspension stabilized by ammonium, as starting material. Suquet et al. (1977) and Lipsicas et al. (1984) prepared a gel according to the procedure described extensively by Hamilton and Henderson (1968). Hickson (1974, 1975) made an aqueous slurry of hydrous alumina, magnesia, and silica within ammonium hydroxide, while Iwasaki et al. (1989) dissolved magnesium chloride and aluminum chloride in an acidified sodium silicate solution, which was subsequently mixed with an alkali solution. All these syntheses have in common that they were performed at temperatures ranging from 150 to 450°C and a pressure from the autogeneous water pressure to 1500 bar. An exception is the method described by Decarreau (1980, 1985), who precipitated saponite nuclei at room temperature from sodium silicate and sodium aluminate in a solution of a magnesium salt acidified with the corresponding acid. These nuclei were aged for three weeks in water at temperatures between 5°C and 90°C.

The aim of this study is a precise characterization of synthetic ammonium-saponites from gels with variable ammonium concentrations and water content in the temperature range 125°C to 280°C.

6.2 EXPERIMENTAL METHODS

The gel was prepared starting from a homogeneous mixture of stoichiometric amounts of powders of amorphous silica (SiO_2), aluminium-triisopropylate ($\text{Al}[\text{OCH}(\text{CH}_3)_2]_3$), and magnesiumacetate-tetrahydrate ($(\text{CH}_3\text{COO})_2\text{Mg}\cdot 4\text{H}_2\text{O}$). The mixture of the powders was brought into aqueous ammonium hydroxide solutions (NH_4OH), in order to produce a saponite with a theoretical composition of $(\text{NH}_4)_{0.6}\text{Mg}_3\text{Al}_{0.6}\text{Si}_{3.4}\text{O}_{10}(\text{OH})_2$. Approximately 125 g of the gel was hydrothermally treated in a 250 ml autoclave for 72 hours at temperatures between 125°C and 280°C, and autogeneous water pressure. After cooling the solid product was washed two times with demineralized water followed by an ion-exchange with a 1 M ammoniumchloride solution at room temperature, to ensure that all

exchangeable sites are occupied by ammonium. Finally, the solid product was washed another three times, sedimented by centrifugation, and dried overnight at 120°C. The sieve fraction smaller than 64 μm was used for characterization, assuming that amorphous material possibly present would have a particle size larger than 64 μm (based on unpublished data KSLA).

The pH of the coexisting hydrothermal liquid after the synthesis was measured, as well as the pH of the water after washing the resulting solid for the first time with 2 l water.

X-ray powder diffraction (XRD) patterns were recorded with a Philips diffractometer, equipped with PW 1700 hardware and APD1700 software, using $\text{CuK}\alpha$ radiation.

Thermogravimetric and differential thermal analyses (TGA/DTA) were made with a Dupont 1090 Thermal Analyzer using heating rates of 10°C/min and 20°C/min, respectively.

Elemental analyses were performed with X-ray fluorescence (XRF). The coexisting hydrothermal fluid was analyzed with Inductively Coupled Plasma (ICP) atomic emission spectrometry. Infrared (IR) absorption spectra were obtained on powdered samples in KBr tablets (sample concentration 1 wt%) using a Perkin Elmer 580 IR spectrophotometer.

The cation exchange capacity (CEC) of the saponite was determined from the NH_4^+ content in solution, after exchange with NaCl, using an ammonia-selective electrode. Surface areas of the ammonium saponites were determined using a commercial apparatus from Micro Meretics, applying the BET equation. The samples were first calcined at 550°C, and subsequently degassed at 300°C in vacuum. Measurements were performed at liquid nitrogen temperature, using nitrogen as the sorbate, assuming the surface area of adsorbed nitrogen to be 16.2 \AA^2 .

The morphology and particle sizes of the products obtained, were investigated with a Philips EM 420 transmission electron microscope (TEM), operated at 120 kV.

Table 6.1 X-ray powder diffraction data for synthetic NH_4 -saponite obtained with a diffractometer (CuK α radiation).

$d(\text{obs})^1$	I/I_{max}^1 (%)	Indices ²	$d(\text{lit})^2$ Ca	$d(\text{lit})^3$ Na	Intensity ^{2,4}
12.34	87	001	15.29	12.6	vvvs
		002	7.65	6.3	w
4.58	72	020/110	4.61		vs
3.24	24	113	3.256		vw
2.60	84	-202	2.598		m
2.55	84	201	2.560		s
2.38	1	202	2.418		s
1.738	11	-311	1.7454		m
		-242	1.7259		vw
1.529	100	060	1.5389		vvvs
		-332	1.5320		vs

¹ NH_4 -saponite from run HTSAP2b.

² Two-water layer Kozákov saponite (Guinier de Wolff camera) (Suquet et al., 1975).

³ Na-exchanged Kozákov saponite (Suquet et al., 1975).

⁴ v = very; s = strong; m = medium; w = weak.

Low temperature synthesis of ammonium-saponites from gels with variable ammonium concentrations and water content

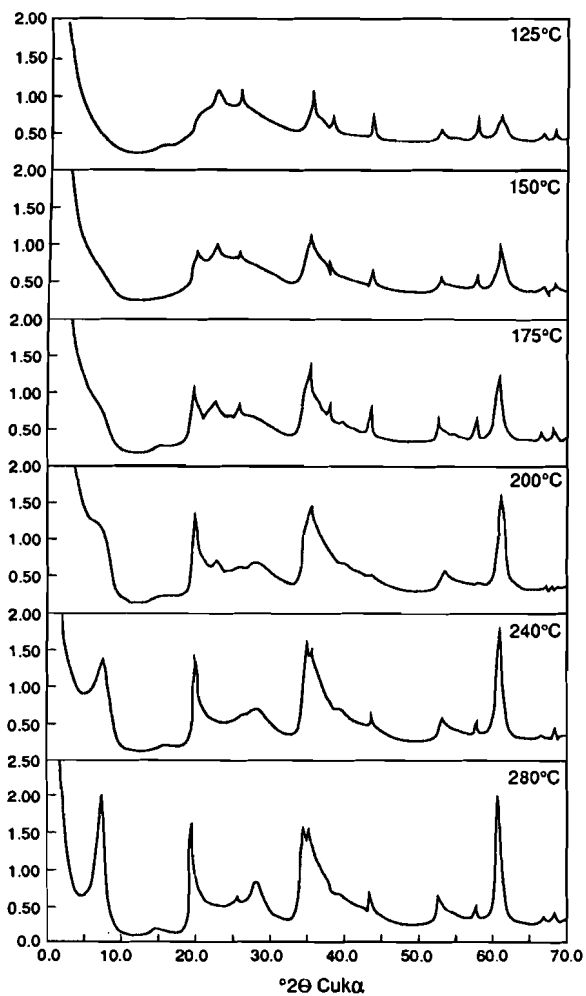
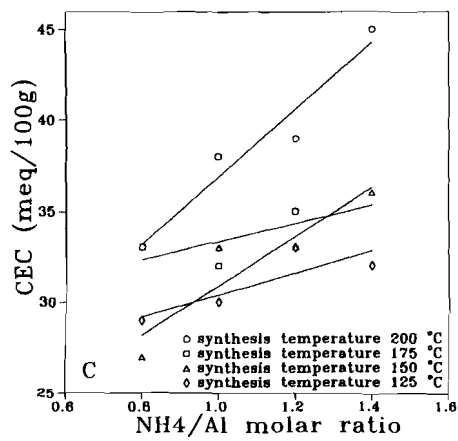
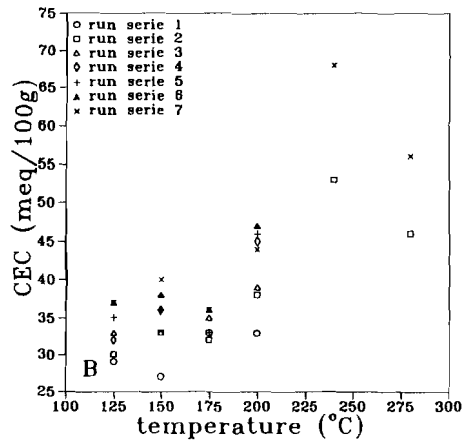
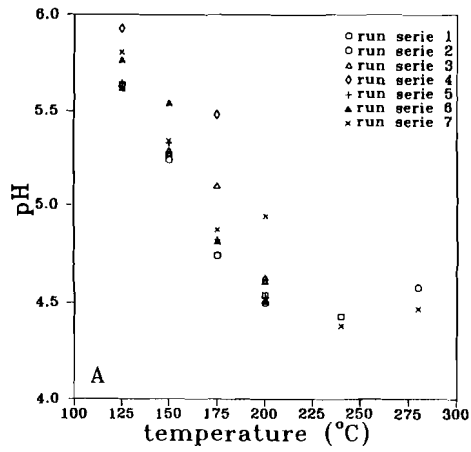


Figure 6.1 X-ray powder diffraction patterns of saponites synthesized at different temperatures (serie 2). c = corundum.



Low temperature synthesis of ammonium-saponites from gels with variable ammonium concentrations and water content

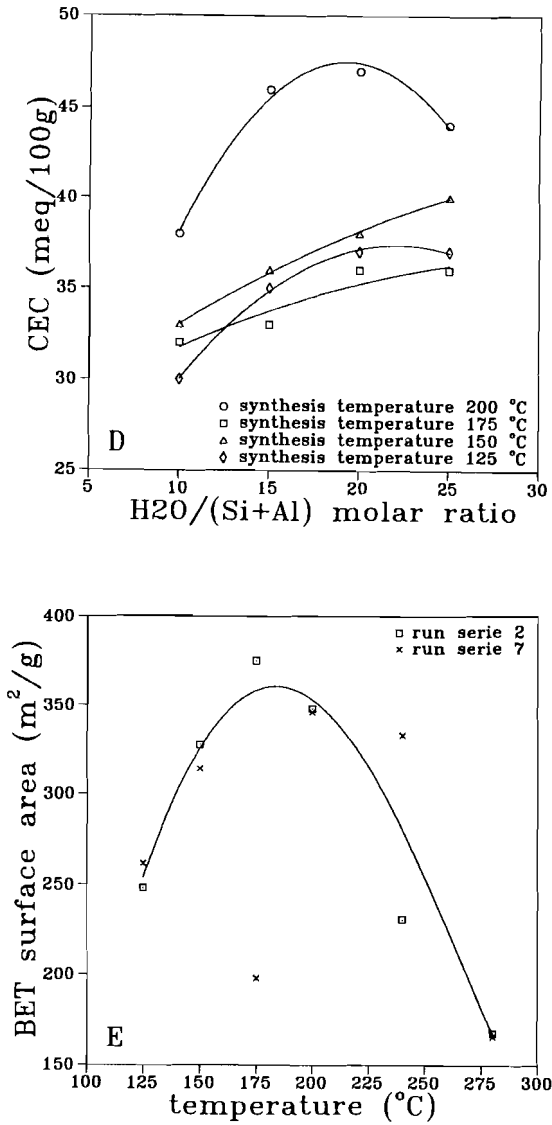


Figure 6.2(a) pH of the water after the first washing as function of the synthesis temperature; **(b)** CEC as function of the synthesis temperature; **(c)** NH₄/Al molar ratio; **(d)** H₂O/(Si + Al) molar ratio and **(e)** BET surface area as function of the synthesis temperature

6.3 RESULTS

The XRD patterns of the solid products display the diffraction pattern of saponite, with a small amount (1-3%) of corundum, α -Al₂O₃ (Fig. 6.1). The corundum is not produced during the synthesis, but is an artifact from the mortar in which the powders for the gel preparation were ground. The basal spacings of the saponites vary between 12.08 Å (7.31° 2 θ) and 12.35 Å (7.15° 2 θ). The intensity of the (001) reflection decreases with decreasing synthesis temperature. At synthesis temperatures of 200°C and lower, the (001) reflection can only be distinguished as a shoulder on the intensity of the primary X-ray beam.

The (hkl) values of the synthetic NH₄-saponite were indexed according to the values of the Kozákov saponite (Suquet et al., 1975) (Table 6.1). A discrepancy shows up in the d-values of the reflections with $l \neq 0$, because of the presence of ammonium as interlayer cation, instead of mainly Ca, which results in a higher basal spacing (Table 6.1). After sodium exchange the basal spacing of the Kozákov saponite decreases to 12.6 Å, which agrees better with the basal spacing of ammonium-saponite. Upon calcination at 550°C the basal reflection broadened and exhibited two not clearly separated maxima at 12.5 Å and 10.2 Å.

Table 6.2a and b summarizes the pH of the fluid after washing for the first time, the cation exchange capacities (CEC), and the BET surface areas of the solid products obtained. The pH decreases monotonically with increasing temperature from 125° to 200°C (Fig. 6.2a). The CEC values never represent more than 45% of the theoretical CEC of 155 meq/100 gr. A decrease in the CEC value is observed with decreasing synthesis temperature at constant water content and initial ammonium concentration (Fig. 6.2b). Higher CEC values are obtained with higher ammonium concentrations at the same synthesis temperature (Fig. 6.2c). A similar trend is observed with the water content, except for the syntheses performed at 200°C, which show a maximum at a molar H₂O/(Si + Al) ratio of 20 (Fig. 6.2d). The BET surface areas do not depend on the ammonium concentration

Low temperature synthesis of ammonium-saponites from gels with variable ammonium concentrations and water content

Table 6.2 Experimental runs at autogeneous water pressure for 72 hours.

a. gels with mol ratio $H_2O/(Si + Al) = 10$

Run	NH ₄ / Al	T (°C)	pH wash	CEC meq/ 100g	BET m ² /g
LTSAP1a	0.8	200	4.50	33	-
LTSAP1b	0.8	175	4.74	33	-
LTSAP1c	0.8	150	5.24	27	-
LTSAP1d	0.8	125	5.63	29	-
HTSAP2a	1.0	280	4.58	46	168
HTSAP2b	1.0	240	4.43	53	231
LTSAP2a	1.0	200	4.54	38	348
LTSAP2b	1.0	175	4.74	32	375
LTSAP2c	1.0	150	5.27	33	328
LTSAP2d	1.0	125	5.64	30	248
LTSAP3a	1.2	200	4.61	39	-
LTSAP3b	1.2	175	5.10	35	-
LTSAP3c	1.2	150	5.29	33	-
LTSAP3d	1.2	125	5.62	33	-
LTSAP4a	1.4	200	4.62	45	-
LTSAP4b	1.4	175	5.48	6	-
LTSAP4c	1.4	150	5.28	36	-
LTSAP4d	1.4	125	5.93	32	-

b. gels with mol ratio $\text{NH}_4/\text{Al} = 1.0$

Run	$\text{H}_2\text{O}/$ $\text{Si} + \text{Al}$	T (°C)	pH wash	CEC meq/ 100g	BET m^2/g
LTSAP5a	15	200	4.53	46	-
LTSAP5b	15	175	4.82	33	-
LTSAP5c	15	150	5.33	36	-
LTSAP5d	15	125	5.65	35	-
LTSAP6a	20	200	4.51	47	-
LTSAP6b	20	175	4.81	36	-
LTSAP6c	20	150	5.54	38	-
LTSAP6d	20	125	5.77	37	-
HTSAP7a	25	280	4.47	56	166
HTSAP7b	25	240	4.38	68	333
LTSAP7a	25	200	4.94	44	346
LTSAP7b	25	175	4.87	36	198
LTSAP7c	25	150	5.34	40	314
LTSAP7d	25	125	5.81	37	262

or water content. With increasing synthesis temperature a maximum BET surface area is observed at 175° to 200°C (Fig. 6.2e).

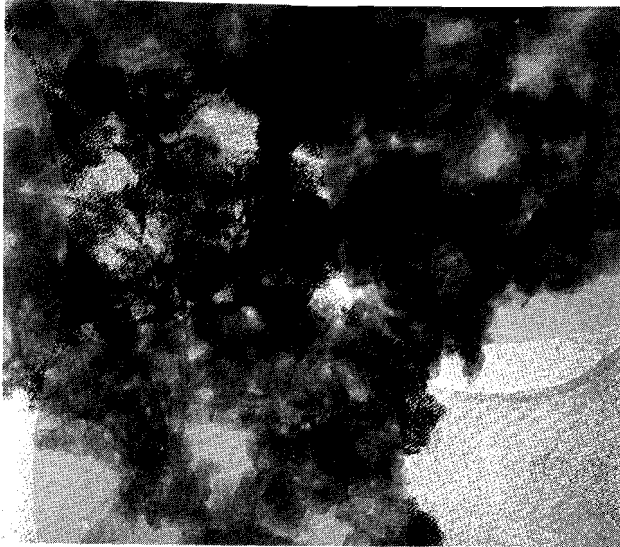
TEM illustrates that the hydrothermal product synthesized at 280°C using a molar ratio $\text{H}_2\text{O}/(\text{Si} + \text{Al})$ of 10 (HTSAP2a) consists of a homogeneous mass of small flakes of approximately 60 Å thick and 400 - 800 Å in diameter (Fig. 6.3a). Only a small amount of amorphous material is observed in HTSAP2a. With decreasing synthesis temperature the amount of amorphous material increases. At 125°C (LTSAP2d) the bulk product consists mainly of amorphous material with only a few

Low temperature synthesis of ammonium-saponites from gels with variable ammonium concentrations and water content

A



B



50 nm

Figure 6.3 Transmission electron micrographs of saponites synthesized at: (a) 280°C, $H_2O/(Si + Al) = 10$ and $NH_4/Al = 1.0$ (HTSAP2a), (b) 125°C, $H_2O/(Si + Al) = 10$ and $NH_4/Al = 1.0$ (LTSAP2d).

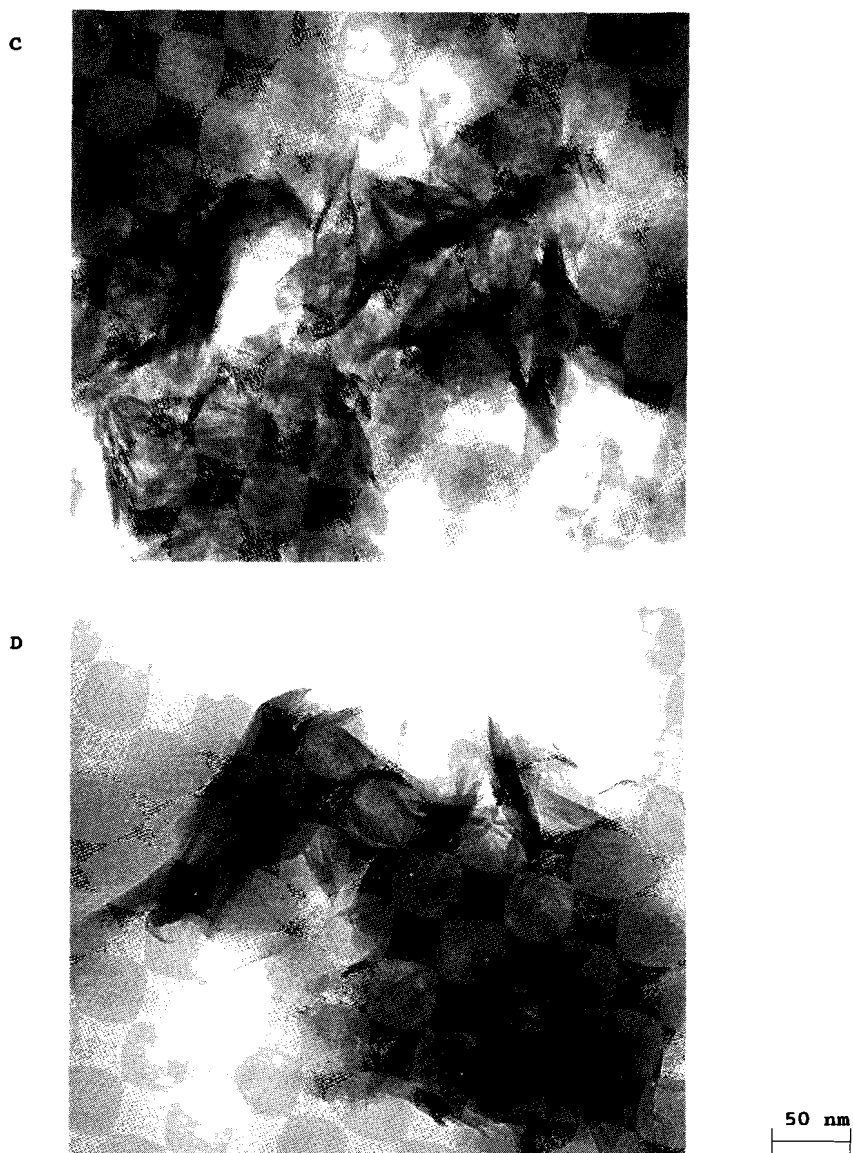


Figure 6.3 Transmission electron micrographs of saponites synthesized at: (c) 280°C, $H_2O/(Si + Al) = 10$ and $NH_4/Al = 1.4$ (HTSAP4a), (d) 280°C, $H_2O/(Si + Al) = 25$ and $NH_4/Al = 1.0$ (HTSAP7a).

Table 6.3. X-ray fluorescence analyses of the run products bulk samples < 64 μm (wt%). For comparison N analyses based on CEC determinations are given.

sample	T °C	SiO ₂	Al ₂ O ₃	MgO	N run pr.	CEC sap.	wt% sap.	CEC
HTSAP2a	280	50.0	20.5	25.0	0.77	0.66	98	0.67
HTSAP2b	240	51.1	20.7	25.5	0.78	0.77	100	0.77
LTSAP2a	200	51.1	21.5	23.7	0.67	0.55	93	0.59
LTSAP2b	175	52.2	22.0	20.2	0.72	0.46	79	0.58
LTSAP2c	150	56.5	23.2	14.9	0.78	0.48	58	0.82
LTSAP2d	125	59.7	25.5	9.6	0.89	0.43	37	1.14
HTSAP7a	280	49.8	22.7	26.2	0.71	0.81	100	0.81
LTSAP7a	200	52.8	19.3	23.1	0.79	0.64	88	0.73
LTSAP7b	175	54.5	26.1	18.2	0.77	0.52	70	0.74
LTSAP7c	150	62.7	20.9	13.1	1.09	0.58	50	1.16
LTSAP7d	125	61.0	27.1	9.5	1.10	0.54	36	1.50
theory*		52.5	15.7	31.1	2.16	2.16		

*theoretical composition $(\text{NH}_4)_{0.6}\text{Mg}_3(\text{Si}_{3.4}\text{Al}_{0.6})\text{O}_{10}(\text{OH})_2$

saponite flakes with diameters less than 200 Å (Fig. 6.3b). The thickness could not be determined, but is less than 30 Å. A rise of the ammonium concentration in the starting gel results in an increase of amorphous material. The particle size of the saponite flakes is not influenced by the ammonium concentration (Fig. 6.3c). The saponite synthesized at $\text{H}_2\text{O}/(\text{Si} + \text{Al}) = 25$ (280°C, HTSAP7a) consists of particles of approximately 110 Å thick and a diameter of 1100 Å, together with a few larger particles with a diameter up to 6500 Å and a thickness up to 470 Å (Fig. 6.3d).

The XRF analyses (Table 6.3) reveal a variation in bulk composition in the products due to the presence of amorphous material and corundum. Different

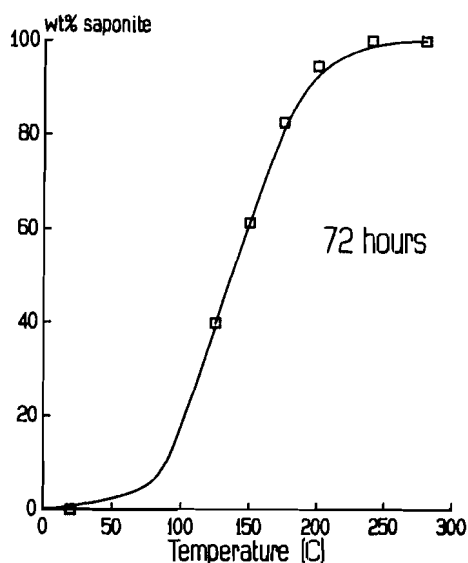


Figure 6.4 Weight percentage of saponite in the run product as function of the synthesis temperature.

concentrations of magnesium, aluminum, and silicon in the hydrothermal fluid are also reflected in the XRF bulk analyses. In all analyses higher Al and lower Mg contents are observed in comparison with the theoretical composition (52.46 wt% SiO₂, 15.72 wt% Al₂O₃, 31.05 wt% MgO, and 2.78 wt% NH₄). An increase in the Si and Al content, together with a drop in the Mg content is observed with decreasing temperature (Table 6.3). Based on the assumption that all magnesium is incorporated in the saponite, the XRF data reflect a relatively increasing amount of saponite in the products with increasing synthesis temperature (Fig. 6.4).

ICP analyses of the hydrothermal fluid (Table 6.4) from runs up to 200°C are in agreement with the XRF analyses. The fluids exhibit increasing Mg concentrations with lower synthesis temperatures (Fig. 6.5).

The infrared spectra of a characteristic sample (HTSAP2a) before and after calcination at 500°C are shown in Figure 6.6. The absorption maxima of the synthetic ammonium-saponite, natural saponite (Krugersdorp Transvaal, van der

Low temperature synthesis of ammonium-saponites from gels with variable ammonium concentrations and water content

Marel and Beutelspacher, 1976), and tobelite, an ammonium-mica (Voncken et al., 1987), are listed in **Table 6.5**. The observed absorption maxima of the synthetic saponite agree well with those of the natural saponite, although some Si-O vibrations are very weak or absent in the spectra of the synthetic saponite. The vibrations due to ammonium agree with the vibrations reported by Voncken et al.

Table 6.4. Representative ICP analyses of the hydrothermal fluid.

sample	Si ppm	Al ppm	Mg wt%
LTSAP6a	87	110	1.20
LTSAP6b	29	84	1.98
LTSAP6c	25	56	2.57
LTSAP6d	12	98	3.08

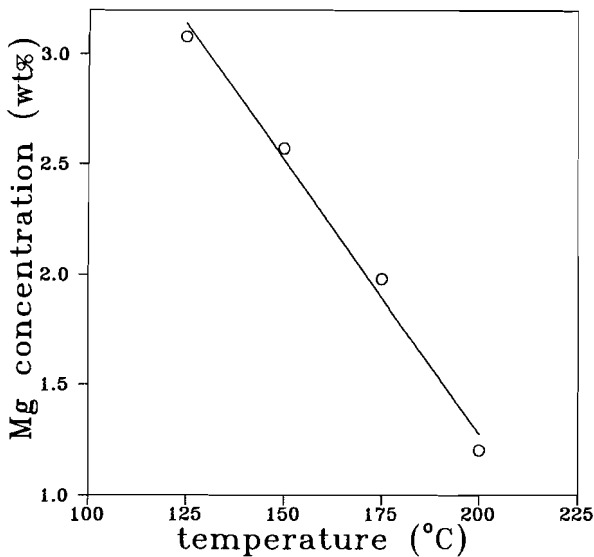


Figure 6.5 MgO concentration in the hydrothermal fluid as function of the synthesis temperature.

Table 6.5. Infrared absorption maxima of ammonium-containing saponite HTSAP2a before and after calcination at 500°C, natural saponite and synthetic tobelite.

HTSAP2a	calcined 500°C	van der Marel & Beutelspacher (1976)	Voncken et al. (1987) Tobelite
3675	3675	3680 Si-O-H	
3625	3620	3625 (Mg)Al-O-H	3630 Al-O-H stretch
3440	3450	3420 H-O-H	
3260	3260		3300 NH ₄ stretch
		3222 H-O-H	
3030			3070 NH ₄ stretch
2840			2850 NH ₄ stretch
1635	1635	1630 H-O-H	
1430			1430 NH ₄ bending
1400			
		1103 Si-O	
		1058 Si-O/Si-O-Si	
1000	1000	1005 Si-O-Al	
835	840		
780	780	750 Si-O-Al	
740			
		693 Si-O-Al	
666	670	652 Si-O-Mg	
		610 Si-O	
528		528 Si-O-Al/Mg	
		480 Si-O	
		462 Si-O-Mg	
450	450	449 Si-O-Mg	425 Si-O

(1987) for ammonium-mica, although they are systematically shifted towards lower wavenumbers.

TGA and DTA plots of HTSAP2a exhibit loss of water, due to dehydration and dehydroxylation, and loss of ammonia (Fig. 6.7). During heating to 140°C 6 wt%

Low temperature synthesis of ammonium-saponites from gels with variable ammonium concentrations and water content

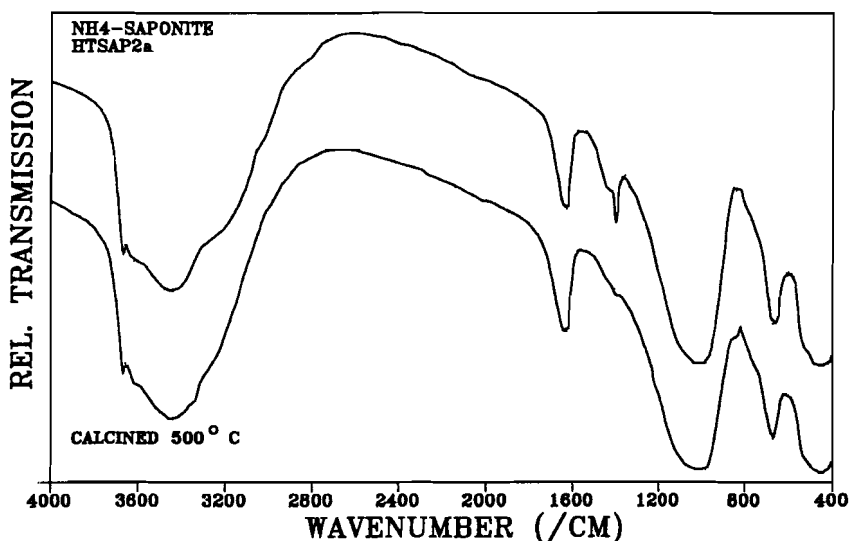


Figure 6.6 IR spectra of saponite HTSAP2a at roomtemperature (upper spectrum) and after calcination at 500°C (lower spectrum).

of absorbed water is lost. The DTA curve shows an endothermic maximum at 100°C. In the range 140° to 525°C an additional amount of 3 wt% of chemically bound water together with some ammonia is lost. The gradual loss between 525°C and 750°C is interpreted as an overlap of ammonia loss and dehydration with dehydroxylation (Kloprogge et al., 1990b). Between 750°C and 860°C the dehydroxylation reaches its maximum weight loss of 2.8 wt% . In the DTA plot the dehydroxylation is represented by an endothermic peak with its maximum at 845°C, just before the exothermic peak, due to the breakdown of saponite, at 875°C. No further weight loss is observed during breakdown.

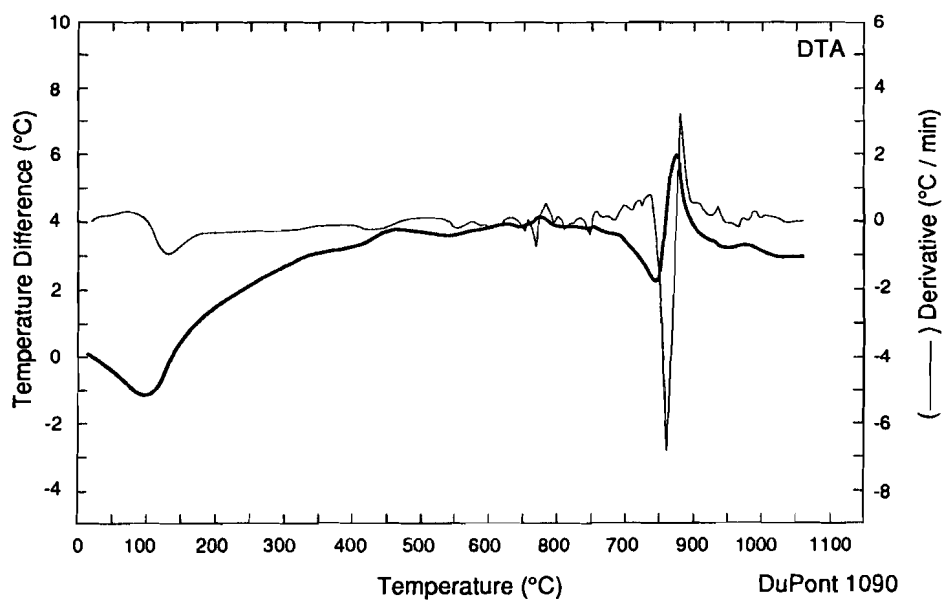
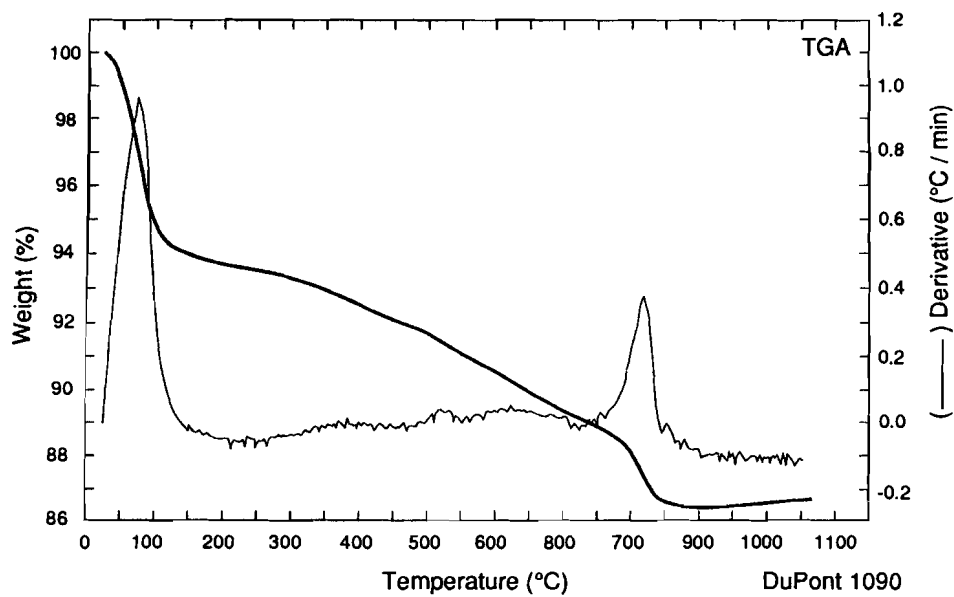


Figure 6.7 Thermogravimetric (upper) and differential thermal analyses of saponite (HTSAP2a).

6.4 DISCUSSION

6.4.1 Saponite crystallinity

The synthesis of NH_4^+ -saponite was successful in all experiments. The degree of crystallinity increases with increasing temperature as evidenced by the increasing intensities of, especially, the (001) and (060) reflections in the diffractograms. Both TEM and sharpening of the XRD reflections, especially the (001) and (060), demonstrate an increasing crystallite size and a decreasing amount of amorphous material with higher synthesis temperatures. Higher ammonium concentrations in the starting gel influence only the CEC of the product and the formation of amorphous material. In contrast to the influence of higher ammonium concentrations in the starting gel, which does not consistently affect the particle size, an increase of the water content results in an increasing particle size. It could be envisaged that the higher ammonium concentration results in an increasing pH, which causes an increasing solubility of silica from the gel. This silica does not participate in the early stage of the crystallization of saponite. During the crystallization the pH drops and the silica is precipitated as amorphous material, due to the decreased solubility. The most crystalline material is obtained at 280°C, autogeneous water pressure (\approx 63 bar), and a $\text{H}_2\text{O}/(\text{Si} + \text{Al})$ ratio of 25. This temperature and the corresponding pressure agree well with those applied by Lipsicas et al. (1984) and Iwasaki et al. (1989). In contrast, Koizumi and Roy (1959) and Suquet et al. (1977) applied much higher pressures (1 kbar and 1.5 kbar, respectively).

The XRD spectra of the saponites synthesized by Iwasaki et al. (1989) indicate a very low crystallinity in comparison with our saponites, due to their very short run times of 3 hours. Although Suquet et al. (1977) selected a run time of 15 days, they still observed a small, undetermined amount of amorphous material. As already stated by Koizumi and Roy (1959), it seems that after a certain time longer run times do not have any further effect on either the crystallite dimensions or the

saponite yield. As we applied a run time of 3 days only, we cannot ascertain whether such a limiting time exists in our experiments.

6.4.2 Saponite chemistry

The theoretical structure formulae based on the starting mixture differs substantially from the observed chemical analyses and cation exchange capacities (Table 6.3). The chemical analyses indicate a considerably higher amount of aluminum. ^{27}Al MAS NMR data (Kloprogge et al., 1992b) show the presence of excess Al^{VI} within the interlayer or within octahedral sites of the saponite structure. The rather low CEC, based on exchangeable ammonium ions only, can be explained by the presence of Al^{3+} and/or Mg^{2+} as interlayer cations. Both possibilities are in agreement with the mass and charge balance. For example, ammonium-saponites with a theoretical structure formula of $(\text{NH}_4)_{0.27}\text{Al}_{0.11}(\text{Mg})_3(\text{Si}_{3.4}\text{Al}_{0.6})\text{O}_{10}(\text{OH})_2$ and $(\text{NH}_4)_{0.27}\text{Mg}_{0.165}(\text{Mg}_{2.835}\text{Al}_{0.11}\text{vac}_{0.055})(\text{Si}_{3.4}\text{Al}_{0.6})\text{O}_{10}(\text{OH})_2$ result in exactly the same mass and charge balance. ^{27}Al MAS-NMR did not provide conclusive evidence, because interlayer Al^{3+} exhibit a resonance at approximately the same frequency as the aluminum present in the octahedral layer (Kloprogge et al., 1992b). Saponites with Mg^{2+} within the interlayer sites have a basal spacing of 15.7 Å (Suquet et al., 1977; Kloprogge et al., 1992a), which is larger than the observed basal spacing of approximately 12.3 Å. Therefore, the observed basal spacing and the doublet of the basal spacing after calcination, indicate that NH_4^+ and Al^{3+} ions reside on the exchange sites. The diffraction profile after calcination indicates the presence of H^+ , Al^{3+} , and some remaining NH_4^+ .

For the saponites produced at the higher synthesis temperatures (240°C and 280°C), the ammonium content of the products, based on the XRF data, are in reasonable agreement with the CEC values. At temperatures below 200°C the CEC values are up to 50 % lower than the XRF values (Table 6.3), indicating that ammonium resides within nonexchangeable sites, possibly of amorphous material, which is present in considerable amounts in the products of the runs performed at temperatures below 200°C.

Calculation of the magnesium distribution between the solid products after the NH_4Cl treatment and the coexisting hydrothermal fluid reveals that the amount of magnesium present in the hydrothermal fluid and in the solid state is equal to the total amount of magnesium in the gel. This is an additional indication that no Mg^{2+} was present as exchangeable cation. A too low amount of magnesium in the analyses should have been found, as the magnesium is expected to be exchanged during the NH_4Cl treatment.

6.4.3 Crystallisation model

^{27}Al MAS-NMR has shown that approximately 60 % of the aluminum, which is initially octahedrally coordinated in aluminium-triisopropylate, changes its coordination during gelation and is incorporated into the silica gel structure as tetrahedral aluminum (Kloprogge et al., 1992b). During the synthesis the pH decreases from approximately 10 to 4.5. In this range the silica is only slightly soluble, i.e., 490 ppm at pH 10.26 to 130 ppm at pH 4.2 (Yariv and Cross, 1979). The magnesium remains highly soluble within the entire pH range. Aluminum, which is incorporated in the gel structure, is only slightly soluble, whereas the aluminum not incorporated is highly soluble at high and low pH, but not in the neutral range. In agreement with the model for the crystallization of hectorite that Decarreau (1980) has proposed, it is suggested that crystallization of the saponite at temperatures above 150°C starts with the formation of the tetrahedral layer with a certain amount of aluminum substitution, which is not fixed by the amount of tetrahedral aluminum in the gel. The initial ratio Si/Al of 5.67 and the $\text{Al}^{\text{IV}}/\text{Al}^{\text{VI}}$ of 1.5 in the gel should result in a $\text{Si}/\text{Al}^{\text{IV}}$ ratio of 9.44. However, values between 5 and 5.9 are observed in the products (Kloprogge et al., 1992b), indicating that Al^{VI} is dissolved from the gel and due to the basic conditions of the hydrothermal fluid changes to Al^{IV} . At lower temperatures the substitution is not only determined by the amount of tetrahedral aluminum in the gel and the hydrothermal solution, but also by the amount of Al^{VI} captured in the amorphous phase. With higher

synthesis temperatures the rate of crystallization is higher. Syntheses at increasing temperatures and constant run time can be considered as an equivalent of syntheses at increasing run time and constant temperature. Assuming this equivalence it is possible to propose a crystallization model based on the results of this study. The intensities of the (00l) reflections increase, while the intensities of the other hk reflections remain nearly constant. Furthermore, the CEC of the saponite decreases with increasing synthesis temperature. These facts support the hypothesis that the crystallization initiates from separated sheets, which later on stack to form thicker saponite flakes. The sharpening of the XRD reflections, especially the (060), indicates that the lateral growth continues during stacking. During the crystallization the pH decreases, due to the formation of acetic acid. The remaining magnesium together with a small amount of aluminum forms octahedral brucite (and gibbsite) layers upon the available tetrahedral layers. Both XRF of the solid product and ICP measurements of the hydrothermal fluid show that during crystallization an increasing amount of magnesium is found in the product. The remaining aluminum, due to its small ionic radius combined with its high charge, is incorporated into the interlayer instead of ammonium. This model elucidates the lower (Si/Al)^{IV} ratio observed with ²⁹Si MAS-NMR (Kloprogge et al., 1992b) as compared to the starting gel and the relatively high degree of aluminum substitution in the interlayer.

ACKNOWLEDGMENTS

The authors thank A. E. de Winter for his help and advice in the laboratory and T. Zalm for the TGA and DTA analyses. M. K. Titulaer is thanked for critically reviewing this manuscript.

REFERENCES

- Decarreau, A. (1980) Cristallogène expérimentale des smectites magnésiennes: hectorite, stevensite: *Bull. Mineral.* **103**, 579-590.
- Decarreau, A. (1985) Partitioning of divalent transition elements between octahedral sheets of trioctahedral smectites and water: *Geochim. Cosmochim. Acta* **49**, 1537-1544.
- Hamilton, D. L. and Henderson, C. M. B. (1968) The preparation of silicate compositions by a gelling method: *Mineral. Mag.* **36**, 832-838.
- Hickson, D. A. (1974) Layered clay minerals, catalysts, and processes for using: *U.S. Patent 3,844,979*.
- Hickson, D. A. (1974) Layered clay minerals, catalysts, and processes for using: *U.S. Patent 3,887,454*.
- Hickson, D. A. (1974) Layered clay minerals, catalysts, and processes for using: *U.S. Patent 3,892,655*.
- Iiyama, J. T. and Roy, R. (1963) Controlled synthesis of heteropolytypic (mixed layer) clay minerals: *Clays & Clay Minerals* **10**, 4-22.
- Iwasaki, T., Onodera, Y. and Torii, K. (1989) Rheological properties of organophillic synthetic hectorites and saponites: *Clays & Clay Minerals* **37**, 248-257.
- Kloprogge, J. T., van der Eerden, A. M. J., Jansen, J. B. H. and Geus, J. W. (1990a) Hydrothermal synthesis of Na-beidellite: *Geologie en Mijnbouw*, **69**, 351-357.
- Kloprogge, J. T., Jansen, J. B. H. and Geus, J. W. (1990b) Characterization of synthetic Na-beidellite: *Clays & Clay Minerals* **38**, 409-414.
- Kloprogge, J. T., Breukelaar, J., Geus, J. W. and Jansen, J. B. H. (1992a) Characterization of Mg-saponites synthesized with gels containing small amounts of Na⁺, K⁺, Rb⁺, Ca²⁺, Ba²⁺, or Ce⁴⁺: *This Thesis Ch. IX*.

- Klopprogge, J. T., Breukelaar, J., Wilson, A. E., Geus, J. W. and Jansen, J. B. H. (1992b) Solid-state nuclear magnetic resonance spectroscopy on synthetic saponites: aluminum on the interlayer site: *This Thesis Ch. VII*.
- Koizumi, M. and Roy, R. (1959) Synthetic montmorillonoids with variable exchange capacity: *Amer. Mineral.* **44**, 788-805.
- Lipsicas, M., Raythatha, R. H., Pinnavaia, T. J., Johnson, I. D., Giese, R. F. Jr., Costanzo, P. M. and Roberts, J.-L. (1984) Silicon and aluminium site distributions in 2:1 layered silicate clays: *Nature* **309**, 604 -607.
- van der Marel, H. W. and Beutelspacher, H. (1976) *Atlas of Infrared Spectroscopy of Clay Minerals and their Admixtures*: Elsevier, Amsterdam, 396 pp.
- Plee, D., Gatineau, L. and Fripiat, J. J. (1987) Pillaring processes of smectites with and without tetrahedral substitution: *Clays & Clay Minerals* **35**, 81-88.
- Sanz, J. and Serratos, J. M. (1984) ^{29}Si and ^{27}Al high-resolution MAS-NMR spectra of phyllosilicates: *J. Amer. Ceram. Soc.* **106**, 4790-4793.
- Schutz, A., Stone, W. E. E., Poncelet, G. and Fripiat, J. J. (1987) Preparation and characterization of bidimensional zeolitic structures obtained from synthetic beidellite and hydroxy-aluminum solutions: *Clays & Clay Minerals* **35**, 251-261.
- Shabtai, J., Rosell, M. and Tokarz, M. (1984) Cross-linked smectites. III. Synthesis and properties of hydroxy-aluminum hectorites and fluorhectorites: *Clays & Clay Minerals* **32**, 99-107.
- Sterte, J. and Shabtai, J. (1987) Cross-linked smectites. V. Synthesis and properties of hydroxy-silicoaluminum montmorillonites and fluorhectorites: *Clays & Clay Minerals* **35**, 429-439.
- Suquet, H., Iiyama, J. T., Kodama, H. and Pezerat, H. (1977) Synthesis and swelling properties of saponites with increasing layer charge: *Clays & Clay Minerals* **25**, 231-242.
- Suquet, H., De La Çalle and Pezerat, H. (1975) Swelling and structural organization of saponite: *Clays & Clay Minerals* **23**, 1-9.
- Torii, K. and Iwasaki, T. (1987) Synthesis of hectorite: *Clay Science* **7**, 1- 16.

Low temperature synthesis of ammonium-saponites from gels with variable ammonium concentrations and water content

- Voncken, J. H. L., Wevers, J. M. A. R., Van der Eerden, A. M. J., Bos, A. and Jansen, J. B. H. (1987) Hydrothermal synthesis of tobelite, $\text{NH}_4\text{Al}_2\text{Si}_3\text{O}_{10}(\text{OH})_2$, from various starting materials and implications for its occurrence in nature: *Geologie en Mijnbouw* **66**, 259-269.
- Woessner, D. E. (1989) Characterization of clay minerals by ^{27}Al nuclear magnetic resonance spectroscopy: *Amer. Mineral.* **74**, 203-215.
- Yariv, S. and Cross, H. (1979) *Geochemistry of Colloid Systems for Earth Scientists*, Springer Verlag, Berlin, 450 pp.

CHAPTER VII

SOLID-STATE NUCLEAR MAGNETIC RESONANCE SPECTROSCOPY ON SYNTHETIC AMMONIUM-SAPONITES; ALUMINUM ON THE INTERLAYER SITE

ABSTRACT

Using ^{27}Al and ^{29}Si solid-state Magic-Angle Spinning NMR techniques it is demonstrated that synthetic ammonium-saponites have a rather constant Si/ Al^{IV} ratio (≈ 5.5) and an $\text{Al}^{\text{VI}}/\text{Al}^{\text{IV}}$ ratio, which varies between 1.5 and 3.8. The above ratios are independent of the synthesis temperature, although an increasing amount of Si, N and to a lesser extent, Al are incorporated in an amorphous phase. ^{27}Al MAS-NMR is unable to differentiate between Al at octahedral and Al^{3+} at interlayer sites. CEC, XRD and the inability to swell prove the Al^{VI} to be mainly on the interlayer sites. Based on the ammonium exchange capacity, X-ray fluorescence, ^{27}Al and ^{29}Si MAS-NMR it is possible to calculate a relatively accurate structural formula.

7.1 INTRODUCTION

Saponite is a trioctahedral 2:1 phyllosilicate, which is composed of sheets formed by a central octahedral sublayer containing predominantly magnesium ions sharing oxygens with two Si-containing tetrahedral sublayers on both sides. A negative charge is created by isomorphous substitution of Si by aluminum in the tetrahedral sublayers. This negative charge may be compensated by cations, such as, Na^+ , K^+ , Ca^{2+} , in the interlayer separating successive sheets (Fig. 7.1). Aluminum can also substitute magnesium in the octahedral sublayer following the muscovite substitution: $3\text{Mg} = 2\text{Al} + \text{vacancy}$, without creation of a positive charge. Suquet et al. (1981), on the other hand, suggest a substitution of $1\text{Mg} = 1\text{Al}$ creating a positive charge, which compensates a negative charge of the tetrahedral sublayer, instead of an interlayer cation. Additionally both Al^{3+} and Mg^{2+} can be present as

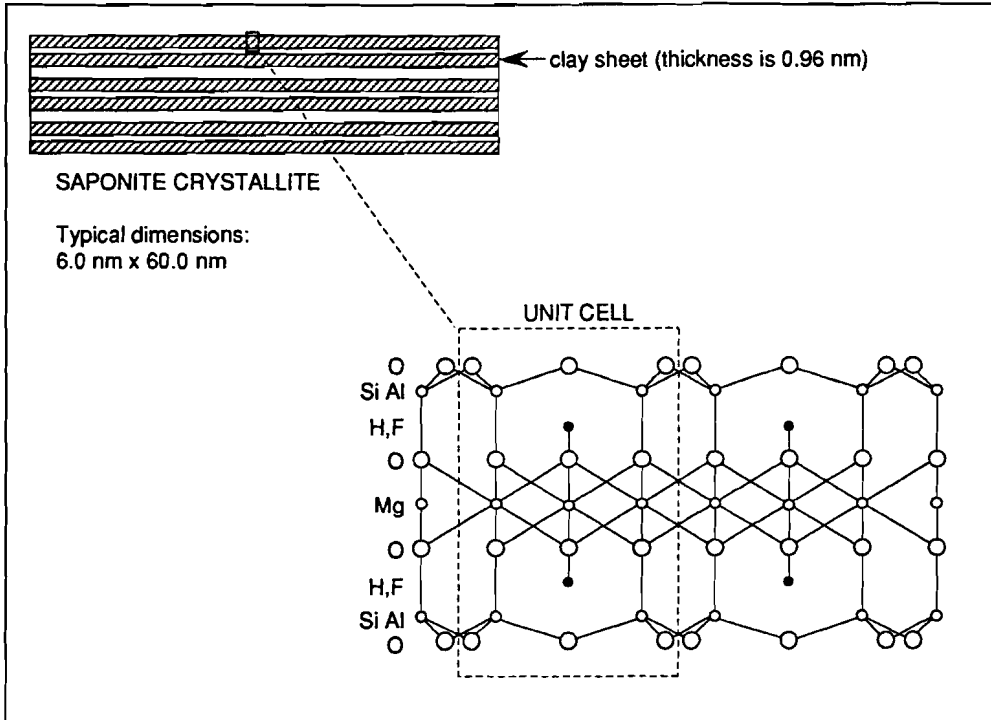


Figure 7.1 [010] view of a trioctahedral 2:1 phyllosilicate structure.

interlayer cation.

Usual techniques, such as, XRD, XRF, IR or TGA/DTA, are unable to determine the precise distribution of the aluminum in saponites. In recent years Magic Angle Spinning Nuclear Magnetic Resonance (MAS-NMR) spectroscopy has proven to be a powerful tool to obtain such structural information (Sanz and Serratosa, 1984; Kinsey et al., 1985, Woessner, 1989).

With ^{29}Si MAS-NMR it has been demonstrated that the resonance positions (chemical shifts) of silicon atoms are dependent on the branching of the silicon atoms and on the degree of tetrahedral aluminum substitution in the second coordination sphere (Wilson, 1987). Silicon atoms of sheet silicates exhibit

resonances between -91 and -102 ppm, while each aluminum substitution causes an additional chemical shift downfield of approximately 5 - 6 ppm (Lippmaa et al., 1980; Kirkpatrick et al., 1985). These ^{29}Si spectra offer the possibility to establish the extent of the tetrahedral substitution $\text{Si}/(\text{Si} + \text{Al}^{\text{IV}})$ in clay structures.

The relevance of magic angle spinning at high field strength is the possibility to observe the $+1/2 \leftrightarrow -1/2$ transition of the quadrupolar nucleus ^{27}Al , which has a spin 5/2. In general octahedral aluminum and tetrahedral aluminum show resonances in the ranges 0 - 30 ppm and 50 - 90 ppm, respectively (Wilson, 1987). Due to quadrupolar effects the determination of the $\text{Al}^{\text{IV}}/\text{Al}^{\text{VI}}$ ratio is less accurate than that of the $\text{Si}/\text{Al}^{\text{IV}}$ ratio.

The aim of this study is to characterize the aluminum and magnesium substitutions in ammonium-saponites synthesized by Klopogge et al. (1991) by means of Magic Angle Spinning Nuclear Magnetic Resonance Spectrometry, for the purpose of establishing the structural formulae.

7.2 EXPERIMENTAL SECTION

7.2.1 Saponite synthesis

Saponite samples were synthesized using a gel prepared of amorphous silica, magnesium acetate, aluminum triisopropylate, and ammonium hydroxide. The saponites resulting from a hydrothermal treatment were characterized by means of XRD, XRF, TEM, ICP, and TGA/DTA (Klopogge et al., 1991). Some physical characteristics are given in Table 7.1. The synthesis temperature was varied between 125°C and 280°C. The initial molar Si/Al ratio in the starting mixture was constant at 5.67 and NH_4^+ was supposed to become interlayer cation. The small amount (<3 %) of corundum in all run products is an artifact caused by the preparation method applied (Klopogge et al., 1992).

Table 7.1 Products, Cation Exchange Capacities (CEC), and basal spacings of the saponites examined in this study.

Sample	T(°C)	Products ¹	CEC ² meq/mol	d ₀₀₁ (sap) (Å)
HTSAP2a	280	NH ₄ -sap + cor	183	12.2
HTSAP2b	240	NH ₄ -sap + cor	206	12.3
LTSAP2a	200	NH ₄ -sap + cor + am	159	12.3
LTSAP2b	175	NH ₄ -sap + cor + am	156	12.3
LTSAP2c	150	NH ₄ -sap + cor + am	221	12.3

¹ sap = saponite; cor = corundum; am = amorphous material.

² CEC only based on NH₄

7.2.2 Solid-State NMR

²⁹Si solid-state MAS-NMR spectra were recorded at 59.62 MHz on a Bruker CXP-300 spectrometer (magnetic field 7.05 T). ²⁷Al solid-state MAS-NMR spectra were obtained on a Bruker WM-500 spectrometer (130.32 MHz, magnetic field 11.7 T). Both instruments apply a sample spinning rate of approximately 14 kHz. Normally approximately 4500 Free Induction Decays (FIDs) were accumulated for the ²⁹Si spectra and 3000 FIDs were accumulated at a repetition time of 0.8 s for the ²⁷Al spectra. Chemical shifts are given in ppm relative to tetramethylsilane (TMS) and [Al(H₂O)₆]³⁺, respectively. Upfield shifts are taken to be negative. Due to the fact that the spectra were recorded with a shielded aluminum-free probe, no correction was needed for background signals.

7.3 RESULTS AND DISCUSSION

The samples were identified mainly as NH_4 -saponite, with a basal spacing between 12.0 and 12.3 Å, containing 1-3 % corundum. At lower synthesis temperatures, a gradually increasing amount of mainly Si-containing amorphous material as impurities (Kloprogge et al., 1992) was observed.

Solid-state ^{27}Al NMR enables one to differentiate between tetrahedrally and octahedrally coordinated aluminum. The ^{27}Al NMR spectra show octahedral resonances between 4.5 ppm and 9.5 ppm and tetrahedral resonances between 55 ppm and 70 ppm (Fig. 7.2a). Analogous to other clay minerals (Woessner, 1989) the 65.9 ppm and 4.8 ppm resonances are therefore assigned to tetrahedral and octahedral aluminum in the synthetic saponite, respectively. Exchange experiments of ammonium-saponite with $\text{Al}(\text{NO}_3)_3$ have shown that ^{27}Al NMR can not discriminate between aluminum on octahedral sites and on interlayer sites (Fig. 7.2b). Aluminum exchanged beidellite, in comparison, exhibits a resonance of octahedral aluminum (about 3 ppm) together with a recognizable shoulder due to interlayer aluminum (about -3 ppm) (Diddams et al., 1984). The presence of aluminum at interlayer sites is indicated by (i) the measured low ammonium exchange measurements, (ii) no measurable Mg^{2+} exchange (Kloprogge et al., 1992), and (iii) the inability to swell in water. The 58.3 ppm resonance is comparable to the tetrahedral resonance at 57.3 ppm of the starting gel (Fig. 7.2c) and is interpreted to be aluminum present in the amorphous phase. The remaining resonance at 9.3 ppm is assigned to corundum, $\alpha\text{-Al}_2\text{O}_3$ (John et al., 1983), which has only octahedral aluminum in its structure. Due to the fact that aluminum has a quadrupolar nucleus, the $\text{Al}^{\text{IV}}:\text{Al}^{\text{VI}}$ ratio being less precise than the $\text{Si}/\text{Al}^{\text{IV}}$ ratio based on ^{29}Si NMR is roughly estimated only. Fortunately, the inaccuracy due to spinning sidebands is excluded in a high magnetic field (11.7 T) and with a high sample spin frequency (14 kHz). Table 7.2 lists the $\text{Al}^{\text{IV}}:\text{Al}^{\text{VI}}$ ratio of the run products and the percentages of total aluminum present in the mentioned phases.

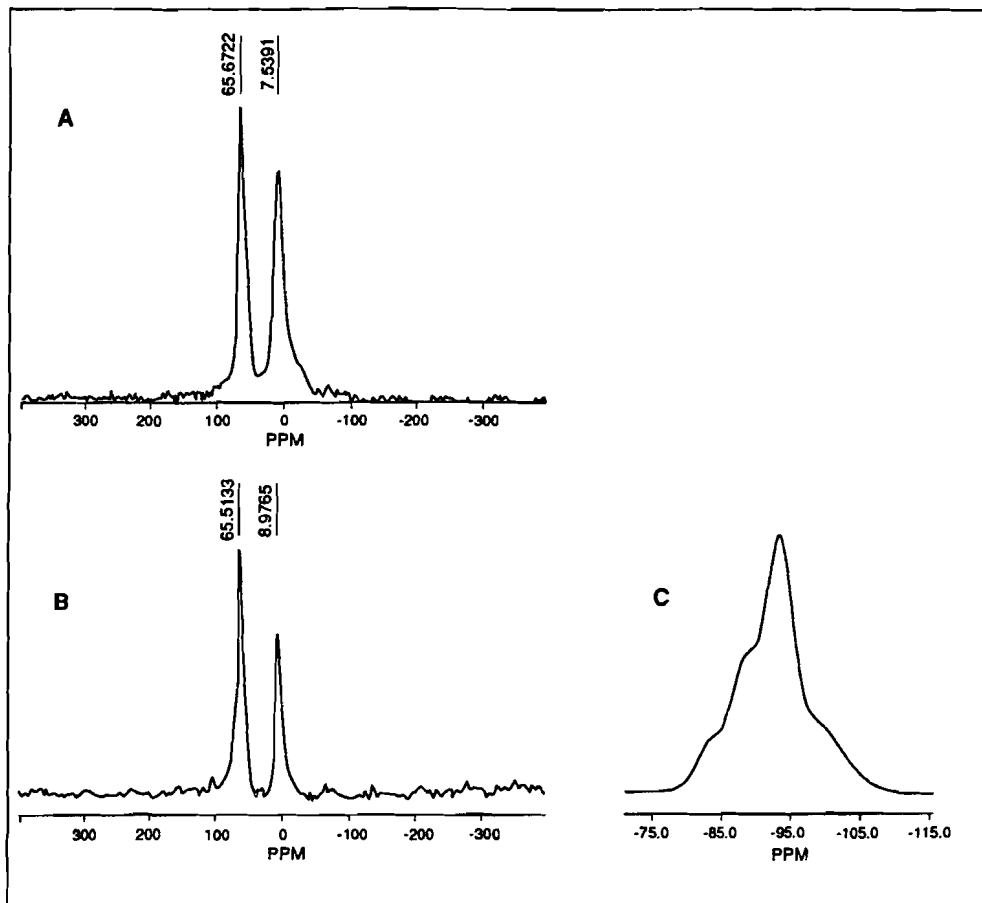


Figure 7.2 a) ^{27}Al MAS-NMR spectrum of NH_4 -saponite, b) ^{27}Al MAS-NMR spectrum of an Al^{3+} -exchanged saponite, and c) ^{28}Si MAS-NMR spectrum of NH_4 -saponite.

Table 7.2 Aluminum distribution in percentages of total aluminum in the NH₄-saponite samples based on ²⁷Al MAS-NMR spectra.

Sample	saponite		Al ^{IV} :Al ^{VI}	Amorphous	Corundum
	Al ^{IV}	Al ^{VI}			
HTSAP2a	64	17	3.8	0	19
HTSAP2b	61	20	3.1	0	18
LTSAP2a	60	21	2.9	0	19
LTSAP2b	49	14	3.5	22	15
LTSAP2c	32	21	1.5	36	10

²⁹Si MAS-NMR spectra reveal three resonances of silicon atoms coordinated with one or more next nearest tetrahedral aluminum atoms in the tetrahedral sublayer of the saponite structure. The resonance with the highest intensity is located at -93.1 ± 0.4 ppm. In addition, a shoulder at -88.5 ± 0.4 ppm and a small shoulder at -83.2 ± 1.2 ppm can be clearly identified. According to results on other synthetic trioctahedral clays by Lipsicas et al. (1984) the -93.1 ppm signal is attributed to Si(0Al), while the two shoulders at -88.5 ppm and -83.2 ppm are assigned to Si(1Al) and Si(2Al), respectively (Fig. 7.2c). An additional resonance can be observed at -102 ppm, which is due to amorphous material.

Similar to zeolites, the fraction of tetrahedral Al(1Al) linkages and Si(2Al) linkages can be calculated (Lipsicas et al., 1984). If Loewensteins avoidance principle holds (Loewenstein, 1954), the fraction of tetrahedral Al(1Al) linkages should be zero. The tetrahedral aluminum substitution can be calculated directly from the ²⁹Si NMR spectra with the expression (Sanz and Serratosa, 1984)

$$(\text{Si}/\text{Al})^{\text{IV}} = \frac{\sum_{n=0}^3 I_{\text{Si}(n\text{Al})}}{\sum_{n=0}^3 (n/3) I_{\text{Si}(n\text{Al})}} \quad (1)$$

Table 7.3 Si distribution in percentages of total Si and ^{29}Si MAS-NMR line intensities and tetrahedral site distribution parameters of the saponites.

Sample	$I_{\text{Si(0Al)}}$	$I_{\text{Si(1Al)}}$	$I_{\text{Si(2Al)}}$	fraction Al(1Al)	fraction Si(2Al)	Si/Al ^{IV}
HTSAP2a	0.494	0.442	0.064	0.05	0.05	5.3
HTSAP2b	0.652	0.160	0.188	0.05	0.18	5.6
LTSAP2a	0.517	0.378	0.105	0.06	0.08	5.1
LTSAP2b	0.590	0.310	0.100	0.04	0.08	5.9
LTSAP2c	0.568	0.332	0.100	0.05	0.08	5.6

Line intensities obtained by fitting the spectra to three independent Gaussian lines using a least-squares method.

am. = amorphous Si; sap. = ammonium-saponite

The values of the experimental ^{29}Si NMR line intensities and site distribution parameters are given in Table 7.3. The very small fraction of Al(1Al) linkages indicates that the distribution of aluminum in the tetrahedral sheet is close to statistical (Alma et al., 1984).

The ^{29}Si chemical shifts depend on the total layer charge and the tetrahedral rotation within the a-b plane. The correlation between the chemical shift δ of Si(0Al) and mean Si-O-Si bond angle θ can be represented by (Wilson, 1987)

$$\delta_{\text{Si(0Al)}} \text{ (ppm)} = -0.619 \theta - 18.7 \text{ ppm} \quad (2)$$

The average deviation α of the Si-O-Si bond angle θ from hexagonal symmetry ($\theta = 109.47^\circ$) enables one to determine b_{NMR} with the relationship (Weiss et al., 1987)

$$\cos \alpha = \frac{b_{\text{NMR}}}{b_{\text{ideal}}} \quad (3)$$

with b_{ideal} being defined by Guggenheim (1984) as

Table 7.4 ^{29}Si MAS-NMR data and structural parameters, based on the relations (2), (3), (4) and (5), of NH_4 -saponites examined in this study.

Sample	$\delta_{\text{Si(OAl)}}$ ppm	$\theta^{\circ}_{\text{obe}}$	$\alpha^{\circ}_{\text{obe}}$	b_{ideal}		b_{NMR}		b_{XRD}
				(Å) ¹	(Å) ²	(Å) ¹	(Å) ²	(Å)
HTSAP2a	-92.6	119.39	9.92	9.267	9.219	9.128	9.081	9.188
HTSAP2b	-92.8	119.71	10.24	9.261	9.217	9.113	9.070	9.174
LTSAP2a	-93.7	121.16	11.69	9.270	9.220	9.078	9.029	9.184
LTSAP2b	-93.0	120.03	10.56	9.254	9.208	9.097	9.052	9.175
LTSAP2c	-93.4	120.68	11.21	9.261	9.212	9.084	9.036	9.175

¹ based on Guggenheim (1984)

² based on Suquet et al. (1981)

$$b(\text{Si}_{1-x}\text{Al}_x) = 9.15 - 0.74x \quad (4)$$

An alternative way to determine b_{ideal} is offered by the relationship formulated by Suquet et al. (1981)

$$b_{\text{ideal}} = 9.174 + 0.079 \text{Al}^{\text{IV}} - 0.07\text{Al}^{\text{VI}} \quad (5)$$

with Al^{IV} measured by ^{29}Si NMR and Al^{VI} with ^{27}Al NMR. The above mentioned relations provide an estimation of b_{NMR} , following either Guggenheim (4) or Suquet et al. (5) from the ^{29}Si NMR data. The latter values can be compared with b_{XRD} from XRD data (Table 7.4). The b_{NMR} values based on the ^{29}Si and ^{27}Al NMR data obtained with both procedures are considerably smaller than the b-values observed by XRD. The relation (5) derived by Suquet et al. (1981) is based on the assumption of a one-to-one $\text{Mg}^{2+} \leftrightarrow \text{Al}^{3+}$ substitution instead of the normally occurring muscovite substitution $3\text{Mg}^{2+} \leftrightarrow 2\text{Al}^{3+} + 1$ vacancy, which substitution is followed in relation (4).

Table 7.5 Structural formula of the NH₄-saponite, based on the Si/Al^{IV} and Al^{IV}/Al^{VI} ratio's, CEC values and assuming that all magnesium is incorporated in the saponite structure.

Sample	unit cell structural formula
HTSAP2a	(NH ₄) _{0.18} Al _{0.15} (Mg _{2.97} Al _{0.02} vac _{0.01})(Si _{3.37} Al _{0.63})O ₁₀ (OH) ₂
HTSAP2b	(NH ₄) _{0.21} Al _{0.13} (Mg _{2.90} Al _{0.06} vac _{0.03})(Si _{3.40} Al _{0.60})O ₁₀ (OH) ₂
LTSAP2a	(NH ₄) _{0.18} Al _{0.16} (Mg _{2.94} Al _{0.04} vac _{0.02})(Si _{3.35} Al _{0.65})O ₁₀ (OH) ₂
LTSAP2b	(NH ₄) _{0.18} Al _{0.13} (Mg _{2.95} Al _{0.03} vac _{0.02})(Si _{3.44} Al _{0.56})O ₁₀ (OH) ₂
LTSAP2c	(NH ₄) _{0.22} Al _{0.13} (Mg _{2.59} Al _{0.27} vac _{0.14})(Si _{3.40} Al _{0.60})O ₁₀ (OH) ₂

Recalculation of α based on b_{XRD} and b_{ideal} (4) results in a small correction of relation (2)

$$\delta_{\text{Si(OAl)}} \text{ (ppm)} = -0.619 \theta - 20.6 \pm 0.4 \text{ ppm} \quad (6)$$

whereas recalculation based on b_{ideal} (5) results in a slightly larger correction of relation (2)

$$\delta_{\text{Si(OAl)}} \text{ (ppm)} = -0.619 \theta - 22.2 \pm 0.5 \text{ ppm} \quad (7)$$

Wilson (1987) already indicated that depending on the input data, slightly different relations can be found. The somewhat smaller correction in relation (6) supports the use of the muscovite substitution in further calculations of the structural formula. The Al^{IV}/Al^{VI} and Si/Al^{IV} ratios based on the ²⁷Al and ²⁹Si NMR spectra enables one to calculate the structural formulae of the synthesized saponites, which are in agreement with the chemical data given by Klopogge et al. (1992). Based on these data and the assumptions that the amount of N determined by the ammonium exchange capacity and all magnesium present in the run products are incorporated in the saponite structure (Table 7.5b), it is possible to calculate the structural formulae.

Based on the observations that at decreasing synthesis temperature i) increasing amounts of silicium, aluminum, and nitrogen are found, ii) a positive correlation exists between the contents of amorphous silica and nitrogen, and iii) the amount

of exchangeable ammonium decreases, it is suggested that with decreasing synthesis temperatures an increasing amount of N, but not as exchangeable ammonium, is bound to the silica in the amorphous phase.

REFERENCES

- Alma, N. C. M., Hays, G. R., Samoson, A. V. and Lippmaa, E. T. (1984) Characterization of Synthetic Dioctahedral Clays by Solid-State Silicon-29 and Aluminum-27 Nuclear Magnetic Resonance Spectrometry: *Anal. Chem.* **56**, 729-733.
- Diddams, P. A., Thomas, J. M., Jones, W., Ballantine, J. A. and Purnell, J. H. (1984) Synthesis, Characterization, and Catalytic Activity of Beidellite-Montmorillonite Layered Silicates and their Pillared Analogues: *J. Chem. Soc., Chem. Commun.* 1984, 1340-1342.
- Guggenheim, S. (1984) The Brittle Micas: in *Micas, Reviews in Mineralogy* **13**, S. W. Bailey ed., Mineralogical Society of America, 61-104.
- John, C. S., Alma, N. C. M. and Hays, G. R. (1983) Characterization of Transitional Alumina by Solid-State Magic Angle Spinning Aluminium NMR: *Appl. Catal.* **6**, 341-346.
- Kinsey, R. A., Kirkpatrick, R. J., Hower, J., Smith, K. A. and Oldfield, E. (1985) High Resolution Aluminum-27 and Silicon-29 Nuclear Magnetic Resonance Spectroscopic Study of Layer Silicates, including Clay Minerals: *Amer. Mineral.* **70**, 537-548.
- Kirkpatrick, R. J., Smith, K. A., Schramm, S., Turner, G. and Yang, W.-H. (1985) Solid-State Nuclear Magnetic Resonance Spectroscopy of Minerals: *Ann. Rev. Earth Planet. Sci.* **13**, 29-47.
- Kloprogge, J. T., Breukelaar, J., Jansen, J. B. H. and Geus, J. W. (1992) Low Temperature Synthesis of Ammonium-Saponites from Gels with variable

- Ammonium Concentrations and Water Contents: *This Thesis Ch VI, Clays & Clay Minerals*, accepted.
- Lippmaa, E., Mägi, M., Samoson, A., Engelhardt, G. and Grimmer, A.-R. (1980) Structural Studies of Silicates by Solid-State High-Resolution ^{29}Si NMR: *J. Amer. Chem. Soc.* **102**, 4889-4893.
- Lipsicas, M., Raythatha, R. H., Pinnavaia, T. J., Johnson, I. D., Giese, R. F. Jr., Costanzo, P. M. and Roberts, J.-L. (1984) Silicon and Aluminium Site Distributions in 2:1 Layered Silicate Clays: *Nature* **309**, 604-607.
- Loewenstein, W. (1954) The Distribution of Aluminum in the Tetrahedra of Silicates and Aluminates: *Amer. Mineral.* **39**, 92-96.
- Sanz, J. and Serratosa, J. M. (1984) ^{29}Si and ^{27}Al High-Resolution MAS-NMR Spectra of Phyllosilicates: *J. Amer. Chem. Soc.* **106**, 4790-4793.
- Suquet, H., Malard, C., Copin, E. et Pezerat, H. (1981) Variation du Parametre b et de la Distance Basale d_{001} dans une Serie de Saponites a Charge Croissante: I Etats Hydrates: *Clay Minerals* **16**, 53-67.
- Weiss, C. A., Altaner, S. P. and Kirkpatrick, R. J. (1987) High Resolution ^{29}Si NMR Spectroscopy of 2:1 Layer Silicates: Correlation among Chemical Shift, Structural Distortions, and Chemical Variations: *Amer. Mineral.* **72**, 935-942.
- Wilson, M. A. (1987) *NMR Techniques and Applications in Geochemistry and Soil Chemistry*. Pergamon Press, Oxford, 353 pp.
- Woessner, D. E. (1989) Characterization of Clay Minerals by ^{27}Al Nuclear Magnetic Resonance Spectroscopy: *Amer. Mineral.* **74**, 203-215.

CHAPTER VIII

HYDROTHERMAL CRYSTALLIZATION OF AMMONIUM-SAPONITE AT 200 °C AND AUTOGENEOUS WATER PRESSURE

ABSTRACT

The effects of the reaction time (2 to 72 hours) and the $\text{NH}_4^+/\text{Al}^{3+}$ molar ratio (1.6, 2.4, and 3.2) on the hydrothermal synthesis of ammonium-saponites are investigated. The gels are obtained by mixing powders, resulting in a stoichiometric composition $\text{Mg}_3\text{Si}_{3.4}\text{Al}_{0.8}\text{O}_{10}(\text{OH})_2$, with aqueous ammonium solutions, with and without F, to result in initial $\text{NH}_4^+/\text{Al}^{3+}$ molar ratios of 1.6, 2.4, and 3.2. The solid bulk products are characterized by X-ray Diffraction, X-ray Fluorescence, and Scanning Electron Microscopy combined with energy-dispersive analysis. The cation exchange capacity (CEC) is determined with an ammonia selective electrode and the pH of the water from the first washing is measured. Ammonium-saponite is formed rapidly within 16 hours. A higher $\text{NH}_4^+/\text{Al}^{3+}$ molar ratio and the presence of F facilitate the crystallization of saponite. Small metastable amounts of bayerite, $\text{Al}(\text{OH})_3$, present at low $\text{NH}_4^+/\text{Al}^{3+}$ molar ratios and after short reaction times disappear upon raising synthesis time. During the first 4 hours the pH decreases rapidly, to drop subsequently slowly to a constant level of approximately 4.6 after 60 hours. With increasing reaction time saponite crystallites particularly grow in the a-b directions of the individual sheets with almost no stacking to thicker flakes. The NH_4^+ CEC of the solid products increases strongly within the first 24 hours. A maximum of 53.3 meq/100 g is observed. The saponite yield increases from approximately 25 % after 2 hours to almost 100 % after 72 hours.

8.1 INTRODUCTION

In recent years the interest has increased in the synthesis of smectites, such as, beidellite (Plee et al., 1987; Schutz et al., 1987; Klopogge et al., 1990a,b), (fluor)hectorite (Shabtai et al., 1984; Sterte and Shabtai, 1987), and saponite (Suquet et al., 1977; Klopogge et al., 1992a,b), because of their high purity and adjustable composition. The smectites can be applied as catalysts and molecular sieves.

At temperatures ranging from 125° to 280°C Kloprogge et al. (1992a,b) have synthesized ammonium-saponite within 72 hours. They proposed a crystallization model, in which the crystallization starts with the growth of individual sheets. During the synthesis individual sheets apparently stack to thick flakes, while lateral growth more slowly continues.

A major problem with the synthesis is the incorporation of aluminum into the saponite structure. Theory predicts all Al^{3+} to be present at the tetrahedral sites replacing Si^{4+} , but actually Al^{3+} is additionally built in at octahedral and even at interlayer sites, instead of Mg^{2+} and NH_4^+ , respectively. The resulting incorporation of an excess of aluminum influences disastrously the physico-chemical properties of the saponite, such as, layer charge, swelling, cation exchange, and acidity. Incorporation of Al^{3+} at other sites than the tetrahedral sites may be avoided by raising the ammonium concentration.

The aims of this study are 1) to characterize the ammonium-saponite crystallites grown for increasing periods of time at constant temperature and pressure, in order to elucidate when and under which conditions aluminum is incorporated at octahedral and interlayer sites 2) to monitor the development of the size and the stacking of the individual sheets as a function of synthesis time to corroborate the sheets stacking model of Kloprogge et al. (1992a), and 3) to force Al^{3+} exclusively into the tetrahedral sites and ammonium into the interlayer sites by varying i) the $\text{NH}_4^+/\text{Al}^{3+}$ molar ratio, ii) the starting chemicals, and iii) by addition of F.

8.2 EXPERIMENTAL METHODS

8.2.1 Saponite synthesis

Gels are prepared from homogeneous mixtures of stoichiometric amounts of the powdered compounds listed in Table 8.1, subsequently mixed with the desired amounts of aqueous solutions of ammonium chloride or ammonium

Table 8.1 List of used chemicals.

SiO ₂	Amorphous Silica, Baker no. 0254.
SiO ₂ /Al ₂ O ₃	Amorphous Silica/alumina, CLA 26554.
Al[OCH(CH ₃) ₂] ₃	Aluminum-triisopropoxide, Merck no. 801079.
Al(NO ₃) ₃ ·9H ₂ O	Aluminum-nitrate-nonahydrate, Merck no. 2437832.
(CH ₃ COO) ₂ Mg·4H ₂ O	Magnesium-acetate-tetrahydrate, Merck no. 5819.
Mg(NO ₃) ₂ ·6H ₂ O	Magnesium-nitrate-hexahydrate, Baker no. 0164.
Mg(OH) ₂	Magnesium-hydroxide, Venton no. 89184.
NH ₄ OH (25%)	Ammonium-hydroxide solution, Baker no. 6051.
NH ₄ Cl	Ammonium-chloride, Baker no. 0018.
NH ₄ F	Ammonium-fluoride, Baker no. 0023.
NaOH	Sodium-hydroxide, Merck no. 6498.
H ₂ O	Demineralized and double distilled water.

fluoride. The Al compound is dissolved into the ammonium solution before mixing with the powdered Si and Mg compounds. Due to the high pH level of the ammonium solution, all dissolved Al³⁺ will be fourfold coordinated, which is required for incorporation at tetrahedral sites in saponites. The theoretical composition of the ammonium-saponite is (NH₄)_{0.6}Mg₃Si_{3.4}Al_{0.6}O₁₀(OH)₂. **Table 8.2** lists the variation in compounds used for the preparation of the gels.

Approximately 125 g of the gel is hydrothermally treated in 250 ml Teflon beakers in autoclaves at 200°C and autogeneous water pressure (approximately 10-15 bar). After cooling the solids are washed twice with demineralized water followed by centrifugation. The pH of the coexisting hydrothermal fluid could not be determined, since the solid product had completely absorbed the fluid. Klopogge et al. (1992a) have shown that the pH of the hydrothermal fluid is

Table 8.2 List of the compounds (mol of oxide) used in the starting gels.

Sample	amorph silica/alumina			Al triiso- propoxide	Mg Al(NO ₃) ₃	Mg				
	SiO ₂	SiO ₂	Al ₂ O ₃			acetate	Mg(NO ₃) ₂	Mg(OH) ₂	NH ₄ OH	NH ₄ F
8A	0.283	-	-	0.050	-	0.250	-	-	0.080	-
9A	0.283	-	-	0.050	-	0.250	-	-	0.160	-
10A	0.283	-	-	0.050	-	0.250	-	-	0.080	0.040
11A	-	0.283	0.025	-	-	0.250	-	-	0.080	0.040
12A	-	0.283	0.025	-	-	-	-	0.250	0.080	0.040
13A	0.283	-	-	-	0.050	0.250	-	-	0.080	-
14A	0.283	-	-	-	0.050	0.250	-	-	0.160	-
15A	0.283	-	-	-	0.050	0.250	-	-	0.080	0.040
16A	0.283	-	-	0.050	-	0.125	0.125	-	0.080	-
17A	0.283	-	-	0.050	-	0.125	0.125	-	0.160	-
18A	0.283	-	-	0.050	-	0.125	0.125	-	0.080	0.040
19A	0.283	-	-	0.050	-	0.250	-	-	0.120	-
20A	0.283	-	-	0.050	-	0.250	-	-	0.080	0.080

only slightly lower than that of the water obtained from the first washing procedure. Therefore, the pH of the water of the first washing procedure is determined. The washed solid is suspended into 1 M ammonium chloride to ensure that all exchangeable sites are occupied by ammonium. Finally, the bulk solids are washed twice with demineralized water to remove excess ammonium chloride, sedimented by centrifugation, and dried overnight at 120°C.

8.2.2 Analytical techniques

X-ray powder diffraction (XRD) patterns are recorded with a Philips diffractometer, equipped with PW 1700 hardware and APD 1700 software, using CuK α radiation.

The cation exchange capacity (CEC) of the saponite is determined after exchange with 0.2 M NaCl from the NH₄⁺ content in the resulting solution with

Table 8.3 Experimental runs at 200°C and autogeneous water pressure

Run	Time hours	NH ₄ / Al	F/ Al	pH ¹	CEC meq/ 100 g	Products ²
LTSAP8A-1	2	1.6		6.34	9.2	S BA
LTSAP8A-2	4	1.6		5.40	13.8	S BA
LTSAP8A-3	8	1.6		5.26	18.2	S
LTSAP8A-4	16	1.6		5.19	23.8	S
LTSAP8A-5	24	1.6		5.08	23.7	S
LTSAP8A-6	48	1.6		4.85	22.5	S
LTSAP8A-7	72	1.6		4.77	24.7	S
LTSAP8A-8	168	1.6		4.67	23.6	S
LTSAP9A-1	2	3.2		7.87	8.1	S
LTSAP9A-2	4	3.2		5.27	15.7	S
LTSAP9A-3	8	3.2		5.01	28.6	S
LTSAP9A-4	16	3.2		4.68	23.3	S
LTSAP9A-5	24	3.2		4.64	30.8	S
LTSAP9A-6	48	3.2		4.60	26.6	S
LTSAP9A-7	72	3.2		4.68	50.2	S
LTSAP9A-8	168	3.2		4.66	42.2	S
LTSAP10A-1	2	2.4	0.8	6.98	7.4	S F
LTSAP10A-2	4	2.4	0.8	5.14	21.0	S F
LTSAP10A-3	8	2.4	0.8	4.76	32.0	S
LTSAP10A-4	16	2.4	0.8	4.78	31.1	S F
LTSAP10A-5	24	2.4	0.8	4.72	28.3	S F
LTSAP10A-6	48	2.4	0.8	4.73	28.3	S F
LTSAP10A-7	72	2.4	0.8	4.64	31.5	S F
LTSAP10A-8	168	2.4	0.8	4.60	23.9	S F

Table 8.3 Experimental runs at 200°C and autogeneous water pressure

Run	Time hours	NH ₄ / Al	F/ Al	pH ¹	CEC meq/ 100 g	Products ²
LTSAP11A	72	2.4	0.8	4.86	53.3	S Q F
LTSAP12A	72	2.4	0.8	9.94	52.1	S Q F B
LTSAP13A	72	1.6		4.78	15.3	S L
LTSAP14A	72	3.2		4.65	18.8	S L
LTSAP15A	72	2.4	0.8	4.75	20.7	S L F
LTSAP16A	72	1.6		4.52	14.5	S L
LTSAP17A	72	3.2		4.53	18.6	S L
LTSAP18A	72	2.4	0.8	4.41	19.1	S L F
LTSAP19A	72	2.4		4.51	21.9	S L
LTSAP20A	72	1.6	1.6	4.62	32.4	S L F

¹ measured after the first washing

² S = saponite, F = sellaite, Q = quartz, L = lizardite, B = brucite, BA = bayerite and all experiments contain various amounts of amorphous material.

an ammonia-selective electrode. Saponites of LTSAP8A-7, LTSAP9A-7, and LTSAP10A-7 have been exchanged with Al(NO₃)₃ instead of NaCl prior to XRF measurements.

Elemental analyses of Si, Al, Mg, N, and F are performed by wavelength-dispersive X-ray fluorescence (XRF).

The morphology of the products obtained is investigated with a scanning electron microscope (SEM), equipped with energy-dispersive X-ray (EDX) analyzers.

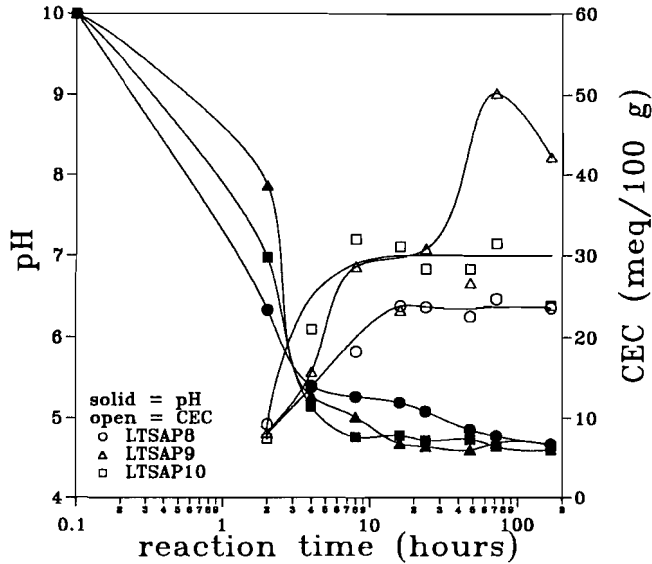


Figure 8.1 Decrease of pH (solid symbols) and the development of the NH_4 cation exchange capacity (CEC) (open symbols) as function of synthesis time at 200°C.

8.3 RESULTS

Table 8.3 summarizes the pH of the fluid obtained from the first washing procedure, the cation (ammonium) exchange capacity (CEC), and the crystalline products. The pH decreases very rapidly during the first 16 hour, followed by a slow decrease towards a constant value of approximately 4.6 upon prolonged synthesis time (Fig 8.1). The pH of LTSAP12A (Table 8.2), being 9.94 is very high as compared to that of all other experiments. The pH values of the series LTSAP16A/LTSAP17A/LTSAP18A and LTSAP19A are slightly lower as compared to those measured with the other experiments.

The NH_4 -CEC values are low, never representing more than 35 % of the theoretical CEC of 155 meq/100 g for pure ammonium-saponite. The CEC increases strongly within the first 24 hours, while longer synthesis times result in essentially constant CEC values (Fig. 8.1). The very high, more than 50 meq/100 g, CEC values for LTSAP9A-7, LTSAP11A and LTSAP12A are

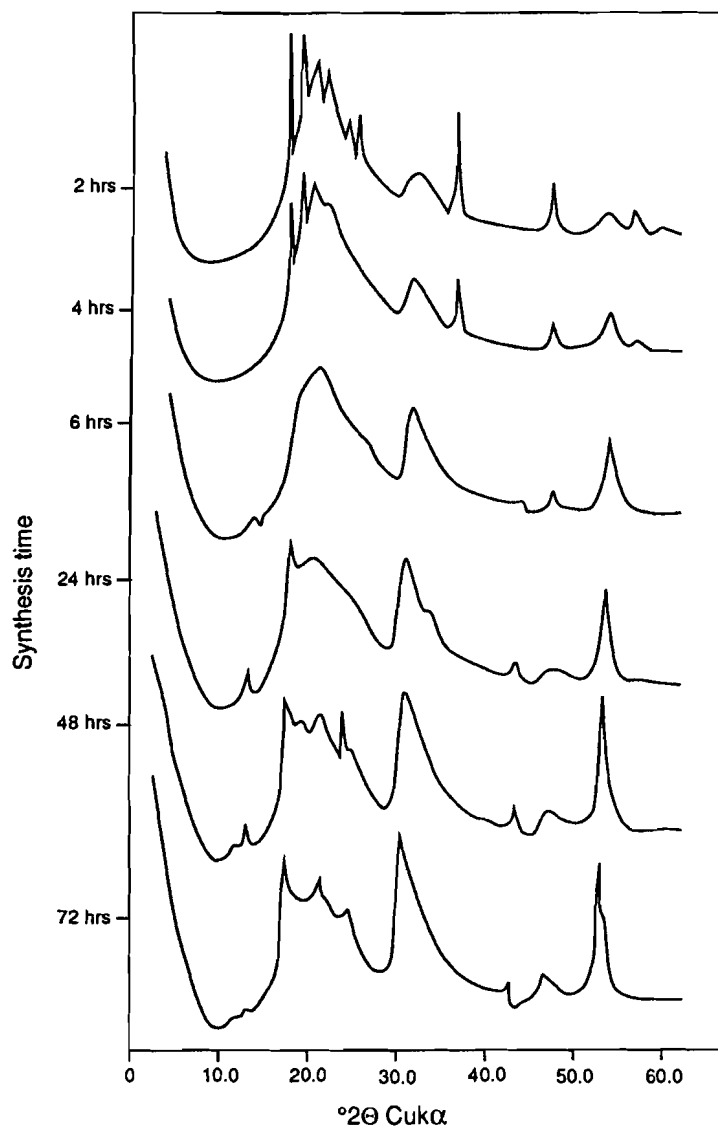


Figure 8.2. X-ray powder diffraction patterns with increasing synthesis time at 200°C: a) LTSAP8A.

remarkable. Exchange of ammonium for aluminum instead of sodium results in an additional lowering of the NH_4 -CEC to values of approximately 3.4 meq/100 g.

The XRD patterns display the development of the saponite structure at increasing synthesis times (Fig. 8.2). LTSAP8A exhibits after 2 hours, together with bayerite, $\text{Al}(\text{OH})_3$, badly crystalline saponite. After 4 hours the amount of bayerite has decreased, while the bayerite diffraction maxima have completely disappeared after 8 hours. The XRD patterns show that the (060) saponite reflection increases in relative intensity and sharpens during the first 48 hours. With long periods of hydrothermal treatment the (060) reflection remains constant, while the other (hkl) reflections sharpen. LTSAP9A shows a much

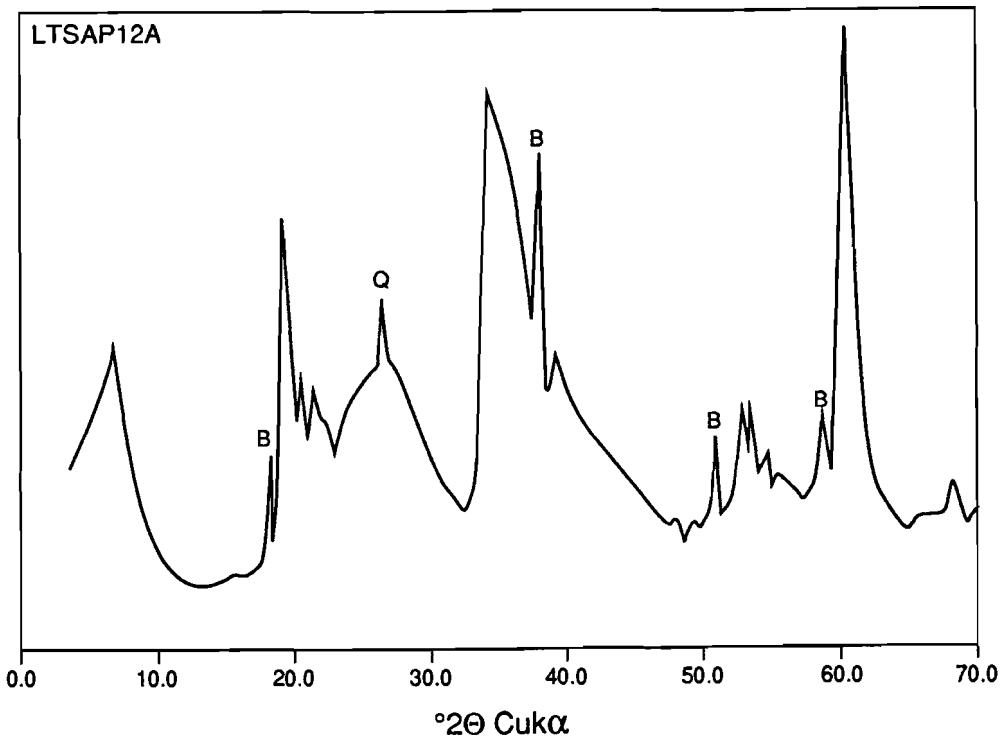


Figure 8.3 a) X-ray powder diffraction patterns of LTSAP12A. Q = quartz, B = brucite.

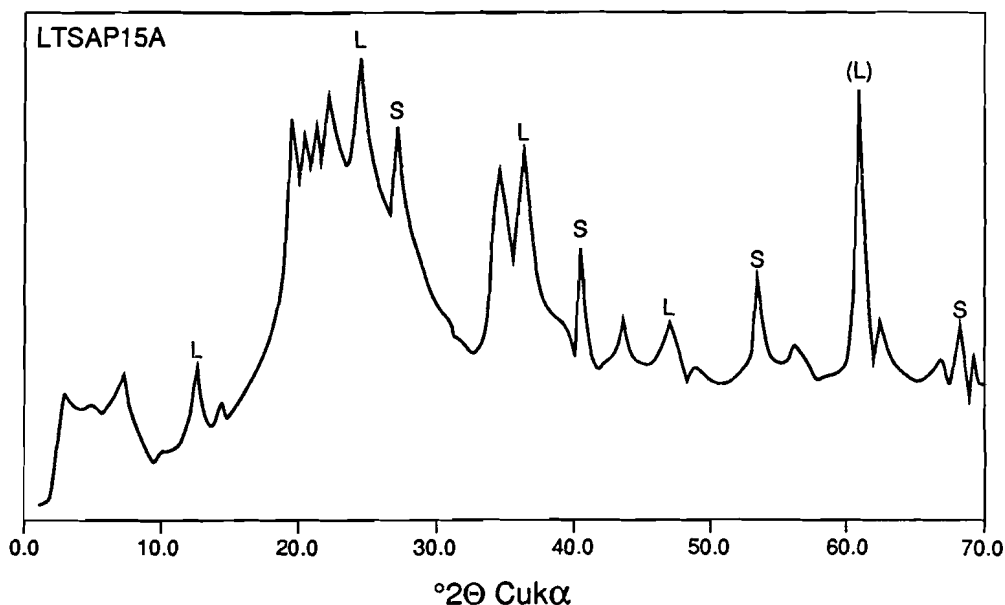


Figure 8.3 b) X-ray powder diffraction patterns of LTSAP15A. S = sellaite, L = aluminum-lizardite.

faster development of saponite as LTSAP8A, e.g., XRD intensities of saponite in LTSAP9A-1 (2 hours) can be compared with those of LTSAP8A-4 (16 hours). LTSAP10A is intermediate in between LTSAP8A and LTSAP9A.

Sellaite, MgF_2 , is observed in all patterns independent of the synthesis time due to the presence of F. In LTSAP10A no bayerite is found. The XRD pattern of LTSAP12A reveals also quartz and brucite as secondary products together with very well crystallized saponite (Fig. 8.3a). LTSAP11A contains quartz as secondary product. The saponites of LTSAP13A, LTSAP14A and LTSAP15A are rather badly crystalline. These series contain a second sheetsilicate, viz., being aluminum-lizardite $(Mg,Al)_3(Si,Al)_2O_5(OH)_4$, whereas LTSAP15A also

Hydrothermal crystallization of ammonium-saponite at 200°C and autogeneous water pressure

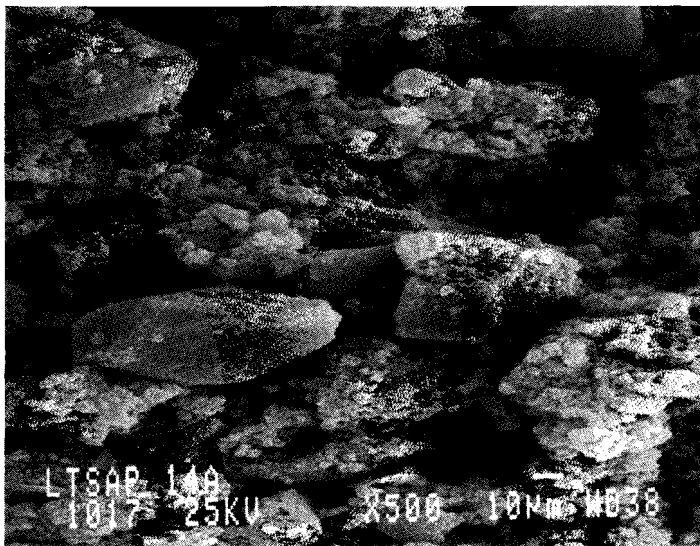
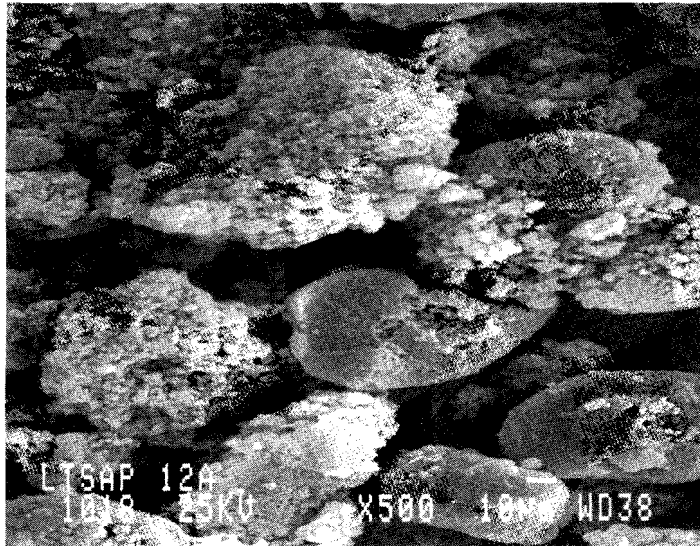


Figure 8.4 SEM photographs of LTSAP12A and LTSAP14A.

Table 8.4 X-ray fluorescence analyses of the run products. Samples with the extension E represent analyses after exchange with aluminumnitrate.

sample	MgO wt%	Al ₂ O ₃ wt%	SiO ₂ wt%	N _{CEC} wt%	N _{XRF} wt%	F wt%	Si/Al
LTSAP8A-1	6.05	10.20	67.71	0.13	0.17	na	5.86
LTSAP8A-2	7.59	7.43	72.27	0.19	0.25	na	8.60
LTSAP8A-3	8.80	5.02	48.32	0.25	0.35	na	7.52
LTSAP8A-4	9.25	5.93	51.37	0.33	0.37	na	7.65
LTSAP8A-5	13.10	6.56	67.77	0.33	0.35	na	9.13
LTSAP8A-6	18.14	8.20	62.00	0.32	0.30	na	6.68
LTSAP8A-7	18.37	6.86	60.63	0.35	0.30	na	7.81
LTSAP8A-8	20.23	8.90	54.83	0.33	0.29	na	5.44
LTSAP9A-1	12.62	10.75	60.27	0.11	0.16	na	4.95
LTSAP9A-2	18.06	8.90	58.62	0.22	0.22	na	5.82
LTSAP9A-3	23.96	8.12	51.45	0.40	0.57	na	5.59
LTSAP9A-4	24.53	8.01	51.26	0.33	0.45	na	5.65
LTSAP9A-5	22.64	7.48	47.34	0.43	0.47	na	5.59
LTSAP9A-6	19.48	8.69	55.15	0.37	0.37	na	5.60
LTSAP9A-7	23.91	7.92	50.64	0.70	0.72	na	5.65
LTSAP9A-8	24.63	7.80	54.64	0.59	0.59	na	6.18
LTSAP10A-1	8.42	10.37	66.13	0.10	0.15	2.89	5.63
LTSAP10A-2	16.48	8.77	59.94	0.29	0.36	na	6.04
LTSAP10A-3	22.30	8.43	56.44	0.45	0.48	na	5.91
LTSAP10A-4	22.44	8.69	55.54	0.44	0.50	2.35	5.64
LTSAP10A-5	23.02	8.46	55.75	0.40	0.47	na	5.82
LTSAP10A-6	22.73	8.99	53.76	0.40	0.42	2.38	5.28
LTSAP10A-7	23.96	8.50	53.03	0.44	0.47	na	5.51
LTSAP10A-8	23.95	8.37	52.61	0.33	0.43	na	5.55

sample	MgO wt%	Al ₂ O ₃ wt%	SiO ₂ wt%	N _{CEC} wt%	N _{XRF} wt%	F wt%	Si/Al
LTSAP11A	19.02	11.22	54.49	0.75	na	na	4.29
LTSAP12A	30.26	8.80	43.58	0.73	na	na	4.37
LTSAP13A	8.99	10.66	68.63	0.21	na	na	5.69
LTSAP14A	17.46	9.58	61.27	0.26	na	na	5.65
LTSAP15A	12.90	10.17	65.34	0.29	na	na	5.68
LTSAP16A	15.87	9.50	61.53	0.20	na	na	5.72
LTSAP17A	19.87	8.82	56.50	0.26	na	na	5.66
LTSAP18A	18.90	8.96	58.06	0.27	na	na	5.73
LTSAP8A-7E	18.13	8.56	61.14	0.13	na	na	6.31
LTSAP9A-7E	22.44	9.95	50.64	0.14	na	na	4.49
LTSAP10A-7E	22.36	9.48	51.79	0.13	na	na	4.82
theory*	31.04	7.86	52.47	2.16			5.67

* theoretical saponite composition $(\text{NH}_4)_{0.6}\text{Mg}_3\text{Si}_{3.4}\text{Al}_{0.6}\text{O}_{10}(\text{OH})_2$, which was intended in the bulk chemistry of the gel.

na = not analyzed.

contains a relatively large amount of sellaite (Fig. 8.3b). The XRD patterns of LTSAP16A, LTSAP17A and LTSAP18A are largely comparable with those of LTSAP13A, LTSAP14A and LTSAP15A.

The XRF analyses (Table 8.4) reveal a systematic change in bulk composition with synthesis time. During the first 8 hours SiO₂ and Al₂O₃ decrease, whereas MgO and N increase. Longer synthesis times have no influence on the composition with the series LTSAP9A and LTSAP10A. For LTSAP8A SiO₂ and Al₂O₃ continue to drop and MgO and nitrogen to increase slowly. The increase of the nitrogen content of the solids with time runs more or less parallel with the rise in CEC, although the CEC is always lower than the analytically assessed

nitrogen content. XRF analyses after cation exchange of Al^{3+} for $[\text{NH}_4]^+$ display only a slight decrease of magnesium, within the XRF accuracy.

SEM (Fig. 8.4) illustrates the products formed after 72 hours (LTSAP8A-7, LTSAP9A-7, LTSAP12A, LTSAP14A, and LTSAP19A). Except for LTSAP19A, all samples exist of large, up to $100\mu\text{m}$, amorphous particles overgrown with clusters of small flakes (diameter less than $10\mu\text{m}$). A small amount of smooth flakes has a diameter larger than $20\mu\text{m}$. LTSAP19A shows better developed crystallites with a few large flakes of diameters up to $50\mu\text{m}$, and only small amorphous particles (mostly less than $10\mu\text{m}$). The EDX analyses, although only providing relative amounts, reveal that the large amorphous particles contain only SiO_2 , with some MgO on their surfaces. The large flakes consist of SiO_2 , Al_2O_3 , and MgO of a weight ratio of 3 : 0.5 : 1. The small flakes also contain SiO_2 , Al_2O_3 , and relatively more MgO as compared to the large flakes.

8.4 DISCUSSION

The synthesis of ammonium-saponite was successful in all experiments, although the amount and crystallinity strongly depend on synthesis time, ammonium concentration, and the constituents of the initial gels.

During the first four hours of the hydrothermal treatment the pH decreases strongly, due to the release of mainly acetate ions, while part of the Mg is incorporated into the crystalizing saponite. After four hours the pH has reached levels between 6.4 and 5.4, being exactly the range in which $\text{Al}(\text{OH})_3$ has its minimum solubility (Hem and Roberson, 1967). The drop in pH explains the formation of bayerite in LTSAP8A-1 and LTSAP8A-2. After eight subsequent hours the bayerite disappears as a separate phase. The bayerite may dissolve due to the removal of Al from the solution by incorporation of octahedral Al into the saponite structure. Alternatively, the small bayerite units may be incorporated as a kind of octahedral building units. The second alternative is

avored, because $\text{Al}(\text{OH})_3$ has a very low solubility when the pH is between 6.4 and 5.4 (Hem and Roberson, 1967). The incorporation of octahedral aluminum in the saponite structure, as established by Kloprogge et al. (1992a,b), is caused by the formation of bayerite during the first hours of the hydrothermal treatment. It has been suggested that the formation of bayerite is due to the fact that the aluminum of the isopropoxide remains sixfold coordinated during gelling. The series LTSAP8 shows that the incorporation is not prevented by dissolving the Al compound in basic ammonium solution, which forces the Al^{3+} into a tetrahedral coordination, before being mixed with the other compounds in the gel preparation method.

In the series LTSAP9A and LTSAP10A no bayerite is observed. The very rapid crystallization of saponite and the resulting drop in pH to levels below 5.3 within the first four hours may prevent the formation of bayerite or, alternatively, the initially formed bayerite has already disappeared after two hours.

Based on the facts that magnesium nitrate and acetate are highly soluble within the observed pH range and that almost all magnesium apparent in the XRF bulk analyses has been incorporated into the saponite structure and assuming that all magnesium is present at the octahedral sites, it is adequate to calculate the saponite yield in the solid products (Table 8.5) with the data of Kloprogge et al. (1992a) for pure ammonium-saponite of identical compositions. After correction for adsorbed water, their pure ammonium-saponite contains 17.07 wt% Mg (31.04 wt% MgO). With this value the other Mg values can be recalculated to saponite percentages. The trend of percentages with increasing synthesis time runs parallel with the increase in CEC of the bulk product.

The use of $\text{Mg}(\text{OH})_2$ in LTSAP12A results in the absence of acid formed from the magnesium compound, as it is the case with magnesium acetate and nitrate, resulting in the high pH levels observed. The high pH adversely affect the saponite crystallinity. The presence of brucite, which is due to the low

Table 8.5 Ammonium-saponite content (in %) of the solid product determined from the Mg content and corresponding CEC values for the ammonium-saponite.

sample	sap%	NH ₄ -CEC meq/100 g
LTSAP8A-1	25.2	36.5
LTSAP8A-2	30.4	45.4
LTSAP8A-3	34.8	52.3
LTSAP8A-4	48.2	49.4
LTSAP8A-5	51.9	45.7
LTSAP8A-6	70.7	31.8
LTSAP8A-7	73.5	33.6
LTSAP8A-8	82.5	28.6
LTSAP9A-1	52.3	15.5
LTSAP9A-2	72.5	21.7
LTSAP9A-3	97.7	29.3
LTSAP9A-4	99.5	23.4
LTSAP9A-5	99.4	31.0
LTSAP9A-6	80.1	33.2
LTSAP9A-7	98.7	50.9
LTSAP9A-8	96.3	43.8
LTSAP10A-1	34.6	21.4
LTSAP10A-2	66.7	31.5
LTSAP10A-3	87.5	36.6
LTSAP10A-4	88.4	35.2
LTSAP10A-5	90.0	31.4
LTSAP10A-6	90.7	31.2
LTSAP10A-7	95.5	33.0
LTSAP10A-8	96.0	24.9

solubility of magnesium hydroxide, explains the high magnesium content observed with the XRF.

The decreasing difference in nitrogen contents based on the XRF and the CEC determinations with increasing synthesis time indicates that a part of the ammonium resides in nonexchangeable sites, possibly of amorphous material, which agrees with the data of Kloprogge et al. (1992a).

The data of this study point to the following crystallization model. The saponite crystallization starts with the formation of separate sheets with hexameric rings containing Si and Al in distributions determined by the Loewenstein rule (Loewenstein, 1954) together with bayerite. During the first period the separate sheets grow mainly in the a-b directions. Meanwhile the bayerite sheets are incorporated as building units, instead of brucite sheets, into the saponite structure, resulting in a considerable amount of octahedral aluminum and a lack of magnesium in the saponite structure. Later stacking occurs as indicated by the increasing intensities of the (hkl) reflections relative to (060). The low NH_4 -CEC values indicate the presence of other interlayer cations, most probably aluminum. This is supported by the XRF analyses, which exhibit too low MgO and too high Al_2O_3 contents as compared to the theoretical values. The cation exchange experiments with aluminum nitrate result in nearly no exchange of magnesium, demonstrating that practically no magnesium was available as interlayer cation. This model is largely in accordance with the model proposed by Kloprogge et al. (1992a,b), who established the exact Al distribution with ^{27}Al and ^{29}Si MAS-NMR.

8.5 CONCLUSIONS

- 1) The crystallinity of synthetic ammonium-saponite strongly depends on synthesis time, ammonium concentration and initial constituents of the gel.
- 2) During the synthesis the pH decreases strongly due to the formation of acetic acid, which results in the formation of bayerite.
- 3) The use of magnesium hydroxide leads to an almost constant high pH level, which leads to the presence of brucite in the solid products due to its low solubility.
- 4) A crystallization model is proposed in which i) separate sheets with hexameric rings containing Si and Al are formed, followed by lateral growth; ii) incorporation of bayerite as octahedral building unit proceeds; iii) separate sheets are subsequently stacked; iv) remaining Al from the solution is incorporated as interlayer cations together with a small amount of ammonium.

ACKNOWLEDGMENT

The authors wish to thank A. de Winter for his help and advice in the laboratory.

REFERENCES

- Hem, J. D. and Roberson, C. E. (1967) Form and stability of aluminum hydroxide complexes in dilute solutions: *U.S. Geol. Surv. Water-Supply Paper*, **1827-A**, 1-55.
- Kloprogge, J. T., van der Eerden, A. M. J., Jansen, J. B. H. and Geus, J. W. (1990a) Hydrothermal synthesis of Na-beidellite: *Geologie en Mijnbouw*, **69**, 351-357.
- Kloprogge, J. T., Jansen, J. B. H. and Geus, J. W. (1990b) Characterization of synthetic Na-beidellite: *Clays & Clay Minerals*, **38**, 409-414.
- Kloprogge, J. T., Breukelaar, J., Jansen, J. B. H. and Geus, J. W. (1992a) Low temperature synthesis of ammonium-saponites from gels with variable ammonium concentration and water content: *This Thesis Ch VI, Clays & Clay Minerals*, accepted.
- Kloprogge, J. T., Breukelaar, J., Wilson, A. E., Geus, J. W. and Jansen, J. B. H. (1992b) Solid-state nuclear magnetic resonance spectroscopy on synthetic saponites: aluminum on the interlayer site: *This Thesis Ch VII, Clays & Clay Minerals*, intended for submission.
- Loewenstein, W. (1954) The distribution of aluminum in the tetrahedra of silicates and aluminates. *Amer. Mineral.* **39**, 92-96.
- Plee, D., Gatinéau, L. and Fripiat, J. J. (1987) Pillaring processes of smectites with and without tetrahedral substitution: *Clays & Clay Minerals*, **35**, 81-88.
- Schutz, A., Stone, W. E. E., Poncelet, G. and Fripiat, J. J. (1987) Preparation and characterization of bidimensional zeolitic structures obtained from synthetic beidellite and hydroxy-aluminum solutions: *Clays & Clay Minerals*, **35**, 251-261.
- Shabtai, J., Rosell, M. and Tokarz, M. (1984) Cross-linked smectites. III. Synthesis and properties of hydroxy-aluminum hectorites and fluorhectorites: *Clays & Clay Minerals*, **32**, 99-107.

- Sterte, J. and Shabtai, J. (1987) Cross-linked smectites. V. Synthesis and properties of hydroxy-silicoaluminum montmorillonites and fluorhectorites: *Clays & Clay Minerals*, **35**, 429-439.
- Suquet, H., Iiyama, J. T., Kodama, H. and Pezerat, H. (1977) Synthesis and swelling properties of saponites with increasing layer charge: *Clays & Clay Minerals*, **25**, 231-242.

CHAPTER IX

CHARACTERIZATION OF Mg-SAPONITES SYNTHESIZED WITH GELS CONTAINING SMALL AMOUNTS OF Na⁺, K⁺, Rb⁺, Ca²⁺, Ba²⁺, OR Ce⁴⁺

ABSTRACT

Saponites are hydrothermally grown in the presence of small amounts of NH₄⁺, Na⁺, K⁺, Rb⁺, Ca²⁺, Ba²⁺ and Ce⁴⁺, with or without F⁻, at a temperature of 200°C for 72 hours. XRD and CEC data reveal the formation of a two water layer saponite with mainly Mg²⁺ as interlayer cation. Dehydration proceeds between 25° and 450°C and dehydroxylation in two steps between 450° and 790°C and between 790° and 890°C. The relatively small length of the b-axis is explained by a considerable octahedral Al substitution and a minor tetrahedral Al substitution. The presence of F⁻ has little influence on the saponite properties.

9.1 INTRODUCTION

The research of synthetic saponites has been focused on Na-saponites (Koizumi and Roy, 1959; Suquet et al., 1977; Iwasaki et al., 1989) and on their saturation with various other cations at the interlayer position (Suquet et al., 1977; 1981a,b; 1982; 1987). Recently, Kloprogge et al. (1992) reported on the synthesis of ammonium-saponite, which is interesting as an acid catalyst.

Saponite is a trioctahedral 2:1 smectite of a theoretical composition M_xMg₃Al_xSi_{4-x}O₁₀(OH)₂, with M representing one equivalent of the interlayer cation, e.g., Na⁺, K⁺, NH₄⁺, or 1/2 Ca²⁺, 1/2 Mg²⁺, or even 1/3 Al³⁺. A single sheet is normally organized with a central Mg²⁺ octahedral layer and on both sides tetrahedral layers of Si⁴⁺, which is partly substituted by Al³⁺. The substitution of Si⁴⁺ by Al³⁺ causes the layer to have an overall negative charge, which is compensated by interlayer cations. Actually, substitution of Al³⁺ also at octahedral and interlayer sites, and of Mg²⁺ at the interlayer sites may additionally proceed during the hydrothermal synthesis. Saponites with Na⁺, Ca²⁺, Mg²⁺ or Ba²⁺ as interlayer cations contain

two water layers resulting in a basal spacing of approximately 15 - 16 Å, whereas interlayer cations such as K^+ or NH_4^+ have only one water layer resulting in a basal spacing of approximately 12.5 Å (Suquet et al. 1975).

This investigation reports on (i) the synthesis of Mg-saponite in the presence of Na^+ , K^+ , Rb^+ , Ca^{2+} , Ba^{2+} , and Ce^{4+} cations, (ii) the influence of F^- on the synthesis of Mg-saponite, and (iii) the influence of partial replacement of hydroxyl groups by F^- on the saponite characteristics. The resulting products are characterized with XRD, XRF, TGA, and ICP. The data will be compared with those reported by Suquet et al. (1975, 1981a,b), who exchanged Na-saponite to saturation with the above cations.

9.2 EXPERIMENTAL METHOD

A homogeneous powder mixture of amorphous silica (SiO_2), aluminum triisopropylate ($Al[OCH(CH_3)_2]_3$), and magnesium acetate-tetrahydrate ($[CH_3COO]_2Mg \cdot 4H_2O$) (Kloprogge et al., 1992b) was mixed with a solution of the desired cation in the form of a hydroxide or fluoride, resulting in a stoichiometric gel having the theoretical saponite composition of $M_{0.6}Mg_3Al_{0.6}Si_{3.4}O_{10}(OH)_2$. M represents one equivalent of the cation involved, which competes for substitution on the interlayer positions.

Approximately 125 g of the above gel was hydrothermally treated for 72 hours at 200°C under autogeneous water pressure. After cooling the solids were separated from the coexisting hydrothermal fluid, washed twice, centrifuged, and dried overnight at 120°C.

Characterization of the solid product was based on the fraction smaller than 64 μm (Kloprogge et al., 1992b). The coexisting hydrothermal fluid was analyzed with Inductively Coupled Plasma- Atomic Emission Spectrometry (ICP-AES). The pH of the coexisting hydrothermal fluid, as well as the pH of the water after washing the

Characterization of Mg-saponites synthesized with gels containing small amounts of Na⁺, K⁺, Rb⁺, Ca²⁺, Ba²⁺, or Ce⁴⁺

solid for the first time were measured with a Consort P514 pH meter. X-ray powder diffraction (XRD) patterns were recorded with a Philips PW 1050/25 diffractometer, using CuK α radiation. Heating stage X-ray diffraction was carried out at 350°C using a HT Guinier CuK α 1 (Enraf Nonius FR553) focussing powder camera. Thermogravimetric analyses were made with a Dupont 1090 Thermal Analyzer using a heating rate of 10°C/min. Elemental analyses of the solid products were obtained by X-ray fluorescence (XRF). The cation exchange capacity (CEC) was determined by exchanging the product with a solution of 1 N ammoniumchloride brought at pH = 7 by addition of ammoniumhydroxide. The exchanged solution was analyzed with Inductively Coupled Plasma-Atomic Emission Spectrometry (ICP-AES) for the competitive interlayer cations, Mg, and Al.

Table 9.1 Experimental runs at 200°C for 72 hours.

Run LTSAP	pH		CEC meq/100 g			d ₀₀₁ (Å) 20°C	b(Å)
	fluid	wash	M ⁺	Mg ²⁺	total		
NA	4.46	4.53	8.4	134.0	142.4	14.1	9.163
K	4.41	4.48	10.5	140.0	150.5	15.3	9.180
CA	-	4.48	13.3	101.4	114.7	14.6	9.169
BA	4.47	4.58	21.2	77.4	98.6	14.7	9.173
CE	4.33	4.54	0.0	74.3	74.3	14.7	9.172
NHF	4.43	4.54	40.0	19.8	58.8	14.7	9.164
NAF	4.41	4.52	4.8	85.0	89.8	-	9.157
KF	4.42	4.50	13.5	74.4	87.9	-	9.152
RBF	4.62	4.70	16.0	76.1	92.1	15.1	9.173
CAF	4.32	4.52	13.4	75.5	88.9	14.0	9.151
BAF	4.43	4.56	21.2	88.0	109.2	-	9.160

Table 9.2 X-ray fluorescence analyses of the saponite bulk samples.

Run	SiO ₂	Al ₂ O ₃	MgO	Na ₂ O	K ₂ O	Rb ₂ O	CaO	BaO	CeO ₂	F
LTSAP	wt%	wt%	wt%	wt%	wt%	wt%	wt%	wt%	wt%	wt%
NA	51.77	9.16	24.71	bd						
K	52.63	9.47	24.71		0.57					
CA	54.13	9.01	23.55				0.31			
BA	54.34	9.35	21.23					2.04		
CE	55.84	9.64	19.40						2.10	
NHF	52.84	11.98	21.72							0.06
NAF	51.99	12.05	22.88	bd						0.06
KF	53.06	12.45	22.22		0.78					0.11
RBF	52.41	9.75	22.22			2.94				0.20
CAF	55.19	9.07	23.05				0.33			0.02
BAF	51.34	13.04	19.40					2.31		0.03

bd = below detection limit

9.3 RESULTS

The results of the different runs are summarized in Table 9.1, 9.2, and 9.3. The runs are denoted, for example, by LTSAPNA, when the run was performed with sodium as the ion to be taken up at the interlayer positions. When also fluorine ions were present, the run is indicated by LTSAPNAF.

XRD on the synthesis products of all experiments prove mainly (hkl) saponite reflections. The (001) reflections are very weak (LTSAPNA, -K, -CA, -BA, -CE, -NHF, -RBF, -CAF), or absent (LTSAPNAF, -KF, -BAF). Experiment LTSAPCE led to an X-ray pattern showing additionally 2 wt% cerianite, CeO₂ (Fig. 9.1). The presence of corundum ($\leq 5\%$), which is mainly observed in the patterns of the experiments where fluorine ions were present, is caused by contamination during grounding in the corundum mortar of the starting compounds (Kloprogge et al., 1992b).

Table 9.3 Structural formulae of the Mg-saponites, based on XRF and CEC data.

Run	formula	amorph
LTSAP		
NA	Na _{0.03} Mg _{0.27} (Mg _{2.58} Al _{0.28} □ _{0.14})(Al _{0.57} Si _{3.43})O ₁₀ (OH) ₂	0.61 SiO ₂
K	K _{0.04} Mg _{0.27} (Mg _{2.57} Al _{0.29} □ _{0.14})(Al _{0.58} Si _{3.42})O ₁₀ (OH) ₂	0.64 SiO ₂
CA	Ca _{0.03} Mg _{0.19} (Mg _{2.41} Al _{0.39} □ _{0.20})(Al _{0.41} Si _{3.59})O ₁₀ (OH) ₂	0.42 SiO ₂
BA	Ba _{0.04} Mg _{0.15} (Mg _{2.29} Al _{0.47} □ _{0.24})(Al _{0.38} Si _{3.62})O ₁₀ (OH) ₂	0.57 SiO ₂
CE	Ce _{0.00} Mg _{0.14} (Mg _{2.11} Al _{0.80} □ _{0.29})(Al _{0.26} Si _{3.72})O ₁₀ (OH) ₂	0.62 SiO ₂
NHF	(NH ₄) _{0.15} Mg _{0.04} Al _{0.07} (Mg _{2.27} Al _{0.49} □ _{0.24})(Al _{0.45} Si _{3.55})O ₁₀ (OH) _{1.99} F _{0.01}	0.22 SiO ₂
NAF	Na _{0.02} Mg _{0.16} Al _{0.04} (Mg _{2.24} Al _{0.50} □ _{0.26})(Al _{0.46} Si _{3.54})O ₁₀ (OH) _{1.99} F _{0.01}	0.12 SiO ₂
KF	K _{0.05} Mg _{0.14} Al _{0.05} (Mg _{2.23} Al _{0.51} □ _{0.26})(Al _{0.49} Si _{3.51})O ₁₀ (OH) _{1.98} F _{0.02}	0.29 SiO ₂
RBF	Rb _{0.06} Mg _{0.14} (Mg _{2.26} Al _{0.49} □ _{0.25})(Al _{0.34} Si _{3.66})O ₁₀ (OH) _{1.96} F _{0.04}	0.13 SiO ₂
CAF	Ca _{0.03} Mg _{0.14} (Mg _{2.34} Al _{0.44} □ _{0.22})(Al _{0.34} Si _{3.66})O ₁₀ (OH) _{1.99} F _{0.01}	0.32 SiO ₂
BAF	Ba _{0.04} Mg _{0.17} (Mg _{1.95} Al _{0.70} □ _{0.35})(Al _{0.42} Si _{3.58})O ₁₀ (OH) _{1.99} F _{0.01}	0.18 SiO ₂

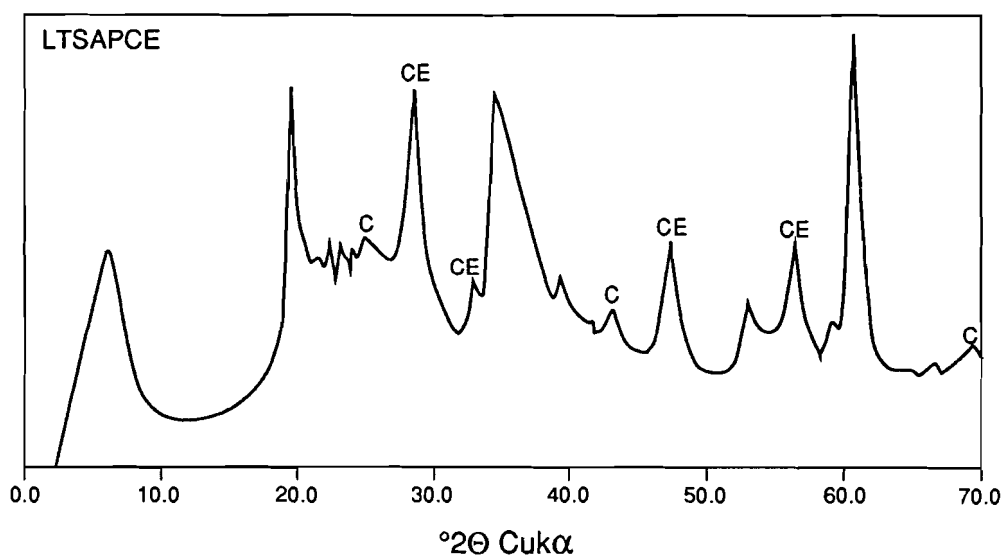


Figure 9.1 X-ray powder diffraction pattern of Mg-saponite synthesized in the presence of Ce⁴⁺ as competitive cation. CE = cerianite, C = corundum.

As shown in **Table 9.1** the basal spacing of the saponites varies between 14.0 Å and 15.3 Å independently of the various interlayer cations present during the synthesis. During dehydration to 350°C the basal spacing slightly decreased to a rather uniform value between 14.0 Å and 14.5 Å.

The length of the b-axis based on the (060) reflection is relatively small, and varies between 9.151 and 9.184 Å. The mean values of the b-axes of the fluor-containing saponites are 0.1 % smaller than those containing only hydroxyl groups with the same interlayer cation. After dehydration the b-axis became 9.150 Å for all saponites.

CEC determinations on the possible interlayer cations (NH_4^+ , Na^+ , K^+ , Rb^+ , Ca^{2+} , Ba^{2+} , Ce^{4+}) yield values between 4.8 and 21.2 meq/100 g, except for LTSAPNHF with an extreme of 40 meq/100 g (**Table 9.1**). These values are extremely low with respect to the theoretical saponite composition (155 meq/100 g). ICP analyses of the exchanged CEC-fluids revealed high concentrations of Mg, corresponding with CEC values of about 74.3 to 140 meq/100 g. No Al was measured in these fluids.

The XRF data on the bulk synthetic product (**Table 9.2**) exhibit relative high Al, intermediate Si, and low Mg contents in comparison with the intended theoretical saponite composition, $\text{M}_{0.6}\text{Mg}_3\text{Al}_{0.6}\text{Si}_{3.4}\text{O}_{10}(\text{OH})_2$. With $\text{M} = \text{NH}_4^+$ the SiO_2 , Al_2O_3 , and MgO wt% is 52.5, 15.7, and 31.1, respectively.

Analyses of the coexisting hydrothermal fluids yield very low concentrations of Si and Al, whereas the Mg concentrations are too high for congruent solution. No clear relationship is observed between the fluid composition concerning Si, Al, and Mg on the one hand and the interlayer cation or F⁻, on the other hand. The concentration of the alternative interlayer cation in the fluid of runs with fluor is 4 to 20 % higher than those with water. The Ce concentration is extremely low, due to the precipitation of crystalline cerianite, which is insoluble.

The pH of the coexisting hydrothermal fluid is rather constant at levels between 4.33 and 4.62, independent of the presence or absence of F⁻. The pH of the water after the first washing is consequently slightly higher (**Table 9.1**).

Characterization of Mg-saponites synthesized with gels containing small amounts of Na⁺, K⁺, Rb⁺, Ca²⁺, Ba²⁺, or Ce⁴⁺

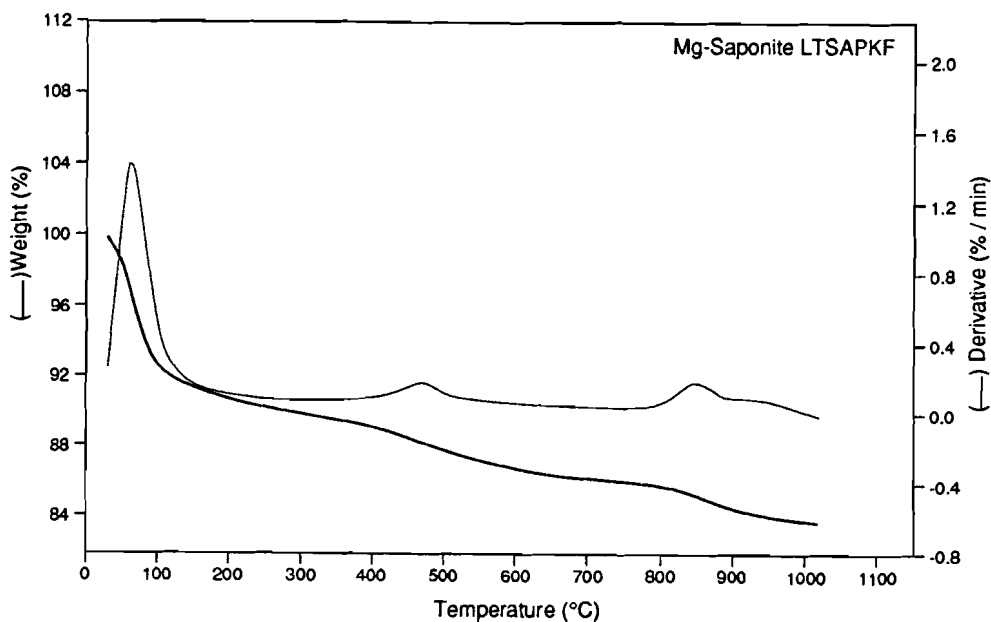


Figure 9.2 Thermogravimetric analysis (heating rate 10°C/min) of Mg-saponite.

The TGA plots of all experimental products exhibit the same profile (**Fig. 9.2**). Below 125°C up to 9.0 wt% physically adsorbed water is lost. The profile in the temperature range 125 - 790°C can be divided in two parts. In the range between 125°C and approximately 450°C 3.7 to 4.9 wt% water present within the interlayer is lost. The weight loss of approximately 1.6 - 2.2 % in the range from 500 to 790°C is attributed to the start of dehydroxylation. Between 790 and 890°C the dehydroxylation reaches a maximum and the sample lost approximately 1.8 - 2.3 % in weight.

9.4 DISCUSSION

The synthesis of saponite was successful in all experiments as demonstrated by the XRD spectra and the drop of the pH level of the coexisting fluid to relatively low values, due to the release of acetate ions (Kloprogge et al., 1992b; Vogels et al., 1992).

The very low intensity of the basal spacings indicates that the stacking of the saponite sheets is very poor. The basal spacings measured for the saponites prepared in the presence of sufficient Na^+ , Ca^{2+} , Ba^{2+} , and Ce^{4+} should be within a range of approximately 14 to 16 Å at 25°C, as reported for saponites with two water layers (Suquet et al., 1975). Saponite synthesized in the presence of K (LTSAPK) yielded a similar basal spacing of 15.29 Å, while K-saponite, like NH_4 -saponite (Kloprogge et al. 1992a), normally should have only one water layer leading to a basal spacing of approximately 12.6 Å.

Upon dehydration all basal spacings decrease to 14 to 15 Å. After dehydration Suquet et al. (1975) observed basal spacings of 12.4 Å for Na-, 10.0 Å for K-, 12.0 Å for Ca-, 12.2 Å for Ba-, and 14.3 Å for Mg-saponites. The uniform basal spacings of 14 to 15 Å of our samples and the CEC results (Table 9.1) point to Mg^{2+} as the main interlayer cation with the whole set of saponites synthesized. Based on the initial gel composition also Al^{3+} may be taken up at interlayer positions. Kloprogge et al. (1992b) have shown that saponites with Al^{3+} as interlayer cation exhibit a behavior corresponding to one water layer within the interlayer, and thus a basal spacing of 12.4 Å. Therefore, the presence of Al^{3+} as major interlayer cation is excluded by the analyses of the exchanged CEC-fluid and the basal spacing.

The length of the b-axis correlates 1) with the interlayer cation and its ionic radius, when the saponite is in the dehydrated state, and 2) with the Al substitution on tetrahedral and octahedral sites (Suquet et al., 1981a,b). For two water layer saponites (Li, Mg, Ca, Ba and Na) in the hydrated state with a

negligible influence of the interlayer cation the relation between b-axis and Al substitution is expressed as (Suquet et al., 1981a):

$$b = 9.178 + 0.076 x \pm 0.01 \text{ \AA}, \quad (1)$$

where x is the layer charge, which is considered to be equal to the difference between Al^{IV} and Al^{VI}. The Al^{IV}-Si substitution results in a negative charge, which is compensated by the positive charge due to the one-to-one Al^{VI}-Mg substitution. These considerations lead to relation (2):

$$b = 9.174 + 0.079 \text{ Al}^{\text{IV}} - 0.07 \text{ Al}^{\text{VI}} \pm 0.01 \text{ \AA} \quad (2)$$

Kloprogge et al. (1992) argued for the normal muscovite substitution $3\text{Mg}^{2+} = 2\text{Al}^{3+} + 1 \text{ vacancy}$ to be more appropriate, which results in a zero charged octahedral layer and, therefore, a slightly higher layer charge in comparison with the one-to-one Al-Mg substitution. According to these relations the small values of the b-axes displayed by our samples can be explained by a considerable octahedral Al substitution or a minor tetrahedral Al substitution. Kloprogge et al. (1992c) confirm a substantial octahedral Al substitution based on ²⁷Al MAS-NMR, whereas the ²⁹Si MAS-NMR data indicate a tetrahedral Al substitution of approximately 0.6 Al per four tetrahedral sites in the saponite structure. The substitution of Al at octahedral sites is also evident from the low CEC values of **Table 9.1**.

The presence of only 20 - 200 ppm F in the saponite structure, replacing 0.5 - 3 % of the hydroxyl groups, has no noticeable effect on the basal spacing, although it is known that trioctahedral fluor-micas exhibit a smaller basal spacing due to increasing interlayer bond strength (Giese, 1984; Munoz, 1984). However, a small influence is found on the b-axis, which has become a little smaller as compared to the corresponding saponites without F. A comparable influence is found on the Mg²⁺ CEC, whereas the NH₄⁺ exchange remains unaltered.

Approximate structure formulae of the saponites can be calculated using the CEC data and XRF data, assuming that 1) all of the exchangeable cations are at the interlayer sites of the saponite, 2) all Mg and Al measured with XRF are present in the saponite structure, and 3) the bulk consists of approximately 80-85 wt%

saponite and 15-20 wt% amorphous SiO₂ (Kloprogge et al., 1992a) (Table 9.3). Our XRD, XRF, and CEC data combined with earlier published NMR data indicate that the muscovite substitution of 3Mg²⁺ by 2Al³⁺ and one vacancy is more appropriate, leaving a zero charge on the octahedral sheet. The negative charge of the tetrahedral sheet is completely compensated by the interlayer cations, of which a considerable amount is Mg²⁺.

The two step weight loss between 25° and approximately 450°C shown in the TGA plots is due to bulk water sorbed at the surface and the interlayers of the saponite. This agrees well with the decrease in basal spacing during dehydration exhibited within the same temperature range. Between 450° and 790° the saponites dehydroxylate very slowly, followed by the main hydroxylation peak between 790° and 890°C. The corresponding DTA plot reveals its main dehydroxylation peak between 800 and 850°C and a very weak, subsidiary peak at approximately 600°C supporting the interpretation of the TGA plot. The weight loss of 3.7 to 4.5 % is in good agreement with the theoretical value of approximately 4.5 to 5 wt%, which depends on the exact saponite composition.

Kloprogge et al. (1992) and Vogels et al. (1992) have proposed a crystallization model for NH₄-saponites consisting of the formation of separate tetrahedral sheets with Si and Al together with bayerite, followed by the incorporation of the bayerite as building unit and stacking of the sheets. The differences with their starting conditions are in found in the 2.5 times increased amount of water and the use of other cations instead of ammonium. The results of this study exhibit two marked differences with those of Kloprogge et al. (1992) and Vogels et al. (1992), being, firstly, the presence of interlayer Mg and the absence of interlayer Al and, secondly, synthesis experiments with fluorine do not result in incorporation of F⁻ into the saponite structure replacing hydroxyl groups, nor in the formation of sellaite, MgF₂. The amounts of Mg²⁺ and F⁻ in the hydrothermal fluid largely exceeds the solubility product of sellaite, indicating complexation with the organic constituents in the fluid prohibiting sellaite crystallization.

ACKNOWLEDGMENTS

The authors are indebted to A. de Winter for his help and advice in the laboratory, H. M. V. C. Govers for the XRD patterns, and T. Zalm for the TGA analyses. R. J. M. J. Vogels is thanked for critically reviewing this manuscript.

REFERENCES

- Giese, R. F. (1984) Electrostatic energy models of micas: in *Micas, Reviews in Mineralogy* vol 13, S. W. Bailey, ed., Mineralogical Society of America, Washington, D.C., 105-141.
- Kloprogge, J. T., Breukelaar, J., Geus, J. W. and Jansen, J. B. H. (1992a) Solid state nuclear magnetic resonance spectroscopy on synthetic ammonium-saponites; aluminum on the interlayer site: *This Thesis Ch VII, Clays & Clay Minerals, intended for submission.*
- Kloprogge, J. T., Breukelaar, J., Jansen, J. B. H. and Geus, J. W. (1992b) Low temperature synthesis of ammonium-saponites from gels with variable ammonium concentration and water content: *This Thesis Ch VI, Clays & Clay Minerals, accepted.*
- Kloprogge, J. T., Breukelaar, J., Geus, J. W. and Jansen, J. B. H. (1992c) Solid state nuclear magnetic resonance spectroscopy on synthetic saponites; magnesium on the interlayer site: *Clays & Clay Minerals, in prep.*
- Koizumi, M. and Roy, R. (1959) Synthetic montmorillonoids with variable exchange capacity: *Amer. Mineral.* 44, 788-803.
- Munoz, J. L. (1984) F-OH and Cl-OH exchange in micas with applications to hydrothermal ore deposits: in *Micas, Reviews in Mineralogy* vol 13, S. W. Bailey, ed., Mineralogical Society of America, Washington, D.C., 469-491.

- Suquet, H., De La Calle, C. et Pezerat, H. (1975) Swelling and structural organization of saponite: *Clays & Clay Minerals* **23**, 1-9.
- Suquet, H., Iiyama, J. T., Kodama, H. and Pezerat, H. (1977) Synthesis and swelling properties of saponites with increasing layer charge: *Clays & Clay Minerals* **25**, 231-242.
- Suquet, H., Malard, C., Copin, E. and Pezerat, H. (1981a) Variation du parametre b et de la distance basale d_{001} dans une serie de saponites a charge croissante: I. Etats hydrates: *Clay Minerals* **16**, 53-67.
- Suquet, H., Malard, C., Copin, E. and Pezerat, H. (1981b) Variation du parametre b et de la distance basale d_{001} dans une serie de saponites a charge croissante: II. Etats 'zero couche': *Clay Minerals* **16**, 181-193.
- Suquet, H., Prost, R. et Pezerat, H. (1982) Etude par spectroscopie infrarouge et diffraction X des interactions eau-cation-feuillet dans les phases a 14.6, 12.2 and 10.1 Å d'une saponite-Li de synthese: *Clay Minerals* **17**, 231-241.
- Suquet, H. and Pezerat, H. (1987) Parameters influencing layer stacking types in saponite and vermiculite: a review: *Clays & Clay Minerals* **35**, 353-362.
- Vogels, R. J. M. J., Breukelaar, J., Kloprogge, J. T., Jansen, J. B. H. and Geus, J. W. (1992) Hydrothermal crystalization of ammonium-saponite with time at 200°C and autogeneous water pressure: *This Thesis Ch VIII, Clays & Clay Minerals*, intended for submission.

CHAPTER X

An ^{27}Al Nuclear Magnetic Resonance Study on the Optimalization of the Development of the Al13 Polymer

Abstract

The synthesis conditions are strongly influencing the yield of the tridecameric polymer Al13 ($[\text{AlO}_4\text{Al}_{12}(\text{OH})_{24}(\text{H}_2\text{O})_{12}]^{7+}$). An amount of 68 % tridecamer was achieved by injection of alkali through a capillary tube into a 5×10^{-2} M Al solution at a rate of 0.015 ml/s up to an OH/Al ratio of 2.2. Dropwise addition of alkali yielded significantly less tridecameric polymer. During progressive hydrolysis the monomeric Al NMR resonance moved from 0.1 ppm to 0.9 ppm and the linewidth increased from 37 to 112 Hz. Simultaneously the resonance at 63.3 ppm due to tridecameric fourfold coordinated Al was changed by 0.02 ppm. During aging the tridecamer rearranged to polymers undetectable by NMR, due to loss of the tetrahedral symmetry of the central Al, which was evidenced from the decrease in intensity and the broadening of the 63.3 ppm resonance. The formation of tetrahedral $\text{Al}(\text{OH})_4^-$, due to the inhomogeneous conditions at the point of base introduction, is essential for the synthesis of Al13. Aging over a period of 1 year caused a strong decrease in Al13 concentration, which shows that Al13 is a metastable polymer.

10.1 INTRODUCTION

The existence of the $\text{AlO}_4\text{Al}_{12}(\text{OH})_{24}(\text{H}_2\text{O})_{12}]^{7+}$ polymer (Al13), first suggested by Johansson (1960,1962,1963), has been a matter of debate among geochemists and soil chemists. In a favored model the polymer is composed of hexameric rings structurally similar to the rings in the lattice of gibbsite ($\text{Al}(\text{OH})_3$) (Brosset et al., 1954; Hsu, 1977). Later on the mineral Zunyite $[\text{Al}_{13}(\text{OH},\text{F})_{16}\text{F}_2]\text{Si}_5\text{O}_{20}\text{Cl}$ has been shown to have a structure with the tridecameric polymers as building blocks (Lampe et al., 1982). ^{27}Al NMR investigations (Akitt et al., 1972; Akitt and Farthing, 1978, 1981; Bottero et al., 1980, Bertsch et al., 1986a,b) and Small Angle X-ray Scattering (Rausch and Bale, 1964; Bottero et al., 1982) have

provided finally unequivocal evidence for the, probably metastable, existence of the Al13 polymer.

The Al13 polymer is of interest as an important pillaring agent in natural and synthetic smectites, e.g. (Shabtai et al., 1984; Plee et al., 1987; Schutz et al., 1987; Sterte and Shabtai, 1987, Kloprogge et al., 1990), which can be used as molecular sieves or shape-selective catalyst.

NMR studies have indicated that synthesis conditions, such as, OH/Al molar ratio, rate of neutralization, mixing conditions (Bertsch et al, 1986a; Bertsch, 1987), and preparation temperature (Kloprogge et al., 1992) are important for the genesis and yield of the tridecameric polymer. Also experimental conditions, such as, concentration, pH, and viscosity (Akitt and Elders, 1985a,b) influence, however, the chemical shifts and linewidth of the ^{27}Al NMR resonances of the monomeric and tridecameric species. Furthermore it has been established that the exact position of the NMR signals is to a limited extent dependent on the choice of reference solution and its concentration (Akitt and Elders, 1985a), magnetic field strength, and dilution with D_2O (Berchier et al., 1986).

The purpose of this investigation is to evaluate the effects on Al13 polymer formation in 0.052 M Al solutions of the following factors, viz., (i) variation of OH/Al molar ratio within the range 1.2 to 2.6, (ii) procedure of base addition, (iii) base injection rate, (iv) mixing rate, and (v) aging for a period of 1 year. The effects are assessed by measuring the chemical shifts and the linewidths of the ^{27}Al NMR resonances. The aim of this study is to optimise the Al13 yield for the use as pillaring agent.

10.2 EXPERIMENTAL METHOD

0.2 M Al stock solutions were prepared by dissolving reagent grade $\text{AlCl}_3 \cdot 6\text{H}_2\text{O}$ (Merck) or $\text{Al}(\text{NO}_3)_3 \cdot 9\text{H}_2\text{O}$ (Merck) in deionized water. Dissolution of reagent grade NaOH (Merck) in deionized water under a N_2 atmosphere provided a 0.2 M alkali

stock solution. The amount of alkali solution required to provide the desired OH/Al molar ratio, ranging from 0.5 to 2.6 with intervals of 0.2, was either injected below the solution surface at various rates using a Gilson pump (capillary diameter 0.5 mm) into, or added dropwise (0.5 ml/drop) to 250 ml of the Al solution, which was vigorously stirred in a vessel described by Vermeulen et al. (1975). The experiments were performed under N_2 atmosphere to exclude effects of carbonate ions. All solutions were adjusted to the same volume to get an identical final Al concentration of 5.2×10^{-2} M. Additionally some Al13 polymer solutions were prepared using 0.5 M $\text{Al}(\text{NO}_3)_3$ and NaOH solutions. The Al concentrations in these solutions were 8.3×10^{-2} and 15.6×10^{-2} M.

The ^{27}Al NMR spectra were recorded with a Bruker WP 200 spectrometer operating at 52.148 MHz (4.6 Tesla) at the Department of Organic Chemistry of the University of Utrecht. For comparative purposes concerning chemical shifts and linewidths some spectra were recorded on a Bruker WM 500 spectrometer operating at 130.321 MHz (11.7 Tesla) at the Department of Physical Chemistry, Faculty of Science, University of Nijmegen. An aluminum nitrate solution was used as standard reference with respect to the chemical shift. The accuracy in the chemical shift measurements is ± 0.01 ppm. Before measurement the solutions were diluted with D_2O (1:1).

10.3 RESULTS

The ^{27}Al NMR spectra exhibited distinct resonances at approximately 0.1 ppm and 63.3 ppm due to monomeric sixfold coordinated Al and to the central fourfold coordinated Al of the Al13 polymer, respectively (Fig. 10.1). Relative concentrations were based on integrated intensities of the measured resonances. The exact position of both resonances depends on the degree of hydrolysis (OH/Al molar ratio) and to a limited extend on the reference solution used.

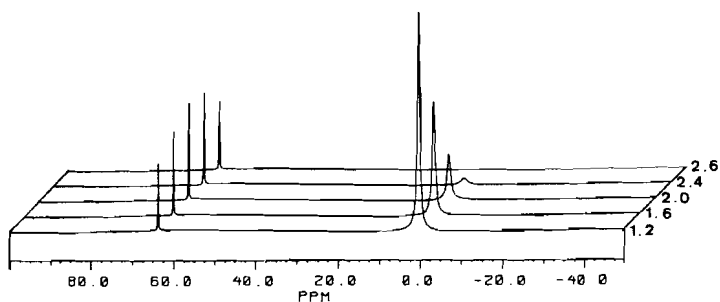


Figure 10.1 ^{27}Al NMR spectra of Al in 0.05 M Al-nitrate solutions with OH/Al molar ratio's 1.2, 1.6, 2.0, 2.4 and 2.6 (dropwise addition at 25°C, stirring rate 300 rpm).

Table 10.1 Influence of the reference solution and its concentration, of the magnetic field strength and of dilution with D_2O on the chemical shift δ .

sample	mol/l	$\delta(\text{ppm})$	
		4.6 Tesla	11.7 Tesla
$\text{Al}_2(\text{SO}_4)_3$	0.5	0.00	0.00
AlCl_3	0.5	-0.18	-0.19
$\text{Al}(\text{NO}_3)_3$	0.5	-0.15	-0.15
$\text{Al}(\text{NO}_3)_3$	0.052	-0.08	-0.10

$\text{D}_2\text{O}/\text{reference}$ vol ratio	$\delta(\text{ppm})$
	4.6 Tesla
1.000	0.02
0.333	0.07
0.176	0.10

Using $\text{Al}_2(\text{SO}_4)_3$ as a reference, 0.5 M AlCl_3 displayed a resonance at -0.18 ppm at 4.6 Tesla and at -0.19 ppm at 11.7 Tesla, while 0.5 M $\text{Al}(\text{NO}_3)_3$ showed a resonance at -0.15 ppm and at both 4.6 and 11.7 Tesla, respectively. At the same field strengths a 5.2×10^{-2} M $\text{Al}(\text{NO}_3)_3$ exhibited resonances at -0.08 ppm and at -0.10 ppm, respectively (Table 10.1). Dilution with 50 vol% D_2O causes a shift of 0.08 ppm to higher field as compared to dilution with 7.5 vol% D_2O .

Solutions of an OH/Al ratio increasing from 1.2 to 2.6 with an interval of 0.2 displayed a strong continuous decline in the amount of monomeric Al (Fig. 10.1 and 10.2). The yield of Al13 after addition of alkali up to an OH/Al molar ratio of 2.2 displayed a maximum of 56.5 % for dropwise addition and 68.0 % for injection at a rate of 0.015 ml/s. At OH/Al molar ratios higher than 2.2, a considerable decrease in the amount of monomeric Al and Al13 was observed. The amount of undetectable Al rose more strongly during injection than during dropwise

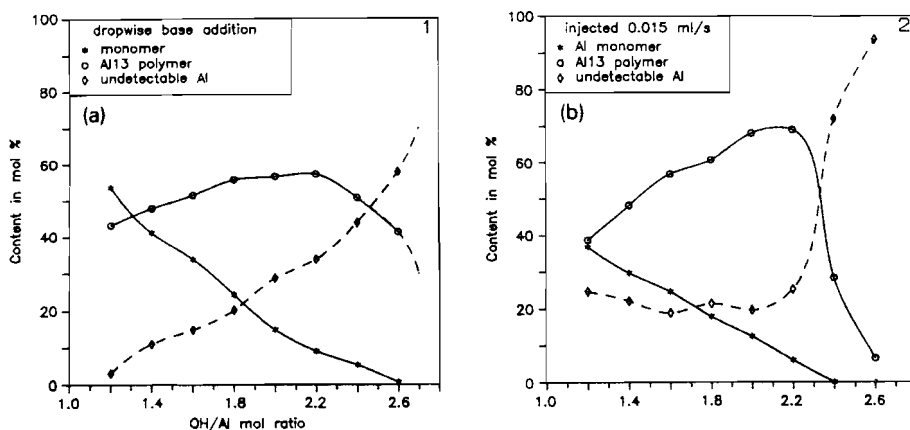


Figure 10.2 The percentages of monomer Al, Al13 and undetectable Al as analyzed with ^{27}Al NMR in 0.05 M Al-nitrate solution as function of OH/Al molar ratio: a) dropwise NaOH addition at 25°C, stirring rate 300 rpm, b) NaOH injection, rate 0.015 ml/s (25°C, stirring rate 300 rpm).

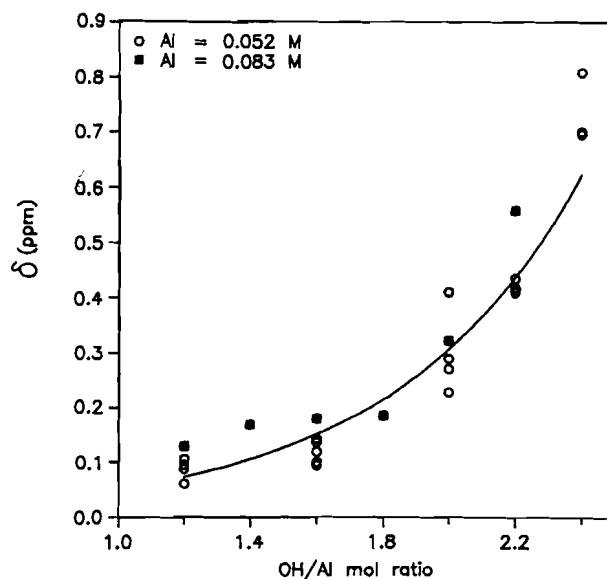


Figure 10.3 The influence of OH/Al molar ratio on the chemical shift of the monomeric sixfold coordinated Al.

addition. During dropwise addition a faint white amorphous precipitate frequently developed, which redissolved within 12 hours of aging. Dropwise neutralization resulted in a less pronounced Al13 maximum and a higher monomer content than continuous injection at 0.015 ml/s.

Upon progressive hydrolysis a small shift to lower field was observed for the sixfold and the fourfold coordinated Al resonance (Fig. 10.3 and 10.4). With the OH/Al molar ratio increasing from 1.2 to 2.4 the resonance of sixfold coordinated Al shifted parabolically from about 0.07 ppm to 0.81 ppm for solutions with Al concentrations of 5.2×10^{-2} M and 8.3×10^{-2} M. A solution of an Al concentration of 15.6×10^{-2} M exhibited a linear shift from 0.09 ppm to 0.15 ppm over the same range of OH/Al molar ratio's, while the linewidth increased from 37 Hz to 112 Hz (Fig. 10.5). The change in chemical shift for fourfold coordinated Al amounted \pm

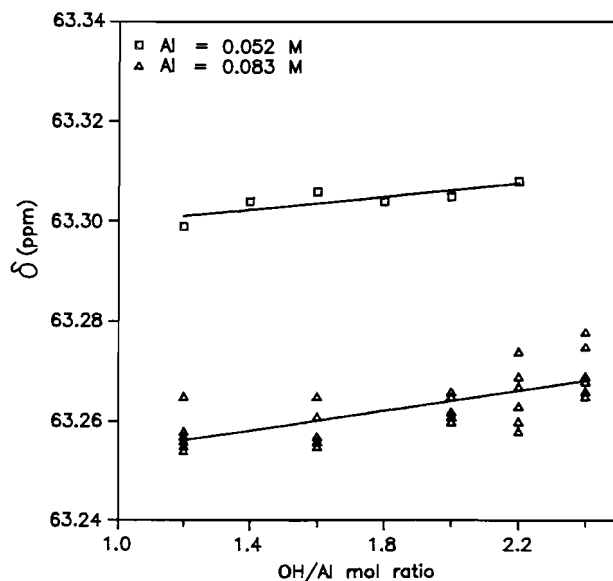


Figure 10.4 The influence of OH/Al molar ratio on the chemical shift of the central fourfold coordinated Al from the Al13 complex.

0.02 ppm, which is much smaller than the shift observed for sixfold coordinated Al. No change in linewidth was observed.

The amount of Al13 is found to be a function of the injection rate of alkali, while at an OH/Al molar ratio of 1.2 the maximum Al13 yield was exhibited at a rate of injection of 0.020 ml/s, whereas the maximum Al13 yield at an OH/Al molar ratio of 2.2 was obtained at an injection rate of 0.10 ml/s (Fig. 10.6). At injection rates above 0.035 ml/s, the solution became transiently cloudy, due to the formation of a colloidal, amorphous precipitate.

The stirring rate during neutralization of $\text{Al}(\text{NO}_3)_3$ also affected the formation of Al13 and monomeric Al (Table 10.2). At stirring rates lower than 210 rpm, precipitation was observed. At higher stirring rates, the solutions remained clear.

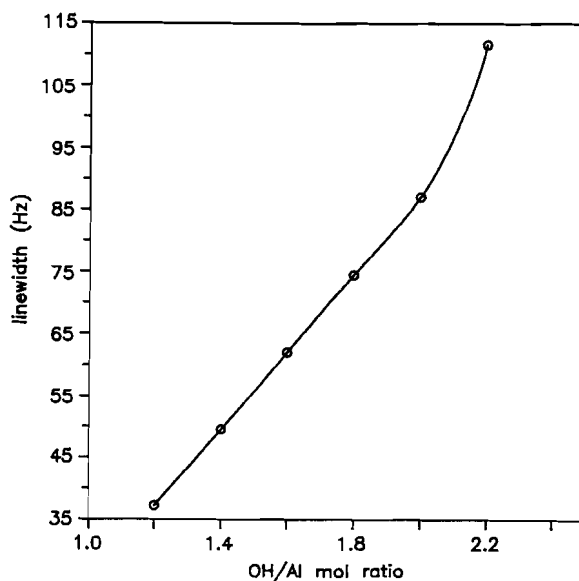


Figure 10.5 The variation with OH/Al molar ratio of the linewidth at half height of the monomeric sixfold coordinated Al in solution with Al concentration of 0.052 M.

Table 10.2 Concentrations of monomeric Al, Al13 and undetectable Al in a 0.05 M Al nitrate solution. The solution was neutralized to an OH/Al molar ratio of 2.4 as function of the stirring rate (dropwise addition at 25°C).

stirring rate rpm	Al monomer %	Al13 polymer %	undetect. Al %
120	3.7	48.0	48.3
180	4.0	49.8	46.2
240	4.4	52.0	43.6
300	4.0	53.7	42.3

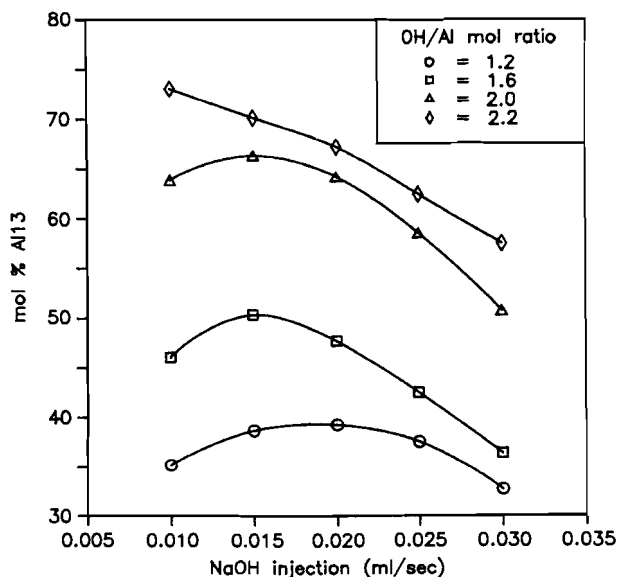


Figure 10.6 The Al13 concentration in 0.05 M Al-nitrate solution with OH/Al molar ratio of 2.5 as function of base injection rate (25°C, stirring rate 300 rpm).

The NMR spectra displayed an increase of Al13 content from 48.0 to 53.7 % without any change in the monomeric resonance upon increasing the stirring rate from 120 rpm to 300 rpm. The amount of undetectable Al decreased simultaneously from 48.3 to 42.3 % .

After aging for 1 year the NMR spectra of a solution of an OH/Al ratio of 2.4 showed no Al13 and 0.49 % of monomeric Al. The *pH* diminished asymptotically from 4.22 to 3.83. The solutions of OH/Al molar ratio's 1.8 and 1.2 decreased in *pH* from 3.93 and 3.80 to 3.65 and 3.41, respectively. NMR spectra of a solution of an OH/Al molar ratio of 1.2 taken at aging periods of 176 and 355 days displayed a decrease of Al13 from 42.9 to 13.2 % and of monomeric Al from 54.9 to 45.5 % (Fig. 10.7). The linewidth of the 63.2 ppm resonance broadened from

20.8 Hz to 41.1 Hz (accuracy 10 %), indicating a decrease in the symmetry of the fourfold coordinated Al in the Al13 polymer upon aging.

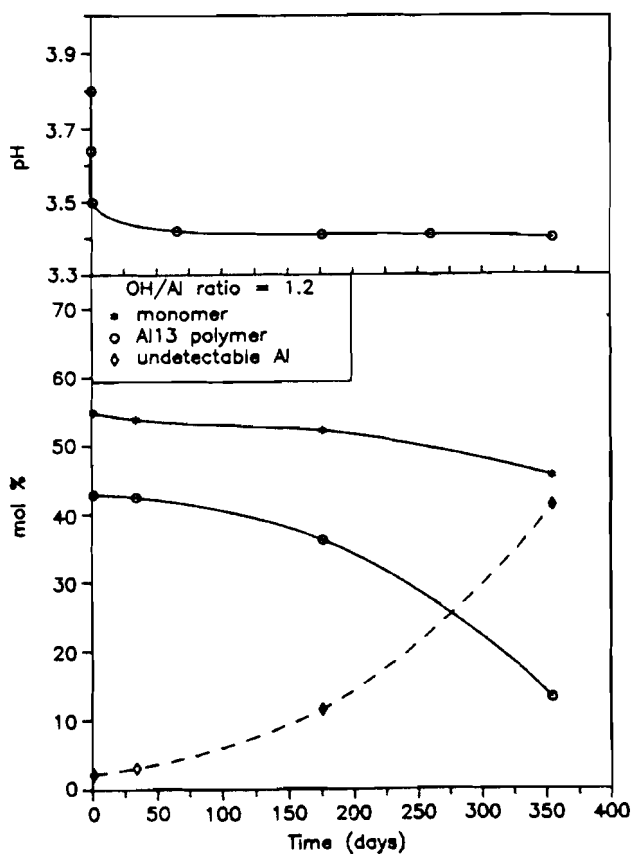


Figure 10.7 The decrease of pH and corresponding changes in concentration of monomeric Al, Al13 and undetectable Al as function of aging time. The concentrations are analyzed with NMR in a partially neutralized Al nitrate solution with OH/Al molar ratio of 1.2.

10.4 DISCUSSION

10.4.1 Reference chemical shift

Most studies performed so far have been based on the assumption that the chemical shift of the reference does not depend on the concentration and the Al salt used. Recent recordings by Akitt and Elders (1985a) as well as the present results have demonstrated that the chemical shift varies to a small extent. Dilute aluminum chloride or aluminum perchlorate solutions are assumed to be the most appropriate references. The 5.2×10^{-2} M aluminum nitrate reference used in this study, instead of aluminum chloride, exhibits a resonance shift of approximately 0.10 ppm to high field in comparison with aluminum chloride. The chemical shift at a high magnetic field strength of 11.7 Tesla is increased by another 0.10 ppm to high field as compared to the shift at 4.6 Tesla. The dilution with D₂O instead of H₂O (Akitt, 1989) finally shifts the resonance by about 0.08 ppm. The same effect has been observed on organosilanes and siloxanes with ²⁹Si NMR (Berchier et al., 1986). The effect of the anion, the concentration, the magnetic field strength, and the dilution with D₂O can account for the chemical shift of the six and fourfold coordinated Al measured in this work being different from the shifts published in most papers concerning Al hydrolysis (Table 10.3).

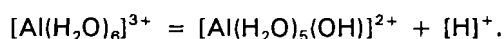
10.4.2 Relation between OH/Al molar ratio and chemical shift and linewidth

The shift of a resonance can be explained by a change in magnetic susceptibility and ionic strength. In our solutions the ionic strength increases during hydrolysis due to the addition of NaOH. The small shift for the fourfold coordinated Al resonance is due to the shielding by the 12 sixfold coordinated Al ions, forming a cage-like structure around the central fourfold coordinated Al in the Al13 complex (Keggin structure). Akitt et al. (1988) pointed out that the linewidth of quadrupolar nuclei is directly proportional to the bulk viscosity of the solution. Upon hydrolysis

Table 10.3 Variation in chemical shift δ as published in previous articles concerning Al13.

Authors	frequency (MHz)	reference	$\delta(\text{Al}^{\text{VI}})$ ppm	$\delta(\text{Al}^{\text{IV}})$ ppm
Kloprogge et al., 1992	52.142	$\text{Al}(\text{NO}_3)_3$	0.1-0.9	63.3
Akitt and Farthing, 1978	23.45	AlCl_3		62.5
Akitt and Elders, 1988	104.2	$\text{Al}(\text{OD})_4^-$	0	62.5
Bertsch et al., 1986b	52.1	Al Fisher	0	62.5
Bottero et al., 1980	23.45	$\text{Al}(\text{OH})_4^-$	0.1	63
Denney and Hsu, 1986	20.727	$\text{Al}(\text{OH})_4^-$	0	63
Thompson et al., 1987	130.3	AlCl_3	0	62.8

the NaOH concentration increases, while the Al nitrate concentration remains the same in all solutions. The ratio of the viscosity of the NaOH solution and that of pure water increases from 1.000 to approximately 1.025, if no polymerization takes place. The polymerization and aggregation of Al13 polymers (Bottero et al., 1987) may raise the viscosity even more. The linewidth of the monomer resonance is not only influenced by the viscosity of the solution but also by the *pH* (Akitt and Elders, 1985b). The increase in linewidth observed during forced hydrolysis may be partly explained by the reaction



Assuming that this is the only effective reaction, the increase in linewidth can be calculated with the expression of Akitt and Elders (1985b), resulting in a broadening of 17.5 Hz. This is only a fraction of the observed linewidth, viz. 37 to 112 Hz, which indicates that this reaction can only play a minor rôle.

10.4.3 Quadrupole relaxation

The isotropic chemical shifts and linewidths of resonances from quadrupolar nuclei such as Al are largely influenced by the dimension of the quadrupole

coupling constant e^2qQ/h . Deviations introduced by the field-dependent second-order quadrupole-induced shift from the isotropic value, can be calculated according to the following relation (Thompson et al., 1987):

$$\delta(\text{ppm}) \approx 6(1 + \eta^2/3)(e^2qQ/h\nu_0)^2 10^3 \quad (1)$$

where ν_0 is the Larmor frequency, e^2qQ/h the nuclear quadrupole coupling constant and η the asymmetry parameter. In solutions under conditions of rapid, isotropic tumbling the spin-lattice (T_1) and spin-spin (T_2) relaxation times for ²⁷Al are given by:

$$1/T_1 = 1/T_2 = (12\pi^2/125)(1 + \eta^2/3)(e^2qQ/h)^2\tau_c \quad (2)$$

where τ_c is the rotational correlation time. The linewidth at half height provides the opportunity to calculate T_2 with the relation $T_2 = 1/\pi\nu_{1/2}$, where $\nu_{1/2}$ is the linewidth at half height in Hz. The fourfold coordinated Al at 63.3 ppm has at half height a linewidth of 18.2 Hz, which results in a T_2 of 1.75×10^{-2} s. This spin-spin relaxation time is of the same order of magnitude as the value reported by Thompson et al. (1987). Substitution in expression (2) using $\tau_c = 1.3 \times 10^{-10}$ s (Thompson et al., 1987) and assuming $\eta = 0$, gives for e^2qQ/h a value of 0.68 MHz. Deviation from the isotropic value can be derived by substitution of these values in equation (1). The calculated result is a shift of 1 ppm from the isotropic value. The T_2 value for monomeric Al is calculated to be approximately 0.9×10^{-2} s for an OH/Al molar ratio of 1.2 and changes to 0.3×10^{-2} for an OH/Al molar ratio of 2.2. The T_1 values of 5.3×10^{-2} s for fourfold coordinated Al and 1.2×10^{-2} for sixfold coordinated Al reported by Bertsch et al. (1986b) for an OH/Al molar ratio of 2.25 are much higher than the values in this paper and those reported by Thompson et al. (1987).

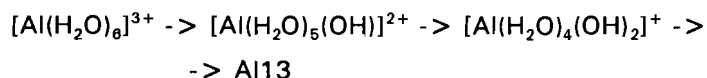
10.4.4 Relation between OH/Al molar ratio and Al13 concentration

Bottero et al. (1980) and Bertsch et al. (1986a,b) have studied the effect of the OH/Al molar ratio on the development of Al13 complexes. The results of the present study, in which solutions of a final Al concentration of 5.2×10^{-2} and

8.3×10^{-2} M were investigated, are comparable with those of Bertsch et al. (1986a,b, 1987). The latter authors had a final Al concentration of 3.34×10^{-2} M. The amorphous precipitate formed during dropwise addition does not contribute to the formation of Al13 during the neutralization or the aging, causing a lower Al13 yield as compared to the alkali injection experiments. The optimal Al13 yield of 68.9 % is reached at an OH/Al molar ratio of 2.2, which is significantly lower than the theoretical effective degree of hydrolysis 2.46 (32 OH/13 Al) based on $[\text{Al}_{13}(\text{OH})_{32}]^{7+}$ (Akitt and Farthing, 1978). Bottero et al. (1980, 1982) obtained with a 10×10^{-2} M Al solution an optimum Al13 yield of 95.8 % at an OH/Al molar ratio of 2.1, which is 0.1 lower than the OH/Al molar ratio at which we observed the maximum yield. Bertsch et al. (1986a,b) observed a maximum Al13 concentration at an OH/Al molar ratio of approximately 2.25 with a 0.03×10^{-2} M Al (69.7 %) and a 3.34×10^{-2} M Al (68.6 %) solution. Akitt and Elders (1988) determined a maximum Al13 concentration of 100 % using $50\text{-}80 \times 10^{-2}$ M Al salt solutions rapidly neutralized at 90°C to an OH/Al molar ratio of 2.5. This agrees with unpublished data from this laboratory.

10.4.5 Alkalis solution injection and mixing conditions

The Al13 yield is a function of the base injection rate, which has an optimum depending on the OH/Al molar ratio. The optimum injection rate shifts from 0.020 ml/sec for solutions with OH/Al molar ratio = 1.2 to approximately 0.010 ml/sec for solutions with OH/Al molar ratio 2.2. At higher rates the fraction of undetectable Al rapidly increased and the solution became cloudy. Bertsch et al. (1986a) and Bottero et al. (1980) suggested that at high injection rates more $\text{Al}(\text{OH})_4^-$ is generated than can be consumed by the formation of Al13. The excess $\text{Al}(\text{OH})_4^-$ reequilibrates with the bulk solution resulting in colloidal or precipitated $\text{Al}(\text{OH})_3$. At addition rates below 0.010 ml/s too low amounts of $\text{Al}(\text{OH})_4^-$ are created, which have reequilibrated with the solution before Al13 can be formed, which represents the other limitation. An alternative is a series of sequential reactions during the slow injection of the alkali solution



It is assumed by several authors (Akitt and Farthing, 1981; Bertsch et al, 1987) that $\text{Al}(\text{OH})_4^-$ formed at the point of alkali introduction is needed as a precursor for the formation of Al13. Akitt and Farthing (1981) hydrolyzed Al^{3+} via solid Na_2CO_3 . They assumed a very rapid $\text{Al}(\text{OH})_4^-$ production under the inhomogeneous conditions at the interface of solid Na_2CO_3 and the solution. As discussed above several equilibria exist in partly neutralized Al solutions, all depending on the rate of alkali injection. Low OH/Al molar ratio's and slow injection favors the formation of mono- and dimer. Fast injection favors precipitation instead. Slow stirring rates causes the $\text{Al}(\text{OH})_4^-$ to reequilibrate with the acid solution. The Al13 and monomer concentrations are similar up to an OH/Al molar ratio of 2.6 for the neutralization reaction of AlCl_3 and $\text{Al}(\text{NO}_3)_3$ solutions, as confirmed by Akitt and Farthing (1981).

10.4.6 Aging

The decrease of the Al13 content upon aging confirms that the Al13 is actually a metastable complex in solution. The Al13 polymer rearranges with time into large polymers unobservable with the NMR technique. Formation of other polymers is evident from the strong increase of the amount of undetectable Al, the disappearance of Al13, and the decrease of monomeric Al in the solution. Several authors have suggested that these polymers consists of hexameric rings (Bottero et al., 1982; Bertsch et al., 1986a,b; Denney and Hsu, 1986). The constant *pH* upon aging suggests a structural rearrangement without changing the degree of hydrolysis of the polymer (Tsai and Hsueh, 1984). Small angle X-ray scattering data suggest that the alumina tetrahedra present in Al13 are squeezed between growing octahedral layers and that tetrahedra are totally lost at the end of the aging process (Bottero et al., 1982, 1987). The broadening of the 63.3 ppm resonance upon aging, indicating a decrease in tetrahedral symmetry, support this structural rearrangement.

10.5 CONCLUSIONS

- 1) Chemical shifts are influenced by i) the choice of reference solution and its concentration, ii) magnetic field strength and iii) dilution with D₂O.
- 2) The increasing chemical shift and linewidth of the monomer resonance upon hydrolysis is mainly caused by increasing ion strength and viscosity.
- 3) The maximum amount of Al₁₃ formed is influenced by the hydrolysis conditions, such as, OH/Al molar ratio, injection rate and mixing conditions.
- 4) The Al₁₃ rearranges into large polymers with a hexameric ring structure upon aging.

ACKNOWLEDGMENTS

The authors wish to thank G. Nachtegaal for the technical assistance at the SON HF-NMR facility at Nijmegen. W. Veeman, A. M. J. van der Eerden, P. Buining and J. van Beek are thanked for critically reviewing this article.

REFERENCES

- Akitt, J. W. (1989) Multinuclear studies of aluminum compounds: *Prog. Nucl. magn. Reson. Spectrosc.* **21**, 1-149.
- Akitt, J. W. and Elders, J. M. (1985a) The hexa-aquo aluminum cation as reference in aluminum-27 NMR spectroscopy: *J. Magn. Reson.* **63**, 587-589.
- Akitt, J. W. and Elders, J. M. (1985b) Aluminium-27 nuclear magnetic resonance studies of the hydrolysis of aluminium(III). Part 7. Spectroscopic evidence for the cation $[\text{AlOH}]^{2+}$ from linebroadening studies at high dilution: *J. Chem. Soc. Faraday Trans.* **81**, 1923-1930.
- Akitt, J. W. and Elders, J. M. (1988) Multinuclear magnetic resonance studies of the hydrolysis of aluminium(III). Part 8. Base hydrolysis monitored at very high magnetic field: *J. Chem. Soc. Dalton Trans.*, 1347-1355.
- Akitt, J. W. and Farthing, A. (1978) New ^{27}Al NMR studies of the hydrolysis of the aluminum(III) cation: *J. Magn. Reson.* **32**, 345-352.
- Akitt, J. W. and Farthing, A. (1981) Aluminum-27 nuclear magnetic resonance studies of the hydrolysis of aluminum(III). Part 4. Hydrolysis using sodium carbonate: *J. Chem. Soc. Dalton Trans.*, 1617-1623.
- Akitt, J. W., Gessner, W. and Weinberger, M. (1988) High-field aluminium-27 nuclear magnetic resonance investigations of sodium aluminate solutions: *Magn. Reson. Chem.* **26**, 1047-1050.
- Akitt, J. W., Greenwood, N. N., Khandelwal, B. L. and Lester, G. D. (1972) ^{27}Al nuclear magnetic resonance studies of the hydrolysis and polymerisation of the hexa-aquo-aluminum(III) cation: *J. Chem. Soc. Dalton Trans.*, 604-610.
- Berchier, F., Pai, Y.-M., Weber, W. P. and Servis, K. L. (1986) Deuterium isotope effects on silicon-29 chemical shifts: *Magn. Reson. Chem.* **24**, 679-680.
- Bertsch, P. M. (1987) Conditions for Al13 polymer formation in partially neutralized aluminum solutions: *Soil Sci. Soc. Amer. J.* **51**, 825-828.

- Bertsch, P. M., Thomas, G. W. and Barnhisel, R. I. (1986a) Characterization of hydroxy-aluminum solutions by aluminum-27 nuclear magnetic resonance spectroscopy: *Soil Sci. Soc. Amer. J.* **50**, 825-830.
- Bertsch, P. M., Layton, W. T. and Barnhisel, R. I. (1986b) Speciation of hydroxy-aluminum solutions by wet chemical and aluminum-27 NMR methods: *Soil Sci. Soc. Amer. J.* **50**, 1449-1454.
- Bottero, J. Y., Axelos, M., Tchoubar, D., Cases, J. M., Fripiat, J. J. and Fiessinger, F. (1987) Mechanism of formation of aluminum trihydroxide from Keggin Al_{13} polymers: *J. Coll. Interf. Sci.* **117**, 47-57.
- Bottero, J. Y., Cases, J. M., Fiessinger, F. and Poirier, J. E. (1980) Studies of hydrolyzed aluminum chloride solutions. 1. Nature of aluminum species and composition of aqueous solutions: *J. Phys. Chem.* **84**, 2933-2939.
- Bottero, J. Y., Tchoubar, D., Cases, J. M. and Fiessinger, F. (1982) Investigation of the hydrolysis of aqueous solutions of aluminum chloride. 2. Nature and structure by small angle X-ray scattering: *J. Phys. Chem.* **86**, 3667-3673.
- Brosset, C., Biedermann, G. and Sillén, L. G. (1954) Studies on the hydrolysis of metal ions XI. The aluminium ion, Al^{3+} : *Acta Chem. Scand.* **8**, 917-1926.
- Denney, D. Z. and Hsu, P. H. (1986) ^{27}Al nuclear magnetic resonance and ferron kinetic studies of partially neutralized $AlCl_3$ solutions: *Clays & Clay Minerals* **34**, 604-607.
- Hsu, P. H., in: *Minerals in Soil Environments*, J. B. Dixon and S. B. Weed, eds., Soil Science Society of America, Madison, WI (1977) 99-143.
- Johansson, G. (1960) On the crystal structure of some basic aluminum salts: *Acta Chem. Scand.* **14**, 771-773.
- Johansson, G. (1962) The crystal structures of $[Al_2(OH)_2(H_2O)_8](SO_4)_2 \cdot 2H_2O$ and $[Al_2(OH)_2(H_2O)_8](SeO_4)_2 \cdot 2H_2O$: *Acta Chem. Scand.* **16**, 403-420.
- Johansson, G. (1963) The crystal structure of a basic aluminum selenate: *Ark. Kemi* **20**, 305-319.
- Johansson, G. (1963) On the crystal structure of the basic aluminum sulfate $13Al_2O_3 \cdot 6SO_3 \cdot xH_2O$: *Ark. Kemi* **20**, 321-342.

- Kloprogge, J. T., Jansen, J. B. H. and Geus, J. W. (1990) Characterization of synthetic Na-beidellite: *Clays & Clay Minerals* **38**, 409-414.
- Kloprogge, J. T., Seykens, D., Geus, J. W. and Jansen, J. B. H. (1992) Temperature influence on the Al13 complex in partially neutralized aluminum solutions: an ²⁷Al nuclear magnetic resonance study: *J. Non-Cryst. Solids* **142**, 87-93.
- Lampe, F., Müller, D., Gessner, W., Grimmer, A.-R. und Scheler, G. (1982) Vergleichende ²⁷Al-NMR-Untersuchungen am Mineral Zunyit und basischen Aluminium-Salzen mit tridekameren Al-oxo-hydroxo-aquo-Kationen: *Z. Anorg. Allg. Chem.* **489**, 16-22.
- Plee, D., Gatineau, L. and Fripiat, J. J. (1987) Pillaring processes of smectites with and without tetrahedral substitution: *Clays & Clay Minerals* **35**, 81-88.
- Rausch, W. V. and Bale, H. D. (1964) Small-angle X-ray scattering from hydrolyzed aluminum solutions: *J. Chem. Phys.* **40**, 3391-3394.
- Schutz, A., Stone, W. E. E., Poncelet, G. and Fripiat, J. J. (1987) Preparation and characterization of bidimensional zeolitic structures obtained from synthetic beidellite and hydroxy-aluminum solutions: *Clays & Clay Minerals* **35**, 251-261.
- Shabtai, J., Rosell, M. and Tokarz, M. (1984) Cross-linked smectites. III. Synthesis and properties of hydroxy-aluminum hectorites and fluorhectorites: *Clays & Clay Minerals* **32**, 99-107.
- Sterte, J. and Shabtai, J. (1987) Cross-linked smectites. V. Synthesis and properties of hydroxy-silicoaluminum montmorillonites and fluorhectorites: *Clays & Clay Minerals* **35**, 429-439.
- Thompson, A. R., Kunwar, A. C., Gutowsky, H. S. and Oldfield, E. (1987) Oxygen-17 and aluminium-27 nuclear magnetic resonance spectroscopic investigations of aluminium(III) hydrolysis products: *J. Chem. Soc. Dalton Trans.*, 2317-2322.

- Tsai, P. P. and Hsu, P. H. (1984) Studies of aged Oh-Al solutions using kinetics of Al-feron reactions and sulfate precipitation: *Soil Sci. Soc. Amer. J.* **48**, 59-65.
- Vermeulen, A. C., Geus, J. W., Stol, R. J. and de Bruyn, P. L. (1975) Hydrolysis-precipitation studies of aluminum(III) solutions. I. Titration of acidified aluminum nitrate solutions: *J. Coll. Interf. Sci.* **51**, 449-458.

CHAPTER XI

Temperature Influence on the Al₁₃ Complex in Partially Neutralized Aluminum Solutions: an ²⁷Al Nuclear Magnetic Resonance Study

Abstract

Stepwise heating to 85°C in the NMR apparatus does not notably change the monomer and tridecamer (Al₁₃) concentrations in a 0.2 M Al(NO₃)₃ solution neutralized with 0.2 M NaOH up to a OH/Al molar ratio of 2.4. Upon heating the fourfold coordinated ²⁷Al NMR signal of Al₁₃ at 63.3 ppm and the very broad sixfold coordinated ²⁷Al NMR signal of Al₁₃ at 12 ppm, exhibit an increasing intensity and decreasing linewidth, due to diminishing "missing intensity" and "quadrupole relaxation", respectively. An analogous effect for a Na₂CO₃ neutralized 0.2 M AlCl₃ solution confirmed that the 12 ppm signal must be assigned to the sixfold coordinated Al of the Al₁₃ complex. The surface ratio of fourfold coordinated Al to sixfold coordinated Al of the Al₁₃ complex experimentally established, is smaller than the theoretical 1:12 ratio. During heating a more intensive exchange interaction between monomer and other Al- species is proposed without any effect on the actual concentrations. High symmetry in the Al₁₃ complex is determined at elevated preparation temperatures from the decreasing linewidth of the 63.3 ppm resonance. Above 85°C the tridecamer transforms in other species, which can not be observed with NMR.

11.1 INTRODUCTION

From X-ray powder diffraction data of basic aluminum sulfate and selenate Johansson (1960,1962,1963) and Johansson et al. (1960) were the first to propose the existence of the tridecameric complex $[AlO_4Al_{12}(OH)_{24}(H_2O)_{12}]^{7+}$ (Al₁₃) (Fig. 11.1a). ²⁷Al NMR (Akitt et al., 1972; Akitt and Farthing, 1978) and small angle X-ray scattering (Rausch and Bale, 1964; Bottero et al., 1982) confirmed the existence of the metastable tridecamer. Upon aging no physical changes are described (Akitt and Farthing, 1981; Tsai and Hsu, 1984,1985; Kloprogge et al., 1992), whereas decreases of approximately 15 % and 70 % in tridecamer content were determined after aging periods of 176 and 355 days, respectively (Kloprogge

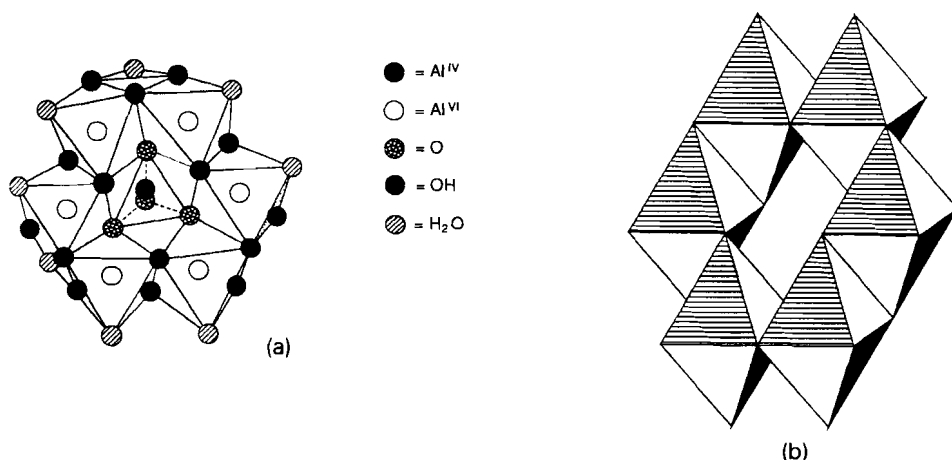


Figure 11.1 a) The tridecameric (Al₁₃) complex (Karlík et al., 1983; Bottero et al., 1987) and b) The hexameric ring complex (modified after Smith and Hem, 1972).

et al., 1992). Together with the decrease of the concentration of the tridecamer, the fact that the pH does not change indicates a structural rearrangement of the tridecameric polymer that does not involve further hydrolysis of Al(III) ions. A rearrangement of the Al₁₃ polymer in hexameric ring polymers (Fig. 11.1b) resembling fragments of the gibbsite structure (Brosset et al., 1954; Smith and Hem, 1972; Bottero et al., 1982; Bertsch et al., 1986a,b; Denney and Hsu, 1986) is supported by small angle X-ray scattering, which points to the growth of elongated platelets. Infrared spectroscopy showed the platelets to be bayerite, while ²⁷Al NMR revealed a decrease of fourfold coordinated Al and an increasing perturbation of the symmetry of the tetrahedral site (Bottero et al., 1987).

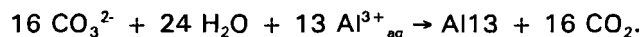
The tridecameric complex is appropriate for pillaring clays. Clays thus pillared exhibit physico-chemical properties attractive for shape-selective catalysts and molecular sieves (Plee et al., 1985, 1987; Schutz et al., 1987; Kloprogge et al., 1990). Usually, the clays are pillared at 25°C, but pillaring at higher temperatures

may increase the quality of the resulting porous structure. It is therefore important to establish optimal conditions for the formation and storage of tridecameric complexes (Kloprogge et al., 1992). Since pillaring at higher temperatures calls for an assessment of the stability of the tridecameric complex at the temperatures to be used, the behavior of the complex is investigated at temperatures from 20 to 95°C.

In this study the behavior of the tridecameric complex has been investigated with ²⁷Al Nuclear Magnetic Resonance (NMR). Samples prepared by partial neutralization of Al(III) solutions at temperatures up to 80°C were measured. During the NMR measurement, the temperature of the differently prepared samples was also varied from 20 to 95°C. Since the mode of addition of the alkaline solution affects the resulting fraction of the Al₁₃ complex, dropwise addition of a NaOH solution and addition of small amounts of solid Na₂CO₃ was used.

11.2 EXPERIMENTAL

A 0.2 M Al(NO₃)₃ solution kept at room temperature was partially neutralized in a nitrogen atmosphere by dropwise adding 0.2 M NaOH over a period of 1 hour to a final OH/Al molar ratio of 2.4. The nitrogen atmosphere was used to exclude an effect of carbon dioxide of atmospheric air. A 0.2 M AlCl₃ solution was partially neutralized by adding solid Na₂CO₃ in amounts of 1 mg over a period of 1 hour resulting in a final OH/Al molar ratio of 2.5. The neutralization proceeded according to the simplified overall reaction



Furthermore, a series of solutions was prepared with an OH/Al molar ratio of 2.5 at 25°, 40° and 75°C, using the 0.2 M AlCl₃ and 0.2 M NaOH stock solutions.

The ^{27}Al NMR spectra were recorded with a Bruker WP200 spectrometer operating at 52.148 MHz (4.6 Tesla). Spectra obtained with this instrument had to be corrected for background signals due to aluminum containing ceramics present in the probe. For comparative reasons some spectra were recorded on a Bruker WM 500 spectrometer operating at 130.321 MHz (11.7 Tesla), designed for solid state work with an aluminum-free probe. This spectrometer was installed at the Department of Physical Chemistry, Faculty of Science, University of Nijmegen. Directly before the NMR measurements the solution was diluted with D_2O (1:1) for field frequency lock. After neutralization and dilution the solutions had an actual Al concentration of 0.05 M. As reference for the chemical shift an aluminum ammonium sulfate solution was used.

To determine the total Al concentration, $\text{Al}(\text{NO}_3)_3$ standard solutions were measured. The percentage of Al monomer relative to the total Al content was directly calculated from the integrated intensity of the 0.3 ppm signal. The percentage of the tridecamer complex was calculated by multiplying the integrated intensity of the 63.3 ppm signal due to fourfold coordinated Al with 13. The fraction of undetectable Al was obtained by subtracting the amount of monomeric and polymeric Al from the total Al of the standard.

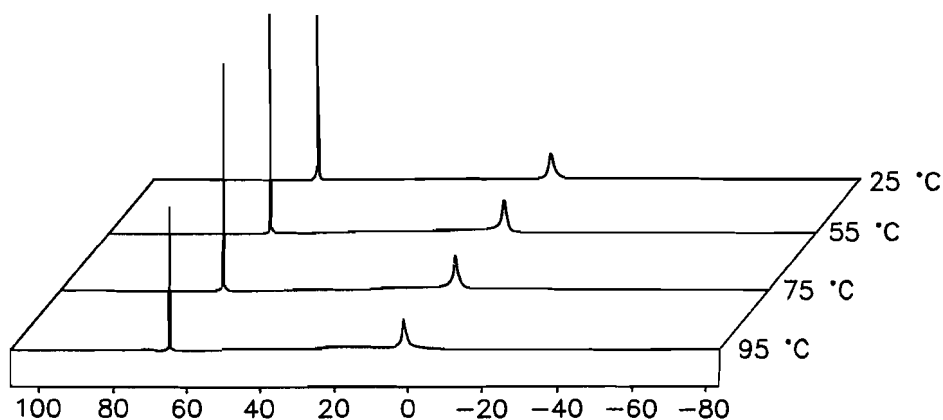


Figure 11.2 ^{27}Al NMR spectra of a at 25 °C NaOH partially neutralized $\text{Al}(\text{NO}_3)_3$ solution with an OH/Al molar ratio of 2.4 measured at temperatures of 25, 55, 75 and 95 °C.

11.3 RESULTS

Monomeric sixfold coordinated Al produced a relatively broad signal at 0.3 ppm (0.1 ppm at 11.7 T), and fourfold coordinated Al of the Al₁₃ complex a sharp signal at 63.3 ppm (63.2 ppm at 11.7 T)(Fig. 11.2). Slightly downfield of the signal due to the sixfold coordinated Al monomer an extremely broad signal of low intensity with its maximum at 12 ppm is hardly detectable in spectra measured at 25°C. The latter signal can be distinguished more easily in the spectra measured at temperatures higher than 55°C (Fig. 11.2). The signal peaking at 12 ppm may be attributed to sixfold coordinated Al present within the tridecameric complexes and to dimeric sixfold coordinated Al.

Raising the temperature slightly broadened the monomeric signal at 0.3 ppm, but narrowed signal at 63.3 ppm due to the fourfold coordinated Al from 18.2 Hz at 25°C to 13.7 Hz at 75°C. The accuracy of the determination of the linewidth is about 10 % . The fraction of Al present as monomeric and tridecameric species calculated from surface integrals of the NMR signals show an apparent increase at temperatures rising to 65°C (Table 11.1, Fig. 11.3). At temperatures increasing to 75°C the very broad signal at 12 ppm exhibited a stronger increase in both surface integral and peak height than the 63.3 ppm signal, as evident from the observed Al^{VI}:Al^{IV} ratio (Table 11.1). At 25°C the 12 ppm signal had a width of 9100 Hz (11.7 T). At 75°C the width had decreased to 2700 Hz (4.6 T). Simultaneously, a significant drop in the fraction of undetectable Al from 18 to 2 % was observed. Up to 85°C the apparent changes in surface integrals and linewidths of the NMR signals were reversible on cooling. The final step of the temperature program in which the temperature was increased from 85°C to 95°C brought about a decrease in the fraction of Al present as the tridecameric complex and, consequently, an increase in the fraction of undetectable Al. Typically the 63.3 ppm signal due to fourfold coordinated Al as well as the 12 ppm signal due

Table 11.1 Apparent distribution of Al among monomeric, tridecameric species and undetectable Al in a solution with OH/Al molar ratio of 2.4 as a function of measurement temperature.

T °C	monomer % 0.3 ppm	Al ^{VI} % 12 ppm	tridecamer % 63.3 ppm	undet. Al%	Al ^{VI} :Al ^{IV}
25	9.9	15.23	72.3	17.8	1 : 2.74
35	11.3	20.50	74.3	14.5	1 : 2.82
45	10.7	26.50	78.2	11.1	1 : 3.38
55	13.1	32.22	81.8	5.1	1 : 5.12
65	12.0	41.18	86.2	1.8	1 : 6.21
75	12.6	38.70	84.2	3.2	1 : 5.98
85	10.8	32.41	86.7	2.5	1 : 4.86
95	9.8	27.65	68.6	21.6	1 : 5.24

to sixfold coordinated Al sharply decreased upon raising the temperature to 95°C (Fig. 11.3).

The sodium-carbonate neutralized Al chloride solution yielded a sharp signal at 63.3 ppm due to fourfold coordinated Al of the tridecameric complex and a peculiar broad signal near 12 ppm. When this solution was heated to 80°C in the NMR apparatus, no significant change in the signal due to fourfold coordinated Al of the tridecameric complex developed, while the surface of the 12 ppm signal increased (Table 11.2). The amount of approximately 30 % of undetectable Al is high as compared to that of the NaOH neutralized solutions.

Raising the temperature during the partial neutralization to 75°C caused the tridecamer content of a solution with an OH/Al molar ratio of 2.5 prepared with dropwise NaOH addition to increase from 52.0 to 80.6 % (Table 11.3). The linewidth of the 63.3 ppm resonance measured at 25°C declined from 18.2 Hz for

Temperature influence on the Al13 complex in partially neutralized aluminum solutions: an ^{27}Al nuclear magnetic resonance study

a solution neutralized at 25°C to 15.6 Hz for a solution neutralized at 75°C (accuracy 10 %).

Table 11.2 Distribution of Al among monomeric, Al13 polymeric species and undetectable Al in percentages in a Na_2CO_3 neutralized Al solution with OH/Al molar ratio of 2.4 at temperatures of 20°C and 80°C.

T °C	Al ^{VI} % 12 ppm	tridecamer %	undet. Al %	Al ^{IV} :Al ^{VI}
20	34.25	69.36	30.64	1 : 6.42
80	42.27	71.73	28.27	1 : 7.66

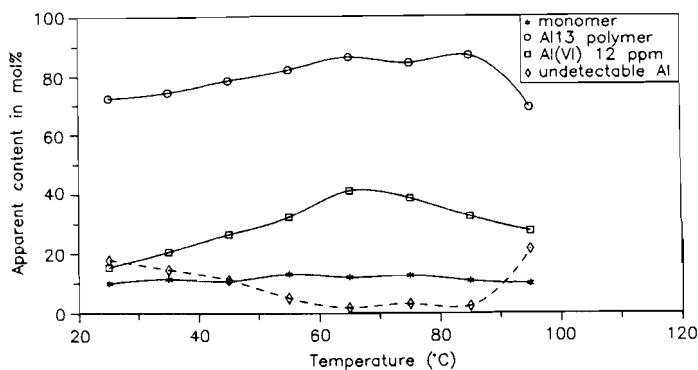


Figure 11.3 Al-distribution among monomer, tridecamer and undetectable Al in an Al nitrate solution with OH/Al molar ratio of 2.4 plotted against temperature.

Table 11.3 Concentrations of monomer, tridecamer and undetectable Al in a 0.05 M Al chloride solution dropwise neutralized till an OH/Al molar ratio of 2.5 as function of the preparation temperature.

T °C	monomer %	Al ^{VI} % 12 ppm	tridecamer %	undet. Al %	Al ^{IV} :Al ^{VI}
25	4.4	6.1	52.0	43.6	1 : 1.53
40	6.7	11.8	70.4	22.9	1 : 2.17
75	5.6	12.2	80.6	13.8	1 : 1.96

11.4 DISCUSSION

Results of this laboratory (Kloprogge et al., 1992) have shown that the precise position of the ²⁷Al NMR resonances depends to a limited extent on the choice of reference solution and its concentration (Akitt and Elders, 1985), the dilution with D₂O, and the magnetic field strength. As dealt with earlier, an Al(NO₃)₃ solution, diluted with an equal volume of D₂O, measured at a magnetic field strength of 4.7 Tesla was used as reference. The use of this reference leads to the observed position of the resonance of the monomeric sixfold coordinated Al at 0.3 ppm, that of the tridecameric sixfold coordinated Al at 12 ppm and that of the fourfold coordinated Al at 63.3 ppm. In the literature resonances at 0 ppm/0.1 ppm (Bottero et al., 1980; Akitt and Elders, 1985), 8 ppm/12 ppm (Akitt and Elders, 1985; Bertsch et al., 1986a,b), and 62.5 ppm/62.8 ppm/63 ppm (Bottero et al., 1980; Akitt and Elders, 1985; Denney and Hsu, 1986; Thompson et al., 1987), respectively, have been reported.

Heating of a partially neutralized Al nitrate solution within the NMR spectrometer to 85°C caused no significant change in the monomer content and a small apparent increase in the tridecamer content. Resonances from a quadrupolar

nucleus as ²⁷Al are known to suffer from the so called "missing intensity" (Akitt, 1989). Especially the resonance at 12 ppm of the Al within the tridecameric complex shows the missing intensity. The missing intensity can be diminished measuring at higher temperatures. The observed intensity is given by

$$I = I_0 \exp(-t/T_2)$$

where I_0 is the initial intensity of the Free Induced Decay (FID), t the time between the appearance of the signal at the filter output and the start of the data collection, and T_2 the spin-spin relaxation time, which is inversely proportional to the linewidth. This explains the apparent increase in the tridecamer and the decrease in the undetectable Al content. The apparent intensity of the 12 ppm signal increased more strongly upon heating than the 63.3 ppm signal due to the fact that T_2 of the sixfold coordinated Al increased more strongly, as evident from the linewidth. The linewidth of the resonance at 12 ppm dropped from 9100 Hz at 25°C to 2700 Hz at 75°C; that of the resonance at 63.3 ppm from 18.2 Hz to 13.7 Hz.

Between 85°C and 95°C a decrease in the signals due to the tridecameric polymer was observed, indicating a structural rearrangement of the tridecamer to a species unobservable by NMR. Heating can be considered to be an accelerated aging. It has been suggested that upon aging the tridecamer rearranges into a larger polymer exhibiting a hexameric ring structure (Brosset al., 1954; Smith and Hem, 1972; Bottero et al., 1982; Bertsch et al., 1986a,b; Denney and Hsu, 1986). ²⁷Al NMR has shown that the fourfold coordinated Al is finally squeezed to a very distorted sixfold coordination. These polymers form elongated platelets, which were identified by IR as bayerite (Bottero et al., 1987), which provides evidence for the hexameric ring structure.

The gradual broadening of the Al monomer resonance at 0.3 ppm with the temperature is presumably due to an increase in exchange-interaction with other Al-species in the solution. The exchange-interactions are usually intensified by heating (Akitt and Farthing, 1978).

In the whole temperature range the resonance at 63.3 ppm due to fourfold coordinated Al of the tridecameric complex is relatively narrow indicating a small distortion of the symmetry (Karlik et al., 1983). The 12 ppm and 63.3 ppm resonance signals sharpen by heating in the NMR apparatus due to the quadrupole relaxation of Al, which contains two temperature-dependent terms, viz., the Electric Field Gradient (EFG), and the correlation time of the EFG. The correlation time diminishes with increasing temperature and thus the linewidth. The EFG is related to the symmetry of the bonding electrons around the nucleus. Unfortunately, it is impossible to gain information on the EFG and thus on the symmetry at increasing measurement temperature due to lack of data on the correlation time of the EFG (Akitt, 1989). The observed width of 2700 Hz at 75°C and 9100 Hz at 25°C (11.7 T) is slightly higher than the linewidth of 2000 Hz and 8100 Hz reported by Akitt and Farthing (1981), and Akitt (1989), respectively. The width of the resonances is attributed to the susceptibility of very broad signals to the background correction applied.

Bertsch et al. (1986a,b) described a broad resonance at 8 ppm downfield of the Al monomer resonance, which is situated at 0 ppm in an 0.1 M AlCl_3 solution of an OH/Al molar ratio of 2.5. The resonance at 8 ppm is presumably comparable to the broad resonance at 12 ppm recorded in the partially neutralized Al nitrate and Al chloride solutions in this work. Bertsch et al. (1986a,b) attributed the signal at 8 ppm to the twelve sixfold coordinated Al of the tridecamer and to the available dimers, which led them to a proportion of fourfold coordinated Al(Al13) and sixfold coordinated Al(Al13 + dimer) of 1/14. In our experiments the proportion of fourfold coordinated Al and sixfold coordinated Al is much smaller than 1/12, the proportion which is expected theoretically for the tridecameric complex (Table 11.2). We observed an optimum ratio of 1/6.2 at a temperature of about 70°C (Table 11.1) for the solution neutralized with NaOH and a maximum ratio of 1/7.7 at 80°C (Table 11.2) for the solution neutralized with Na_2CO_3 . These proportions are even lower than presented by Bertsch et al. (1986a,b), although the observations were made at the same magnetic field strength. Akitt (1989) has

stated that it is required to perform the measurements at high magnetic field strength in an aluminum-free probe, applying a broad bandwidth coupled with a very large sweepwidth in order to obtain a correct proportion. The proportion mentioned by Bertsch et al. (1986a,b) therefore may be inaccurate, while the low proportions presented here are due to the low magnetic field. The increase of the broad resonance at 80 °C in the AlCl₃ solution neutralized by carbonate supports the fact that the signal at 12 ppm is mainly due to the sixfold coordinated Al of the tridecameric complex.

Hydrolysis at a preparation temperature of 75 °C yielded the highest content of the tridecameric complex. The decrease of the linewidth of the resonance at 63.3 ppm at high preparation temperatures indicates a higher symmetry of the tridecameric polymer. The higher symmetry leads to a change in the EFG, whereas the correlation time of the EFG remains constant during the NMR measurement, which was performed at 25 °C. It is suggested that a smaller distortion of the Al-octahedra favours the formation of the tridecameric polymer.

11.5 CONCLUSIONS

- 1) Heating to 85 - 95 °C in the NMR apparatus results in a structural rearrangement of the tridecamer into a larger polymer with a bayerite structure.
- 2) The linewidth decrease and intensity increase of the octahedral and tetrahedral resonances of the tridecameric polymer is caused by an increase in T₂ upon heating.
- 3) Heating in the NMR apparatus intensifies the exchange interaction of the monomer with other species in the solution and thus to a broadening of the monomer resonance.

- 4) The symmetry of the tridecamer tetrahedrals becomes higher at elevated preparation temperatures, causing a sharpening of the resonance at 63.3 ppm due to fourfold coordinated Al.
- 5) Preparation at 75 °C results in a smaller distortion of the Al-octahedra, favouring the formation of the tridecameric polymer.

ACKNOWLEDGMENTS

The authors are grateful to G. Nachtegaal for the technical assistance at the NWO-SON HF-NMR facility at Nijmegen. W. Veeman, A. M. J. van der Eerden, P. Buining, J. van Beek and M. K. Titulaer are thanked for critically reviewing this article.

REFERENCES

- Akitt, J. W. (1989) Multinuclear studies of aluminium compounds: *Prog. NMR Spectr.* **21**, 1-149.
- Akitt, J. W. and Elders, J. M. (1985) Aluminium-27 nuclear magnetic resonance studies of the hydrolysis of aluminium(III). Part 7. Spectroscopic evidence for the cation [Al(OH)]²⁺ from linebroadening studies at high dilution: *J. Chem. Soc. Faraday Trans.* **81**, 1923-1930.
- Akitt, J. W. and Farthing, A. (1978) New ²⁷Al NMR studies of the hydrolysis of the aluminium(III) cation: *J. Magn. Reson.* **32**, 345-352.
- Akitt, J. W. and Farthing, A. (1981) Aluminum-27 nuclear magnetic resonance studies of the hydrolysis of aluminum(III). Part 4. Hydrolysis using sodium carbonate: *J. Chem. Soc. Dalton Trans.*, 1617-1623.
- Akitt, J. W., Greenwood, N. N., Kandelwahl, B. L. and Lester, G. D. (1972) ²⁷Al nuclear magnetic resonance study of the hydrolysis and polymerisation of the hexa-aquo-aluminum(III) cation: *J. Chem. Soc. Dalton Trans.*, 604-610.
- Bertsch, P. M., Layton, W. J. and Barnhisel, R. I. (1986a) Speciation of hydroxy-aluminum solutions by wet chemical and aluminum-27 NMR methods: *Soil Sci. Soc. Amer. J.* **50**, 1449-1454.
- Bertsch, P. M., Thomas, G. W. and Barnhisel, R. I. (1986b) Characterization of hydroxy-aluminum solutions by aluminum-27 nuclear magnetic resonance spectroscopy: *Soil Sci. Soc. Amer. J.* **50**, 825-830.
- Bottero, J. Y., Axelos, M., Tchoubar, D., Cases, J. M., Fripiat, J. J. and Fiessinger, F. (1987) Mechanism of formation of aluminum trihydroxide from Keggin Al₁₃ polymers: *J. Coll Interf. Sci.* **117**, 47-57.
- Bottero, J. Y., Cases, J. M., Fiessinger, F. and Poirier, J. E. (1980) Studies of hydrolyzed aluminum chloride solutions. 1. Nature of aluminum species and composition of aqueous solutions: *J. Phys. Chem.* **84**, 2933-2939.

- Bottero, J. Y., Tchoubar, D., Cases, J. M. and Fiessinger, F. (1982) Investigation of the hydrolysis of aqueous solutions of aluminum chloride. 2. Nature and structure by small angle X-ray scattering: *J. Phys. Chem.* **86**, 3667-3673.
- Brosset, C., Biedermann, G. and Sillén, L. G. (1954) Studies on the hydrolysis of metal ions XI. The aluminum ion, Al^{3+} : *Acta Chem. Scand.* **8**, 1917-1926.
- Denney, D. Z. and Hsu, P. H. (1986) ^{27}Al nuclear magnetic resonance and ferron kinetic studies of partially neutralized AlCl_3 solutions: *Clays & Clay Minerals* **34**, 604-607.
- Johansson, G. (1960) On the crystal structure of some basic aluminum salts: *Acta Chem. Scand.* **14**, 771-773.
- Johansson, G. (1962) The crystal structures of $[\text{Al}_2(\text{OH})_2(\text{H}_2\text{O})_8](\text{SO}_4)_2 \cdot 2\text{H}_2\text{O}$ and $[\text{Al}_2(\text{OH})_2(\text{H}_2\text{O})_8](\text{SO}_4)_2 \cdot 2\text{H}_2\text{O}$: *Acta Chem. Scand.* **16**, 403-420.
- Johansson, G. (1963) The crystal structure of a basic aluminum selenate: *Ark. Kemi* **20**, 305-319.
- Johansson, G. (1963) On the crystal structure of the basic aluminum sulfate $13\text{Al}_2\text{O}_3 \cdot 6\text{SO}_3 \cdot x\text{H}_2\text{O}$: *Ark. Kemi* **20**, 321-342.
- Johansson, G., Lundgren G., Sillén L. G. and Söderquist, R. (1960) On the crystal structure of a basic aluminum sulfate and the corresponding selenate: *Acta Chem. Scand.* **14**, 769-771.
- Karlik, S. J., Tarien, E., Elgavish, G. A. and Eichhorn, G. (1983) Aluminum-27 nuclear magnetic resonance study of aluminum(III) interactions with carboxylate ligands: *Inorg. Chem.* **22**, 525-529.
- Kloprogge, J. T., Jansen, J. B. H. and Geus, J. W. (1990) Characterization of synthetic Na-beidellite: *Clays & Clay Minerals* **38**, 409-414.
- Kloprogge, J. T., Seykens, D., Jansen, J. B. H. and Geus, J. W. (1992) An ^{27}Al nuclear magnetic resonance study on the optimization of the development of the Al13 polymer: *J. Non-Cryst. Solids* **142**, 94-102.
- Plee, D., Borg, F., Gatineau, L. and Fripiat, J. J. (1985) High-resolution solid-state ^{27}Al and ^{29}Si nuclear magnetic resonance study of pillared clays: *J. Amer. Chem. Soc.* **107**, 2362-2369.

- Plee, D., Gatineau, L. and Fripiat, J. J. (1987) Pillaring processes of smectites with and without tetrahedral substitutions: *Clays & Clay Minerals* **35**, 81-88.
- Rausch, W. V. and Bale, H. D. (1964) Small-angle X-ray scattering from hydrolyzed aluminum nitrate solutions: *J. Chem. Phys.* **40**, 3391-3394.
- Schutz, A., Stone, W. E. E., Poncelet, G. and Fripiat, J. J. (1987) Preparation and characterization of bidimensional zeolitic structures obtained from synthetic beidellite and hydroxy-aluminum solutions: *Clays & Clay Minerals* **35**, 251-261.
- Smith, R. W. and Hem, J. D. (1972) Effect of aging on aluminum hydroxide complexes in dilute aqueous solutions: *U.S. Geol. Surv. Water-supply Paper* **1827-D**, 1-51.
- Thompson, A. R., Kunwar, A. C., Gutowsky, H. S. and Oldfield, E. (1987) Oxygen-17 and aluminium-27 nuclear magnetic resonance spectroscopic investigations of aluminium(III) hydrolysis products: *J. Chem. Soc. Dalton Trans.*, 2317-2322.
- Tsai, P. P. and Hsu, P. H. (1984) Studies of aged OH-Al solutions using kinetics of Al-ferrous reactions and sulfate precipitation: *Soil Sci. Soc. Amer. J.* **48**, 59-65.
- Tsai, P. P. and Hsu, P. H. (1985) Aging of partially neutralized aluminum solutions of sodium hydroxide/aluminum molar ratio = 2.2: *Soil Sci. Soc. Amer. J.* **49**, 1060-1065.

CHAPTER XII

ALUMINUM MONOMER LINE-BROADENING AS EVIDENCE FOR THE EXISTENCE OF $[\text{AlOH}]^{2+}$ AND $[\text{Al}(\text{OH})_2]^+$ DURING FORCED HYDROLYSIS; A ^{27}Al NUCLEAR MAGNETIC RESONANCE STUDY

ABSTRACT

The ^{27}Al monomer resonance of 0.05 M aluminum nitrate solutions gradually broadens from 7.82 to 89.40 Hz upon forced hydrolysis from an OH/Al molar ratio of 0.0 to 2.2. The broadening is due to increasing amounts of $[\text{AlOH}]^{2+}$ and $[\text{Al}(\text{OH})_2]^+$ up to 2.24 % and 0.11 %, respectively. To calculate the linewidth of the monomer resonance, it is assumed that $[\text{AlOH}]^{2+}$ and $[\text{Al}(\text{OH})_2]^+$ have identical linewidths as the isoelectronic compounds $[\text{AlF}]^{2+}$ and $[\text{AlF}_2]^+$, respectively. The calculation is based on pK values of 4.99 for $[\text{AlOH}]^{2+}$ and 10.13 for $[\text{Al}(\text{OH})_2]^+$. The results of the theoretical calculations agree well with observed linewidth data.

12.1 INTRODUCTION

In recent years the formation of monomeric, oligomeric and tridecameric polymers of Al(III) upon forced hydrolysis is studied with ^{27}Al nuclear magnetic resonance spectroscopy (Bottero et al., 1980; Bertsch et al., 1986; Akitt, 1989; Kloprogge et al., 1992). It is generally accepted that the monomer $[\text{Al}(\text{H}_2\text{O})_5(\text{OH})]^{2+}$, usually written as $[\text{AlOH}]^{2+}$, is generated during self-hydrolysis of $[\text{Al}(\text{H}_2\text{O})_6]^{3+}$ with formation constants (pK values) ranging from 4.9 to 5.33 (Mesmer and Baes, 1971; Baes and Mesmer, 1976; May et al., 1979; Bottero et al., 1980, 1982; Brown et al., 1985). In addition, the development of $[\text{Al}(\text{H}_2\text{O})_4(\text{OH})_2]^+$, shortened as $[\text{Al}(\text{OH})_2]^+$, has been established upon forced hydrolysis, with pK values from 8.71 to 10.91 (Mesmer and Baes, 1971; Baes and Mesmer, 1976; May et al., 1979; Bottero et al., 1980, 1982; Brown et al., 1985).

The two hydroxo-monomers $[\text{AlOH}]^{2+}$ and $[\text{Al}(\text{OH})_2]^+$ cannot be observed directly with ^{27}Al NMR, due to their fast proton exchange. In spite of the lack of separate resonances for the hydroxo-monomers, Akitt et al. (1969) and Akitt

and Elders (1985) argued that there must be a measurable influence on the linewidth of the monomer resonance during self-hydrolysis. The same effect may be, of course, expected during forced hydrolysis.

The purpose of this study is i) to determine the formation of both the $[\text{AlOH}]^{2+}$ and the $[\text{Al}(\text{OH})_2]^+$ species during forced hydrolysis, ii) to evaluate the influence of these species on the ^{27}Al NMR linewidth of the monomer resonance and iii) to compare the pK data reported in literature by calculation of the monomer linewidth based on the amounts of the monomer species and comparison with the observed linewidth data.

12.2 EXPERIMENTAL

Aluminum and alkali stock solutions of a concentration of 0.2 M were prepared by dissolving $\text{Al}(\text{NO}_3)_3 \cdot 9\text{H}_2\text{O}$ (Merck no. 1063) and NaOH (Merck no. 6498) in CO_2 free deionized water. The amount of alkali solution required to obtain the desired OH/Al molar ratio was injected at 25°C into the Al solution with an injection rate of 0.015 ml/s using a Gilson pump (Kloprogge et al., 1992). The OH/Al molar ratio was varied between 0 and 2.4. All solutions were diluted up to a final Al concentration of 0.05 M, which was checked by ICP-AES.

From all solutions the pH was measured with a pH meter Consort P514 with an accuracy of 0.02.

The ^{27}Al NMR spectra were recorded at 25°C with a Bruker WP 200 spectrometer operating at 52.148 MHz (4.2 Tesla) at the Bijvoet Institute of the University of Utrecht. Standard 1024 Free Induction Decays (FIDs) were recorded applying no relaxation delay. Other parameters are: puls width 47.6 $\mu\text{sec.}$, acquisition time 0.819 sec. and spectral width 10000.00 Hz. An 0.05 M aluminum nitrate solution was used as external reference with respect to the

Aluminum monomer line-broadening as evidence for the existence of $[Al(OH)]^{2+}$ and $[Al(OH)_2]^+$ during forced hydrolysis; an ^{27}Al nuclear magnetic resonance study

concentrations of the various Al species and to their chemical shifts. The accuracy in the linewidth measurements is $\pm 10\%$. Immediately before the NMR measurements the solutions were diluted with 5 vol% D_2O for field frequency lock. This has no measurable influence on the pH or the ^{27}Al NMR linewidths. Spectra obtained with the Bruker WP 200 are corrected for a broad low intensity background signal between 50 and -40 ppm, due to aluminum present in the probe, by subtracting a H_2O/D_2O blanco spectrum from the measured spectra. Subtraction has no influence on the linewidth data.

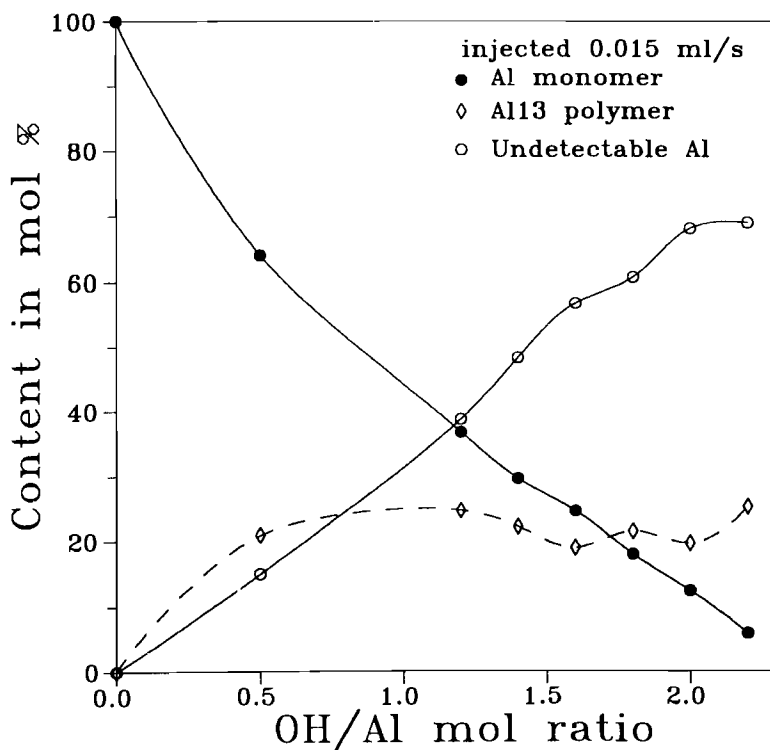


Figure 12.1 Al species distribution as function of OH/Al molar ratio in 0.05 M aluminum nitrate solution, results after Klopogge et al. (1992).

12.3 RESULTS

The ^{27}Al NMR spectra exhibit two resonances at approximately 0 ppm, due to sixfold coordinated Al in the monomers, and at approximately 63 ppm, due to fourfold coordinated Al of the tridecamer. Figure 12.1 shows the Al monomer and tridecamer distribution as a function of the OH/Al molar ratio between 0.0 and 2.2, a part of which was previously reported by Klopogge et al. (1992). In the range between OH/Al molar ratios of 0.0 and 2.2, the monomer decreases continuously, whereas the tridecamer almost linearly increases. The small differences from a linear increase are most probably due to the inaccuracy of

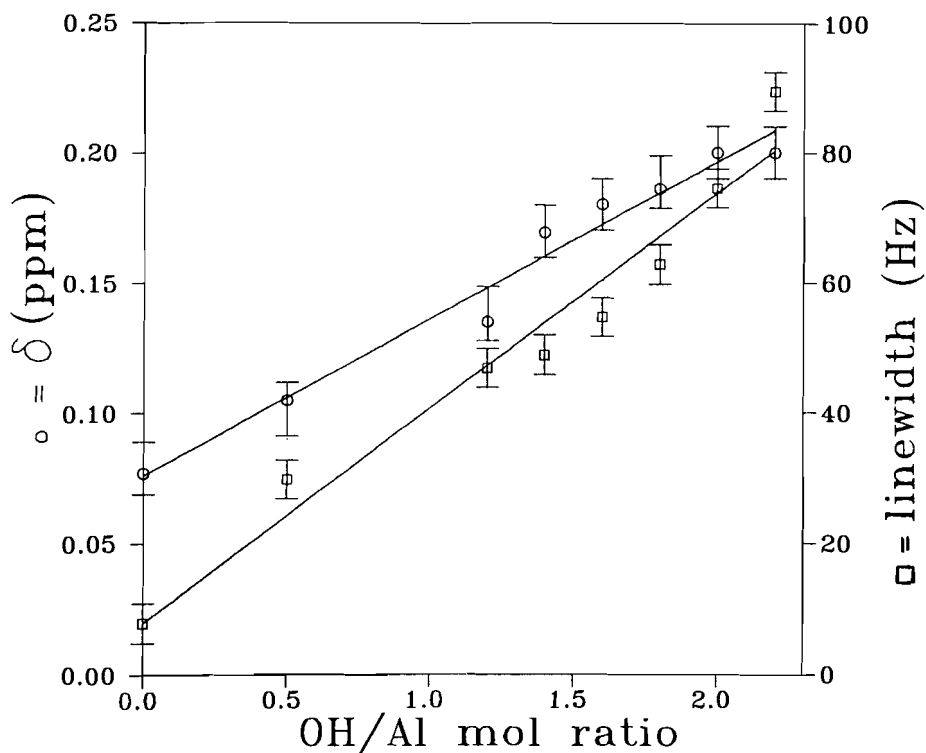


Figure 12.2 ^{27}Al NMR chemical shift and linewidth of the monomer as function of OH/Al molar ratio.

the NMR determinations. The undetectable Al species contain Al polymers too large to be observed with ^{27}Al NMR, but are observed with others techniques, such as, Ferron colorometry and based on the absolute Al concentrations as measured with ICP-AES.

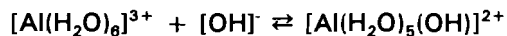
The chemical shift δ of the monomer resonance correlates linearly with the OH/Al molar ratio from 0.008 ppm for the reference aluminum nitrate solution (OH/Al molar ratio 0.0) to 0.18 ppm for the hydrolyzed solution with OH/Al molar 2.2. The linewidth at half height broadens simultaneously from 7.82 Hz to 89.40 Hz (Fig. 12.2). The measured pH increases from 2.90 to 4.14 during hydrolysis of respective solutions.

12.4 DISCUSSION

With k_{xy} being the formation constant for the formation of $[Al_x(OH)_y]^{3-x-y}$, the reactions between $[Al(H_2O)_6]^{3+}$, $[Al(OH)]^{2+}$ and $[Al(OH)_2]^+$ upon hydrolysis can be expressed as:



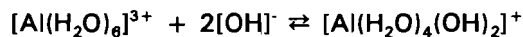
with $k_{11} = [Al(OH)^{2+}][H_3O^+]/[Al^{3+}]$, or, alternatively, upon forced hydrolysis:



with $k_{11}' = [Al(OH)^{2+}]/[Al^{3+}][OH]^-$ and



with $k_{12} = [Al(OH)_2^+][H_3O^+]^2/[Al^{3+}]$, or, alternatively, upon forced hydrolysis:



with $k_{12}' = [Al(OH)_2^+]/[Al^{3+}][OH]^{-2}$.

The concentrations of the mono- and dihydroxy monomers become higher with forced hydrolysis, that is causing an increase of pH. These increasing concentrations are monitored by the increasing linewidth of the ^{27}Al monomer resonance. The amounts of hydroxy-monomers formed upon hydrolysis can be

calculated with an appropriate set of k-values from in the literature (Table 12.1) in combination with the amount of monomer measured with ^{27}Al NMR.

The exchange rate of protons between $[\text{Al}(\text{H}_2\text{O})_6]^{3+}$ and $[\text{AlOH}]^{2+}$ is very high (Akitt and Elders, 1985) and is equivalent with the rate at which the aluminum changes its environment between these two species. It is reasonable to assume also a rapid exchange with $[\text{Al}(\text{OH})_2]^+$. Therefore, the ^{27}Al resonance of the monomer will be a weight average of the three species. The linewidth of the respective monomer resonances are calculated taking i) a linewidth of 2 Hz for $[\text{Al}]^{3+}$ (Akitt and Elders, 1985), ii) 620 Hz for $[\text{AlOH}]^{2+}$ and 890 Hz for $[\text{Al}(\text{OH})_2]^+$ being identical with $[\text{AlF}]^{2+}$ and $[\text{AlF}_2]^+$ (Akitt and Elders, 1985) and iii) the amounts of the various monomers derived from the equilibrium calculations. The calculations of Akitt and Elders showing that, although the linewidths of both unsymmetrical hydroxy- and fluorine- monomers are only a coarse approximation, a good agreement exists between observations and calculations justify the hypothesis of equal linewidths.

In the test of the k-values, those reported by May et al. (1979) result in the best fit between calculated and observed linewidth of the monomer resonance upon hydrolysis (Fig. 12.3, Table 12.2). The calculations show the existence of small amounts of $[\text{AlOH}]^{2+}$ with a maximum of 2.24 % at an OH/Al molar ratio

Table 12.1 Formation constants from literature, which are used successively in calculations of the Al monomer speciation.

pK	Mesmer & Baes 1971	Baes & Mesmer 1976	May et al. 1979	Bottero et al. 1982	Brown et al. 1985
11	4.9	4.97	4.99	5.02	5.33
12	10.3	9.3	10.13	8.71	10.91

Aluminum monomer line-broadening as evidence for the existence of $[Al(OH)]^{2+}$ and $[Al(OH)_2]^+$ during forced hydrolysis; an ^{27}Al nuclear magnetic resonance study

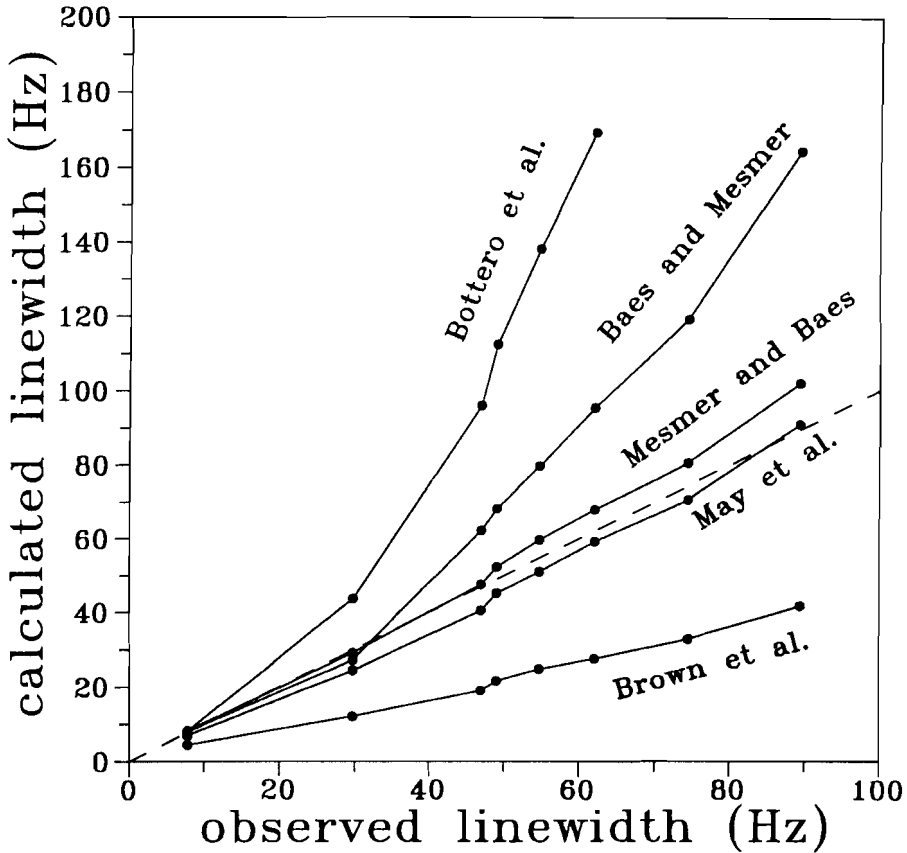


Figure 12.3 Calculated linewidth as function of the observed linewidth based on the pK-values listed in Table 12.1.

of 0.5, and of $[Al(OH)_2]^+$ with a maximum of 0.11 % at an OH/Al molar ratio of 1.6. The OH/Al molar ratios are slightly lower than the expected values of 1.0 and 2.0, due to the simultaneous formation of the tridecameric polymer. Our calculations based on linewidth data demonstrate that the formation of $[Al(OH)_2]^+$ also influences the linewidth of the monomer resonance. It contradicts the conclusions of Akitt and Elders (1985) that the monomer linewidth data upon forced hydrolysis are identical to those upon self-hydrolysis, considering $[Al(OH)]^{2+}$ as the only source of linebroadening. They

calculated a pK_{11} value of 4.93 based on their data, which is well matching calculated and observed linewidth. Applying their pK -value of 4.93 in our calculations, disregarding the presence of small amounts of $[Al(OH)_2]^+$, results in very small values for the monomer linewidth. However, the difference between their pK_{11} -value of 4.93 ± 0.08 and 4.99 as reported by May et al. (1979) is within the experimental error (Akitt and Elders, 1985). The presence of small amounts of the dihydroxy-monomer may be expected in their experiments.

Table 12.2 Calculated monomer species distribution (mol % of total Al) based on the pK -values reported by May et al. (1979), pH, and calculated and observed monomer linewidths (Hz) as function of OH/Al molar ratio.

OH/ Al	pH	total monomer	mol % of total Al in solution			fraction of Al-monomer			linewidth (Hz)	
			$[Al]^{3+}$	$[Al(OH)]^{2+}$	$[Al(OH)_2]^+$	$[Al]^{3+}$	$[Al(OH)]^{2+}$	$[Al(OH)_2]^+$	F_{calc}	F_{obs}
0.0	2.90	100.00	99.19	0.81	0.005	0.992	0.008	0.000	6.94	7.82
0.5	3.55	64.10	61.80	2.24	0.060	0.964	0.035	0.001	24.52	29.80
1.2	3.78	36.70	34.47	2.13	0.099	0.939	0.058	0.003	40.51	46.93
1.4	3.83	29.60	27.58	1.92	0.100	0.932	0.065	0.003	45.19	49.02
1.6	3.89	24.50	22.59	1.80	0.109	0.922	0.073	0.004	51.02	54.75
1.8	3.95	17.91	16.30	1.50	0.105	0.910	0.084	0.006	59.15	62.08
2.0	4.03	12.41	11.07	1.23	0.105	0.892	0.099	0.009	70.73	74.49
2.2	4.14	5.90	5.09	0.73	0.082	0.862	0.124	0.014	90.88	89.40

The results presented in this paper provide insight in the processes of forced hydrolysis in aluminum nitrate solutions and prove the formation of not only the monohydroxy-monomer $[AlOH]^{2+}$, but also the dihydroxy-monomer $[Al(OH)_2]^+$. For the first time the formation of both species has been determined with the monomer linewidth broadening upon forced hydrolysis.

12.5 CONCLUSIONS

1) Calculation of the Al monomer species distribution demonstrate the existence of not only $[Al]^{3+}$ and $[AlOH]^{2+}$, but also $[Al(OH)_2]^+$ in partly hydrolyzed Al-solutions. This last species is a significant source of linebroadening of the ^{27}Al monomer resonance.

2) Calculations based on the k-values of May et al. (1979) result in the best fit between calculated and observed ^{27}Al monomer linewidths.

REFERENCES

- Akitt, J. W. (1989) Multinuclear studies of aluminum compounds: *Prog. NMR Spectr.* **21**, 1-149.
- Akitt, J. W. and Elders, J. M. (1985) Aluminum-27 nuclear magnetic resonance studies of the hydrolysis of aluminium(III). Part 7. Spectroscopic evidence for the cation $[AlOH]^{2+}$ from line-broadening studies at high dilution: *J. Chem. Soc. Faraday Trans.* **81**, 1923-1930.
- Akitt, J. W., Greenwood, N. N. and Lester, G. D. (1969) Hydrolysis and dimerisation of aqueous aluminum salt solutions: *Chem. Commun.*, 988-989.
- Baes, C. F. and Mesmer, R. E. (1976) *"The Hydrolysis of Cations"*, Wiley Interscience, New York, 189 pp.
- Bertsch, P. M., Thomas, G. W. and Barnhisel, R. I. (1986) Characterization of hydroxy-aluminum solutions by aluminum-27 nuclear magnetic resonance spectroscopy: *Soil Sci. Soc. Am. J.* **50**, 825-830.
- Bottero, J. Y., Cases, J. M., Fiessinger, F. and Poirier, J. E. (1980) Studies of hydrolyzed aluminum chloride solutions. 1. Nature of aluminum species and composition of aqueous solutions: *J. Phys. Chem.* **84**, 2933-2939.
- Bottero, J. Y., Tchoubar, D., Cases, J. M. and Fiessinger, F. (1982) Investigation of the hydrolysis of aqueous solutions of aluminum chloride. 2. Nature and structure by small angle X-ray scattering: *J. Phys. Chem.* **86**, 3667-3673.
- Brown P. L., Sylva, R. N., Batley, G. E. and Ellis, J. (1985) The hydrolysis of metal ions. Part 8. Aluminum(III): *J. Chem. Soc. Dalton Trans.*, 1967-1970.
- Kloprogge, J. T., Seykens, D., Jansen, J. B. H. and Geus, J. W. (1992) An ^{27}Al nuclear magnetic resonance study on the optimization of the development of the Al13 polymer: *J. Non-Cryst. Solids* **142**, 94-102.

Aluminum monomer line-broadening as evidence for the existence of $[AlOH]^{2+}$ and $[Al(OH)_2]^+$ during forced hydrolysis; an ^{27}Al nuclear magnetic resonance study

May, H. M., Helmke, P. A. and Jackson, M. L. (1979) Gibbsite solubility and thermodynamic properties of hydroxy-aluminum ions in aqueous solution at 25°C: *Geochim. Cosmochim. Acta* **43**, 861-868.

Mesmer, R. E. and Baes, C. F. (1971) Acidity measurements at elevated temperatures. V. Aluminum ion hydrolysis: *Inorg. Chem.* **10**, 2290-2296.

CHAPTER XIII

THE EFFECTS OF CONCENTRATION AND HYDROLYSIS ON THE OLIGOMERIZATION AND POLYMERIZATION OF Al(III) AS EVIDENT FROM THE ^{27}Al NMR CHEMICAL SHIFTS AND LINEWIDTHS

ABSTRACT

The Al concentration and forced hydrolysis influence the polymerization of aqueous Al(III) and thus the ^{27}Al NMR spectra. An increase of the Al concentration results in a drop of the fraction present as monomer, in the formation of an oligomer of an OH/Al molar ratio of 2.42, and in the disappearance of the tridecamer above an Al concentration of 0.15 M. Increasing the OH/Al molar ratio at a constant Al concentration leads to a linear drop of the fraction present as monomer over the whole range between 1 and 2.5 and a maximum in oligomer fraction between 1.5 and 2.5. At low Al concentrations the fraction of tridecamer exhibits an optimum yield between OH/Al ratios of 2.2 and 2.4. At ratios higher than 2.4 NMR unobservable polymers are formed. The chemical shift and the linewidth of the monomer resonance are lowered by increasing spin-spin relaxation (T_2) and a consequently decreasing quadrupole coupling constant upon increasing Al concentration. With increasing OH/Al molar ratio $[\text{Al}(\text{H}_2\text{O})_6]^{3+}$ is mainly replaced by $[\text{Al}(\text{H}_2\text{O})_5(\text{OH})]^{2+}$ and $[\text{Al}(\text{H}_2\text{O})_4(\text{OH})_2]^+$ and subsequently the chemical shift and linewidth of the monomer resonance increase. The Al concentration or OH/Al molar ratio hardly affect the resonance of the central fourfold coordinated Al of the tridecamer, due to its very strong shielding.

13.1 INTRODUCTION

Over the past few decades many studies have been devoted to the hydrolysis and polymerization of aluminum(III). In the investigations titration and precipitation (Vermeulen et al., 1975); Stol et al., 1976), ^{27}Al NMR (Akitt et al., 1972; Akitt and Farthing, 1978, 1981; Bottero et al., 1980; Betsch et al., 1986a,b; Klopogge et al., 1992a,b), and small-angle X-ray scattering (Rausch and Bale, 1964; Bottero

et al., 1982) have been used. ^{27}Al NMR spectroscopy has directly evidenced the existence of monomeric ($[\text{Al}(\text{H}_2\text{O})_6]^{3+}$, $[\text{Al}(\text{H}_2\text{O})_5\text{OH}]^{2+}$ and $[\text{Al}(\text{H}_2\text{O})(\text{OH})_2]^+$), oligomeric ($[\text{Al}(\text{OH})_{2.5}(\text{H}_2\text{O})_x]_n^{3n+}$), and tridecameric, $[\text{AlO}_4\text{Al}_{12}(\text{OH})_{24}(\text{H}_2\text{O})_{12}]^{7+}$, species in partially hydrolyzed Al solutions (Akitt et al., 1969; Akitt et al., 1972; Akitt and Mann, 1981, Akitt, 1989, Klopogge et al., 1992c).

The formation of the above mentioned species depends on the hydrolysis conditions: the OH/Al molar ratio, the rate of neutralization, the mixing conditions (Bertsch et al., 1986a; Bertsch, 1987; Klopogge et al., 1992b) and the preparation temperature (Klopogge et al., 1992a). The effects of the experimental conditions have been studied usually at fixed Al concentrations. Klopogge et al. (1992c) have shown that forced hydrolysis at a final Al concentration of 0.05 M not only leads to $[\text{Al}(\text{H}_2\text{O})_6]^{3+}$ and $[\text{Al}(\text{H}_2\text{O})_5\text{OH}]^{2+}$, but also to $[\text{Al}(\text{H}_2\text{O})(\text{OH})_2]^+$. The dihydroxy-monomer significantly influences the linewidth of the ^{27}Al monomer resonance at low Al concentrations. The best fit between the observed and the calculated linewidth is obtained using pK values of 4.99 for $[\text{Al}(\text{H}_2\text{O})_5\text{OH}]^{2+}$ and 10.13 for $[\text{Al}(\text{H}_2\text{O})(\text{OH})_2]^+$ as reported by May et al. (1979). The same pK values will be used in this study. Recently, Akitt and Elders (1988) determined that the Al concentration is an important additional parameter, which may control the distribution of the Al species upon hydrolysis and thus the ^{27}Al NMR spectra.

The purposes of this study are a) to evaluate the influence of the Al concentration on (i) different dissolved Al(III) species, (ii) the ^{27}Al NMR chemical shifts, and (iii) the linewidths during hydrolysis of Al solutions with sodium hydroxide solutions, and b) to combine the effects of the concentration with the influence of the OH/Al molar ratio between 0.0 and 2.5.

13.2 EXPERIMENTAL

Al^{3+} and alkali stock solutions with concentrations of 0.20, 0.51, 0.85, 1.70, and 2.55 M were prepared by dissolving $\text{Al}(\text{NO}_3)_3 \cdot 9\text{H}_2\text{O}$ (Merck) and NaOH (Merck)

in CO₂ free deionized water. The Al solutions were hydrolyzed with alkali solutions of the corresponding hydroxide concentration. The amount of the alkali solution required to establish a desired OH/Al molar ratio was injected at 25°C into the Al solution at an injection rate of 0.015 ml/s using a Gilson pump (Kloprogge et al., 1992b). The final Al concentration was chosen at 0.05, 0.15, 0.25, 0.50 and 0.75 M. At a fixed Al concentration the OH/Al molar ratio was varied between 0.0 and 2.4.

The ²⁷Al NMR spectra were recorded with a Bruker WP 200 spectrometer operating at 52.148 MHz (4.2 Tesla) at the Department of Organic Chemistry of the University of Utrecht. Standard 1024 Free Induction Decays (FIDs) were recorded applying no relaxation delay. All parameter are identical to those reported in Ch. XII. Aluminum nitrate solutions with identical Al concentrations as the hydrolyzed solutions were used as external standard with respect to the concentration. The 0.05 M aluminum nitrate solution was also used as reference with respect to the chemical shift for all solutions. Directly before NMR measurements the solutions were diluted with D₂O for field frequency lock. Spectra obtained with the Bruker WP 200 are corrected for background signals, due to aluminum present in the probe, by subtracting a H₂O/D₂O blanco spectrum from the measured spectra.

13.3 RESULTS

13.3.1 Al hydrolysis products

The ²⁷Al NMR spectra exhibit three resonances at approximately 0 ppm and 4 ppm, both due to sixfold coordinated Al in the monomers and oligomers, respectively, and at approximately 63 ppm due to the central, fourfold coordinated Al of tridecamers. (Fig. 13.1). Relative concentrations are based on integrated intensities of the resonances. The errors in the calculated concentrations, which

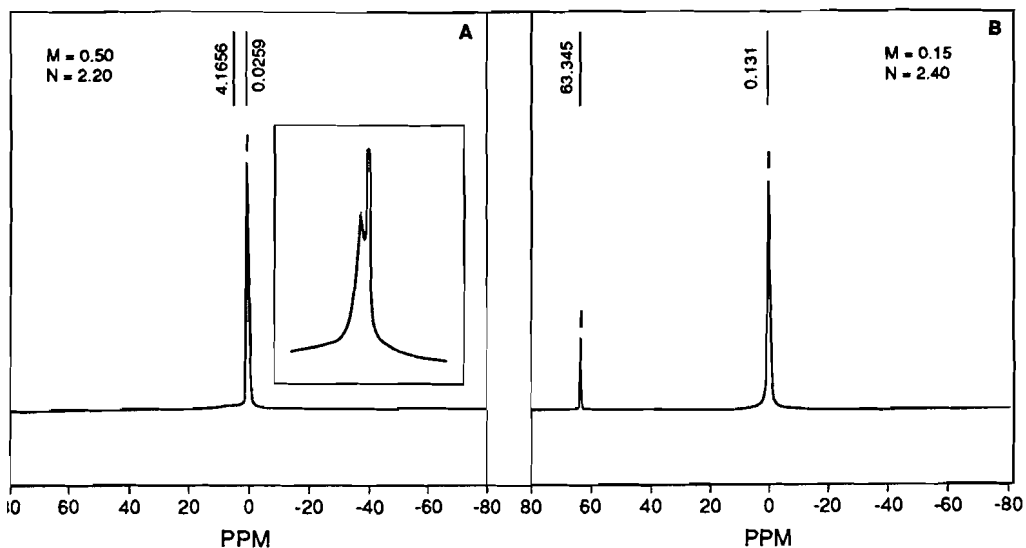
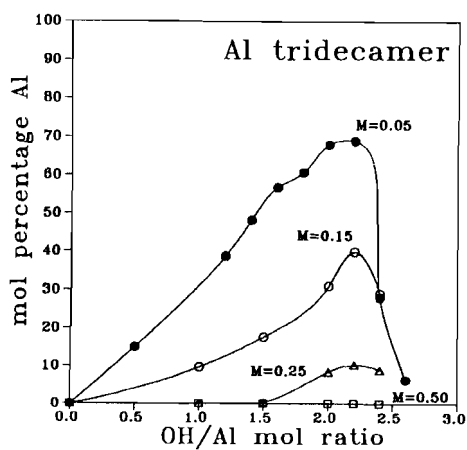
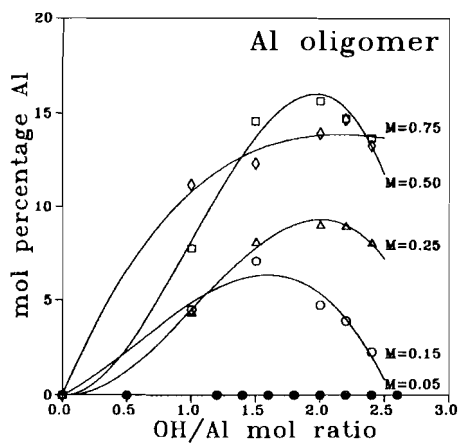
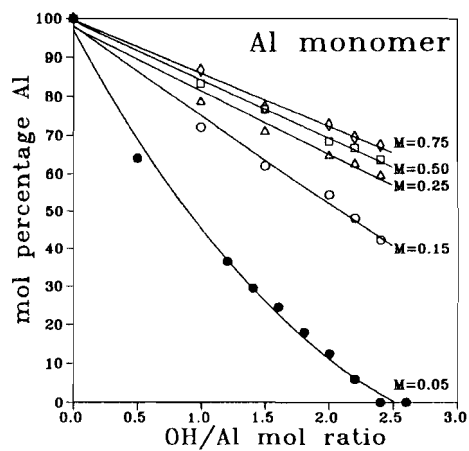


Figure 13.1 ^{27}Al NMR spectra of solutions of 0.15 M final Al concentration and OH/Al molar ratio of 2.4 (a) and 0.50 M final Al concentration and OH/Al molar ratio of 2.2 (b).

are caused by overlap of the monomeric and oligomeric resonances, and the calculation of the tridecamer concentration from a narrow resonance representing only 1/13 (7.7 mol%) of its total Al content, are estimated to be smaller than 10 %.

Figure 13.2 shows plots of the individual Al species present as a function of the OH/Al molar ratio. The relative amount of monomeric Al increases with the Al concentration and decreases linearly with increasing OH/Al molar ratio from 1.0 to 2.4 (**Fig. 13.2a**). The fraction present as oligomer becomes generally more important at higher Al concentrations. The oligomer fraction does not clearly depend on the degree of hydrolysis. A maximum yield of oligomers can be observed between OH/Al molar ratios of 1.5 ($M = 0.15$) and 2.2 ($M = 0.75$) (**Fig. 13.2b**). At Al concentrations of 0.05, 0.15, and 0.25 M the tridecamer fraction

The effect of concentration and hydrolysis on the oligomerization and polymerization of Al(III) as evident from the ^{27}Al NMR chemical shifts and linewidths



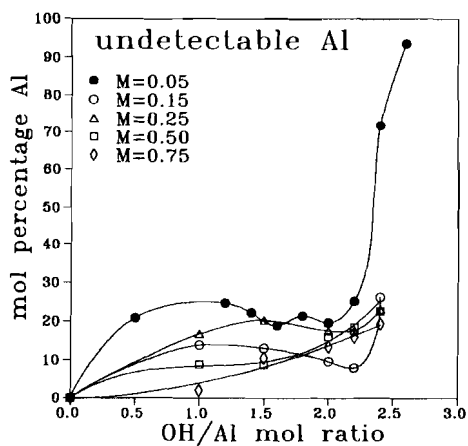
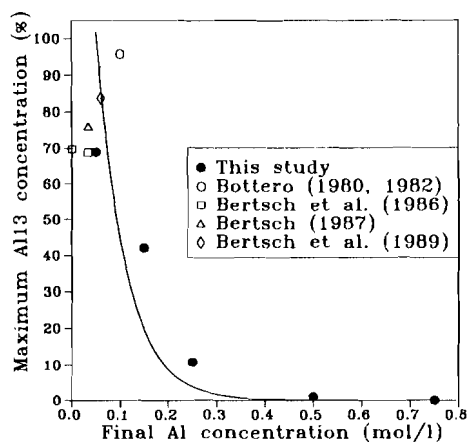


Figure 13.2 Distribution of monomer (a), oligomer (b), and tridecamer (c) as a function of the OH/Al molar ratio at different final aluminum concentrations, the optimum tridecamer yield as a function of the final Al concentration (d), and the unobservable Al as a function of the OH/Al molar ratio at different final aluminum concentrations (e).

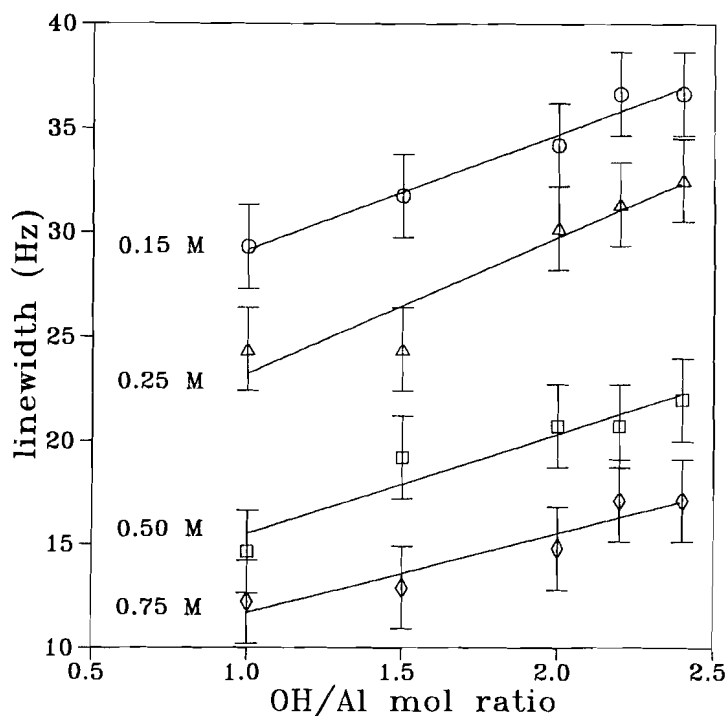


Figure 13.4 Change in linewidth at half height as a function of the OH/Al molar ratio and Al concentration of the monomer resonance.

in the solution with 0.75 M Al and an OH/Al molar ratio of 1.0, and the highest shift of approximately 0.18 ppm in the solution with 0.05 M Al and an OH/Al molar ratio of 2.4. The linewidth at half height exhibits a linear trend in the range from 12 to 90 Hz with increasing OH/Al ratio (Fig. 13.4). No visible influence on the sixfold coordinated Al resonance of the oligomer can be established, due to the overlap with the monomeric resonance, the low intensity, and the relatively large linewidth.

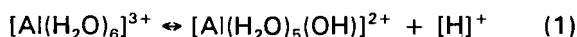
The influence of the Al concentration on the central fourfold coordinated Al of the tridecamer cannot be determined at high concentrations due to the absence of the tridecamer. At concentrations less than 0.50 M Al the chemical shift seems to

exhibit no tendency for a linear increase as a function of the OH/Al molar ratio in the entire range from 1.0 to 2.4, unlike the shift of the monomeric resonance (Fig. 13.5). The difference between 63.29 ppm and 63.34 ppm is smaller than the experimental error. The linewidth at half height remains constant at 7.3 Hz, independent of both the Al concentration and the degree of hydrolysis.

13.4 DISCUSSION

13.4.1 Changes in the fractions of the different Al species

The hydrolysis of aluminum solutions leads to a decrease in monomer content at OH/Al molar ratios between 1.0 and 2.5. At an Al concentration of 0.05 M the decrease in monomer content is equivalent to the addition of 3 OH⁻ per monomer, which is only slightly higher than the expected 2.5 OH⁻ per monomer needed for the formation of the tridecamer (Akitt, 1989). When the final aluminum concentration is raised, higher amounts of hydroxyls, up to 7.35 OH⁻ per monomer, are consumed, due to the formation of the oligomer and other NMR undetectable polymers. The presence of these polymers prohibits the determination of the OH/Al ratio of the oligomer in most solutions. An exception is the solution with 0.75 M Al and an OH/Al molar ratio 1.0, in which the amount of undetectable polymers is less than 2%. Based on the equilibrium:



with a reaction constant pK_s of 4.99 (May et al., 1979), the amount of monohydroxy monomer can be calculated to be 72.9%. This implies an OH/Al molar ratio for the oligomer of approximately 2.42. Oligomers proposed in literature, such as, $\text{Al}_2(\text{OH})_2$ and $\text{Al}_3(\text{OH})_4$, do not support our results and those of Akitt and Elders (1988). Alternatively, Akitt and Elders (1988) have suggested the possible existence of the species: $\text{Al}_3(\text{OH})_8$, $\text{Al}_5(\text{OH})_{13}$, $\text{Al}_2(\text{OH})_5$, and $\text{Al}_4(\text{OH})_{10}$. Their observation of the variation in chemical shift and linewidth in the Al spectra

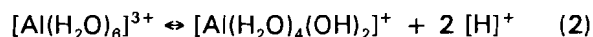
and their information from proton spectra may implicate that the 4 ppm resonance is a composite resonance with two or more broad, overlapping signals. Recently, Akitt (1989) stated that the oligomer has to be the $\text{Al}_2(\text{OH})_5$ with an OH/Al ratio of 2.5, which is close to the value of 2.42 observed in this study.

The absence of the tridecamer in hydrolyzed solutions of high Al concentrations can be explained by a model (Akitt and Farthing, 1981; Bertsch, 1987; Kloprogge et al., 1992b), in which $\text{Al}(\text{OH})_4^-$ is formed inhomogeneously at the point of alkali introduction, due to local supersaturation, as precursor for the formation of the tridecamer. An increase of the Al concentration will result in less or no supersaturation at the point of alkali introduction preventing the formation of the $\text{Al}(\text{OH})_4^-$ precursor.

13.4.2 Resonance changes

The degree of hydrolysis and the Al concentration hardly affect the central fourfold coordinated Al resonance of the tridecamer, whereas the monomer resonance is strongly modified. The absence of an effect is caused by the strong shielding of the central fourfold coordinated Al of the tridecamer, which prohibits exchange with its environment. The less shielded sixfold coordinated Al of the monomer is much more liable to a change in resonance.

The linewidth at half height ($\nu_{1/2}$) of the monomer resonance increases with progressive hydrolysis and decreases with the final aluminum concentration. Akitt and Elders (1985) and Kloprogge et al. (1992c) have shown that the monomer linewidth is influenced by the exchange equilibria (1) and (2):



Using data about the aluminum self hydrolysis they obtained a linear relationship between the logarithm of the linewidth and the pH:

$$\log [(W_{\text{meas}} - 2)/(620 - W_{\text{meas}})] = \text{pH} + \log[K_6] \quad (3)$$

with W_{meas} the measured linewidth in Hz and $\text{p}K_6$ the rate constant of reaction (1). Upon forced hydrolysis the pH and linewidth data followed precisely the same pattern as during self hydrolysis, indicating that polymerization does not influence

the linewidth of the monomer resonance. Bertsch et al. (1986a) reached the same conclusion based on spin-lattice relaxation rates (T_1). In solution the quadrupole coupling constant e^2qQ/h influences NMR spectra through relaxation processes, and under conditions of rapid isotropic tumbling, the spin-lattice (T_1) and spin-spin (T_2) relaxation times (s) are given by (Akitt, 1989):

$$1/T_1 = 1/T_2 = [3\pi^2(2I + 3)/10I^2(2I - 1)][1 + \eta^2/3][e^2qQ/h]^2\tau_c \quad (4)$$

where ²⁷Al has spin $I = 5/2$, η is the asymmetry parameter, e^2qQ/h the quadrupole coupling constant (Hz), and τ_c is the rotational correlation time (s). T_2 is related to the width at half height ($\nu_{1/2}$) by (Akitt and Elders, 1985):

$$T_2 = 1/\pi\nu_{1/2} \quad (5)$$

The linewidth of the monomer decreases with Al concentration, which is not only caused by changes in equilibria (1) and (2), but also by a change in T_2 . Akitt and Elders (1985) observed a maximum change in linewidth less than 2 Hz in solution with concentrations lower than 1 M Al. An increase of the Al concentration results in a drop of the linewidth, which implies, according to equation (5), an increase of T_2 . Substitution of T_2 in equation (4) reveals a subsequent decrease in e^2qQ/h , to which the chemical shift is related by equation:

$$\delta \text{ (ppm)} = 6 \times 10^3(1 + \eta^2/3)(e^2qQ/h\nu_0)^2 \quad (6)$$

where ν_0 is the Larmor frequency (Hz). Based on equation (6) it can be concluded that a decrease in the quadrupole coupling constant e^2qQ/h will result in a shift of δ to lower values. The observation of a decreasing linewidth of the monomer with an increasing Al concentration leads theoretically to a shift of δ to lower values, which, indeed, is experimentally observed (Fig. 13.3). For example, increasing the Al concentration from 0.15 to 0.75 M at a constant OH/Al molar ratio of 1.0 decreases the linewidth from 30 to 12.2 Hz and shifts δ from 0.10 ppm to -0.05 ppm. Substitution of $\nu_{1/2}$ in (5), the resulting T_2 in (4) and the quadrupole coupling constant e^2qQ/h in (6) reveal a maximum shift of δ of approximately 1.3 ppm to lower values. By neglecting (i) the influence of equilibria (1) and (2), (ii) the

Table 13.1 The influence of degree of hydrolysis and final Al concentration on the monomer resonance linewidth.

OH/Al molar ratio	final Al conc. (mol/l)	pH	calculated linewidth (Hz)	observed linewidth (Hz)
0.0	0.75	1.69	7.60	7.30
0.0	0.50	1.96	7.87	9.80
0.0	0.25	2.37	8.77	11.70
0.0	0.15	2.77	11.00	14.65
0.0	0.15	2.77	11.00	14.65
1.0	0.15	3.37	22.01	24.64
1.5	0.15	3.50	27.16	31.74
2.0	0.15	3.63	32.86	34.18
2.2	0.15	3.70	38.83	36.63
2.4	0.15	3.75	42.71	41.07

presence of other polymers, and (iii) assuming a value of 1×10^{-10} s for τ_c the calculated shift is overestimated.

The influence of the degree of hydrolysis on the monomer resonance linewidth is larger than the final aluminum concentration. Increasing the OH/Al molar ratio results in an increase of both pH and ionic strength and in the viscosity due to the formation of large polymers. The effect of changes in the equilibria (1) and (2) will here be much more important as compared to the effect of the Al concentration. **Table 13.1** shows the influence on the linewidth observed during hydrolysis and with the final Al concentration, assuming linewidths of 7.3 Hz for $[\text{Al}]^{3+}$, being the minimal linewidth observed, 620 Hz for $[\text{AlOH}]^{2+}$, and 890 Hz for $[\text{Al}(\text{OH})_2]^+$. The increased value of 7.3 Hz at higher Al concentrations instead of 2 Hz as minimal linewidth is probably due to an increase of the viscosity (Akitt and Elders, 1985). For example, in a solution of a final Al concentration of 0.15 M the pH increases

from approximately 2.77 to 3.75 with the OH/Al molar ratio rising from 0.0 to 2.5. Assuming a $\text{p}K_a$ of 4.99 (May et al., 1979) and substitution of the pH in equation (3) results in a increase of approximately 30 Hz. Accounting for the uncertainties in these calculations, e.g., in τ_c and e^2qQ/h , and neglecting the interference of both effects on the observed linewidths used in these calculations, this is in reasonable agreement with the observed increase of approximately 26 Hz.

13.5 CONCLUSIONS

- 1) The monomer concentration rises at increasing Al concentration and drops at increasing OH/Al molar ratio.
- 2) The oligomer concentration increases with increasing Al concentration. The oligomer can not be observed in solutions of an Al concentration of 0.05 M. No clear dependency upon the OH/Al molar ratio is observed. The OH/Al ratio of the oligomer is approximately 2.42.
- 3) The tridecamer is only formed at low Al concentrations, 0.05 and 0.15 M, and is absent at higher Al concentrations. An optimum yield is observed between OH/Al molar ratios of 2.2 and 2.4.
- 4) The chemical shift and the linewidth of the monomer resonance decreases with rising Al concentration due to an increase in T_2 and a subsequent decrease of the quadrupole coupling constant e^2qQ/h .
- 5) The chemical shift and the linewidth of the monomer resonance increase with increasing OH/Al molar ratio due to the formation of $\text{Al}(\text{H}_2\text{O})_5(\text{OH})^{2+}$.
- 6) The chemical shift of the central fourfold coordinated Al of the tridecamer does not increase with increasing OH/Al molar ratio and is independent of Al concentration. The linewidth remains constant upon increasing both the OH/Al molar ratio and the Al concentration. This is due to the very strong shielding of the central fourfold coordinated Al.

REFERENCES

- Akitt, J. W.(1989) Multinuclera studies of aluminium compounds: *Prog. NMR Spectr.* **21**, 1-149.
- Akitt, J. W. and Elders, J. M.(1985) Aluminum-27 nuclear magnetic resonance studies of the hydrolysis of aluminium(III). Part 7. Spectroscopic evidence for the cation $[AlOH]^{2+}$ from linebroadening studies at high dilution: *J. Chem. Soc. Faraday Trans.*, 1923-1930.
- Akitt, J. W. and Elders, J. M. (1988) Multinuclear magnetic resonance studies of the hydrolysis of aluminium(III). Part 8. Base hydrolysis monitored at very high magnetic field: *J. Chem. Soc. Dalton Trans.*, 1347-1355.
- Akitt, J. W. and Farthing, A. (1978) New ^{27}Al NMR studies of the hydrolysis of the aluminum(III) cation: *J. Magn. Reson.* **32**, 345-352.
- Akitt, J. W. and Farthing, A. (1981) Aluminum-27 nuclear magnetic resonance studies of the hydrolysis of aluminum(III). Part 4. Hydrolysis using sodium carbonate: *J. Chem. Soc. Dalton Trans.*, 1617-1623.
- Akitt, J. W., Greenwood, N. N., Kandelwahl, B. and Lester, G. D. (1972) ^{27}Al nuclear magnetic resonance studies of the hydrolysis and polymerisation of the hexa-aquo-aluminum(III) cation: *J. Chem. Soc. Dalton Trans.*, 604-610.
- Akitt, J. W., Greenwood, N. N. and Lester, G. D. (1969) Hydrolysis and dimerisation of aqueous aluminum salt solutions: *Chem. Commun.*, 988-989.
- Akitt, J. W. and Mann, B. E. (1981) ^{27}Al NMR spectroscopy at 104.2 MHz: *J. Magn. Reson.* **44**, 584-589.
- Bertsch, P. M. (1987) Conditions for Al₁₃ polymer formation in partially neutralized aluminum solutions: *Soil Sci. Soc. Amer. J.* **51**, 825-828.
- Bertsch, P. M., Layton, W. J. and Barnhisel, R. I. (1986a) Speciation of hydroxy-aluminum solutions by wet chemical and aluminum-27 NMR methods: *Soil Sci. Soc. Amer. J.* **50**, 1449-1454.

- Bertsch, P. M., Thomas, G. W. and Barnhisel, R. I. (1966b) Characterization of hydroxy-aluminum solutions by aluminum-27 nuclear magnetic resonance spectroscopy: *Soil Sci. Soc. Amer. J.* **50**, 825-830.
- Bottero, J. Y., Cases, J. M., Fiessinger, F. and Poirier, J. E. (1980) Studies of hydrolyzed aluminum chloride solutions. 1. Nature of aluminum species and composition of aqueous solutions: *J. Phys. Chem.* **84**, 2933-2939.
- Bottero, J. Y., Tchoubar, D., Cases, J. M. and Fiessinger, F. (1982) Investigation of the hydrolysis of aqueous solutions of aluminum chloride. 2. Nature and structure by small-angle X-ray scattering: *J. Phys. Chem.* **86**, 3667-3673.
- Kloprogge, J. T., Seykens, D., Geus, J. W. and Jansen, J. B. H. (1992a) Temperature influence on the Al13 complex in partially neutralized aluminum solutions: an ²⁷Al nuclear magnetic resonance study: *J. Non-Cryst. Solids* **142**, 87-93.
- Kloprogge, J. T., Seykens, D., Jansen, J. B. H. and Geus, J. W. (1992b) An ²⁷Al nuclear magnetic resonance study on the optimization of the development of the Al13 polymer: *J. Non-Cryst. Solids* **142**, 94-102.
- Kloprogge, J. T., Seykens, D., Jansen, J. B. H. and Geus, J. W. (1992c) Aluminum monomer line-broadening as evidence for the existence of [Al(OH)]²⁺ and [Al(OH)₂]⁺ during forced hydrolysis; an ²⁷Al nuclear magnetic resonance study: *This Thesis Ch XII, J. Non-Cryst. Solids*, accepted for publication.
- May, H. M., Helmke, P. A. and Jackson, M. L. (1979) Gibbsite solubility and thermodynamic properties of hydroxy-aluminum ions in aqueous solution at 25°C: *Geochim. Cosmochim. Acta* **43**, 861-868.
- Rausch, W. V. and Bale, H. D. (1964) Small-angle X-ray scattering from hydrolyzed aluminum nitrate solutions: *J. Chem. Phys.* **40**, 3391-3394.
- Stol, R. J., van Helden, A. K. and de Bruyn, P. L. (1976) Hydrolysis-Precipitation studies of aluminum(III) solutions. 2. A kinetic study and model: *J. Coll. Interf. Sci.* **57**, 115-131.

- Thompson, A. R., Kunwar, A. C., Gutowski, H. S. and Oldfield, E. (1987) Oxygen-17 and aluminium-27 nuclear magnetic resonance spectroscopic investigations of aluminium(III) hydrolysis products: *J. Chem. Soc. Dalton Trans.*, 2317-2322.
- Vermeulen, A. C., Geus, J. W., Stol, R. J. and de Bruyn, P. L. (1975) Hydrolysis-precipitation studies of aluminum(III) solutions. I. Titration of acidified aluminum nitrate solutions: *J. Coll. Interf. Sci.* **51**, 449-458.

CHAPTER XIV

THE TRIDECAMERIC ALUMINUM COMPLEX AS AN APPROPRIATE PRECURSOR FOR FIBROUS BOEHMITE: A ^{27}Al NMR STUDY ON THE PARTIAL HYDROLYSIS OF ALUMINUM *SEC*-BUTOXIDE

ABSTRACT

The aging of the aluminum tridecamer in acidified aluminum *sec*-butoxide is studied with ^{27}Al NMR. At 20°C the tridecamer content passes through a maximum of 19.7 % after 133 hours of aging to decline subsequently to a final content of approximately 12 % . At 90°C the tridecamer disappears within 21 hours of aging due to clustering. After 91 hours colloidal gibbsite forms, while the pH drops continuously from 4.3 to 3.5. Simultaneously the monomer concentration increases to approximately 6.6 % . The rise is possibly due to liberation of the central fourfold coordinated Al from the tridecamer that rearrange to hexameric rings, and to dissolution of some gibbsite in the acid solution. The hexameric rings are considered to be the precursor for the crystallization of gibbsite and boehmite. Increase of the preparation temperature from 20° C to 80°C has no effect on the amount of tridecamer, although at 90°C the amount rises from approximately 9 % to 14.1 % . An increase of the preparation temperature leads to changes in the second order quadrupole effects, which results in a line sharpening from 19.5 to 9.8 Hz for the central fourfold coordinated Al signal of the tridecamer at 63.3 ppm.

14.1 INTRODUCTION

Akitt (1989) has extensively reviewed the research on the formation of the tridecameric aluminum complex $[\text{AlO}_4\text{Al}_{12}(\text{OH})_{24}(\text{H}_2\text{O})_{12}]^{7+}$ (Johansson, 1960, 1963) upon hydrolysis of inorganic Al-salts and Al metal.

The hydrolysis of organic aluminum compounds, such as, Al alcoxides has been examined by means of Fourier Transform Infrared (FTIR) Spectroscopy (Chane-Ching and Klein, 1988), X-Ray Diffraction (XRD) (Yoldas, 1973; Kriz et al., 1984; Pierre and Uhlman, 1987), Transmission Electron Microscopy (TEM)

(Yoldas, 1973), and ^{27}Al NMR (Kriz et al., 1984; Olson and Bauer, 1986; Nazar and Klein, 1988; Akitt et al., 1989). The development of the tridecamer during the hydrolysis of aluminum secondary butoxide $\text{Al}[\text{OC}_4\text{H}_7]_3$ (ASB) as recorded by ^{27}Al NMR spectroscopy has not been reported, although it is presumably an important building unit during the hydrothermal synthesis at 150°C of extremely fine fibrous boehmite in acid hydrolyzed ASB (Buining et al., 1990) or aging of ASB in water at 25° and 80°C (Yoldas, 1973).

The aims of this study are: i) to study the effect of aging on the tridecameric complex at 20°C and 90°C in partially acid hydrolyzed ASB solutions; ii) to elucidate the development of the tridecameric complex during acid hydrolysis of ASB at various preparation temperatures between 20° and 90°C ; iii) to determine the breakdown of the tridecameric complex during thermal treatment up to 90°C of a partially hydrolyzed ASB solution in the NMR apparatus; iv) to investigate whether the breakdown products are appropriate precursors for the formation of fibrous boehmite.

14.2 EXPERIMENTAL METHODS

15.2.1 Preparation of the acidified Al alcoxide solutions

0.150 M Al solutions with an Al/Cl molar ratio of 2.60 are prepared by adding 1.80 ml reagent grade aluminumtri-secundair butoxide (ASB, Fluka A.G. no. 06190) to 0.24 ml HCl (37 wt%, Merck no. 317) in 47.96 ml twice distilled water under a N_2 atmosphere. The resulting 50 ml solutions are stirred for 45 minutes with a magnetic stirring bar at the desired preparation temperature. Immediately after the addition a suspension is formed of amorphous aluminum hydroxide containing *sec*-butoxide groups (Yoldas, 1973; Buining et al., 1991), which slowly dissolves upon progressing hydrolysis. The first series of experiments involves the aging the solutions for 17 to 298 hours in closed Erlenmeyers at 20°C . In the second series of experiments the solutions

prepared at 20°C are stored in closed Teflon beakers at 90°C for 7 to 137 hours. In the third series of experiments solutions are prepared at 20°, 40°, 60°, 80°, and 90°C within 5 minutes and stored in closed Erlenmeyers at 20°C for approximately 170 hours.

14.2.2 Analytical techniques

Aliquots of the solutions which contain precipitates are carefully taken with a pipet for the purpose of analyses. Turbid solutions are centrifuged first at 3000 rpm for 30 minutes, Before decantation. All solutions are analyzed with ICP-AES, ²⁷Al NMR and the pH is measured.

The total aluminum concentration in the supernatant is determined by Inductively Coupled Plasma-Atomic Emission Spectroscopy (ICP-AES). The ²⁷Al NMR spectra of the supernatants are obtained with a Bruker WP 200 spectrometer operating at 52.148 MHz (4.6 Tesla). The spectra obtained with this instrument have to be corrected for background signals due to aluminum containing ceramics in the probe by subtracting a blanco H₂O/D₂O spectrum from the experimental spectra. All solutions are diluted with D₂O (1:1), which act as field frequency lock. A 0.15 M aluminum nitrate solution is used as external standard with respect to the chemical shift. Upfield shifts, reported in ppm, are taken to be negative.

The Al monomer content of the total Al present is determined directly from the integrated surface area of the sixfold coordinated Al resonance at approximately 0 ppm (Kloprogge et al., 1992a). The tridecamer Al content is calculated by multiplying by 13 the integrated area of the 63.3 ppm resonance of the central fourfold coordinated Al of the tridecamer (Kloprogge et al., 1992a). The NMR-undetectable Al content is calculated by subtracting the percentage of monomeric and tridecameric Al from the total Al present in solution, as determined by ICP-AES. The error in the surface area determinations is approximately 10 %.

During the aging experiments the pH is measured regularly. After centrifugation of the turbid solutions the resulting precipitate is dried overnight at 120°C. The X-Ray powder Diffraction (XRD) patterns of the precipitates are recorded on a Philips PW 1050/25 diffractometer using $\text{CuK}\alpha$ radiation.

14.3 RESULTS

14.3.1 Colloids

Immediately after mixing the ASB with HCl solutions the resulting solutions become turbid due to an amorphous solid. The turbidity gradually disappears after 32 to 54 hours aging at 20°C. In this period of time the ICP-AES measurements of the supernatant reveal a nearly constant Al concentration. Longer aging leads to an almost linear increase in Al concentration. After extrapolation over 60 days the yield of soluble aluminum amounts to approximately 90 %. The solid residue disappears within 60 days. The residues separated by centrifugation of the freshly mixed turbid solutions do not display XRD patterns, which indicates the presence of X-ray amorphous material only. Aging at 90°C results in the disappearance of turbidity within 7 hours. No visible residue is observed, although particles smaller than 50 nm can still be present. The ICP-AES analyses indicate only the presence of approximately 50 to 60 % of the aluminum totally present in the solution.

Solutions aged at 90°C for more than 91 hours have become again colloidal. Remarkably, the total Al concentration in solution as detected by ICP-AES remains at the same level of approximately 50 to 60 % throughout the whole aging experiment. After 12 days aging at 90°C the colloidal particles of sample RV12A are separated from the solvent by centrifugation and dried overnight at 120°C. The XRD pattern corresponds to the pattern of gibbsite, $\text{Al}(\text{OH})_3$, together with a broad hump between 17 and 33 degrees 2θ characteristic of an amorphous phase. After 3 months aging at 20°C the amount of colloid has

The tridecameric aluminum complex as an appropriate precursor for fibrous boehmite: an ^{27}Al NMR study on the partial hydrolysis of aluminum sec-butoxide

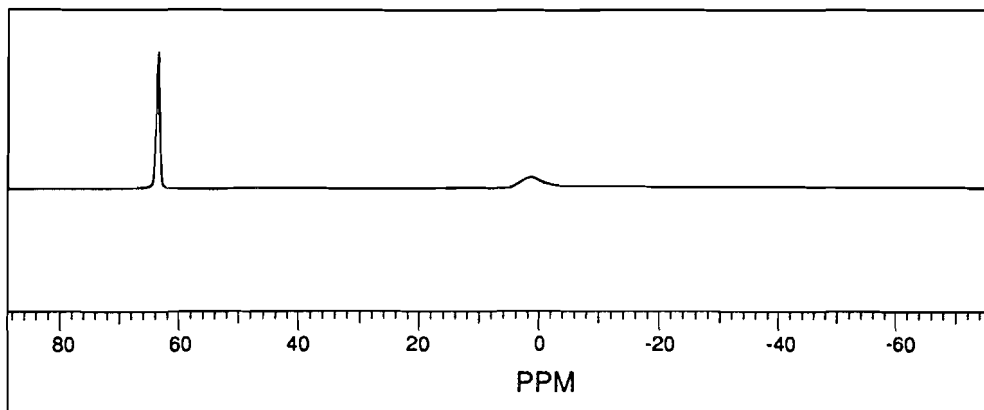


Figure 14.1 ^{27}Al NMR spectrum of a partially hydrolyzed ASB solution aged at 20°C.

increased. XRD patterns of the colloids of the samples RV10A and RV14A confirm the presence of gibbsite.

14.3.2 ^{27}Al NMR

A typical NMR spectrum of a partially hydrolyzed ASB solution displays two distinct resonances (Fig. 14.1). The broad (approximately 170 Hz) resonance at approximately 0 ppm is attributed to monomeric sixfold coordinated Al, present in the following species $[\text{Al}(\text{H}_2\text{O})_6]^{3+}$, $[\text{Al}(\text{H}_2\text{O})_5\text{OH}]^{2+}$, and $[\text{Al}(\text{H}_2\text{O})_4(\text{OH})_2]^+$ (Akitt and Elders, 1985; Bertsch et al., 1986a). The sharp resonance at approximately 63.3 ppm with a linewidth of approximately 14 to 20 Hz is ascribed to the central fourfold coordinate Al of the tridecameric polymer (Kloprogge et al., 1992a,b).

14.3.3 Aging at 20°C

The aluminum percentages of the monomeric and tridecameric Al species measured by ^{27}Al NMR and the total Al concentration determined by ICP-AES are plotted as function of aging time at 20°C in Figure 14.2.

The total Al concentration (ICP-AES) in solution exhibits a clear increase from 0.027 M (17.9 % of total Al added with ASB) to 0.043 M (28.6 %) upon aging. The monomer content varies between 0.5 and 1.6 %, and seems to be independent of aging time. The tridecamer content increases from 9.3 to 18.8 % during the first 133 hours, and decreases to 13.1 % after about 300 hours. Upon 133 hours of aging the total soluble Al percentage (NMR) increases from 10.5 to 19.7 %, while after about 300 hours it has decreased to 14.7 %. The sum of the Al concentrations detected by ^{27}Al NMR is about a factor two lower than that measured with ICP-AES.

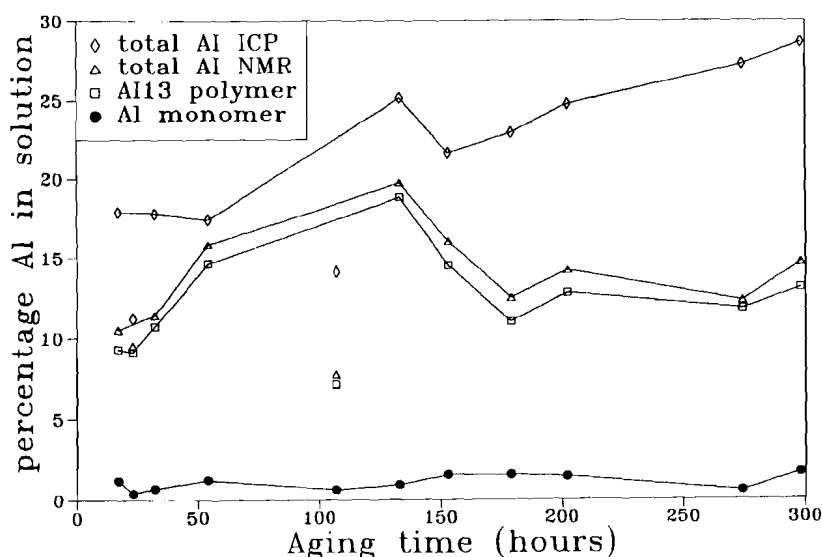


Figure 14.2 Plot of the total Al concentration determined by ICP-AES and ^{27}Al NMR and the tridecamer, and monomer percentages determined by ^{27}Al NMR as function of aging time at 20°C.

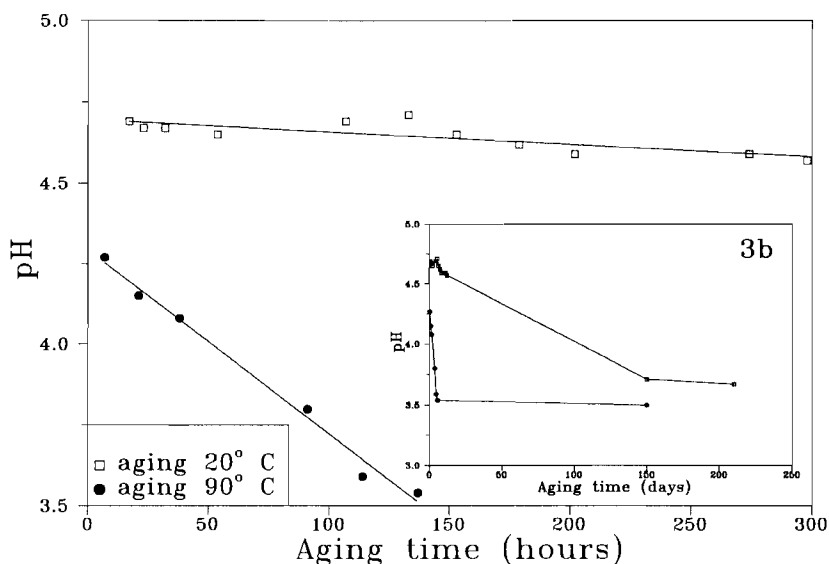


Figure 14.3 a) pH as function of aging time at 20°C and b) long term aging at 20 and 90°C.

During the first 300 hours of aging the pH decreases almost linearly from 4.74 to 4.57 (Fig. 14.3a). After 210 days the pH decreases to 3.67 (Fig. 14.3b), finally resulting in an asymptotic value of approximately 3.5.

14.3.4 Aging at 90°C

The ICP-AES analyses reveal Al concentrations in a range between 50 and 60 % of the total Al added with ASB, independent of aging time (Fig. 14.4). Between 21 and 91 hours a small rise of the monomer content from 3.4 to 6.6 % coincides with the slightly increasing total aluminum content (NMR) to 6.6 %. Within 21 hours the tridecamer content has decreased from 10.3 to approximately 0.0 %. In the same time the total Al (NMR) content decreased from 12.1 to 3.4 %. The total Al contents detected by NMR are considerably

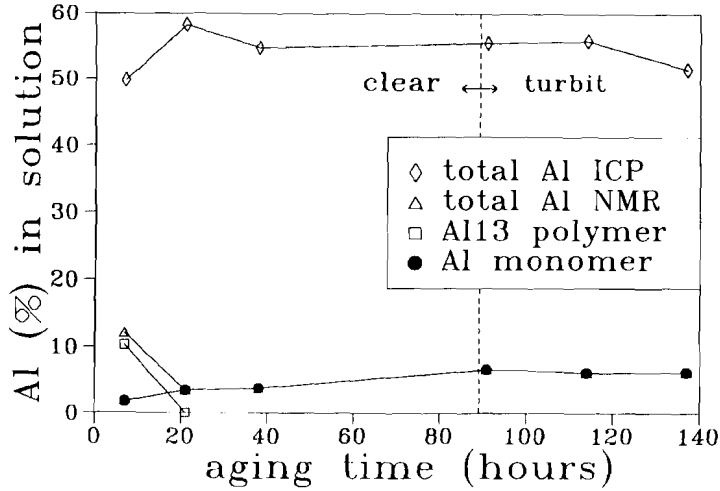


Figure 14.4 Total Al determined by ^{27}Al NMR and ICP-AES, tridecamer, and monomer percentages as function of aging time at 90°C .

lower than those aged at 20°C . Longer aging does not further affect the NMR detectable aluminum species, although after aging for more than 80 hours the solutions have become extremely colloidal.

The pH decreases linearly from 4.27 to 3.54 during 100 hours aging (Fig. 14.3a). After prolonged aging for 150 days all solutions have a pH between 3.5 and 3.7 (Fig. 14.3b).

The linewidth at half height of the monomer resonance gradually diminishes from 132 Hz after 6.7 hours to 32 Hz (accuracy 10 %) after 137 hours of aging. Upon aging at 90°C the monomer resonance shifts towards high field from 0.57 ppm after 10 min to 0.09 ppm after 137 hours. The chemical shift of the tridecamer resonance remains at 63.3 ppm.

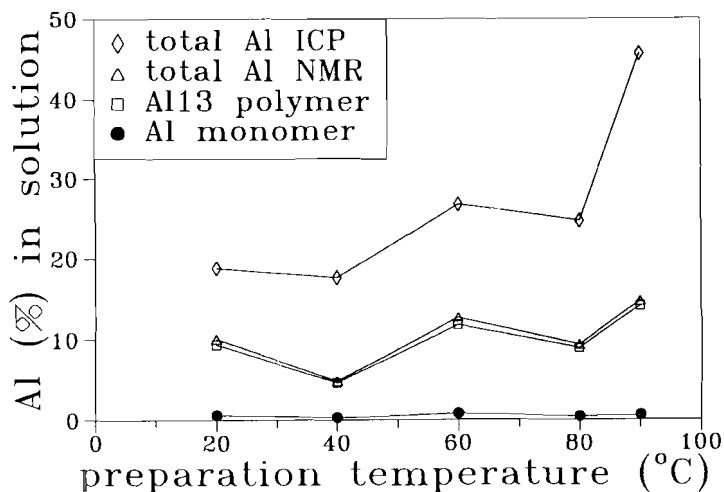


Figure 14.5 Total Al determined by ^{27}Al NMR and ICP-AES, tridecamer, and monomer percentages as function of preparation temperature after aging at 20°C for 170 hours.

14.3.5 Solutions prepared between 20 and 90°C

The ASB and HCl solutions are mixed at the desired temperatures for approximately 5 minutes and subsequently rapidly cooled to room temperature. All solutions prepared below 80°C are clear after aging for 170 hours at 20°C. The solutions prepared at 80° and 90°C are turbid after 170 hours aging.

The total Al concentration after 170 hours of aging detected with ICP-AES exhibit a small, rather irregular increase from approximately 19 % to 25 % of totally added Al with ASB with increasing preparation temperature from 20°C to 80°C. Preparation at 90°C results in an increase of the soluble aluminum content to approximately 46 % (Fig. 14.5).

The monomer and tridecamer contents are nearly at one level of concentration, viz., at less than 1 %, and at approximately 9 %, respectively, for solutions

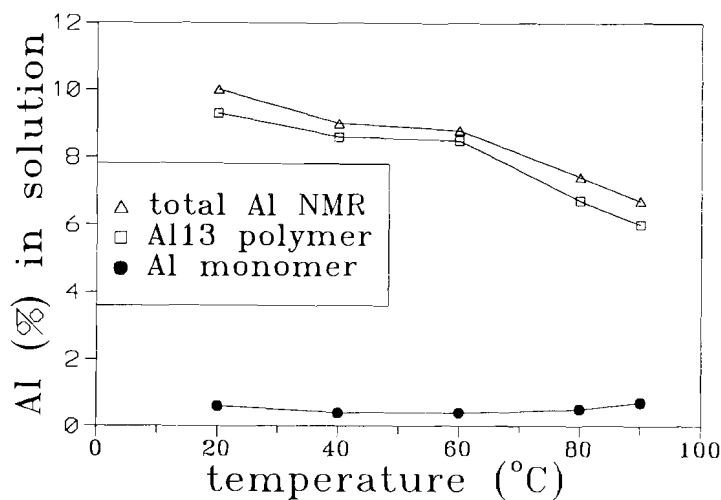


Figure 14.6 Total Al determined by ^{27}Al NMR; tridecamer, and monomer percentages as function of sample temperature in the NMR apparatus. Total Al detected by ICP-AES at 20°C is 18.8 %.

prepared between 20° and 80°C. The sum of Al contents detected with NMR remains nearly constant at 10 % for these solutions. Preparation at 90°C results in an increase to 14.7 %, mainly due to an increase in tridecamer content to 14.1 %.

14.3.6 Heating in the NMR apparatus

Sample RV3B, that had already aged for a period of 175 hours at 20°C, has been studied in the NMR heating experiments. The total soluble Al concentration detected with ICP-AES before the heating experiments was 18.8 %.

The sum of Al contents detected with NMR decreases almost linearly from 10.0 % at 20°C to 6.7 % at 90°C (Fig. 14.6), due to the decrease of the tridecamer content from 9.3 % at 20°C to 6.0 % at 90°C, while the monomer content remains almost unchanged.

The peakwidth at half height of the tridecameric fourfold coordinated Al signal sharpens linearly with increasing preparation temperature from 19.53 Hz for solutions prepared at 20°C to 9.8 Hz for solutions prepared at 90°C. The signal shifts from 63.3 ppm to 64.0 ppm for solutions prepared at increasing temperature from 20° to 90°C.

14.4 DISCUSSION

Hydrolysis proceeding after mixing of ASB and HCl solutions results in the formation of the tridecamer as one of the aluminum species. No other species than monomer and tridecamer are observed with ²⁷Al NMR.

ICP-AES analyses reveal that in all experiments the aluminum concentration increases with aging at 20°C as well as upon increasing preparation temperature. On the other hand, the tridecamer content decreases upon aging. This indicates the formation of aluminum polymers, which are undetectable with NMR, but which are, at least partly, measured with ICP-AES. Aging at 90°C results in a relatively constant aluminum concentration of about 50 - 60 %. This concentration is much higher than the concentrations in solutions aged at 20°C, in which remnants of a residue are present. Although no residue is observed, only 50 to 60 % is detected with the ICP-AES. This can be explained by either the presence of very small, less than 50 nm, colloidal aluminum hydroxide particles, or aluminum (organic) polymers large enough not to be detected by ICP-AES and NMR, but too small to be apparent as a visible colloidal phase. The disappearance of the tridecamer during the first 21 hours is accompanied by an equal increase in the total Al concentration measured with ICP-AES, indicating

that polymers with dimensions larger or equal to that of the tridecamer (± 12 Å) are not detected by ICP-AES. The same is evidenced by increasing the preparation temperature from 80° to 90°C, which results in a strong rise of the total Al concentration (ICP-AES), whereas the tridecamer only slightly increases.

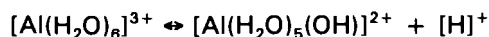
Based on the comparable initial conditions before aging, and on the almost constant tridecamer content in the solutions prepared at increasing temperature, it is reasonable to assume that a maximum tridecamer concentration is rapidly established. After 7 hours aging at 90°C almost no tridecamer is left. Therefore, it can be concluded that clustering and/or breakdown of the tridecamer proceeds within 7 hours aging at 90°C. The simultaneous decrease in pH upon aging indicates a lowering of the degree of hydrolysis of the aluminum accompanying the clustering/breakdown and, therefore, must imply a change in the polymer structure.

High temperature aging results in the disappearance of the tridecamer, a strong increase of NMR undetectable aluminum, and the formation of colloidal gibbsite, which may imply the clustering and rearrangement of the tridecamer into large polymers unobservable with NMR. Based on Small-angle X-ray Scattering (SAX), Infrared spectroscopy, and X-ray diffraction, it is concluded that these clustered polymers consist of hexameric rings (Bottero et al., 1982; Bertsch et al., 1986a,b; Denney and Hsu, 1986). In contrast to this study, a constant pH is reported upon aging, pointing to a structural rearrangement without any change in the degree of hydrolysis of the polymer (Tsai and Hsu, 1984).

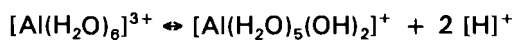
The decrease in tridecamer content upon long term aging (> 133 hours) at 20°C is in agreement with that observed with partly hydrolyzed $\text{Al}(\text{NO}_3)_3$ (Kloprogge et al., 1992b). In contrast with the 20°C data, the 90°C data show an increase of the monomer content upon aging. Based on SAX and ^{27}Al NMR, Bottero et al. (1982, 1987) have suggested that clustering of the tridecamers squeezes the central tetrahedral aluminum ion between the growing octahedral layers. These squeezed aluminum ions are liberated from the cluster into the

acidic solution, which may result in a small increase of the monomer content. The disappearance of the tridecamer upon 90°C aging will then lead to the liberation of approximately 0.8 % of monomer. During long term aging colloidal gibbsite is generated. The low pH between 3.5 and 3.7 will cause partly dissolution of gibbsite, which may again result in an increase of the monomer content in solution. Pereya and Kittrick (1988) have shown that the solubility of gibbsite in the pH range between 3.55 and 3.82 is of the order of $8 \text{ to } 45 \times 10^{-4} \text{ M}$, which is equivalent with an increase of the monomer content of 0.5 to 3.0 %. Based on these data an increase of the monomer content should be of the order of 1.3 to 3.8 %, from which the highest value is in reasonable agreement with our increase of approximately 4.4 %.

The decreasing linewidth of the monomer resonance upon aging may be explained by a shift in the equilibria



and



upon decreasing pH (Akitt and Elders, 1985; Klopogge et al., 1992c).

The internal heating experiments show an increase and sharpening of the monomer resonance intensity with increasing temperature. Both are caused by changing second order quadrupole effects, which are temperature dependent. This results in a change of the relaxation time T_2 and, consequently, diminishes the so called "missing intensity" (Akitt, 1989).

In contrast with the slowly, continuous decrease of the tridecamer upon heating in this study, Klopogge et al. (1992a) noticed an apparent increase of the tridecamer upon heating up to 85°C in the NMR, due to a competition between increasing intensity due to second order quadrupole effects and the clustering/breakdown of the tridecamer. Although quadrupole effects influence the intensities in our experiments, the clustering/breakdown is much more predominant, resulting in a continuous decrease. The large amounts of organic complexes may cause a different chemical environment with respect to the

completely inorganic environment used by Kloprogge et al. (1992a). This change may not only affect the stability of the tridecamer, but also the aluminum quadrupole parameters and the ^{27}Al NMR line intensities.

Buining et al. (1991) synthesized colloidal, hexagonal boehmite plates and colloidal boehmite needles ($l \approx 300\text{nm}$, $d \approx 15\text{ nm}$) by hydrothermal treatment of acidified ASB solutions at 110° and 150°C , respectively. Tokar and Krischner (1962) have determined that at pressures below 300 bar the phase transition from gibbsite to boehmite is found at approximately 100°C . The formation of gibbsite at 90°C in this study and the formation of boehmite at 110°C reported by Buining et al. (1991) agree with the phase transition (Krischner, 1962). Therefore, it can be concluded that the formation of boehmite at 110°C proceeds identically with that of gibbsite via the clustering of Al polymers in hydrolyzed ASB solutions.

14.5 CONCLUSIONS

Acidification of aqueous ASB solutions results in the hydrolysis of aluminum, creating polymers, such as, the tridecamer. During aging at 90°C clustering and partly breakdown of the tridecamer results in the formation of colloidal gibbsite and a small amount of monomer. It is suggested that the formation of boehmite above the boehmite/gibbsite phase transition at approximately 100°C proceeds identically with that of gibbsite.

ACKNOWLEDGMENT

The authors wish to thank A. M. J. van der Eerden for his advice and help in the HPT laboratory, Institute fo Earth Sciences, H. M. V. C. Govers for the XRD patterns, and P. Anten for the ICP-AES analyses.

REFERENCES

- Akitt, J. W. (1989) Multinuclear studies of aluminium compounds: *Prog. NMR Spectr.* **21**, 1-149.
- Akitt, J. W., Elders, J. M., Fontaine, X. L. R. and Kundu, A. K. (1989) Multinuclear magnetic resonance studies of the hydrolysis of aluminium(III). part 10. Proton, carbon-13 and aluminium-27 spectra of aluminium-acetate at very high magnetic field: *J. Chem. Soc. Dalton Trans.*, 1897-1901.
- Akitt, J. W. and Elders, J. M. (1985) Aluminium-27 nuclear magnetic resonance studies of the hydrolysis of aluminium(III). Part 7. spectroscopic evidence for the cation $[AlOH]^{2+}$ from line-broadening studies at high dilution: *J. Chem. Soc. Faraday Trans.*, 1923-1930.
- Bertsch, P. M., Layton, W. J. and Barnhisel, R. I. (1986a) Speciation of hydroxy-aluminum solutions by wet chemical and aluminum-27 NMR methods: *Soil Sci. Soc. Amer. J.* **50**, 1449-1454.
- Bertsch, P. M., Thomas, G. W. and Barnhisel, R. I. (1986b) Characterization of hydroxy-aluminum solutions by aluminum-27 nuclear magnetic resonance spectroscopy: *Soil Sci. Soc. Amer. J.* **50**, 825-830.
- Bottero, J. Y., Tchoubar, D., Cases, J. M. and Fiessinger, F. (1982) Investigation of the hydrolysis of aqueous solutions of aluminum chloride. 2. Nature and structure by small angle X-ray scattering: *J. Phys. Chem.* **86**, 3667-3672.
- Bottero, J. Y., Axelos, M., Tchoubar, D., Cases, J. M., Fripiat, J. J. and Fiessinger, F. (1987) Mechanism of formation of aluminum trihydroxide from Keggin Al_{13} polymers: *J. Coll. Interface Sci.* **117**, 47-57.
- Buining, P. A., Pathmamanoharan, C., Bosboom, M., Jansen, J. B. H. and Lekkerkerker, H. N. W. (1990) : Effect of hydrothermal conditions on the

- morphology of colloidal boehmite particles: Implications for fibril formation and monodispersity: *J. Amer. Ceram. Soc.* **73**, 2385-2390.
- Buining, P. A., Pathmamanoharan, C., Jansen, J. B. H. and Lekkerkerker, H. N. W. (1991) : Preparation of colloidal boehmite needles by hydrothermal treatment of aluminum alkoxide precursors: *J. Amer. Ceram. Soc.* **74**, 1303-1307.
- Chane-Ching J.-Y. and Klein, L. C. (1988) : Hydrolysis in the aluminum sec-butoxide-water-isopropyl alcohol system: II, aging and microstructure: *J. Amer. Ceram. Soc.* **71**, 86-90.
- Denney, D. Z. and Hsu, P. H. (1986) ^{27}Al nuclear magnetic resonance and Ferron kinetic studies of partially neutralized AlCl_3 solutions: *Clays & Clay Minerals* **34**, 604-607.
- Johansson, G. (1960) On the crystal structure of some basic aluminum salts: *Acta Chem. Scand.* **14**, 771-773.
- Johansson, G. (1963) The crystal structure of a basic aluminum selenate: *Ark. Kemi* **20**, 305-319.
- Kloppogge, J. T., Seykens, D., Geus, J. W. and Jansen, J. B. H. (1992a) Temperature influence on the Al_{13} complex in partially neutralized aluminum solutions: an ^{27}Al nuclear magnetic resonance study: *J. Non-Cryst. Solids* **142**, 87-93.
- Kloppogge, J. T., Seykens, D., Jansen, J. B. H. and Geus, J. W. (1992b) An ^{27}Al nuclear magnetic resonance study on the optimization of the development of the Al_{13} polymer: *J. Non-Cryst. Solids* **142**, 94-102.
- Kloppogge, J. T., Seykens, D., Jansen, J. B. H. and Geus, J. W. (1992c) Aluminum monomer line-broadening as evidence for the existence of $[\text{AlOH}]^{2+}$ and $[\text{Al}(\text{OH})_2]^+$ during forced hydrolysis: an ^{27}Al nuclear magnetic resonance study: *this thesis Ch XII*, accepted for publication in *J. Non-Cryst. Solids*.
- Kríz, O. Casensky, B., Lycka, A., Fusek, J. and Hermanek, S. (1984) ^{27}Al NMR behavior of aluminum alkoxides: *J. Magn. Reson.* **60**, 375-381.

- Nazar, L. F. and Klein, L. C. (1988) Early stages of alumina sol-gel formation in acidic media: an ^{27}Al nuclear magnetic resonance spectroscopy investigation: *J. Amer. Ceram. Soc.* **71**, C85-C87.
- Olson, W. L. and Bauer, L. J. (1986) Characterization of the sol-gel transition of alumina sols prepared from aluminum alkoxides via ^{27}Al NMR: *Mat. Res. Soc. Symp. Proc.* **73**, 187-193.
- Pereya, F. J. and Kittrick, J. A. (1988) Relative solubility of corundum, gibbsite, boehmite and diaspore at standard state conditions: *Clays & Clay Minerals* **36**, 391-396.
- Pierre, A. C. and Uhlmann, D. R. (1986) : Amorphous aluminum hydroxide gels: *J. Non-Cryst. Solids* **82**, 271-276.
- Pierre, A. C. and Uhlmann, D. R. (1987) Gelation of aluminum hydroxide sols: *J. Amer. Ceram. Soc.* **70**, 28-32.
- Tokar, K. and Krischner, H. (1962) *Ber. Deut. Keram. Ges.* **39**, 139.
- Tsai, P. P. and Hsu, P. H. (1984) Studies of aged OH-Al solutions using kinetics of Al-Ferron reactions and sulfate precipitation: *Soil Sci. Soc. Amer. J.* **48**, 59-65.
- Yoldas, B. E. (1973) Hydrolysis of aluminium alkoxides and bayerite conversion: *J. Appl. Chem. Biotechnol.* **23**, 803- 809.

CHAPTER XV

THERMAL STABILITY OF BASIC ALUMINUM SULFATE

ABSTRACT

The tridecameric Al polymer $[\text{AlO}_4\text{Al}_{12}(\text{OH})_{24}(\text{H}_2\text{O})_{12}]^{7-}$ is prepared by forced hydrolysis of an $\text{Al}(\text{NO}_3)_3$ solution by NaOH up to an OH/Al mol ratio of 2.2. Upon addition of sulfate the tridecamer crystallizes into macroscopic crystallites of the basic aluminum sulfate $\text{Na}_{0.1}[\text{Al}_{13}\text{O}_4(\text{OH})_{24}(\text{H}_2\text{O})_{12}](\text{SO}_4)_{3.55}$, which is characterized structurally by means of XRD, ^{27}Al MAS-NMR, IR and chemically by ICP. The basic aluminum sulfate has a monoclinic unit-cell with $a = 20.188 \pm 0.045 \text{ \AA}$, $b = 11.489 \pm 0.026 \text{ \AA}$, $c = 24.980 \pm 0.056 \text{ \AA}$, and $\beta = 102.957^\circ \pm 0.022^\circ$. With TGA, DTA and heating stage XRD the thermal decomposition is studied. The tridecamer persists as a stable unit in the sulfate structure to temperatures of 80°C . Approximately 9 moles H_2O are adsorbed in excess to one mole basic aluminum sulfate, which are easily lost by heating to 80°C . From 80° to 360°C the tridecamer unit will gradually decompose losing its 12 water and 24 hydroxyl groups and to become finally X-ray amorphous. From 360° to 950°C , with a maximum between 880° and 950°C , SO_3 is removed, leaving behind primary aluminum oxide.

15.1 INTRODUCTION

Forced hydrolysis of Al solutions by addition of alkali hydroxide solutions results in the formation of the tridecamer $[\text{AlO}_4\text{Al}_{12}(\text{OH})_{24}(\text{H}_2\text{O})_{12}]^{7-}$ (Kloprogge et al., 1992a,b). The tridecamer contains a central tetrahedral AlO_4 unit in a cage of twelve Al octahedrals. The tridecamer is of commercial interest because of its antiperspirant activity, its ability to control viscosity of kaolinite clays (Teagarden et al., 1981) and its pillaring capacity in smectites to form molecular sieves and catalysts (Plee et al., 1987; Schutz et al., 1987; Kloprogge et al., 1990). ^{27}Al nuclear magnetic resonance spectroscopy has confirmed the presence of both octahedral (chemical shift 0 ppm) and tetrahedral Al (chemical shift 62.5 ppm) in the tridecameric complex (Akitt et al., 1972; Akitt and Farthing, 1978; Kloprogge et al., 1992a,b).

Johansson (1960,1962,1963) and Johansson et al. (1960) have precipitated two different basic aluminum sulfates, being monoclinic $\text{Na}[\text{Al}_{13}\text{O}_4(\text{OH})_{24}(\text{H}_2\text{O})_{12}](\text{SO}_4)_4 \cdot x\text{H}_2\text{O}$ and cubic $[\text{Al}_{13}\text{O}_4(\text{OH})_{25}(\text{H}_2\text{O})_{11}](\text{SO}_4)_3 \cdot x\text{H}_2\text{O}$, both consisting of the tridecameric aluminum polymers attached by hydrogen bonding to the oxygen atoms of the sulfate. Solid-state high-resolution ^{27}Al NMR has confirmed the presence of both tetrahedral (Müller et al., 1981, Lampe et al., 1982) and octahedral aluminum in basic aluminum salts (Bottero et al., 1987; Kunwar et al., 1984).

Until now the basic aluminum sulfate has only be characterized by means of X-ray diffraction and solid state ^{27}Al MAS-NMR. In this study basic aluminum sulfate, precipitated from partly hydrolyzed aluminum nitrate solutions, is characterized with ^{27}Al solid-state Magic-Angle Spinning Nuclear Magnetic Resonance spectroscopy (MAS-NMR), X-ray diffraction (XRD), Infrared spectroscopy (IR) and chemically analyzed with Inductively Coupled Plasma-Atomic Emission Spectroscopy (ICP-AES). The thermal decomposition behaviour is studied with Thermal Gravimetric Analysis (TGA), Differential Thermal Analysis (DTA), and heating-stage X-ray diffraction (HT-XRD). This study of the thermal decomposition will help to get a better understanding of the processes that take place during calcination of smectites pillared with the tridecameric polymer.

15.2 EXPERIMENTAL TECHNIQUES

15.2.1 The tridecamer solution

The tridecameric Al polymer is obtained by hydrolysis of an 0.5 M aluminum nitrate solution with an 0.5 M sodium hydroxide solution, until an OH/Al mol ratio of 2.2 is reached. Klopogge et al. (1992b) have described the details of the hydrolysis.

5 ml of the tridecamer solution is diluted with 5 ml D_2O before measurements of solution NMR. The ^{27}Al NMR spectra are recorded on a Bruker WP 200

spectrometer operating at 52.148 MHz (4.6 Tesla) at the Department of Organic Chemistry of the University of Utrecht. Chemical shifts are reported in ppm relative to $[\text{Al}(\text{H}_2\text{O})_6]^{3+}$.

15.2.2 Basic aluminum sulfate

To 100 ml of the tridecameric solution 100 ml of 0.5 M sodium sulfate is added, resulting in final concentrations of 0.085 M Al^{3+} and 0.25 M $(\text{SO}_4)^{2-}$. The precipitate is aged for 42 days before removal from the solution for further investigation.

The precipitates grown at the bottom and the walls of the container are collected separately, washed with distilled water and dried at room temperature. Chemical compositions are obtained by dissolving 500 mg of each precipitate in 50 ml 1M HCl and analyzed for Al, Na, and S by ICP. XRD powder patterns are recorded on a Philips PW 1050/25 diffractometer using $\text{CuK}\alpha$ radiation. Unit-cell dimensions are calculated using the least squares refinement computer program Unitcellc (Strom, 1976). Heating stage X-ray diffraction is carried out using a HT Guinier $\text{CuK}\alpha 1$ (Enraf Nonius FR553) focussing powder camera. The temperature is raised from 35° to 700°C using a heating rate of 10°C per hour. ^{27}Al magic angle spinning (MAS) NMR spectra are recorded on a Bruker WM 500 spectrometer operating at 130.321 MHz (11.7 Tesla) at the Department of Physical Chemistry, Faculty of Science, University of Nijmegen. The sample spin-frequency is approximately 3 kHz. Chemical shifts are reported in ppm relative to $[\text{Al}(\text{H}_2\text{O})_6]^{3+}$. Infrared absorption spectra are obtained on powdered samples in KBr tablets with 1 wt% sample concentration using a Perkin Elmer 580 IR spectrophotometer. Thermogravimetric analyses are performed with a Dupont 1090 Thermal Analyzer, applying a heating rate of 10°C/min.

15.3 RESULTS

15.3.1 Preparation

The hydrolyzed Al solution with an OH/Al ratio of 2.2 contains 27 % monomeric Al and 73 % tridecameric Al based on ^{27}Al NMR resonances at 0.16 ppm and 63.35 ppm, respectively (Fig. 15.1a). Comparison with an external Al^{3+} standard implies that the alumina in the solution was completely recovered, proving that no other aluminum polymer species are present.

Addition of sodium sulfate to the tridecamer solution results after approximately 15 min in the steady growth of small needles from the clear solution on the walls of the container. After 1 hour the solution becomes cloudy white. Overnight aging results again in a clear solution with approximately 0.5 mm long needles at the wall and a precipitate without any visible crystals at the bottom.

15.3.2 Characterization

ICP analysis of the washed crystals from the wall dissolved in HCl results in an atom ratio of 13 Al to 0.1 Na to 3.55 S, which can be recalculated to a structural formula of $\text{Na}_{0.1}[\text{Al}_{13}\text{O}_4(\text{OH})_{24}(\text{H}_2\text{O})_{12}](\text{SO}_4)_{3.55}\cdot x\text{H}_2\text{O}$. The unwashed precipitate of the bottom has an atom ratio of 6 Al to 4 Na to 2 S. Upon washing the precipitate completely redissolves.

The X-ray diffraction pattern of the unwashed bottom precipitate reveals the presence of crystalline NaNO_3 , while no crystalline basic aluminum sulfate has been observed. The XRD pattern of the crystals from the wall resembles the patterns reported by Bersillon et al. (1980) and Tsai and Hsu (1984, 1985). The basic aluminum sulfate exhibits a monoclinic unit cell (Fig. 15.2, Table 15.1). Al was used as internal standard to correct systematic errors in the resulting 2θ values. Based on the unit cell parameters for the monoclinic basic aluminum sulfate (Johansson, 1963), the pattern is indexed and unit cell parameters are recalculated using the first 38 reflections resulting in: $a = 20.188 \pm 0.045 \text{ \AA}$, $b = 11.489 \pm 0.026 \text{ \AA}$, $c = 24.980 \pm 0.056 \text{ \AA}$, and $\beta = 102.957^\circ \pm 0.022^\circ$ (Table 15.1).

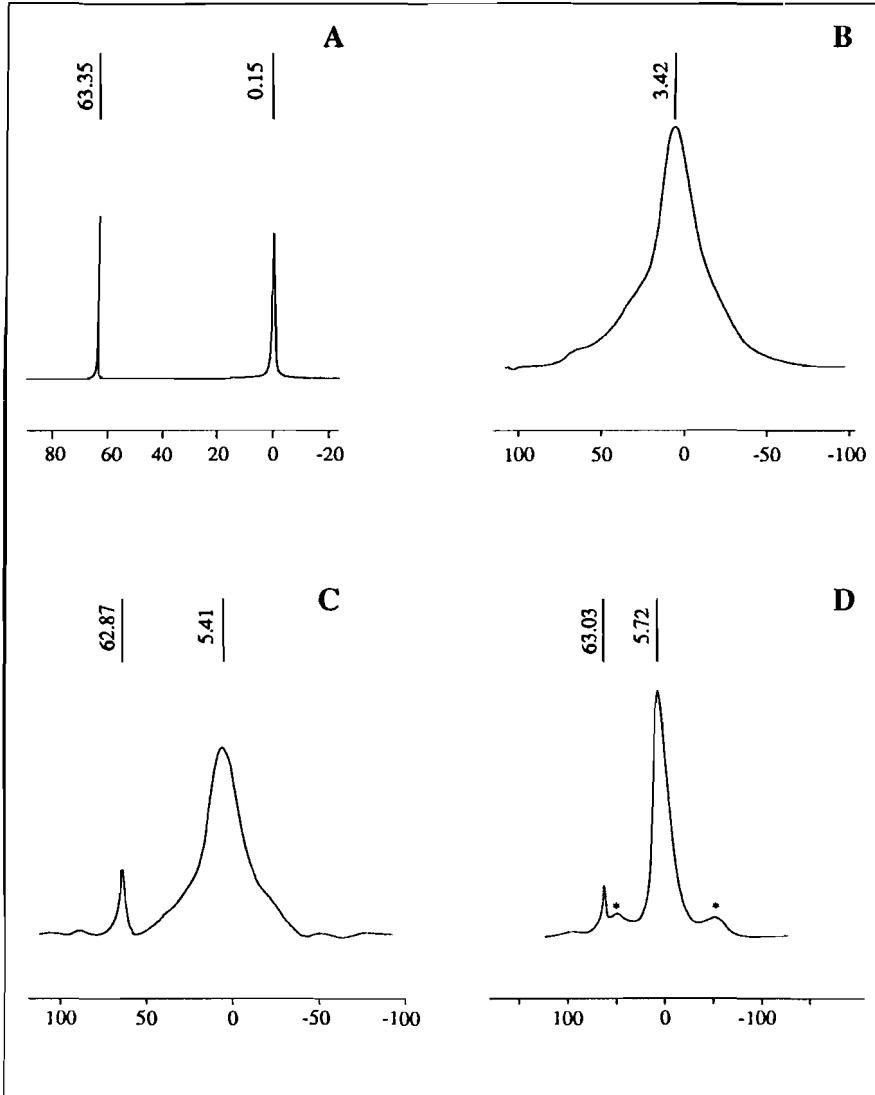


Figure 15.1 a) ^{27}Al NMR spectrum of the partly hydrolyzed solution with an OH/Al ratio of 2.2; ^{27}Al solid-state MAS-NMR spectra of b) the precipitate from the bottom; c) the unwashed and d) the washed crystals from the wall.

Table 15.1 X-ray diffraction data in the range $3 - 50^\circ 2\theta$ of the washed basic aluminum sulfate from the wall.

d(obs) ¹ Å	I(rel)	d(calc) ² Å	hkl	Bersillon et al. (1980)	Tsai and Hsu(1984)
12.07	100	12.18	002	12.3	12.2
11.49	8	11.50	010		
10.29	10	10.40	011	10.0	10.4
9.85	45	9.84	200	9.61	9.89
9.57	19	9.58	-111		
8.86	18	8.85	111	8.85	8.93
8.65	8	8.67	-202		
6.90	9	6.92	-212	6.83	6.53
5.89	6	5.94	212	5.83	
5.80	9	5.79	-204		
5.45	6	5.46	-121	5.37	5.33
5.34	5	5.32	311		
5.15	12	5.15	-122	5.18	5.17
4.69	7	4.69	023		4.60
4.55	13	4.56	-412	4.58	
					4.47
4.37	30	4.37	214	4.37	4.36
4.27	6	4.28	-322		
4.16	25	4.15	321	4.17	4.10
4.05	18	4.05	-414		4.06
3.97	8	3.97	124		3.98
3.82	15	3.83	016	3.83	3.83
3.75	6	3.76	-422		3.65
3.57	6	3.57	511		
3.52	13	3.52	502	3.53	
3.44	8	3.46	-424	3.46	3.44
3.42	8	3.41	422		
3.36	8	3.36	-602 133	3.37	
3.30	13	3.30	324 330	3.33	3.33
3.23	13	3.23	-612	3.24	3.24

Table 15.1

d(obs) ¹ Å	l(rel)	d(calc) ² Å	hkl	Bersillon et al. (1980)	Tsai and Hsu(1984)
3.16	5	3.16	601	3.16	3.15
3.01	8	3.01	-118 504	3.00	3.02
2.97	9	2.97	-433	2.92	2.98
2.85	11	2.85	041	2.86	
2.81	5	2.81	-418	2.79	2.82
2.78	6	2.78	-711 036		
2.72	12	2.72	-714	2.73	
2.68	12	2.68	-328 531		2.69
2.65	19	2.65	604 -518 -341	2.65	
2.57	7	2.57	-419 -721 243	2.58	2.57
					2.50
2.39	8	2.39	-635	2.39	2.38
2.30	11	2.30	-718 -821 -731	2.30	2.32
2.20	11	2.20	-913 -912 -347	2.20	2.23
					2.18
2.12	12	2.12	617 445	2.12	
2.10	8	2.10	-831		2.10
2.03	6	2.03	-454	2.04	2.06
1.919	16	1.919	057	1.92	1.96
1.906	9	1.906	-10-23		

¹ Corrected d-values shift 2θ , using Al as internal standard.

² Calculation based on: $a = 20.2 \text{ \AA}$; $b = 11.5 \text{ \AA}$; $c = 25.0 \text{ \AA}$; $\beta = 103^\circ$; space group Pa or P2/a (Johansson, 1963).

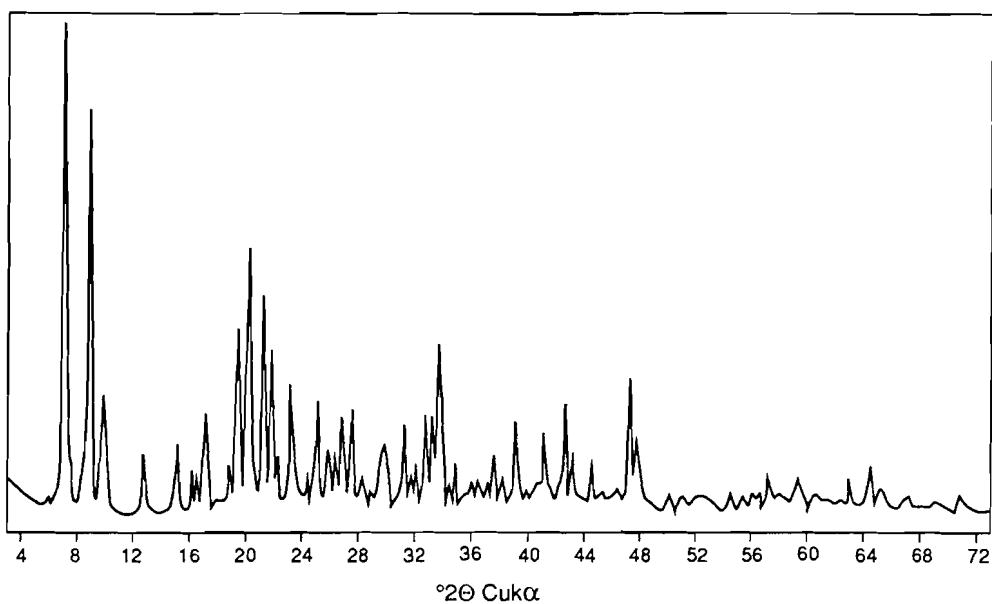


Figure 15.2 X-ray powder diffraction pattern of the basic aluminum sulfate crystals.

The ^{27}Al MAS-NMR spectrum of the unwashed precipitate from the bottom reveals one large 3650 Hz (at half height) broad Al^{VI} resonance at 3.4 ppm (Fig. 15.1b). The crystals grown at the wall exhibit a large 3000 Hz broad Al^{VI} resonance at 5.4 ppm and a small 500 Hz sharp Al^{IV} resonance at 62.9 ppm. The resonances have a surface ratio $\text{Al}^{\text{IV}}:\text{Al}^{\text{VI}}$ of approximately 1:14 (accuracy 10-15%) (Fig. 15.1c). Washing of the wall crystals barely affects the ^{27}Al spectrum. The two signals at 63.0 ppm (700 Hz) and 5.7 ppm (2500 Hz) indicate a comparable surface ratio $\text{Al}^{\text{IV}}:\text{Al}^{\text{VI}}$ of approximately 1:13 (Fig. 15.1d).

The IR spectra of the unwashed precipitates from bottom and wall are comparable (Fig. 15.3a,b) and exhibit typical absorption bands of OH at 3440, 1085 and 980 cm^{-1} , H_2O at 3247 and 1640 cm^{-1} , SO_4 at 1135, 980, 715, 610 and 566 cm^{-1} and NO_3 at 2425, 1787, 1085, 836, and 715 cm^{-1} (Table 15.2). Washing of the wall crystals results in the disappearance of the minor NO_3 absorption bands (Fig. 15.3c).

Table 15.2 IR absorption maxima (cm⁻¹) of the unwashed precipitate from the bottom and the washed crystals from the wall.

bottom	wall	Teagarden et al. (1981)	Nyquist and Kagel (1971) Gadsden (1975)
3440 vs	3440 vs	3400 Al-OH stretch	Al-O-H stretch
3247 sh	3247		H-O-H stretch
2425 m			NO ₃ v ₁ + v ₃ combination
1787 w			NO ₃ v ₁ + v ₄ combination
1640 s	1640 s		H-O-H bending
1405 sh			NO ₃ asym. stretch v ₃
1385 vs			"
1360 sh			"
1135 s	1135 vs		SO ₄ stretch v ₃
1085 sh	1085 sh	1080 Al-OH bend	NO ₃ sym. stretch v ₁
980 m	980 s	970 Al-OH def. bend	SO ₄ v ₁
836 m			NO ₃ v ₂
		780 AlO ₄ asym. stretch	
715 vw sh	715 sh		SO ₄ + NO ₃ v ₄
	636 w	640 AlO ₄ sym. stretch	
610 s	610 s		SO ₄ v ₄
566 sh	566 sh		SO ₄ v ₂
	450 sh		SO ₄ v ₂

v = very, s = strong, m = medium, w = weak, sh = shoulder
 sym. = symmetric, asym. = asymmetric.

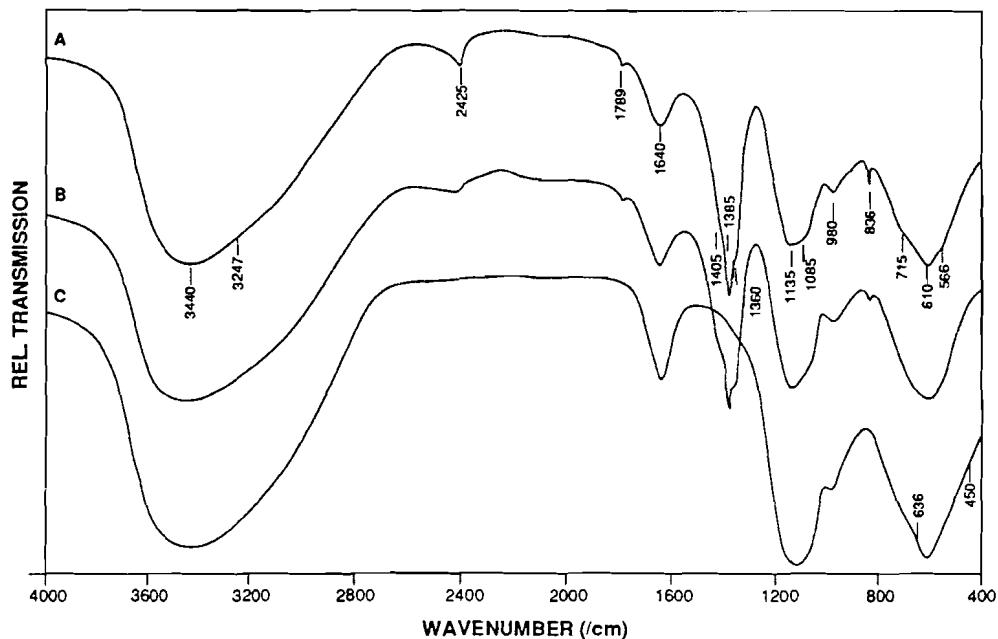


Figure 15.3 Infra-red spectra of a) the unwashed crystals; b) the precipitate on the bottom and c) the washed crystals.

15.3.3 Thermal stability

Up to 80°C the HT X-ray diffraction pattern remains unchanged. Between 80° and 270°C a general decrease in d_{hkl} values is displayed, while the seven diffraction maxima between 5.5 and 4.2 Å merge into one faint band between 5.0 and 4.0 Å. Above 270°C all maxima disappear and the basic aluminum sulfate becomes X-ray amorphous.

TGA of the crystals exhibits four different steps of weight loss (Fig. 15.4a). Between 25°C and 80°C 10.5 wt% physically adsorbed water is lost. 28 wt% is lost in the range 80° to 360°C. A third weight loss of 6.5 wt% is recorded from 360°C to 880°C. Finally, 12.5 wt% is lost between 880°C and 950°C. The

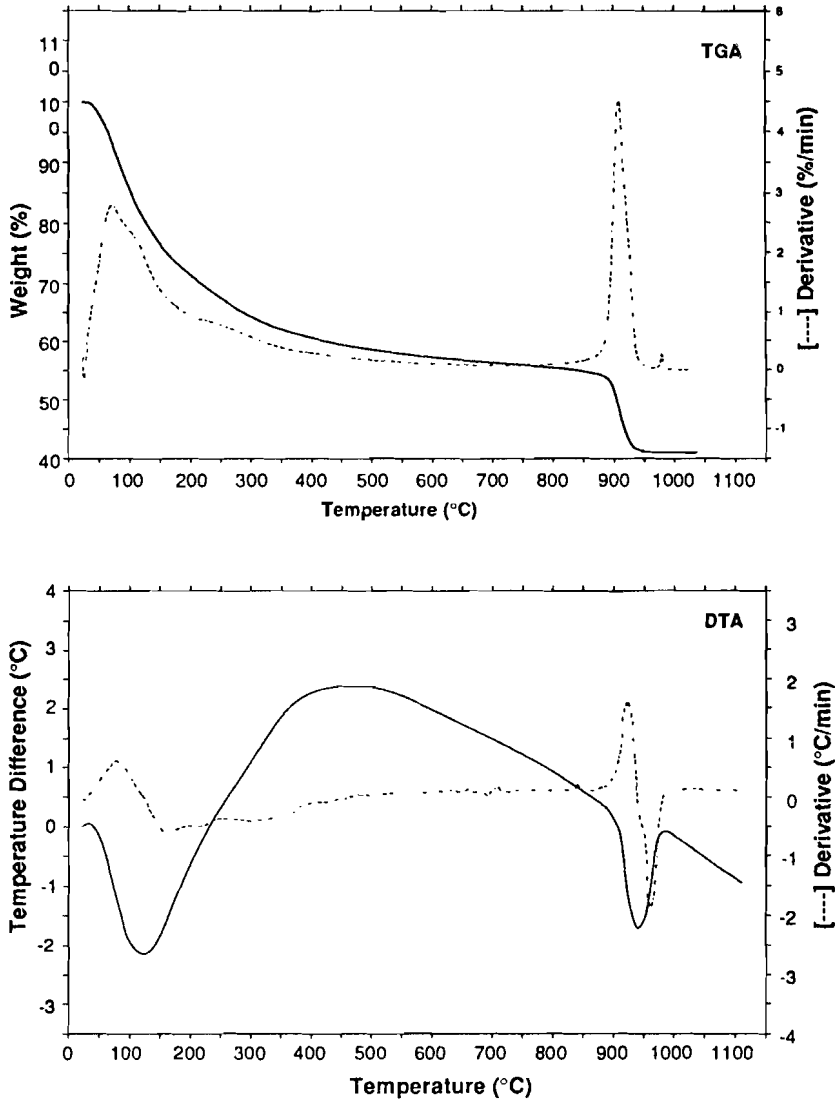


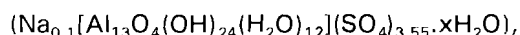
Figure 15.4 a) Thermogravimetric analysis and b) Differential thermal analysis of the basic aluminum sulfate crystals after washing.

corresponding DTA profile (Fig. 15.4b) shows major endothermic peak maxima at 120° and 930°C.

15.4 DISCUSSION

The ^{27}Al MAS-NMR spectra have proven the presence of tetrahedral and octahedral positions in the tridecamer, which is a structural unit in the crystals at the wall. The Al^{IV} to Al^{VI} ratio of about 1:13 is very close to the theoretical ratio of 1:12 of the tridecamer. Previous investigations (Müller et al., 1981; Lampe et al., 1982) reported only the presence of tetrahedral resonances for the tridecameric sulfate and chloride. The absence of the octahedral resonances in these investigations was attributed to broadening due to the second order quadrupolar effects of the (1/2, -1/2) transition at lower magnetic field strength (Kunwar et al., 1984), and strong distortion of the Al octahedra (Lampe et al., 1982) resulting in large quadrupole coupling constants (Kunwar et al., 1984). Only zunyite, $[\text{Al}_{13}(\text{OH},\text{F})_{16}\text{F}_2]\text{Si}_5\text{O}_{20}\text{Cl}$ gave a detectable octahedral signal (Table 15.3). Kunwar et al. (1984) measured both octahedral and tetrahedral resonances at high magnetic field strength, but the Al^{IV} to Al^{VI} ratio was not reported. Bottero et al. (1987) calculated an Al^{IV} to Al^{VI} ratio of 1:6.7, without correction for the overlap of both resonances and their spinning sidebands due to large variations in the quadrupolar coupling constants. After correction for this overlap an $\text{Al}^{\text{IV}}:\text{Al}^{\text{VI}}$ ratio of 1:16.4 was calculated (Bottero et al., 1987).

The X-ray powder diffractograms reveal a monoclinic unit cell, which is in agreement with the chemical analysis of the washed, almost sodium-free crystals. The structural formula:



based on the ICP data points to the presence of $[\text{Al}_{13}\text{O}_4(\text{OH})_{24}(\text{H}_2\text{O})_{12}]^{7+}$ units rather than those of $[\text{Al}_{13}\text{O}_4(\text{OH})_{25}(\text{H}_2\text{O})_{11}]^{6+}$ in the basic aluminum sulfate crystal structure, as was suggested by Schönherr et al. (1981), Müller et al. (1981), and

Table 15.3 ^{27}Al chemical shifts, δ (ppm), Full Width at Half Height (FWHH, Hz) for Al^{IV} and Al^{VI} .

		Al^{VI}		Al^{IV}		$\frac{\text{Al}^{\text{IV}}}{\text{Al}^{\text{VI}}}$
		δ	FWHH	δ	FWHH	
$\text{Na}_{0.1}\text{Al}_{13}(\text{SO}_4)_{3.55}$	(1)	5.4	3000	62.9	500	1:14
$\text{Na}_{0.1}\text{Al}_{13}(\text{SO}_4)_{3.55}$	(2)	5.7	2500	63.0	700	1:13
$\text{Al}_{13}(\text{SO}_4)_3$	(4)			59		
$\text{Al}_{13}(\text{SO}_4)_4$	(5)	8 ± 5		62.8 ± 0.3		
$\text{Al}_{13}(\text{SO}_4)_4$	(6)	3.6	3875	63.3	970	1:15
$\text{Al}_{13}(\text{SeO}_4)_4$	(5)	8 ± 5		62.9 ± 0.3		
$\text{Al}_{13}\text{Cl}_6$	(3)			62.5		
$\text{Al}_{13}\text{Cl}_6$	(4)			62		
Zunyite*	(4)	0		69		
Zunyite*	(5)	8 ± 1		72.0 ± 1.0		

(1) this study unwashed

(2) this study washed

(3) Müller et al. (1981)

(4) Lampe et al. (1982)

(5) Kunwar et al. (1984)

(6) Bottero et al. (1987)

* formula $[\text{Al}_{13}(\text{OH},\text{F})_{16}\text{F}_2]\text{Si}_5\text{O}_{20}\text{Cl}$

Lampe et al. (1982). The calculated unit-cell parameters are almost identical to those for the sodium free basic aluminum sulfate with space group P2/a or Pa (Johansson, 1963). The results of the ^{27}Al MAS-NMR and of the IR spectra, which exhibit vibrations of Al-OH, Al-O₄ and H₂O comparable with those of basic aluminum chloride (Teagarden et al., 1981) and of the SO₄ groups, support the structure determined by Johansson (1960, 1963).

The 10.5 wt% loss of physically adsorbed water during heating from room temperature up to 80°C is equivalent to $x = 9 \text{ H}_2\text{O}$ in the formula:

$\text{Na}_{0.1}[\text{Al}_{13}\text{O}_4(\text{OH})_{24}(\text{H}_2\text{O})_{12}](\text{SO}_4)_{3.55} \cdot x\text{H}_2\text{O}$, which agrees well with the 10 to 14 H_2O reported by Johansson (1960). This observation is comparable with that of Müller et al. (1981) for basic aluminum chloride, which loses adsorbed water during a mild thermal treatment to 104°C. The HT-XRD results prove that this dehydration does not change the lattice of the basic aluminum sulfate. The loss of 28.5 wt% in the temperature range from 80° to 360°C is due to the disappearance of 12 moles of H_2O from the tridecameric unit and another 12 moles of H_2O from the neighbouring 24 hydroxyl groups. Theoretically, based on the presence of the $[\text{Al}_{13}\text{O}_4(\text{OH})_{24}(\text{H}_2\text{O})_{12}]^{7+}$ unit, these losses should represent two times 14 wt%, which agrees well with the determined loss of 28.5 wt%. The HT-XRD results exhibit a decrease in d_{hkl} values in the temperature range from 80° to 270°C, due to the destruction of the basic aluminum sulfate structure, which ultimately results in X-ray amorphous material with a composition of $\text{Na}_{0.1}\text{Al}_{13}\text{O}_{16}(\text{SO}_4)_{3.55}$. The remaining weight loss must be caused by the disappearance of 3.55 moles of SO_3 . This will produce a theoretical loss of 18.5 wt%, which is slightly lower than the observed loss of 19 wt%, leaving mainly aluminum oxide with a small amount of sodium oxide as final products. The observed thermal decomposition of the basic aluminum sulfate indicates that during calcination all water and hydroxyl groups are removed from the tridecameric polymer structure. This implies that at calcination temperatures higher than approximately 360°C the Al-pillars in pillared clays convert into aluminum oxide.

ACKNOWLEDGMENT

The authors thank G. Nachtegaal (Nijmegen) for the help with the MAS-NMR at the NWO-SON HF-NMR Facility, Department of Physical Chemistry, University of Nijmegen, respectively. H. M. V. C. Govers is acknowledged for the help with the XRD patterns, T. Zalm for the assistance with the TGA and DTA, C. Strom for the unit-cell refinements and P. Anten for the ICP analyses. We thank J. van Beek, P. Dirken and M. K. Titulaer for critically reviewing the manuscript.

REFERENCES

- Akitt J. W. and Farthing A. (1978) New ^{27}Al NMR Studies of the Hydrolysis of the Aluminum(III) Cation: *J. Magn. Reson.* **32**, 345-352.
- Akitt J. W., Greenwood N. N., Kandelwahl B. L. and Lester G. D. (1972) ^{27}Al Nuclear Magnetic Resonance Studies of the Hydrolysis and Polymerisation of the Hexa-aquo- aluminum(III) Cation: *J. Chem Soc. Dalton Trans.* **1972**, 604-610.
- Bersillon J. L., Hsu P. H. and Fiessinger F. (1980) Characterization of Hydroxy-Aluminum Solutions: *Soil Sci. Soc. Amer. J.* **44**, 630-634.
- Bottero J. Y., Axelos M., Tchoubar D., Cases J. M., Fripiat J. J. and Fiessinger F. (1987) Mechanism of Formation of Aluminum Trihydroxide from Keggin Al_{13} Polymers: *J. Coll. Interface Sci.* **117**, 47-57.
- Gadsden J. A. (1975) *Infrared Spectra of Minerals and Related Inorganic Compounds*, Butterworths, London, 277 pp.
- Johansson G. (1960) On the Crystal Structure of Some Basic Aluminium Salts: *Acta Chem. Scand.* **14**, 771-773.
- Johansson G. (1962) The Crystal Structures of $[\text{Al}_2(\text{OH})_2(\text{H}_2\text{O})_8](\text{SO}_4)_2 \cdot 2\text{H}_2\text{O}$ and $[\text{Al}_2(\text{OH})_2(\text{H}_2\text{O})_8](\text{SeO}_4)_2 \cdot 2\text{H}_2\text{O}$: *Acta Chem. Scand.* **16**, 403-420.

- Johansson G. (1963) On the Crystal Structure of the Basic Aluminum Sulfate $13\text{Al}_2\text{O}_3 \cdot 6\text{SO}_3 \cdot x\text{H}_2\text{O}$: *Ark. Kemi* **20**, 321-342.
- Johansson G., Lundgren G., Sillén L. G. and Söderquist R. (1960) On the Crystal Structure of a Basic Aluminium Sulfate and Corresponding Selenate: *Acta Chem. Scand.* **14**, 769-771.
- Kloprogge J. T., Jansen J. B. H. and Geus J. W. (1990) Characterization of Synthetic Na-Beidellite: *Clays & Clay Minerals* **38**, 409-414.
- Kloprogge J. T., Seykens D., Geus J. W. and Jansen J. B. H. (1992a) Temperature Influence on the Al₁₃ Complex in Partial Neutralized Aluminum Solutions: An ²⁷Al Nuclear Magnetic Resonance Study: *J. Non-Cryst. Solids* **142**, 87-93.
- Kloprogge J. T., Seykens D., Jansen J. B. H. and Geus J. W. (1992b) An ²⁷Al Nuclear Magnetic Resonance Study on the Optimization of the Development of the Al₁₃ Polymer: *J. Non-Cryst. Solids* **142**, 94-102.
- Kunwar A. C., Thompson A. R., Gutowsky H. S. and Oldfield E. (1984) Solid State Aluminum-27 NMR Studies of Tridecameric Al-Oxo-Hydroxy Clusters in Basic Aluminum Selenate, Sulfate, and the Mineral Zunyite: *J. Magn. Reson.* **60**, 467-472.
- Lampe F., Müller D., Gessner W., Grimmer A.-R. und Scheler G. (1982) Vergleichende ²⁷Al-NMR-Untersuchungen am Mineral Zunyite und basischen Aluminium-Salzen mit tridekameren Al-oxo-hydroxo-aquo-Kationen: *Z. Anorg. Allg. Chem.* **489**, 16-22.
- Müller D., Gessner W., Schönherr S. und Görz H. (1981) NMR-Untersuchungen am tridekameren Al-oxo-hydroxo-Kation: *Z. Anorg. Allg. Chem.* **483**, 153-160.
- Nyquist R. A. and Kagel R. O. (1971) *Infrared Spectra of Inorganic Compounds (3800 - 45 cm⁻¹)*, Academic Press, New York, 495 pp.
- Plee D., Gatineau L. and Fripiat J. J. (1987) Pillaring Processes of Smectites with and without Tetrahedral Substitution: *Clays & Clay Minerals* **35**, 81-88.
- Schönherr S., Görz H., Müller D. und Gessner W. (1981) Darstellung und Charakterisierung eines wasserlöslichen Al₁₃O₄₀-Chlorides: *Z. Anorg. Allg. Chem.* **476**, 188-194.

- Schutz A., Stone W. E. E., Poncelet G. and Fripiat J. J. (1987) Preparation and Characterization of Bidimensional Zeolitic Structures obtained from Synthetic Beidellite and Hydroxy-Aluminum Solutions: *Clays & Clay Minerals* **35**, 251-261.
- Strom C. (1976) *Unitcellc, an Interactive APL Program for Computing Cell Constants*. Geol. Mineral. Institute, State University of Leiden, The Netherlands, Internal Report.
- Teagarden D. L., Kozlowski J. F. and White J. L. (1981) Aluminum Chlorohydrate I: Structure Studies: *J. Pharm. Sci.* **70**, 758-761.
- Tsai P. P. and Hsu P. H. (1984) Studies of Aged OH-Al Solutions using Kinetics of Al-Ferron Reactions and Sulfate Precipitation: *Soil Sci. Soc. Amer. J.* **48**, 59-65.
- Tsai P. P. and Hsu P. H. (1985) Aging of Partially Neutralized Aluminum Solutions of Sodium Hydroxide/Aluminum Molar Ratio = 2.2: *Soil Sci. Soc. Amer. J.* **49**, 1060-1065.

CHAPTER XVI

STUDY OF BASIC ALUMINUM SULFATE BY ONE- AND TWO-DIMENSIONAL ^{27}Al MAS NMR

ABSTRACT

The quadrupole coupling constants (QCC) and asymmetry parameters (η) of the Al^{IV} and Al^{VI} sites in basic aluminum sulfate have been determined by using the field dependent second order quadrupole shift, 2-dimensional nutation NMR and computer simulation. The quadrupole data from these three methods are consistent. The Al^{IV} site has a QCC of 1.6 MHz and an η of 0-0.2, while the 12 Al^{VI} sites have an average QCC of 5-6 MHz and an η of 0-0.2.

16.1 INTRODUCTION

The tridecameric Al cluster $[\text{AlO}_4(\text{Al}_{12}(\text{OH})_{24}(\text{H}_2\text{O})_{12})]^{7+}$ consists of a central AlO_4 tetrahedron surrounded by twelve sixfold coordinated Al atoms. The tridecameric cluster forms the building unit of several basic aluminum salts (chloride, selenate, sulfate) (Johansson, 1960; 1963; Johansson et al., 1960; Lampe et al, 1981) and of the mineral Zunyite $[\text{Al}_{13}(\text{OH},\text{F})_{16}\text{F}_2]\text{Si}_5\text{O}_{20}\text{Cl}$ (Pauling, 1933). The basic salts result from partial hydrolysis of $\text{Al}(\text{H}_2\text{O})_6^{3+}$ followed by precipitation (Kloprogge et al., 1992b,c). Although the basic aluminum sulfate has been extensively investigated by X-ray diffraction (Johansson, 1960; 1963; Kloprogge et al., 1992c) and ^{27}Al magic-angle spinning (MAS) nuclear magnetic resonance (NMR) (Schönherr et al., 1981; Lampe et al., 1982; Kunwar et al., 1984; Bottero et al., 1987; Kloprogge et al., 1992c); some information on quadrupole coupling constants is only available for the sodium-rich cubic species (Kunwar et al., 1984).

Because of its large size, the Al_{13} complex is important in the field of catalysis as an interlayer pillaring species in clays. Calcination of Al_{13} pillared clays results in conversion of the Al_{13} into a $\gamma\text{-Al}_2\text{O}_3$ -like oxide pillar.

The aim of this study is to determine the quadrupole data of a sodium poor monoclinic Al₁₃ sulfate with a variety of experimental techniques. Knowledge of these quadrupole data may facilitate the interpretation of ²⁷Al NMR spectra of pillared clays and especially provide the conversion of Al₁₃ into an oxide pillar.

16.2 THEORETICAL BACKGROUND

Usually, quadrupole coupling constants and asymmetry parameters are determined by Nuclear Quadrupole Resonance (NQR). The determination is based on the splitting of nuclear spin levels, mainly by the quadrupole interaction, in the presence of a small or even in the absence of an external magnetic field. This method is rather insensitive to small quadrupole coupling constants (0 - 10 MHz) and a wide range of frequencies has to be investigated for possible resonances (Kentgens, 1987; Kentgens et al., 1987). Samoson and Lippmaa (1983, 1988) introduced a two-dimensional nutation experiment, which allows one to separate the quadrupole from the chemical shift interaction. The 2D nutation experiment, extensively described by Kentgens (1987) and Kentgens et al. (1987), is divided into two time domains. During the evolution period (t_1) the system is irradiated with a radio frequency (rf) at a certain magnetic field (H_1), in the detection period (t_2) the free induction decay is collected. During t_1 the spins precess around the rf field (= nutation) with specific nutation frequencies, which depend on the magnitude of the quadrupole interaction (H_q). The experiment can be described by a rotating frame Hamiltonian, consisting of a quadrupole interaction term and an rf term:

$$H = \omega_q(3I_z^2 - I(I + 1)) - \omega_{rf}I_x = H_q + H_{rf}$$

where $\omega_q = [e^2qQ/(8I(2I - 1))](3\cos^2\Theta - 1 + \eta\sin^2\Theta\cos 2\phi)$ and

$\omega_{rf} = \gamma B_1$ (Kentgens, 1987; Tjink et al., 1987; Janssen et al., 1989). Two-dimensional Fourier transformation of the acquired signals results in a characteristic pattern. Projection on the F_2 axis will provide the normal (1/2, -

1/2) powder line shape due to the combined effect of the chemical shift anisotropy and the quadrupole interaction, while projection on the F_1 axis provides the nutation spectrum, which is independent of the chemical shift. The nutation spectrum depends only on the quadrupole parameters e^2qQ/h and η , the spin quantum number I , and the rf field strength B_1 . The nutation spectra can easily be simulated and used in a qualitative way to determine quadrupole interactions from experimental spectra.

A second procedure is based on the difference in the second-order quadrupole induced chemical shift at different magnetic field strengths. The shift of the center of gravity of a peak, δ_{CG} (ppm) is a function of the quadrupole parameters e^2qQ/h and η , and the Larmor frequency ν_0 , which depends on the field strength:

$$\delta_{\text{CG}}(\text{ppm}) = -6 \times 10^3 (e^2qQ/h\nu_0)^2 (1 + 1/3\eta^2) \quad [1]$$

(Samoson, 1985; Kentgens et al., 1991). With ν_0 known and assuming a value for η , the quadrupole coupling constant e^2qQ/h can be determined from the experimental spectra. For asymmetric line shapes the center of gravity does not necessarily coincide with the peak maximum. It is important to assure that the peaks are symmetric if peak positions are used. Otherwise centers of gravity have to be calculated.

16.3 EXPERIMENTAL

The basic aluminum sulfate was synthesized by partial hydrolysis of a 0.5 M $\text{Al}(\text{NO}_3)_3$ solution with a 0.5 M NaOH solution until an OH/Al molar ratio of 2.2 was reached, followed by addition of Na_2SO_4 , as described previously by Kloprogge et al. (1991a).

The one-dimensional ^{27}Al NMR spectra were obtained using Bruker CPX-300, AM-500 and AM-600 spectrometers operating at 7.1, 11.7, and 14.1 T respectively. Straightforward one-pulse experiments were performed, using

short (1-2 μ s) pulses, 0.5 s recycle delays, and 100 kHz spectral widths. Per measurement 200-1300 Free Induction Decays (FID) were collected. Magic angle spinning speeds of 12 kHz were used. The two-dimensional ^{27}Al nutation spectrum is collected on a Bruker AM-500 spectrometer at 11.7 T, using 64 t_1 increments of 2 μ s. A recycle delay of 0.5 s was chosen, sufficiently long to ensure that the system can return to equilibrium between the pulses. Establishing equilibrium is important, because too short a recycle delay can cause harmonics of the true frequency in the F_2 spectrum (Kentgens et al., 1987). All ^{27}Al chemical shifts are referenced relative to an aqueous 1M AlCl_3 solution. Simulations of the ^{27}Al spectra were carried out with the ASPECT 3000 computer program POWDER (Müller and Bentrup, 1989).

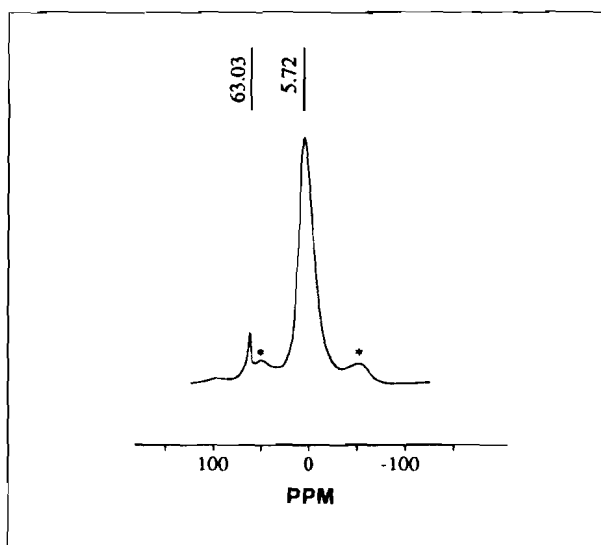


Figure 16.1 ^{27}Al MAS NMR spectrum of basic aluminum sulfate measured at 11.7 T, spinning speed 12 kHz (After Klotz et al., 1992a).

16.4 RESULTS

16.4.1 Second order quadrupole induced shift.

The one-dimensional ^{27}Al spectrum displays a resonance at 63.0 ppm at 11.7 T with a full width at half height (FWHH) of 500 Hz (Fig. 16.1). Resonances in this region are assigned to tetrahedrally coordinated aluminum (Müller et al., 1981; Akitt, 1989). Based on earlier work (Kloprogge et al., 1992a), the 63.0 ppm resonance corresponds to the Al^{IV} of the tridecamer, in agreement with the chemical shift of the tridecamer Al^{IV} in solution (Kloprogge et al., 1992b,c). The signal from the fourfold coordinated Al shifts to 60.1 ppm at 7.1 T, and 63.3 ppm at 14.1 T. The shifts correspond to a Quadrupole Coupling Constant (QCC) of 1.7 ± 0.5 MHz and an isotropic chemical shift (δ_{iso}) of 64 ± 0.5 ppm. The second resonance is observed at 5.7 ppm at 11.7 T with a FWHH of 3650 Hz, and is assigned to the twelve Al^{VI} of the tridecamer. This resonance has a very broad, asymmetric shape, with a steep flank at the low-field side and a more gradually sloping flank at the high-field side. The asymmetry is usually an indication of a spread in electric field gradient (Kohn et al., 1991). This resonance shifts to 2.3 ppm at 7.1 T and 6.1 ppm at 14.1 T. Roughly calculating the QCC from these peak maxima is clearly erroneous, as it ignores the low-field shoulder. Equation [1] is only valid for the center of gravity of the peak. The position of the center of gravity can easily be extracted from the spectra as it is the weighed average of the chemical shift and the intensity. Use of the correct parameters in equation [1] results in a QCC of 5.2 MHz for the sixfold coordinated aluminum and a δ_{iso} of 11 ppm. For purposes of comparison: the use of peak maxima results in a QCC of 2.3 ± 0.5 MHz, and a δ_{iso} of 7.5 ± 0.5 ppm. From the quadrupole data, the contribution of the second order quadrupole broadening to the linewidth ($\delta\nu_{\frac{1}{2}}$) can be calculated. As indicated in Table 16.1 the linewidth $\delta\nu_{\frac{1}{2}}$ varies between 80 and 330 Hz for Al^{IV} , and 1500-9100 Hz for Al^{VI} , depending on the type of procedure used. Residual contributions from un-averaged dipolar interactions and chemical shift dispersion

add up to 150-400 Hz for the fourfold coordinated site and 0-900 Hz for the sixfold coordinated site.

16.4.2 2D Nutation NMR

Projection of the 2D nutation data on the F_1 -axis results in two 1-dimensional nutation spectra of the Al^{IV} and Al^{VI} present in the basic aluminum sulfate (Fig. 16.2). The Al^{IV} nutation spectrum gives a reasonably well resolved structure, which is best simulated by using an asymmetry parameter $\eta \approx 0.2$ and a quadrupole coupling constant e^2qQ/h between 1.2 and 2.4 MHz. The Al^{VI} nutation spectrum exhibits a very poorly resolved pattern, which cannot be simulated by one set of quadrupole parameters. A rough estimate of the quadrupole coupling constant e^2qQ/h for the main signal is between 5 and 12 MHz, based on the presence of a strong peak at $F_1 = 3\omega_{rf}$. This results in a calculated $\delta\nu_{1/2}$ of 1500-9100 Hz.

Table 16.1 ^{27}Al NMR data.

Method	QCC (MHz)	δ_{iso} (ppm)	$\delta\nu_{1/2}$ (Hz)	FWHH (Hz)
Al^{IV}				
2D nutation	1.2-2.4	-	80-330	480
Quadrupole shift	1.7	64	170	
Simulation	1.6	64	150	
Al^{VI}				
2D nutation	5-12	-	1500-8400	2400
Quadrupole shift	5.2	11	1600	
Simulation	6	17	2100	
Structure correlation	9-12.5	-	4700-9100	

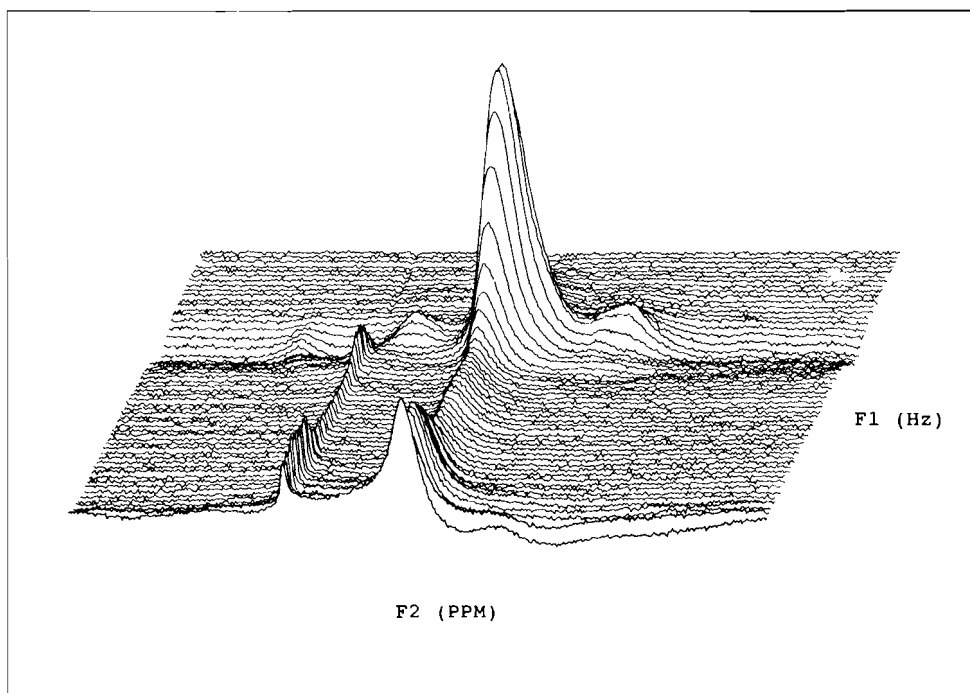


Figure 16.2 Two-dimensional ^{27}Al NMR spectrum of basic aluminum sulfate measured at 11.7 T.

16.4.3 Computer simulation

The Al^{IV}-site in the F₂ spectrum is best simulated by a QCC of 1.6 ± 0.2 MHz and an asymmetry parameter η between 0 and 0.2, the Al^{VI}-site by a QCC of 6 ± 1 MHz and an η between 0 and 0.2.

16.5 DISCUSSION

Quadrupole data from simulation, nutation NMR, and second order quadrupole shift for the tetrahedral site are in good agreement. The QCC of 1.6 MHz is larger than the value of 0.8 MHz reported by Kunwar et al. (1984), who only used the second order quadrupole shift. Our value, obtained by three independent methods, is supposed to be more accurate. Kunwar et al. (1984) furthermore used a sodium rich basic Al salt which has a cubic structure. This will have a little effect on the QCC of Al^{IV} but could probably influence the Al^{VI} QCC. In case of the 12 octahedral Al-sites, the quadrupole data derived from the various methods are also consistent. The results point to an average quadrupole coupling constant of 6 MHz. Kunwar et al. (1984) simulated static NMR spectra of the ²⁷Al site in basic aluminum sulfate and obtained a QCC of 10.2 ± 0.5 MHz and an η of 0.2 ± 0.1. Their sulfate was a sodium-rich species, which, however, does not affect the Al NMR data, as has recently been shown for alkali fluoroaluminates (Dirken et al., 1992).

For the twelve octahedral Al sites in basic aluminum sulfate the octahedral distortions have been calculated. The octahedral distortions are known to be related to the magnitude of the QCC. The distortion parameter used is the longitudinal strain $|\alpha|$, defined by Ghose and Tsang (1973) as

$$|\alpha| = \sum_{i=1}^6 |\ln(l_i/l_0)|$$

where l_i are the individual Al-O bond lengths, and l_0 is the ideal bond length for a perfect octahedron having the same volume as the actual octahedron. Ghose and Tsang (1973) suggested a correlation between $|\alpha|$ and the QCC based on a wide variety of substances. Starting from the crystal structure of basic

Table 16.2 Quadrupole data for octahedral aluminum using the $|\alpha|$ -factor (Ghose and Tsang (1973)).

	$ \alpha $	$ \Psi $	QCC (MHz)
Al1	0.22	1.3	12.5
Al2	0.16	1.0	9.1
Al3	0.18	1.1	10.1
Al4	0.16	1.2	9.1
Al5	0.20	1.1	11.2
Al6	0.18	1.0	10.1

aluminum sulfate as determined by Johanson (1960), the $|\alpha|$ factors for the 12 octahedral sites are calculated (Table 16.2). The last column of Table 16.2 shows the QCC values calculated from the correlation obtained by Ghose and Tsang (1973). Evidently, the calculated QCC values are in good agreement with the data of Kunwar et al (1984), but not with our experimental data. A strong argument against the average 10 MHz QCC value is the fact that the corresponding peak width of 10 kHz exceeds the experimental width by 6.5 kHz, which is beyond any experimental error. Ghose and Tsang (1973) mention three exceptions to their QCC-deformation correlation, viz. corundum, spodumene and chrysoberyl. Our data and the fact that the tridecameric Al

polymer converts into a corundum-like structure upon calcination indicate that basic aluminum-13 sulfate has to be added to this list.

16.6 CONCLUSIONS

- 1) 1-D and 2-D NMR spectroscopy has been used to determine QCC data; the results obtained by three different procedures are consistent.
- 2) ^{27}Al QCC data of Al13 sulfate are :
Fourfold coordinated Al: QCC = 1.6 MHz; η = 0-0.2
Sixfold coordinated Al: QCC = 5-6 MHz; η = 0-0.2.
- 3) Much care must be taken in using QCC-deformation correlations.

ACKNOWLEDGMENTS

The authors wish to thank G. Nachtegaal for the technical assistance at the HF-NMR facility at Nijmegen. R.J.M.J. Vogels, and J. van Beek are thanked for critically reviewing this manuscript.

REFERENCES

- Bottero, J. Y., Axelos, M., Tchoubar, D., Cases, J. M., Fripiat, J. J. and Fiessinger, F. (1987) Mechanism of formation of aluminum trihydroxide from Keggin Al_{13} polymers: *J. Coll. Interf. Sci.* **117**, 47-57
- Dirken, P.J., Jansen, J.B.H., and Schuiling, R.D. (1992) Influence of octahedral polymerization on ^{23}Na and ^{27}Al MAS NMR in alkalifluoroaluminates: *Amer. Mineral.* **77**, 718-724.
- Ghose, S. and Tsang, T. (1973) Structural dependence of quadrupole coupling constant e^2qQ/h for ^{27}Al and crystal field parameter D for Fe^{3+} in aluminosilicates: *Amer. Mineral.* **58**, 748-755.
- Janssen, R., Tijink, G. A. H. and Veeman, W. S. (1989) High-temperature NMR study of zeolite Na-A: detection of a phase transition: *J. Phys. Chem.* **93**, 899-904.
- Johansson, G. (1960) On the crystal structure of some basic aluminum salts: *Acta Chem. Scand.* **14**, 771-773.
- Johansson, G. (1963) On the crystal structure of the basic aluminum sulfate $13\text{Al}_2\text{O}_3 \cdot 6\text{SO}_3 \cdot x\text{H}_2\text{O}$: *Ark. Kemi* **20**, 305-319.
- Johansson, G., Lundgren, G., Sillén, L. G. and Söderquist, R. (1960) On the crystal structure of a basic aluminium sulfate and the corresponding selenate: *Acta Chem. Scand.* **14**, 769-771.
- Kentgens, A. P. M. (1987) Two-dimensional solid state NMR: *Ph. D. Thesis Katholieke Universiteit Nijmegen, The Netherlands.*
- Kentgens, A. P. M., Lemmens, J. J. M., Geurts, F. M. M. and Veeman, W. S. (1987) Two-dimensional solid-state nutation NMR of half-integer quadrupolar nuclei: *J. Magn. Reson.* **71**, 62-74.
- Kentgens, A. P. M., Bayensse, C. R., van Hooff, J. H. C., de Haan, J. W. and van de Ven, L. J. M. (1991) A ^{69}Ga and ^{71}Ga MAS NMR study of the gallium analogue zeolite ZSM-5: *Chem. Phys. Letters* **176**, 399-403.

- Kloprogge, J. T., Geus, J. W., Jansen, J. B. H. and Seykens, D. (1992a) Thermal stability of basic aluminum sulfate: *Thermochim. Acta*, in press.
- Kloprogge, J. T., Seykens, D., Geus, J. W. and Jansen, J. B. H. (1992b) Temperature influence on the Al₁₃ complex in partially neutralized aluminum solutions: an ²⁷Al nuclear magnetic resonance study: *J. Non-Cryst. Solids* **142**, 87-93.
- Kloprogge, J. T., Seykens, D., Jansen, J. B. H. and Geus, J. W. (1992c) An ²⁷Al nuclear magnetic resonance study on the optimalization of the development of the Al₁₃ polymer: *J. Non-Cryst. Solids* **142**, 94-102.
- Kohn, S.C., Dupree, R., and Smith, M.E. (1989) A multinuclear magnetic resonance study of the structure of hydrous albite glasses: *Geochim. Cosmochim. Acta* **53**, 2925-2935.
- Kunwar, A. C., Thompson, A. R., Gutowski, H. S. and Oldfield, E. (1984) Solid state aluminum-27 NMR studies of tridecameric Al-oxo-hydroxy clusters in basic aluminum selenate, sulfate and the mineral Zunyite: *J. Magn. Reson.* **60**, 467-472.
- Lampe, F. von, Müller, D., Gessner, W., Grimmer, A.-R. und Scheler, G. (1982) Über basische Aluminumsalze und ihre Lösungen. XI. Vergleichende ²⁷Al-NMR-Untersuchungen am Mineral Zunyit und basischen Aluminium-Salzen mit tridekameren Al-oxo-hydroxo-aquo-Kationen: *Z. Anorg. Allg. Chem.* **489**, 16-22.
- Müller, D., and Bentrup, U. (1989) ²⁷Al Untersuchungen an alkalifluoroaluminaten: *Z. Anorg. Allg. Chem.* **517**, 167-176.
- Müller, D., Gessner, W., Behrens, H.-J. and Scheler, G. (1981) Determination of the aluminium coordination in aluminium-oxygen compounds by solid-state high-resolution ²⁷Al NMR: *Chem. Phys. Letters* **79**, 59-62.
- Pauling, L. (1933) The crystal structure of Zunyite Al₁₃Si₅O₂₀(OH,F)₁₈Cl: *Z. Kristallogr.* **84**, 442-452.
- Samoson, A. (1985) Satellite transition high-resolution NMR of quadrupolar nuclei in powders: *Chem. Phys. Letters* **119**, 29-32.

- Samoson, A. and Lippmaa, E. (1983) Excitation phenomena and line intensities in high-resolution NMR powder spectra of half-integer quadrupolar nuclei: *Phys. Rev. B* **28**, 65667-6570.
- Samoson, A. and Lippmaa, E. (1988) 2D NMR nutation spectroscopy in solids: *J. Magn. Reson.* **79**, 255-268.
- Schönherr, S., Görz, H., Müller, D. und Gessner, W. (1981) Darstellung und Charakterisierung eines wasserlöslichen $\text{Al}_{13}\text{O}_{40}$ -Chlorides: *Z. Anorg. Chem.* **476**, 188-194.
- Tijink, G. A. H., Janssen, R. and Veeman, W. S. (1987) Investigation of the hydration of zeolite NaA by two-dimensional ^{23}Na nutation NMR: *J. Amer. Chem. Soc.* **109**, 7301-7304.

CHAPTER XVII

THE EFFECT OF THERMAL TREATMENT ON THE PROPERTIES OF HYDROXY-Al AND HYDROXY-Ga PILLARED MONTMORILLONITE AND BEIDELLITE

Abstract

The pillaring process of montmorillonite and beidellite with Al and Ga polymers has been studied with XRD, IR, ^{27}Al , ^{71}Ga , and ^{29}Si MAS NMR, TGA, TEM, N_2 adsorption, and chemical analysis. The Al adsorption maximum of montmorillonite is close to 5.5 meq Al/g clay, whereas the maximum of Ga is higher. The basal spacings of the pillared clays vary between 16.7 and 18.8 Å. Freeze-drying of pillared products followed by calcination yielded more regular pillared structures. Pillaring montmorillonite increased the BET surface area from 35 to 350 m^2/g mainly by creation of micropores < 20 Å in diameter. The Al-pillared clays are thermally stable to approximately 700°C. Calcination of pillared montmorillonite liberates protons from the pillar, which diffuse into the clay sheet thus lowering the thermal stability. In pillared beidellite mainly silanol groups are formed by breaking Si-O-Al bonds. No reaction is observed between pillars and montmorillonite upon calcination, whereas in pillared beidellite a structural transformation links the pillar to inverted tetrahedra of the tetrahedral sheet.

17.1 INTRODUCTION

The use of clay minerals in catalytic reactions was recognized at the end of the nineteenth century (Von Liebig, 1865). Examples of catalytic reactions are simple isomerization and polymerization on palygorskite (Montaland, 1911; Gurwitsch, 1912, 1923). In the period from 1930 to 1950 acid-treated montmorillonites were major cracking catalysts in oil processing, which catalysts were later being replaced by the more thermostable precipitated silica-aluminas and, subsequently, by the more selective zeolites.

The interest for clay mineral catalysts was renewed by the development of clays expanded by organic compounds (Barrer and MacLeod, 1955), because zeolites are not suitable for the conversion of relatively large organic molecules.

However, the disadvantage of organic pillars is the low thermostability and the resulting collapse of the pillared clay structure. The use of inorganic compounds, such as, Al (Brindley and Sempels, 1977; Lahav et al., 1978, Plee et al., 1987; Schutz et al., 1987), and Zr (Yamanaka and Brindley, 1979; Bartley and Burch, 1985; Bartley, 1988) as pillaring agents, solved this problem. On calcination the polyoxocations dehydrate and dehydroxylate, and react to metal oxide pillars providing a permanent microporosity and an increased thermostability.

The polyoxocation, $[\text{AlO}_4\text{Al}_{12}(\text{OH})_{24}(\text{H}_2\text{O})_{12}]^{7+}$ (Al13), is formed by forced hydrolysis of Al^{3+} under specific conditions (Kloprogge et al., 1992a,b). The Al13 species, firstly suggested by Johansson (1962) from the structure of basic aluminum sulfate, was evidenced in solution by small-angle X-ray scattering (Rausch and Bale, 1964) and ^{27}Al NMR (see references in Akitt, 1989).

Based on ^{27}Al and ^{29}Si MAS-NMR of pillared beidellite and Mg-smectites, Plee et al. (1985a) suggested that, unlike montmorillonite, calcining pillared beidellite results in linking the Al13 species and the tetrahedral layer. Inverted tetrahedra are terminated by OH groups, which react with the OH groups of the Al13 to form an $(\text{Si,Al})^{\text{tetrahedral}}\text{-O-Al}^{\text{pillar}}$ bridge.

Based on the similar ionic radii and crystal structures of the oxides and oxohydroxides Johansson (1962) assumed the existence of a Ga13 species, $[\text{GaO}_4\text{Ga}_{12}(\text{OH})_{24}(\text{H}_2\text{O})_{12}]^{7+}$ analogous to the Al13 species. Bradley et al. (1990a,b) provided evidence for Ga13 in solution based on ^{71}Ga NMR and suggested the use of Ga13 as a pillaring agent (Bradley et al., 1990a,b). The use of Ga13 as a pillaring agent can be advantageous, since it allows one to observe independently the structural changes in both the pillar and the clay during calcination. With aluminum it is difficult to distinguish the Al present within the pillar and within the clay sheets

Most of the catalytic properties of clays are due to their acidic character, which is significantly influenced by the clay structure. Upon calcination of octahedrally substituted smectites (e.g., montmorillonite) protons can migrate into vacancies of the octahedral sheet, where they are bound to lattice oxygens.

The migrated protons are no longer available for catalytic reactions. The remaining acid sites are mainly of the Lewis type. In tetrahedrally substituted smectites (e.g., beidellite), however, the protons are attached to surface oxygens of the tetrahedral sheet. These Brönsted sites are similar to those within Y zeolite (Barrer, 1978; Plee et al., 1985b).

The aims of this study are to characterize the structural changes in (i) Al13- and (ii) Ga13-pillared montmorillonite (octahedral substitution), and (iii) Al13- and (iv) Ga13-pillared hydrothermally synthesized beidellite (tetrahedral substitution) upon calcination at increasing temperatures from 25° to 700°C. The characterization is performed by means of X-ray diffraction, ²⁷Al and ²⁹Si magic-angle spinning NMR, Infrared spectroscopy, chemical analysis, transmission electron microscopy, thermogravimetric analyses, and specific surface area determinations.

17.2 EXPERIMENTAL

17.2.1 Starting clays

The montmorillonite used in this study (SWy-1) was obtained from the Source Clay Repository of the Clay Mineral Society. This Na-montmorillonite, found in the Newcastle Formation, Crook County, Wyoming, has an approximate cation exchange capacity (CEC) of 83.4 meq/100g, which is close to the value of 85 meq/100 g reported by van Olphen and Fripiat (1979).

The fraction smaller than 2 μm was obtained by gravity sedimentation. Sodium exchange was completed by washing four times with 1 M NaCl and removing the excess electrolyte by washing with deionized water for at least five times.

Na-beidellite was synthesized according to the procedure described by Klopogge et al. (1990a,b). A gel with composition Na_{0.7}Al_{4.7}Si_{7.3}O₂₂ was hydrothermally treated for seven days at 350°C and 1 kbar in a Tuttle-type

externally heated, cold-seal pressure vessel. The Na-beidellite has a CEC of approximately 70 meq/100 g (Kloprogge et al., 1990b)

17.2.2 Pillaring agents

0.5 M $\text{Al}(\text{NO}_3)_3$ (Merck 1063) solutions were hydrolyzed by injection, using a Gilson pump (rate 0.015 ml/s), of a 0.2 M NaOH (Merck 6498) solution in a specially designed reaction vessel (Vermeulen et al., 1975), until a molar OH/Al ratio of 2.4 was reached (Kloprogge et al., 1992b). The final solutions were aged for 2 hours at 50°C to optimize the Al13 content.

0.2 M GaCl_3 solutions (supplied by P. van Gaans) were hydrolyzed either by injection, similar to the Al hydrolysis, or by dropwise addition of 0.2 M NaOH solution, until a molar OH/Ga ratio of 2.25 was reached. The solutions used for ^{71}Ga NMR were aged for 30 minutes at 50°C. As pillaring agents freshly hydrolyzed Ga solutions prepared by the injection method without aging were used.

17.2.3 Pillaring processes

Adequate volumes of the partly hydrolyzed Al and Ga solutions were rapidly added to the montmorillonite and beidellite suspensions (20 g/l) under constant stirring for several hours. Ratios of 5.5, 10, and 20 meq Al/g montmorillonite and 5.5 meq Ga/g montmorillonite were obtained. For the beidellite an excess of 30 meq Al/g was used, based on the results of Plee et al. (1987) showing that due to the localization of charge in the tetrahedral layer a higher Al13/clay ratio than 20 meq Al/g is needed to achieve maximum swelling. After the exchange was completed, the suspensions were centrifuged, and the remaining clays were washed five times with deionized water to remove excess $\text{Al}^{3+}/\text{Ga}^{3+}$, Na^+ , and $\text{NO}_3^-/\text{Cl}^-$. The washed pillared clays were air- (25°C) or freeze-dried, followed by calcination at temperatures between 100° and 700°C.

17.2.4 Characterization of the pillaring agents and pillared clays

The partly hydrolyzed Al and Ga solutions were characterized by ^{27}Al and ^{71}Ga NMR applying a Bruker WP200 spectrometer operated at 52.148 MHz (4.6 T) at the Department of Organic Chemistry of the University of Utrecht and a Bruker AM500 spectrometer operating at 152.53 MHz (11.7 T) at the SON HF-NMR Facility, University of Nijmegen.

The morphology of the montmorillonite, beidellite, and their pillared analogues were investigated with a Philips EM 420 transmission electron microscope (TEM) operated at 120 kV. X-ray powder diffraction (XRD) patterns were recorded with a Philips PW 1050/25 diffractometer using $\text{CuK}\alpha$ radiation. Heating stage XRD was carried out using a HT Guinier $\text{CuK}\alpha_1$, Enraf Nonius FR553, focussing powder camera, and applying a heating rate of $1^\circ\text{C}/\text{min}$. Infrared spectra were obtained on powdered samples in KBr tablets (sample concentration 1 wt%) using a Perkin Elmer 1700 Fourier Transform Infrared (FTIR) spectrometer. Diffuse reflectance IR (DRIFT) spectra at increasing temperatures were obtained on powdered samples (50 wt% KBr) in a special cell within an argon atmosphere. Thermogravimetical analyses (TGA) were carried out with a Dupont 1090 Thermal analyzer at heating rates of 1° and $10^\circ\text{C}/\text{min}$. Differential thermal analyses (DTA) were obtained at a heating rate of $20^\circ\text{C}/\text{min}$. High-resolution magic-angle-spinning nuclear magnetic resonance (MAS-NMR) spectra were recorded on a Bruker AM500 spectrometer (11.7 T) at the Koninklijke/Shell laboratory, Amsterdam. ^{27}Al , ^{29}Si , and ^{71}Ga were obtained at 130.321 MHz, 99.346 MHz, and 152.53 MHz, respectively. Chemical shifts are reported in ppm relative to $[\text{Al}(\text{H}_2\text{O})_6]^{3+}$, tetramethylsilane (TMS), and $[\text{Ga}(\text{H}_2\text{O})_6]^{3+}$, respectively. Chemical analyses were carried out by dissolution of the clay samples by means of lithium-borate fusion and subsequent analysis of the solution by inductively coupled plasma-atomic emission spectroscopy (ICP-AES). A standard granite STAN-1 of WACOM (fraction 30-2) served as an analytical standard. N_2 adsorption-desorption

isotherms were determined with a ASAP 2400 surface area, pore-volume analyzer (Micromeritics Instrument Corporation). The total surface areas were calculated using the BET equation, micropore surface areas were determined from t-plots, and external surface areas being the difference between the BET and micropore surface areas.

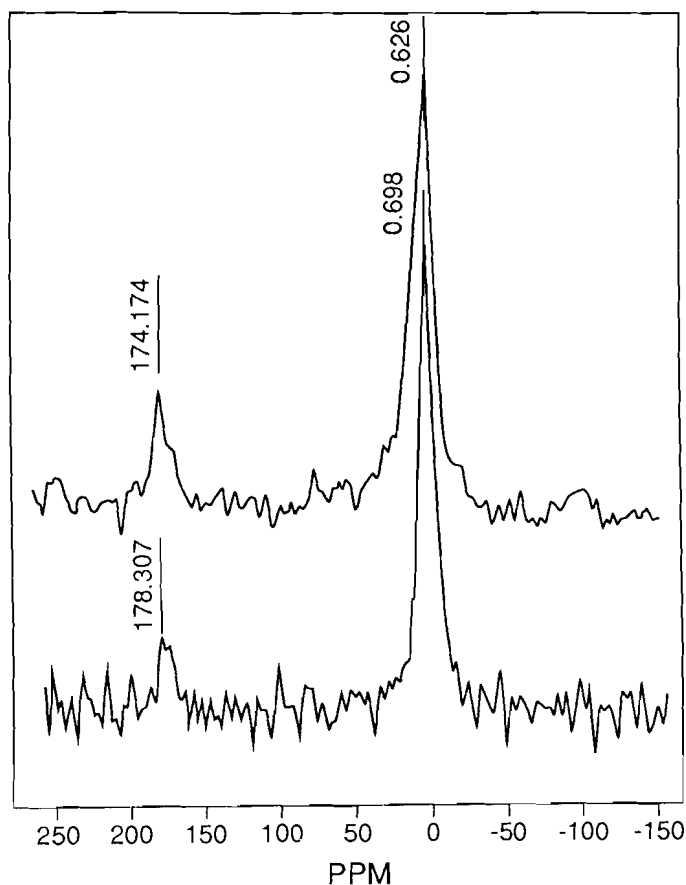


Figure 17.1 ^{71}Ga NMR spectra of partly hydrolyzed Ga solutions prepared by dropwise addition (upper) and by injection (lower).

17.3 RESULTS

17.3.1 Pillaring agents

The ^{27}Al NMR spectra of the partly hydrolyzed Al^{3+} solutions exhibit two peaks at approximately 0.1 and 63.3 ppm, due to monomeric sixfold coordinated Al and to the central fourfold coordinated Al of the Al13, respectively. A detailed description of this hydrolysis has been presented in Klopogge et al. (1992b). The ^{71}Ga spectra (Fig. 17.1) of partly hydrolyzed Ga^{3+} solutions exhibit, analogously to Al^{3+} , two peaks at 0 and at approximately 176 ppm, attributed to monomeric sixfold coordinated Ga and the central fourfold coordinated Ga of the Ga13 polymer (Bradley et al., 1990a,b). In contrast to Al^{3+} , dropwise addition of NaOH to Ga^{3+} solutions yields a slightly higher amount of Ga13 than NaOH injection.

17.3.2 Al-pillared montmorillonite and beidellite

The Al-pillared montmorillonites and beidellites exhibit basal spacings of approximately 18 to 19 Å (Fig. 17.2), irrespective of the method of preparation (Table 17.1). Upon calcination up to 600°C a slight decrease to values around 16.5 Å is observed. Heating stage XRD of uncalcined pillared montmorillonite show that the high basal spacing is retained up to 840°C, above which temperature an abrupt decrease to 9.8 Å is observed. The 9.8 Å reflection disappears at 890°C together with the 06/33, 02/11, and 20/13 reflection bands.

Table 17.2 shows the chemical analyses of pillared montmorillonite and beidellite. The amounts of water are based on the TGA determinations. The pillared montmorillonite has an increased Al content as compared to the starting clay SWy-1, independently of the amount of Al offered per gram of clay during exchange. Calculation of the mineral formulae from the chemical analyses

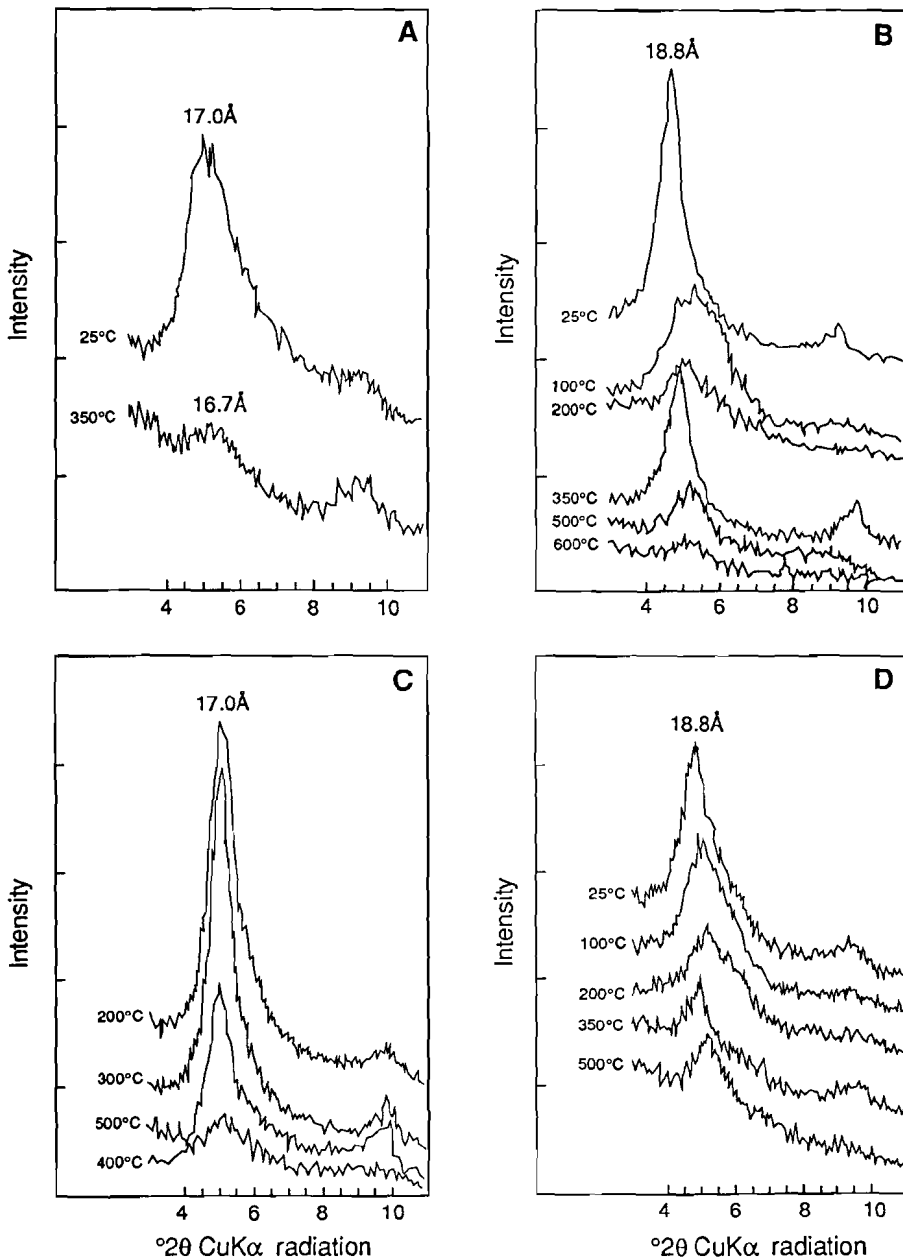


Figure 17.2 001 reflections of Al-pillared montmorillonites: a) 3.0 meq Al/g clay; b) air-dried, 5.5 meq Al/g; c) freeze-dried, 5.5 meq Al/g, d) freeze-dried, 20 meq Al/g, and e) Al-pillared beidellite, 30 meq Al/g.

The effect of thermal treatment on the properties of hydroxy-Al and hydroxy-Ga pillared montmorillonite and beidellite

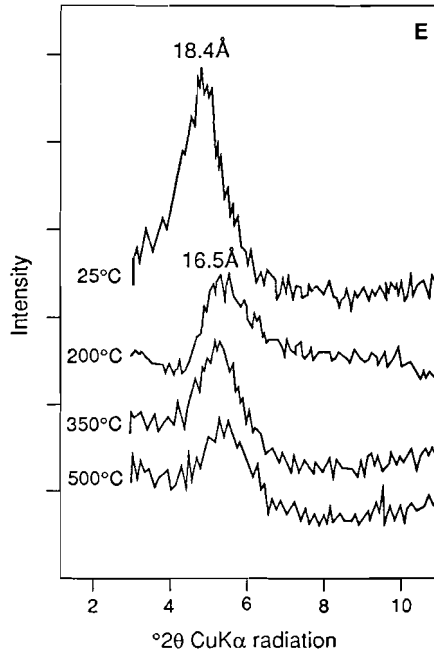


Table 17.1 Basal spacings (Å) of montmorillonite, Al and Ga pillared montmorillonite, beidellite and Al pillared beidellite.

Clay	pillar	meq/g	drying	25°C	350°C	500°C
SWy-1	-	-	air	12.4	10.0	9.8
montm	Ga	5.5	air	17.7	9.5	-
montm	Al	3.0	freeze	17.0	16.7	-
montm	Al	5.5	air	18.8	17.5	17.0
montm	Al	5.5	freeze	-	17.7	16.9*
montm	Al	10.0	air	-	17.9	-
montm	Al	20.0	freeze	18.8	17.4	16.7
beid	-	-	air	12.4	10.0	9.8
beid	Al	30.0	freeze	18.0	17.4	16.4

montm = montmorillonite SWy-1, beid = synthetic beidellite

* value measured at 600°C by lack of 500°C data

Table 17.2 Chemical analyses of the starting clays montmorillonite SWy-1 and synthetic beidellite and their Al pillared analogues.

	SWy-1	PILC6 5.5 meq air	PILC25 5.5 meq freeze	PILC28 20 meq freeze	beid	BPC4 30 meq freeze
SiO ₂	53.57	52.79	50.75	49.12	36.49	
Al ₂ O ₃	18.62	24.13	24.96	23.82	29.62	43.66
TiO ₂	0.14	0.08	0.07	0.07	-	-
Fe ₂ O ₃	3.74	3.51	3.36	3.24	-	-
MgO	2.73	2.12	1.99	1.93	-	-
CaO	1.07	-	-	-	-	-
K ₂ O	0.28	0.52*	-	-	-	-
Na ₂ O	1.10	-	-	-	2.55	-
H ₂ O	6.30	12.60	9.60	nd	8.85	15.29
total	91.80	96.53	92.77	79.81	90.14	95.44

* error in the ICP analysis

structural formula

SWy-1	(Na _{0.29} , Ca _{0.16} , K _{0.05})(Al _{3.01} , Mg _{0.56} , Fe _{0.39})(Si _{7.96} , Al _{0.04})O ₂₀ (OH) ₄
PILC6	([Al13] _{0.09} , K _{0.09})(Al _{3.01} , Mg _{0.56} , Fe _{0.39})(Si _{7.96} , Al _{0.04})O ₂₀ (OH) ₄
PILC25	([Al13] _{0.10})(Al _{3.01} , Mg _{0.56} , Fe _{0.39})(Si _{7.96} , Al _{0.04})O ₂₀ (OH) ₄
PILC28	([Al13] _{0.10})(Al _{3.01} , Mg _{0.56} , Fe _{0.39})(Si _{7.96} , Al _{0.04})O ₂₀ (OH) ₄
beid	(Na _{0.71})(Al _{4.08})(Si _{7.06} , Al _{0.96})O ₂₀ (OH) ₄
BPC4	([Al13] _{0.15})(Al _{4.08})(Si _{7.06} , Al _{0.96})O ₂₀ (OH) ₄

Table 17.3 Surface areas and pore volumes of montmorillonite SWy-1 and Al pillared analogues. PILC6 to PILC14, having 5.5 meq Al/g, are airdried, PILC17 to PILC22 are freeze-dried, PILC26/28 have 20 meq Al/g and are freeze-dried.

	T _{calc} °C	interlayer spacing (Å)	BET m ² /g	P _v [*] vol cm ³ /g	micropore vol calc cm ³ /g	micropore vol cm ³ /g	mesopore vol cm ³ /g	micropore area m ² /g
SWy-1	25	2.1	26	0.104	0.003	0.005	0.101	7
PILC11	25	9.2	349	0.180	0.139	0.321	0.041	337
PILC14	200	7.7	174	0.128	0.066	0.134	0.063	156
PILC6	350	7.9	269	0.188	0.102	0.213	0.086	246
PILC7	500	7.4	150	0.145	0.054	0.111	0.091	129
PILC13	600	7.1	219	0.201	0.081	0.155	0.120	192
PILC17	200	7.4	226	0.196	0.086	0.167	0.110	207
PILC19	300	7.4	270	0.192	0.104	0.200	0.088	252
PILC20	400	7.5	318	0.230	0.122	0.239	0.108	291
PILC22	600	7.3	190	0.146	0.073	0.139	0.073	170
PILC28	25	9.2	297	0.186	0.116	0.273	0.070	281
PILC26	350	7.8	281	0.177	0.110	0.219	0.067	265

reveals the presence of 0.10 pillars per unit cell montmorillonite and 0.15 per unit cell beidellite.

In **Table 17.3** the results from N₂ adsorption and desorption measurements are presented. Assuming that all micropores (< 20 Å) are located within the interlamellar space of the pillared clay, the micropore volumes can be calculated from the interlayer spacing (i.e., the basal spacing, viz., 9.6 Å being the thickness of a single sheet (Grim, 1968)) and the BET surface areas. The air dried montmorillonites exhibit an irregular sequence of BET surface areas, total pore volumes, and micropore volumes, but a linear increase in the mesopore volume with the calcination temperature. The freeze-dried samples show a

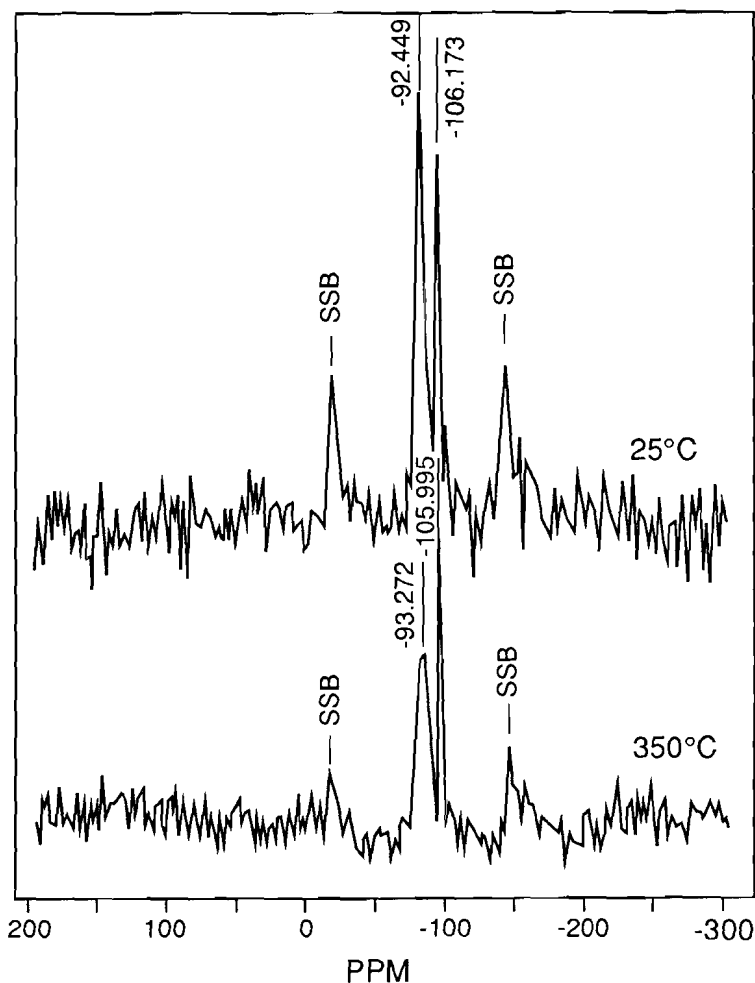


Figure 17.3 ^{29}Si MAS NMR spectra of air-dried (upper) and 350°C calcined Al-pillared montmorillonite (lower).

regular increase of the surface area and of the micropore volume up to a calcination temperature of 400°C, followed by a significant drop after calcination at 600°C. The measured micropore volumes are all approximately 50 % smaller than the calculated values.

The ^{29}Si MAS-NMR spectrum of SWy-1 exhibits two resonances at -92.4 ppm and 106 ppm (Fig. 17.3), the last being due to a minor amount of quartz. The -92.4 ppm resonance from the montmorillonite tetrahedral site shifts to -93.3 ppm upon Al₁₃ intercalation and calcination at 350°C, indicative for small changes in the clay structure.

The ^{27}Al MAS-NMR spectra are interesting, since they can indicate the presence of the Al₁₃ pillars in the clay structure. The ^{27}Al MAS-NMR spectra of SWy-1 reveal a broad signal, which is assigned to octahedral Al at 2.3 ppm (FWHH 5733 Hz) and a small signal at approximately 60 ppm, which is assigned to tetrahedral Al substituting Si. Pillaring results in a signal between 63 and

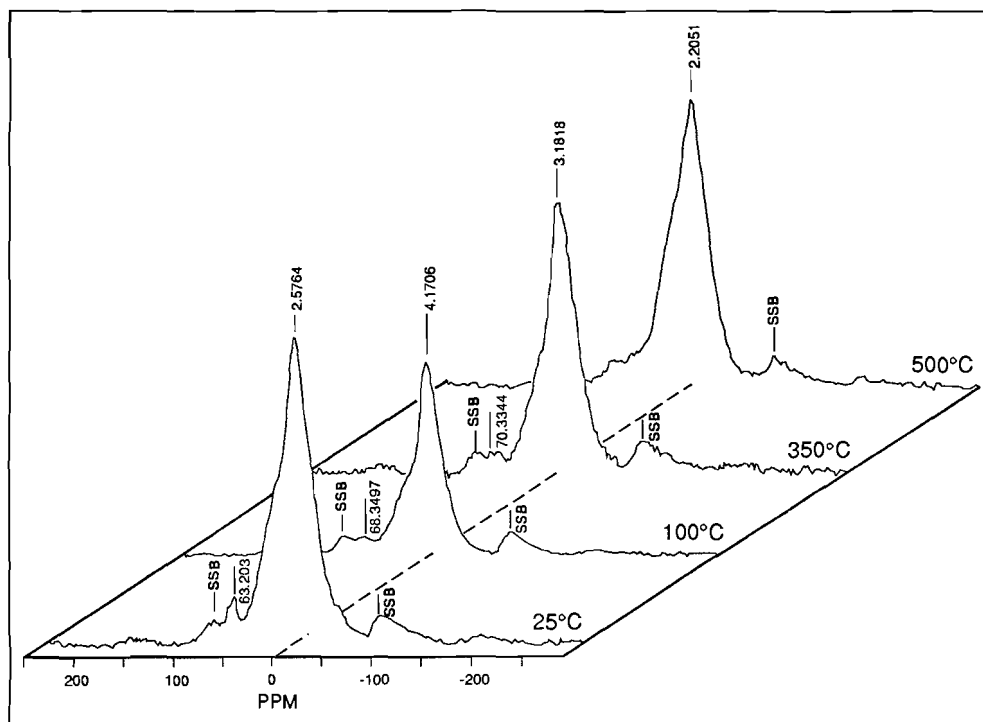


Figure 17.4 ^{27}Al MAS NMR spectra of Al-pillared montmorillonite calcined at various temperatures.

70 ppm, which is mostly assigned to the tetrahedral Al from the Al₁₃ (Plee et al., 1985)(Fig. 17.4). The tetrahedral signal from the clay structure cannot be discriminated from the Al₁₃ signal. Calcination causes a decrease of the intensity and a shift from 63 to 70 ppm. Synthetic beidellite shows two resonances at 3.8 ppm (FWHH 782 Hz) and 68.9 ppm (FWHH 573 Hz) assigned to octahedral and tetrahedral Al, respectively, in the beidellite structure. The intensity ratio Al^{IV}:Al^{VI} of 14.6:85.4 is close to the theoretical value of 14.8:85.2. After pillaring both signals shifts about 0.3 ppm downfield to 4.1 ppm (FWHH 886 Hz) and 69.2 ppm (FWHH 573 Hz)(Fig. 17.5). Here also no distinction can be made between tetrahedral Al from the pillar and from the

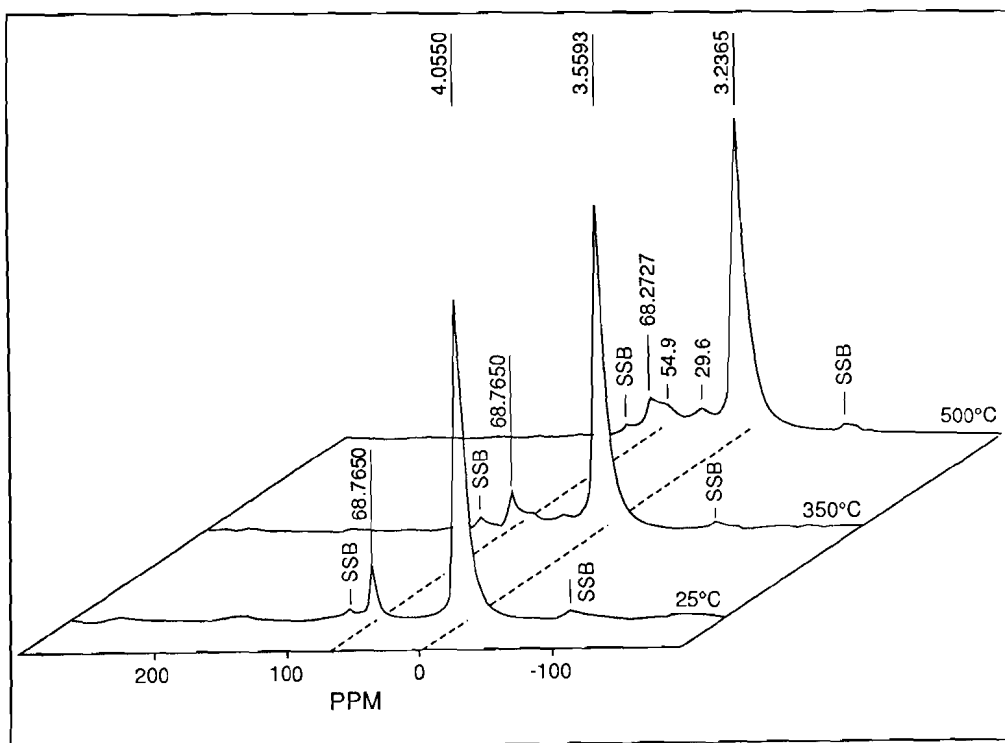


Figure 17.5 ²⁷Al MAS NMR spectra of Al-pillared beidellite calcined at various temperatures.

The effect of thermal treatment on the properties of hydroxy-Al and hydroxy-Ga pillared montmorillonite and beidellite

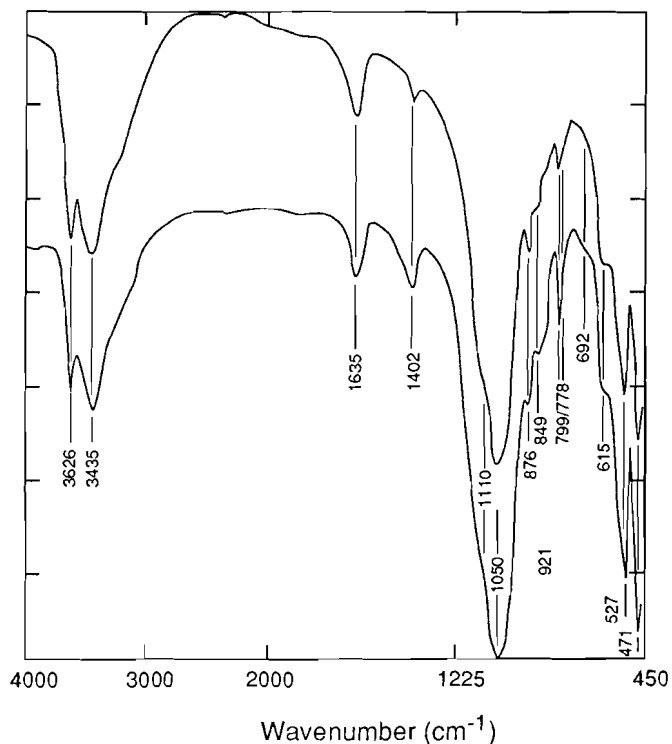


Figure 17.6 IR spectra of montmorillonite (lower) and its Al-pillared analogue calcined at 100°C (upper).

beidellite structure. The intensity ratio Al^{IV}:Al^{VI} changes to 10.5:89.5, which is close to the ratio of 10.2:89.8 based on the chemical analyses. Upon calcination above 350°C two new signals appear at 54.9 ppm and 29.6 ppm.

IR spectra have been measured to observe changes in both the pillar structure and the tetrahedral sheet of the clay structure upon intercalation and calcination. The IR spectra of SWy-1, beidellite, and their pillared analogues are displayed in **Figure 17.6**. The pillaring of SWy-1 results in a slight increase in intensity of the Al--OH and (Mg,Al)--OH modes at 921 and 849 cm⁻¹.

Commencing at approximately 400°C, the structural hydroxy stretching vibration at 3631 cm⁻¹, the Al--OH vibration, and the Si--O--Al bending vibration at 525 cm⁻¹ gradually decrease. The 921 cm⁻¹ vibration has disappeared at 600°C. The three vibrations at 3631, 921, and 525 cm⁻¹ shift to slightly higher wave numbers at increasing calcination temperatures. DRIFT spectra recorded during heating to 400°C show a larger drop in intensity of the Al--OH stretching vibration at 3644 cm⁻¹ than that of the untreated SWy-1. Upon heating to 300°C a shoulder at 3456 cm⁻¹ appears in the spectrum of pillared montmorillonite, which is absent in SWy-1. The IR spectra of beidellite and the pillared analogue reveal upon pillaring decreasing intensities of the 3651 cm⁻¹ Al--OH stretching and the 937 cm⁻¹ Al--OH vibration. DRIFT spectra recorded at 400°C do not exhibit a drop in intensity of the Al--OH stretching vibration, as observed for pillared montmorillonite. At 200°C a band at 3453 cm⁻¹ appears, analogously to the pillared montmorillonite, although it has a stronger intensity.

The TGA plot of SWy-1 (Fig. 17.7a) exhibits below 150°C the loss of 6.3 wt% due to dehydration. Between 150° and 535°C a very small amount of 0.5 wt% is lost, attributed to the removal of interlayer water and the set on of dehydroxylation. The dehydroxylation reached a maximum weight loss of 4.0% between 535° and 680°C. Pillared montmorillonite (Fig. 17.7b) lost more weight both below 150°C, being 14.4 %, and within the range 150° to 525°C, being 4.5 %, attributed to the removal of excess water absorbed into the pillared interlayer and dehydroxylation of the pillars (Occelli and Tindwa, 1983). The DTA plot of the pillared montmorillonite shows the presence of a small endotherm between approximately 410° and 580°C, not present in the DTA plot of SWy-1. Analogously to SWy-1, beidellite lost 8.85 wt% below 120°C. No loss was observed between 120° and 395°C, but an unusual weight loss of 1.5 % was observed between 395° and 565°C. This loss was accompanied by an endothermic peak in the DTA plot, which was probably caused by the dehydroxylation of some amorphous material. Finally a weight loss of 2.85 % was observed between 625° and 725°C. During heating of the

The effect of thermal treatment on the properties of hydroxy-Al and hydroxy-Ga pillared montmorillonite and beidellite

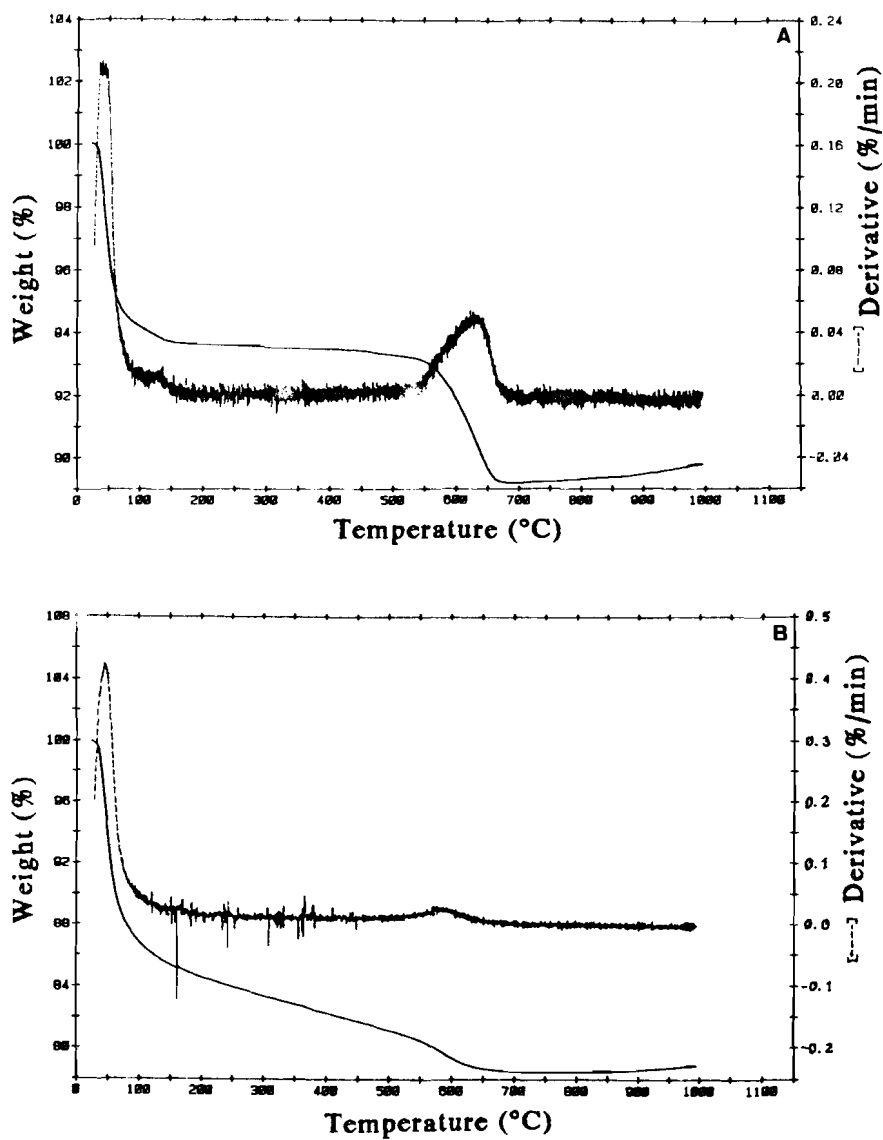
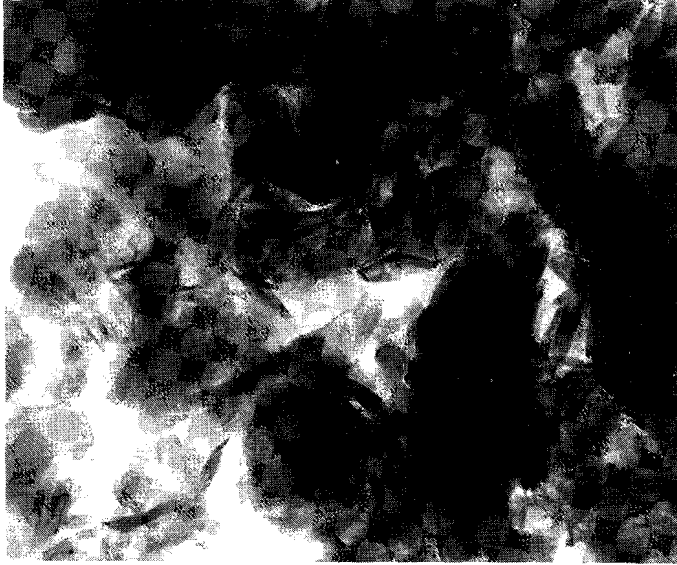


Figure 17.7 TGA plots of a) montmorillonite SWy-1 and b) its Al-pillared analogue.



The effect of thermal treatment on the properties of hydroxy-Al and hydroxy-Ga pillared montmorillonite and beidellite



Figure 17.8 TEM photographs of Al-pillared beidellite BPC3 (upper left, 1 cm = 1700 Å), Al-pillared montmorillonite PILC8 (lower left, 1 cm = 270Å), and PILC12 (right, 1 cm = 330 Å).

freeze-dried pillared beidellite to 150°C 13.6 wt% was lost. Analogously to the beidellite 1.4 wt% was lost between 150° and 350°C, followed by an additional 5.6 wt% loss between 350° and 550°C. From 550° to 700°C, finally, 1.4 wt% was lost. The thermal effects occurring upon heating pillared beidellite were more gradual than that of Na-beidellite.

The TEM photographs (Fig. 17.8) show aggregates, consisting of face-to-face pillared montmorillonite platelets, mainly in edge-to-face contact forming a house of cards morphology as described by van Olphen (1977). Lattice fringe images of PILC8 exhibit a regular pillar distribution over up to several hundreds of ångströms and indicate basal spacings of approximately 16.7 Å, which is close to the value of 16.4 Å determined by XRD.

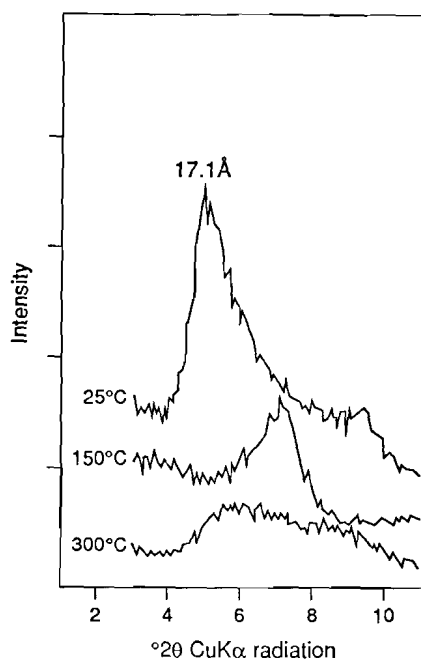


Figure 17.9 001 reflection of Ga-pillared montmorillonite at various calcination temperatures.

17.3.3 Ga-pillared montmorillonite

The basal spacing of Ga pillared montmorillonite decreased from 17.7 Å to approximately 12.3 Å after calcination at 150°C. At 350°C the pillared structure completely collapsed to a basal spacing of 9.52 Å (Fig. 17.9). The ^{71}Ga MAS-NMR spectra (Fig. 17.10) from samples calcined at 25° and 150°C reveal a tetrahedral signal at 172.6 ppm (FWHH 3493 Hz) and an octahedral signal at 30.1 ppm (FWHH 6487 Hz). The octahedral signal is not visible in the spectra of the partly hydrolysed Ga solutions. Upon calcination at 300° C these signals have disappeared and are replaced by a very broad signal at approximately 0 ppm. The IR spectra of Ga-pillared montmorillonite (Fig. 17.11) do not show any vibrations different from that of Al-pillared montmorillonite, although there are no significant changes in intensity upon calcination. The TGA plot is largely the same as for Al-pillared montmorillonite. During heating to

The effect of thermal treatment on the properties of hydroxy-Al and hydroxy-Ga pillared montmorillonite and beidellite

170°C 12.9 wt% was lost, followed by a gradual loss of 3.8 wt% between 170° and 550°C, and finally a loss of 2.3 wt% between 550° and 710°C.

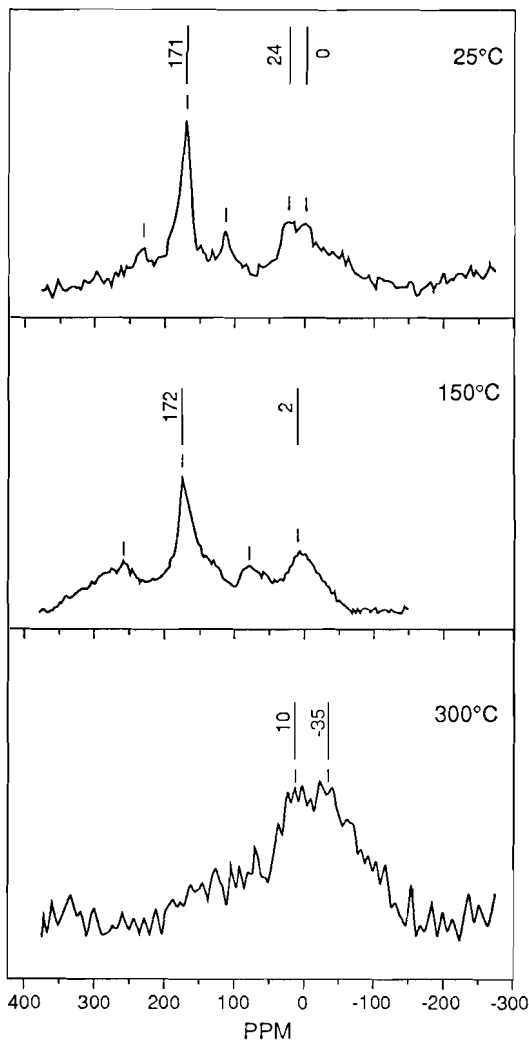


Figure 17.10 ^{71}Ga MAS NMR spectra of Ga-pillared montmorillonite calcined at various temperatures.

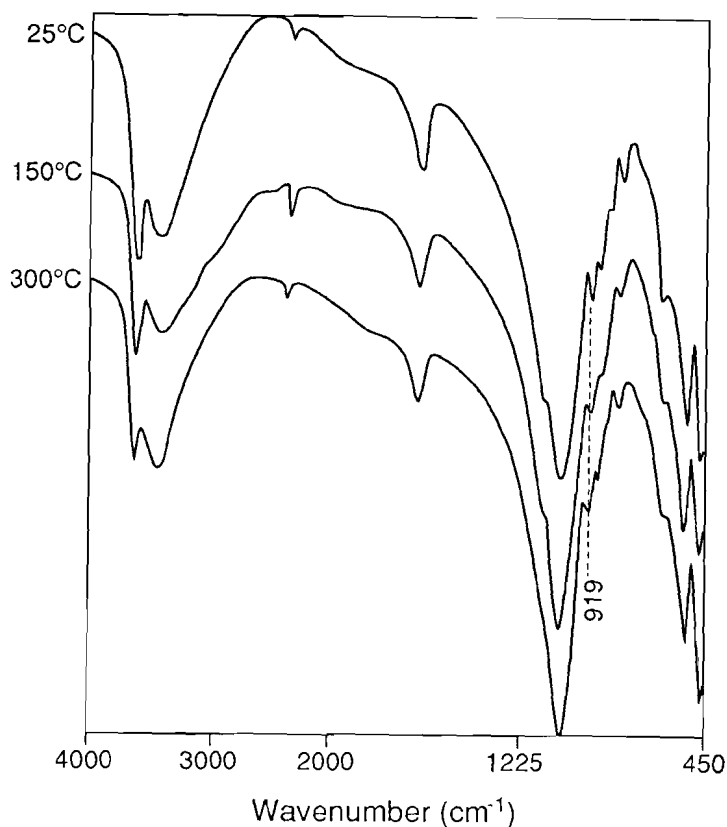


Figure 17.11 IR spectra of Ga-pillared montmorillonite calcined at various temperatures.

17.4 DISCUSSION

XRD patterns have shown that exchanging montmorillonite with amounts of Al13 pillaring solutions (OH/Al molar ratio 2.4) larger than 5.5 meq Al/g clay does not yield basal spacings larger than about 17 Å or more regular pillared structures. The maximum amount of Al13 agrees with the data of Gu and Doner (1990), who found that 5.5 meq Al/g clay is sufficient to saturate montmorillonite with Al13. Large basal spacings are obtained for pillared beidellite after exchange with 30 meq Al/g, whereas 10 meq/g did not result in an increase in basal spacing. The much higher amount of Al13 required supports

the findings of Plee et al. (1987) that high meq Al/g clay levels are required for beidellite, because other non-pillaring Al species are preferentially adsorbed. The montmorillonite exchanged with 5.5 meq Ga/g clay exhibit a basal spacing of 17.1 Å, which rapidly decreases upon calcination. The low apparent thermal stability does not agree with the result of Bellaloui et al. (1990), who observed thermally stable (up to 500°C) expanded montmorillonite exchanged with 30 meq Ga/g clay. The difference in thermal stability may be attributed to the much lower Ga13 concentration in the solution used in our exchange experiments as compared to the Al13 concentration of solutions prepared under identical conditions.

Pillaring increases the specific surface area of the montmorillonite, SWy-1, from 25 to 349 m²/g, essentially by creating micropores of a diameter less than 20 Å. The samples dried in air show an irregular behavior of the BET surface area, whereas the basal spacing continuously decreases. The irregular behaviour may be explained by the calcination procedure in which a preheated furnace was used. Upon heating the clay samples water is released and, due to diffusional problems arising from the sudden increase in temperature, the local water pressure in the clay may become that high that the structure of the clay is affected. The freeze-dried pillared montmorillonites exhibit a surface area and microporosity increasing up to a calcination temperature of 400°C caused by shrinkage of the pillars due to dehydration (Malla and Komarneni, 1990). At higher temperatures, where dehydroxylation of both pillar and clay structure proceeds, a strong decrease in surface area and pore volume is observed, comparable with the results of Schutz et al. (1987) for pillared beidellite.

Increasing the calcination temperature up to 350°C results in sharper, but slightly smaller, basal spacings for both Al-pillared montmorillonite and beidellite, indicating a more regular layered structure. Plee et al. (1987) have shown that increasing the temperature to 75°C of the Al13 solution and the clay slurry during the exchange with Al13 causes a decreasing and,

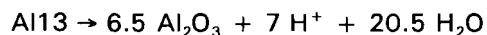
simultaneously, broadening basal spacing. Kloprogge et al. (1992a) proved that heating Al13 solutions to temperatures between 85° and 95°C resulted in a structural rearrangement of the tridecamer. Our results imply a similar mechanism as suggested by Plee et al. (1987), according to which drying of pillared clay slurries at elevated temperatures causes a disorganization of the clay structure and/or a partial depolymerization of the structure and/or a partial depolymerization of the intercalated Al13 polymer. Drying above 500°C yields broader basal spacings; the broadening is mainly attributed to the thermal instability of the pillared structure caused by dehydroxylation.

In contrast to the Al-pillared montmorillonite, the Ga-pillared analogue completely collapses to a basal spacing of 9.52 Å upon calcination at 350°C. This indicates a total collapse of the Ga13 pillar to single Ga cations and not to its oxide form. Although this sample was allowed to rehydrate, it remained completely dehydrated. Hofmann and Klemen (1950) and Chourabi and Fripiat (1981) have shown that at higher temperatures small interlayer cations, such as, H⁺ and Li⁺, can migrate through the hexagonal cavities in the tetrahedral sheets of montmorillonite into the octahedral sheet, where they compensate the charge deficiency. Upon rehydration these ion-exchanged montmorillonites do not show an increase of the basal spacing to their original values, indicating the irreversibility of the migration process. The ionic radius of Ga³⁺ is slightly smaller than that of Li⁺ (0.62 Å versus 0.68 Å) and Ga³⁺ ions should, therefore, be able to migrate into the octahedral sheet as well.

Heating stage XRD of pillared montmorillonite shows that the pillared interlayer is stable at temperatures up to 840°C. At this temperature the basal reflection shifts to 9.8 Å, which is approximately the thickness of a single montmorillonite sheet. The final basal spacing of 9.8 Å indicates that, although the clay is dehydroxylated as evident from the broadening of the 06/33, 02/11 and 24 bands at temperatures ranging from 580° to 600°C, the sheet-like structure is still present. At 890° the reflection at 9.8 Å disappears due to the breakdown of the sheet-like structure. It has to be concluded that not the thermal stability

of the pillars, but that of the montmorillonite structure is the limiting factor for the stability of pillared montmorillonites.

The lower thermal stability of the pillared clay is probably due to the diffusion of protons into the clay sheet. The protons are released from the pillars during dehydroxylation according to the overall reaction:



It is well known that the thermal stability of H^+ exchanged clays is less than that of the initial clay (Ames and Sand, 1958). Moreover, the dehydroxylation of the pillars produces water, causing the local partial water pressure in the clay structure to be sufficiently high to induce hydrolysis (Tichitt et al., 1988). The self-destructive protonic attack on the clay sheets has been confirmed by the TGA analyses, which reveal that dehydroxylation within the pillared clay occurs at lower temperatures than within the original clay.

Upon calcination at 350°C the ^{29}Si MAS-NMR spectrum of pillared montmorillonite exhibits a shift of the Si (OAl) signal from -92.4 ppm to 93.3 ppm. Weiss et al. (1987) have shown that with decreasing total layer charge the ^{29}Si NMR chemical shifts for Si(nAl) in 2:1 layer silicates become progressively shielded. The upfield shift of the Si(OAl) resonance is attributed to the diffusion of protons into the clay sheets lowering the layer charge. The data of Tennakoon et al. (1986a,b) showing an upfield shift of 2 ppm upon heating to 500°C of Li^+ and H^+ exchanged montmorillonites in comparison to the original montmorillonite support the above explanation.

In the IR spectra of pillared montmorillonite the Al-OH vibration at 919 cm^{-1} starts to decrease in intensity upon heating above 300°C and has completely disappeared at 600°C . Yariv and Heller-Kallai (1973) have shown that migration of protons into the octahedral sheets of H^+ clays leads to a decrease in the intensity of the lattice hydroxy bands, due to interaction with the protons. In agreement with the results discussed above, the diminishing intensity of the 919 cm^{-1} vibration is, therefore, also related to the diffusion of protons released

from the pillars into the octahedral layer. Pillared beidellite exhibits a similar decrease in the Al--OH librational vibration at 937 cm^{-1} . The protons released upon dehydroxylation are not likely to migrate into the octahedral layer, because in beidellite the charge deficiency originates from tetrahedral substitutions. The results of Kawano and Tomita (1991) have demonstrated that small interlayer cations like Mg^{2+} migrate into the hexagonal cavities of the tetrahedral network instead of into the octahedral sheet. However, the fact that the TGA and DTA plots of the pillared beidellite also show a lower dehydroxylation temperature suggests that, in spite of the neutrality of the octahedral layer, protons are able to diffuse through the hexagonal cavities of the tetrahedral sheet into the octahedral sheet, where they can interact with the structural hydroxyl groups.

Starting at about 400°C a progressive reduction in intensity and at 700°C the disappearance of the structural stretching vibration at 3631 cm^{-1} is observed. The spectroscopic results, indicating that the dehydroxylation of the pillared montmorillonite is nearly complete at 700°C , are in agreement with the TGA analyses showing no weight loss above 680°C . The shift of the Al--OH stretching and bending vibrations at 3631 and 621 cm^{-1} to higher energies initiating at 600°C may also be associated with dehydroxylation.

IR spectra of in situ calcinated pillared montmorillonite reveal upon heating to 300°C a previously not observed vibration at 3457 cm^{-1} . This vibration may have been present in the uncalcined sample, being obscured by the broad H--O--H vibration at 3435 cm^{-1} , or may originate from the calcination. Pillared beidellites exhibit the same spectral behavior upon calcination, but more strongly. Schutz et al. (1987) observed the same effect in their spectra. Protons released from the pillar may either enter the octahedral layer and recombine with structural hydroxy groups to form water, or react with tetrahedral Si-O-Al bonds, being the weakest bonds, forming Si-OH and/or Al-OH bonds. ^{27}Al NMR has shown that montmorillonite only contains small amounts of tetrahedral Al, which causes reactions to Si-OH and Al-OH bands to be of minor importance. Chourabi and Fripiat (1981) have shown that upon heating NH_4^+ beidellites

silanol stretching bands at 3420 cm^{-1} and 3500 cm^{-1} appear, formed by protons breaking the Si-O-Al linkages. The reaction is fairly similar to the decationization reaction in NH_4^+ exchanged X and Y zeolite (Uytterhoeven et al., 1965).

The small endotherm between $410\text{ }^\circ\text{C}$ and $580\text{ }^\circ\text{C}$ observed in the DTA-plots of pillared montmorillonites calcined between $200\text{ }^\circ\text{C}$ and $500\text{ }^\circ\text{C}$ was not observed with the original SWy-1, indicating that this endotherm is due to the dehydroxylation of the pillars. Differential scanning calorimetry (Occelli and Tindwa, 1983; Pinnavaia et al., 1984) and differential thermal analysis (Sterte, 1990) of pillared montmorillonite revealed also a small endotherm with its maximum at about $500\text{ }^\circ\text{C}$, which has been attributed to the dehydroxylation of the pillars.

The ^{27}Al NMR spectroscopic investigation of pillared clays is obstructed by the difficulty to analyze quantitatively the tetrahedral and octahedral resonances (Diddams et al., 1984; Pinnavaia et al., 1985; Tennakoon et al., 1986) and the changes of the resonances upon calcination. The ^{27}Al spectra of pillared montmorillonite show a decrease in intensity of the tetrahedral resonance upon calcination, indicating the disappearance of the central fourfold coordinated Al from the pillar. ^{71}Ga MAS NMR spectra of the uncalcined pillared montmorillonite sample and of the sample calcined at $150\text{ }^\circ\text{C}$ demonstrate the presence of the Ga13 pillar, which displays a resonance analogous to that of the solution. After calcination at $300\text{ }^\circ\text{C}$ the tetrahedral resonance at 172.6 ppm has completely disappeared and only a very broad signal at about 0 ppm is visible, indicating the presence of octahedral Ga only. The low thermal stability of Ga13 in solution (Bradley et al., 1990) indicated already that the Ga13 pillars are also of a limited thermal stability. Up till now no explanation can be presented for the transformation to Ga^{3+} instead of to the Ga-oxide, which was observed by Bellaloui et al. (1990) upon calcination.

The spectra of Al-pillared beidellite show the development of new resonances at 54.9 ppm and 29.6 ppm upon calcination. Fyfe et al. (1982) have reported a

resonance at 54 ppm in dealuminated Na-Y zeolite, assigned to tetrahedral Al in a silicon-rich tetrahedral network, whereas Kentgens et al. (1983) have mentioned a 53 ppm resonance due to tetrahedral Al in the lattice of zeolite ZSM-5. Plee et al (1985) have suggested a model in which Al tetrahedra in the tetrahedral sheet of beidellite are inverted and oxygens at the apex, pointing into the interlamellar space, are anchored to the pillar. Upon calcination of pillared beidellite, they observed a new resonance at 56.5 ppm, which is thought to be identical to the 54.9 ppm resonance in this paper, which is tentively assigned to the new tetrahedral Al environment.

Reactions between the Al pillar and the beidellite sheets are thought to occur at the Al-substituted tetrahedrons in the tetrahedral sheet. Chourabi and Fripiat (1984) have shown that silanol groups in the form of Si-OH-Al are formed upon heating NH_4^+ -beidellite. A similar, but very limited, proton-induced reaction was observed upon heating pillared montmorillonite. The IR spectra of in situ calcined pillared beidellite exhibit a much stronger absorption band at 3457 cm^{-1} , assigned to silanol groups formed by the breaking of Si-O-Al bonds in the tetrahedral layer. A reaction between the Al pillar and the protonated Si-OH-Al linkage will yield either $\text{Si-O-Al}^{\text{oct}}_{\text{pillar}}$ or $\text{Al}^{\text{tet}}_{\text{sheet}}\text{-O-Al}^{\text{oct}}_{\text{pillar}}$. The fact that silanol groups are observed in the IR spectra of calcined pillared beidellite favor the second assignment. The ^{27}Al MAS NMR and the IR data of pillared beidellite are consistent with the model proposed by Plee et al. (1987), whereas calcination of pillared montmorillonite does not result in such a structural rearrangement.

The observed resonance at 29.6 ppm is assigned to fivefold coordinated Al, analogous to the 29 ppm signal from dehydroxylated pyrophyllite (Fitzgerald et al., 1989). This resonance most probably arises from fivefold coordinated Al developed in the pillar upon calcination, based on an analogous peak at 30.1 ppm in calcined synthetic pillared hectorite, which clay structure is aluminum-free (unpublished data R.J.M.J. Vogels). Still, five-coordinated Al in the non-pillared beidellite structure cannot completely be ruled out, because no data are available for calcined unpillared beidellite.

REFERENCES

- Akitt, J. W. (1989) Multinuclear studies of aluminium compounds: *Progr. NMR Spectr.* **21**, 1-149.
- Ames, L. L. and Sand, L. B. (1958) Factors effecting maximum hydrothermal stability in montmorillonites: *Amer. Mineral.* **43**, 641-648.
- Barrer, R. M. and McLeod, D. M. (1955) Activation of montmorillonite by ion exchange and sorption complexes of tetraalkylammonium montmorillonites: *Trans. Faraday Soc.* **51**, 1290-1300.
- Bartley, G. J. J. (1988) Zirconium pillared clays: *Catal. Today* **2**, 233-241.
- Bartley G. J. J. and Burch, R. (1985) Zr-containing pillared clays. Part III. Influence of method of preparation on the thermal stability: *Appl. Catal.* **19**, 175-185.
- Bellaloui, A., Plee, D. and Meriaudeau, P. (1990) Gallium containing pillared interlayer clays: preparation, characterization and catalytic properties: *Appl. Catal.* **63**, 17-110.
- Bradley, S. M., Kydd, R. A. and Yamdagni, R. (1990a) Detection of a new polymeric species formed through the hydrolysis of gallium(III) salt solutions: *J. Chem. Soc. Dalton Trans.*, 413-417.
- Bradley, S. M., Kydd, R. A. and Yamdagni, R. (1990b) Comparison of the hydrolysis of gallium(III) and aluminium(III) solutions by nuclear magnetic resonance spectroscopy: *J. Chem. Soc. Dalton Trans.*, 2653-2656.
- Brindley, G. W. and Sempels, R. E. (1977) Preparation and properties of some hydroxy-aluminium beidellites: *Clay Minerals* **12**, 229-236.
- Chourabi, B. and Fripiat, J. J. (1981) Determination of tetrahedral substitutions and interlayer surface heterogeneity from vibrational spectra of ammonium in smectites: *Clays & Clay Minerals* **29**, 260-268.
- Diddams, P. A., Thomas, J. M., Jones, W., Ballantine, J. A. and Purnell, J. H. (1984) Synthesis, Characterization and catalytic activity of beidellite-

- montmorillonite layered silicates and their pillared analogues: *J. Chem. Soc., Chem. Commun.*, 1340-1342.
- Fitzgerald, J. J., Dec, S. F. and Hamza, A. (1989) Observation of five-coordinated Al in pyrophyllite dehydroxylate by solid-state ^{27}Al NMR spectroscopy at 14 T: *Amer. Mineral.* **74**, 1405-1408.
- Fyfe C. A., Gobbi, G. C., Hartman, J. S., Klinowski, J. and Thomas, J. M. (1982) Solid-state magic-angle spinning aluminum-27 nuclear magnetic resonance studies of zeolites using a 400-MHz high-resolution spectrometer: *J. Phys. Chem.* **86**, 1247-1250.
- Grim, R. E. (1968) *Clay Mineralogy*. McGraw-Hill, New York, 121-122, 316-328.
- Gu, B. and Doner, H. E. (1990) Adsorption of hydroxy-Al polycations and destabilization of illite and montmorillonite suspension: *Clays & Clay Minerals* **38**, 493-500
- Gurwitsch, L. (1912) Adsorption: *Z. Chem. Ind. Kolloide* **11**, 17-19.
- Gurwitsch, L. (1923) Zur Kenntnis der heterogenen Katalyse: *Z. Phys. Chem.*, Frankfurt **107**, 235-248.
- Hofmann, J. and Klemen, R. (1950) Verlust der Austauschfähigkeit von Lithiumionen an Bentonit durch Erhitzung: *Z. Anorg. Chem.* **262**, 95-99.
- Johansson, G. (1962) The crystal structures of $[\text{Al}_2(\text{OH})_2(\text{H}_2\text{O})_8](\text{SO}_4)_2 \cdot 2\text{H}_2\text{O}$ and $[\text{Al}_2(\text{OH})_2(\text{H}_2\text{O})_8](\text{SeO}_4)_2 \cdot 2\text{H}_2\text{O}$: *Acta Chem. Scand.* **16**, 403-420.
- Kawano, M. and Tomita, K. (1991) X-ray powder diffraction studies of the rehydration properties of beidellite: *Clays & Clay minerals* **39**, 77-83.
- Kentgens, A. P. M., Scholle, K. F. M. G. J. and Veeman, W. S. (1983) Effect of hydration on the local symmetry around aluminium in ZSM-5 zeolites, studied by ^{27}Al nuclear magnetic resonance: *J. Phys. Chem.* **87**, 4357-4360.
- Kloprogge, J. T., van der Eerden, A. M. J., Jansen, J. B. H. and Geus, J. W. (1990a) Hydrothermal synthesis of Na-beidellite: *Geologie & Mijnbouw* **69**, 351-357.

- Kloprogge, J. T., Jansen, J. B. H. and Geus, J. W. (1990b) Characterization of synthetic Na-beidellite: *Clays & Clay Minerals* **38**, 409-414.
- Kloprogge, J. T., Seykens, D., Geus, J. W. and Jansen, J. B. H. (1992a) Temperature influence on the Al₁₃ complex in partially neutralized aluminum solutions: an ²⁷Al nuclear magnetic resonance study: *J. Non-Cryst. Solids* **142**, 87-93.
- Kloprogge, J. T., Seykens, D., Jansen, J. B. H. and Geus, J. W. (1992b) An ²⁷Al nuclear magnetic resonance study on the optimalization of the development of the Al₁₃ polymer: *J. Non-Cryst. Solids* **142**, 94-102.
- Lahav, N., Shani, U. and Shabtai, J. (1978) Cross-linked smectites I. Synthesis and properties of hydroxy-aluminum-montmorillonite: *Clays & Clay Minerals* **26**, 107-115.
- Malla, P. B. and Komarneni, S. (1990) Synthesis of highly microporous and hydrophilic alumina-pillared montmorillonite: water-sorption properties: *Clays & Clay Minerals* **38**, 363-372.
- Montaland, L. (1911) Process for converting pinene into camphene: *U.S. Patent* **999,667**.
- Occelli, M. L. and Tindwa, R. M. (1983) Physicochemical properties of montmorillonite interlayered with cationic-oxyaluminum pillars: *Clays & Clay Minerals* **31**, 22-28.
- van Olphen, H. and Fripiat, J. J. (eds.) *Datahandbook for clay minerals and other non-metallic minerals*. Pergamon Press, Oxford.
- Pinnavaia, T. J., Landau, S. D., Tzou, M.-S. and Johnson, J. D. (1985) Layer cross-linking in pillared clays: *J. Amer. Chem. Soc.* **107**, 7222-7224.
- Pinnavaia, T. J., Tzou, M.-S., Landau, S. D. and Raythatha, R. H. (1984) On the pillaring and delamination of smectite clay catalysts by polyoxo cations of aluminum: *J. Mol. Catal.* **27**, 195-212.

- Plee, D., Borg, F., Gataineau, L. and Fripiat, J. J. (1985a) High-resolution solid-state ^{27}Al and ^{29}Si nuclear magnetic resonance study of pillared clays: *J. Amer. Chem. Soc.* **107**, 2362-2369.
- Plee, D., Gataineau, L. and Fripiat, J. J. (1987) Pillaring processes with and without tetrahedral substitution: *Clays & Clay Minerals* **35**, 81-88.
- Plee, D., Schutz, A., Poncelet, G. and Fripiat, J. J. (1985b) Acid properties of bidimensional zeolite. In *Catalysis by acids and bases*, B. Imelik, C. Naccache, G. Coudurier, J. Ben Taarit and J. C. Vedrine (eds.) Elsevier, Amsterdam, 342-350.
- Rausch, W. V. and Bale, H. D. (1964) Small-angle X-ray scattering from hydrolyzed aluminum nitrate solutions: *J. Chem. Phys.* **40**, 3391-3394.
- Schutz, A., Stone, W. E. E., Poncelet, G. and Fripiat, J. J. (1987) Preparation and characterization of bidimensional zeolitic structures obtained from synthetic beidellite and hydroxy-aluminum solutions: *Clays & Clay Minerals* **35**, 251-261.
- Sterte, J. P. (1990) Preparation and properties of pillared interstratified illite/smectite: *Clays & Clay Minerals* **38**, 609-616
- Tennakoon, D. T. B., Jones, W. and Thomas, J. M. (1986) Structural aspects of metal-oxide pillared sheet silicates: *J. Chem. Soc., Faraday Trans. I*, **82**, 3081-3090 .
- Tennakoon, D. T. B., Thomas, J. M., Jones, W., Carpenter, T. A. and Ramdas, S. (1986) Characterization of clay and clay-organic systems: *J. Chem. Soc., Faraday Trans. I*, **82**, 545-562.
- Tichit, D., Fajula, F., Figueras, F., Ducourant, B., Mascherpa, G. Gueguen, C. and Bosquet, J. (1988) Sintering of montmorillonites pillared by hydroxy aluminum species: *Clays & Clay Minerals* **36**, 369-375.
- Uytterhoeven, J. B., Christner, L. G. and Hall, W. K. (1965) Studies of the hydrogen held by solids VIII: the decationated zeolites: *J. Phys. Chem.* **69**, 2117-2126.

The effect of thermal treatment on the properties of hydroxy-Al and hydroxy-Ga pillared montmorillonite and beidellite

- Vermeulen, A. C., Geus, J. W., Stol, R. J. and de Bruyn, P. L. (1975) Hydrolysis-precipitation studies of aluminum(III) solutions. I. Titration of acidified aluminum nitrate solutions: *J. Coll. Interf. Sci.* **51**, 449-458.
- Von Liebig (1865) *Chemische Briefe*: C.F. Winter'sche Verlagshandlung, Leipzig, 96.
- Yamanaka, S. and Brindley, G. W. (1979) High surface area solids obtained by reaction of montmorillonite with zirconylchloride: *Clays & Clay Minerals* **27**, 119-124.
- Yariv, S. and Heller-Kallai, L. (1973) I.R. evidence for migration of protons in H- and organo-montmorillonites: *Clays & Clay Minerals* **21**, 199-200.

CHAPTER XVIII

CATALYTIC ACTIVITY OF NICKEL SULFIDE CATALYSTS SUPPORTED ON Al-PILLARED MONTMORILLONITE FOR THIOPHENE HYDRODESULFURISATION.

ABSTRACT

Al-pillared clays, prepared by exchange with partly hydrolyzed aluminum nitrate solutions, dried in air or freeze-dried, and calcined, were used as supports for nickel sulfide catalysts. The catalysts were tested on their hydrodesulfurization (HDS) activity for thiophene. The catalysts show a high thiophene HDS activity. It appeared that details in the preparation and calcination of the pillared clays have a strong influence on the catalytic activity.

18.1 INTRODUCTION

Pillared clays are considered to be interesting two-dimensional, shape-selective, molecular sieves of a larger pore size range than zeolites. In 1955 Barrer and MacLeod developed the idea of pillaring montmorillonite with organic compounds. However, these organic pillars decompose at relatively low temperatures, resulting in the collapse of the pillared clay structure. Utilization of inorganic polyoxocations, mainly Al (Brindley and Sempels, 1977) and Zr (Yamanaka and Brindley, 1979; Bartley and Burch, 1985) as pillaring agents dealt with the problem of the thermal stability. On calcination the polyoxocations react to immobile oxide pillars resulting in a permanent microporosity in the clay interlayers.

The Al polyoxocation, $[\text{AlO}_4\text{Al}_{12}(\text{OH})_{24}(\text{H}_2\text{O})_{12}]^{7+}$ (Al13), formed during forced hydrolysis of Al^{3+} under specific conditions (Kloprogge et al., 1992a,b), has a Keggin-type structure, consisting of a central fourfold coordinated Al surrounded by twelve sixfold coordinated Al (Johansson 1960, 1962, 1963). The existence

of Al₁₃ in solution was proven by ²⁷Al NMR (see references in Akitt, 1989) and small-angle X-ray scattering (Rausch and Bale, 1964).

Al-pillared clays exhibit a reduction of the cation exchange capacity (Keren, 1986), an increase in basal spacing, surface area, thermal stability (Plee et al., 1987; Schutz et al., 1987), and both Brønsted and Lewis acidity, the last becoming dominant upon calcination (Schutz et al., 1987, Schoonheydt, 1991).

Only few data have thus far been reported on metal sulfide catalysts supported on pillared clays. Warburton (1988) used clays pillared by Fe-sulfide for the high-pressure demetallization of heavy crude oil. Ocelli and Rennard (1988) applied pillared bentonite as a support for Ni-Mo catalysts for the hydrogenation-hydrocracking of vacuum gas oil feedstocks. In both cases the catalysts exhibited interesting catalytic properties.

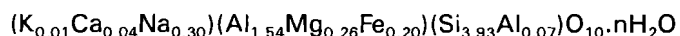
Studies on carbon-supported nickel sulfide catalysts have indicated that during the preparation of the catalyst supports, such as, Al₂O₃ interact significantly more strongly with the Ni²⁺ cations than carbon supports, which only exhibit a weak interaction. Pillared clays provide an interesting intermediate case. Whereas the alumina pillars will react with the Ni²⁺ cations, the expanded clay structure will remain stable. The thus resulting Ni sites in the pillared clay structure are comparable to those in zeolites. Welters et al. (1992) have recently demonstrated that sulfidation of NiNaY zeolites produces highly active desulfurization catalysts. Hence, sulfidation of nickel catalysts supported on pillared clays can be expected to produce highly active metal sulfide catalysts.

This paper compares the activity for thiophene hydrodesulfurisation (HDS) at atmospheric pressure of nickel sulfide catalysts supported on Al₁₃-pillared montmorillonite to alumina and carbon supports (Duchet et. al., 1983; Vissers et. al., 1984).

18.2 EXPERIMENTAL

18.2.1 Starting clay

The Na-montmorillonite SWy-1 from the Newcastle Formation, Crook County, Wyoming, was obtained from the Source Clay Repository of the Clay Mineral Society. Small amounts of quartz, calcite, and K-feldspar are present (van Olphen and Fripiat, 1979). Therefore, chemical analyses can only yield an approximate structural formula of



and a CEC of 85 meq/100 g clay (Brindley and Kao, 1980).

The fraction smaller than 2 μ m was obtained by gravity sedimentation and decantation, followed by washing four times with 1 M NaCl solution and removing the excess electrolyte by washing five times with deionized water.

18.2.2 Pillaring agent

Aluminum tridecamer solutions were prepared by injection at a rate of 0.015 ml/sec of 0.2 M NaOH (Merck) solution using a Gilson pump (capillary diameter of 0.5 mm) below the surface of an 0.5 M Al(NO₃)₃ (Merck) solution, which was vigorously stirred, until the desired OH/Al molar ratio of 2.4 was reached (Kloprogge et al., 1992). These solutions contain approximately 70 % Al13 polymer (Kloprogge et al., 1992).

18.2.3 Pillaring process and characterization of the pillared clays

The Al13 solutions were rapidly added under vigorous stirring to specified volumes of clay slurries, containing 20 g of solid/liter, to attain ratio's of 5.5 and 20 meq Al/g clay. After 12 hours exchange the pillared clays were washed five times with deionized water, followed by air- or freeze-drying and calcination at temperatures between 473 K and 973 K. The pillared clays were characterized by means of X-ray powder diffraction, using a Philips PW

1050/25 diffractometer ($\text{CuK}\alpha$), to measure the basal spacing, and N_2 adsorption to obtain the BET surface area using a ASAP 2400 surface area and pore volume analyzer (Micromeritics Instrument Corporation), .

18.2.4 Catalyst preparation

The catalysts were prepared by pore volume impregnation of the pillared clays with appropriate solutions of nickel chloride ($\text{NiCl}_2 \cdot 6\text{H}_2\text{O}$, Merck p.a.). The concentration of the metal salt solution was adjusted so as to obtain a nickel loading of 4.0 wt% Ni per gram of catalyst. Alumina (Ketjen 001-1.5E) and carbon (Norit RX3-E) supported nickel sulfide catalysts were prepared according to the same procedure. All catalysts were dried in air at 383 K for 16 h.

18.2.5 Activity measurements

Catalyst samples (200 mg, 0.125 to 0.425 mm particle size) were presulfided in situ in a $\text{H}_2\text{S}/\text{H}_2$ flow (10 mol% H_2S , 60 ml/min) using the following temperature program: a 6 K min^{-1} increase from 293 K to 673 K and keeping the catalyst for 2 hours at 673 K. Following the sulfidation the gas flow was switched to the reaction mixture: a hydrogen flow containing 4.0 mol% thiophene (Janssen Chimica). The reaction conditions were: flowrate 50 ml min^{-1} , reaction temperature 673 K, and pressure 1 bar. The thiophene conversion was measured at different time intervals by on-line gas chromatography. First order rate constants for thiophene HDS (k_{HDS}) were calculated as described elsewhere (Duchet et al., 1983).

18.3 RESULTS AND DISCUSSION

Table 18.1 summarizes the basic characteristics of the pillared montmorillonites. Upon pillaring the basal spacings of the montmorillonites increase from approximately 12.5 Å to 18.8 Å. Upon calcination up to 873 K a

Catalytic activity of nickel sulfide catalysts supported on Al-pillared montmorillonite for thiophene hydrodesulfurisation

Table 18.1 Basal spacings (Å), BET surface areas (m²/g), and micropore (<20 Å) volume as percentage of total pore volume of the montmorillonite SWy-1 and the pillared analogues.

sample	meq Al/g	drying	Tcalcination K	d ₀₀₁ Å	BET m ² /g	micropore vol (%)
SWy-1	-	-	298	12.5	25.6	2.9
PILC11	5.5	air	298	18.8	348.8	77.2
PILC6	5.5	air	623	17.6	269.0	54.3
PILC7	5.5	air	773	17.0	150.2	37.2
PILC17	5.5	freeze	473	17.0	226.4	43.9
PILC19	5.5	freeze	573	17.0	270.4	54.2
PILC20	5.5	freeze	673	17.0	317.6	53.0
PILC22	5.5	freeze	873	16.9	189.5	50.0
PILC26	20.0	freeze	623	17.4	280.6	62.4
PILC27	20.0	freeze	773	16.7	n.d.	n.d.

decrease to approximately 16.8 Å is observed. The calcined samples show a considerable drop in BET surface area and micropore (pores < 20 Å) volume fraction. The freeze-dried samples exhibit a BET surface area increasing with calcination at temperatures up to 673 K and a nearly constant micropore volume fraction, followed by a strongly diminishing surface area at 873 K. An extensive characterization of these pillared montmorillonites is given by Boijj et al. (1992).

The results of the activity measurements are represented in the **Figures 18.1 to 18.3**. The reaction rate constant for the hydrodesulfurization of thiophene is plotted as a function of the time on stream for several catalysts. In **Figure 18.1** two catalysts not based on clay are compared with a non-pillared and a pillared montmorillonite (SWy-1 and PILC26) catalyst. The carbon-supported catalyst shows a much better HDS activity than the alumina-supported catalyst, as known from literature (Vissers et. al., 1983; Duchet et. al., 1983). The

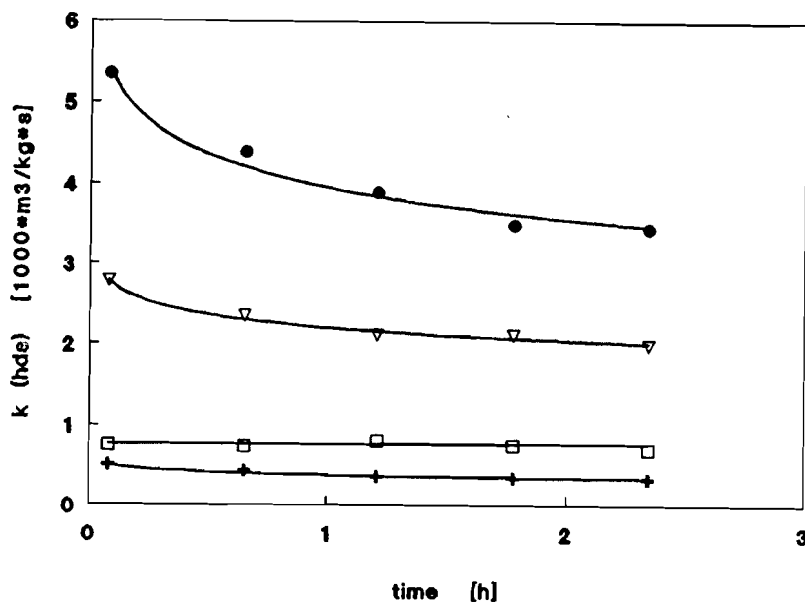


Figure 18.1 Reaction rate constant for thiophene HDS as a function of time on stream for various supports: □ 4 wt% Ni on Al₂O₃; ▽ 4 wt% Ni on C; + 4 wt% Ni on SWy-1; ● 4 wt% Ni on PILC26.

interaction between the metal ions and the support is much stronger for Al₂O₃ than for C, resulting in a lower activity for the alumina-supported catalysts (Visser et al., 1987; Prins et al., 1989).

The montmorillonite-supported sample shows an even lower activity than the alumina-supported sample. This may be due to a low nickel sulfide dispersion caused by the low surface area and the very low fraction of micropores of the non-pillared sample (Table 18.1). The HDS activity of the catalysts prepared from pillared clays, however, is higher than that of the non-pillared clay. As an example the activity of PILC26, which is even higher than that of the carbon-supported catalyst, is given in Figure 18.1. The SiO₄ groups in the tetrahedral

Catalytic activity of nickel sulfide catalysts supported on Al-pillared montmorillonite for thiophene hydrodesulfurisation

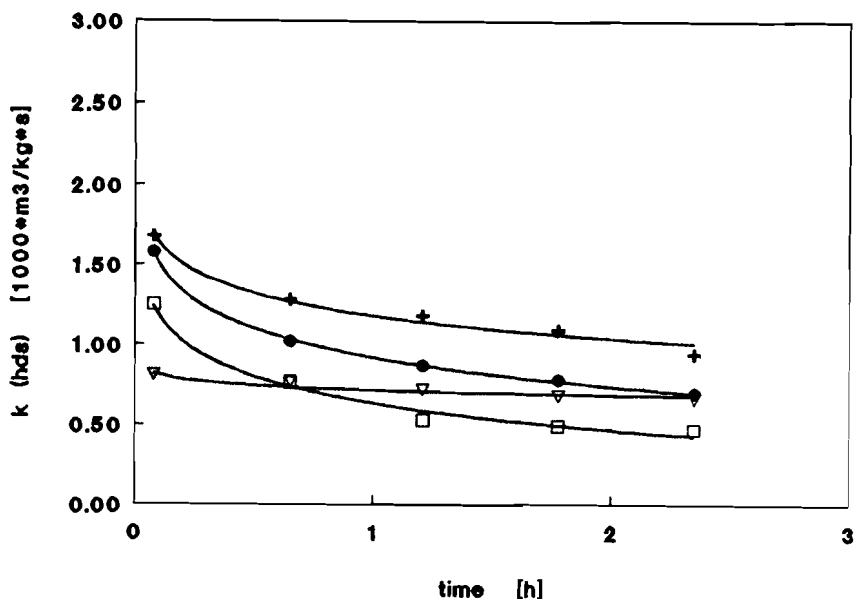


Figure 18.2 Reaction rate constant for thiophene HDS as a function of time on stream for: + 4 wt% Ni on PILC17; ● 4 wt% Ni on PILC19; □ 4 wt% Ni on PILC20; ▽ 4 wt% Ni on PILC22.

layer are, like carbon, inert to nickel. Therefore, catalysts supported on pillared clay are expected to have a rather low metal-support interaction causing a sulfidation chemistry more to resemble that of carbon supports (Vissers et al., 1987).

The thiophene HDS activity of nickel sulfide catalysts supported on pillared clays prepared by freeze-drying and calcining at different temperatures (Fig. 18.2), decreases with increasing calcination temperature. The decrease in activity upon raising the calcination temperature is contradiction with the expectation based on the increasing surface area. Raising the calcination temperature increases the dehydration and dehydroxylation of the Al13 pillars

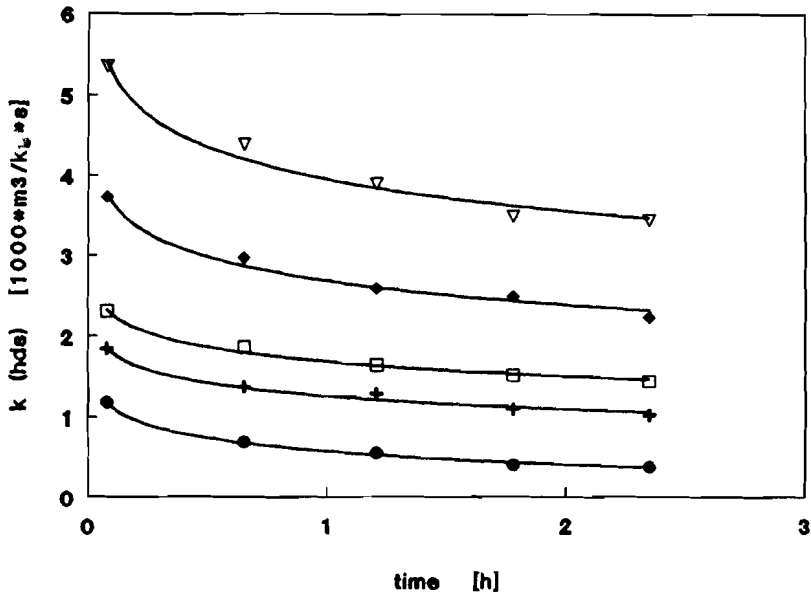


Figure 18.3 Reaction rate constant for thiophene HDS as a function of time on stream for: + 4 wt% Ni on PILC6; ● 4 wt% Ni on PILC7; □ 4 wt% Ni on PILC11; ▽ 4 wt% Ni on PILC26; ◆ 4 wt% Ni on PILC27.

that react to oxide pillars resembling $\gamma\text{-Al}_2\text{O}_3$ (Tennakoon et al., 1986) according to the overall reaction $\text{Al13} \rightarrow 6.5 \gamma\text{-Al}_2\text{O}_3 + 7 \text{H}^+ + 20.5 \text{H}_2\text{O}$. The reaction to the oxide results in differences in the surface properties and a decrease in reactivity of the pillars with respect to the nickel. The calcination experiments, therefore, are indicative that nickel interacts with the pillars. The decreased interaction upon calcination lowers the HDS activity by changing the nickel sulfide dispersion. Welters (pers. comment) has recently found indications for zeolite supports that changes in activity can affect the sulfide dispersion. Increasing the calcination temperature will lower the acidity of the clay due to loss of protons released from the pillars. The release of protons may also have

some influence on the dispersion and HDS activity of the catalyst. The presence of acid sites on the clay support is probably responsible for the deactivation due to coke formation. The PILC22 sample, calcined at 873 K, does not show any deactivation because no Brønsted acidity is left after complete dehydration and dehydroxylation of the pillared clay. The same trend is observed for samples exchanged with 20 meq Al/g clay and for air dried samples (Fig. 18.3).

Montmorillonites exchanged with 20 meq Al/g clay exhibit a much higher HDS activity than those exchanged with 5.5 meq Al/g clay (Fig. 18.3). As compared to the 5.5 meq Al/g pillared clays, the 20 meq Al/g samples do not show any significant difference in basal spacing, BET surface, average micropore size or amount of alumina pillars per gram of clay. The lack of differences indicates that zero charged montmorillonite upon saturation with Al^{III} pillars is established with 5.5 meq Al/g clay, which agrees with the results of Gu and Doner (1990). The only difference observed, accompanying a small increase in absolute pore volume up to calcination at 673 K, is a rise of the micropore volume from approximately 50 % to 62 % of the total pore volume, suggesting a more homogeneous pillar distribution. Figueras et al. (1990) observed an increasing homogeneity of the pillars upon competitive ion exchange of NH₄⁺ and Al^{III}. They argued that diffusion of Al^{III} with a kinetic radius of about 10 Å (Bottero et al., 1982) is restricted in the interlayer space of smectites. The high selectivity of the clay for Al^{III} apparently precludes a good distribution, preventing the Al^{III} polymers from diffusion into the core of the interlayer. Increasing the amount of Al^{III} per gram of clay, without altering the Al concentration in solution, seems to decrease the diffusional limitations. The better distribution of pillars sheets and the higher micropore volume may also influence the distribution of the nickel species, resulting in a higher dispersion of the nickel sulfide phase.

Also the drying procedure of the pillared montmorillonites affects the activity for thiophene HDS. Air-drying of the pillared clays leads to catalysts of slightly

higher reaction rates. The air-dried samples exhibit slightly smaller external surface areas and mesopore volumes in comparison with the freeze-dried samples. The difference may be explained by the aggregation of the montmorillonite platelets in a face-to-face orientation, whereas freeze-dried samples have aggregates mostly formed by three dimensional edge-to-edge and edge-to-face configuration, like a house of cards (van Olphen, 1977; Occelli et al., 1987). These structures are probably retained upon calcination and impregnation with Ni^{2+} , causing small differences in the nickel sulfide dispersion leading to the slightly higher HDS activity of the air-dried samples.

Detailed characterization of the pillared clays after impregnation with Ni^{2+} and sulfidation is required to explain the observed differences in catalytic activity for thiophene hydrodesulfurisation.

18.4 CONCLUSIONS

It has been demonstrated that montmorillonite can be impregnated with nickel followed by sulfidation to provide catalysts exhibiting comparable and even higher thiophene HDS activities than alumina- and carbon-supported nickel sulfide catalysts. The catalytic activity is shown to increase with decreasing calcination temperature of the pillared montmorillonite and by raising the amount of Al₁₃ pillars from 5.5 meq Al/g to 20 meq/g. 5.5 meq Al/g is sufficient to saturate the montmorillonite. Catalytic activity is only slightly dependent on the method of drying.

ACKNOWLEDGEMENTS

The authors wish to thank A. M. J. van der Eerden for his advice, critical comments, and help in the HPT laboratory of the Institute of Earth Sciences. We also thank R. J. M. J. Vogels and P. J. Dirken for critically reviewing this manuscript.

REFERENCES

- Akitt, J. W. (1989) Multinuclear studies of aluminium compounds: *Progr. NMR Spectr.* **21**, 1-149.
- Barrer, R. H. and MacLeod, D. M. (1955) Activation of montmorillonite by ion exchange and sorption complexes of tetraalkylammonium montmorillonites: *Trans. Faraday Soc.* **51**, 1290-1300.
- Bartley, G. J. J. and Burch, R. (1985) Zr-containing pillared clays. Part III. Influence of method of preparation on the thermal and hydrothermal stability: *Appl. Catal.* **19**, 175-185.
- de Beer, V. H. J., Duchet, J. C., Prins, R. (1981) The role of the cobalt and nickel in hydrodesulfurization, promoters or catalysts?: *J. Catal.* **72**, 369-372.
- Booij, E., Kloprogge, J. T., Vogels, R. J. M. J., Geus, J. W., Jansen, J. B. H. and Schuiling, R. D. (1992) The effect of thermal treatment on the properties of hydroxy-Al and hydroxy-Ga pillared montmorillonite and beidellite: in prep.; *This Thesis Ch XVII*.
- Bottero, J. Y., Tchoubar, D., Cases, J. M. and Fiessinger, F. (1982) Investigation of the hydrolysis of aqueous solutions of aluminum chloride. 2. Nature and structure by small angle X-ray scattering: *J. Phys. Chem.* **86**, 3667-3673.
- Brindley, G. W. and Kao, C. -C. (1980) Formation, compositions and properties of hydroxy-Al- and hydroxy-Mg-montmorillonite: *Clays & Clay Minerals* **28**, 435-443.
- Brindley, G. W. and Sempels, R. E. (1977) Preparation and properties of some hydroxy-aluminium beidellites: *Clay Minerals* **12**, 229-236.
- Burch, R. and Warburton, C. I. (1987) Pillared clays as demetallisation catalysts: *Appl. Catal.* **33**, 395-404.

- Duchet, J. C., van Oers, E. M., de Beer, V. H. J. and Prins, R. (1983) Carbon supported sulfide catalysts: *J. Catal.* **80**, 386-402.
- Figueras, F., Klapysa, Z., Massiani, P., Mountassir, Z., Tichit, D., Fajula, F., Gueguen, C., Bousquet, J. and Auroux, A. (1990) Use of competitive ion exchange for intercalation of montmorillonite with hydroxy-aluminum species: *Clays & Clay Minerals* **38**, 257-264.
- Gu, B. and Doner, H. E. (1990) Adsorption of hydroxy-Al polycations and destabilization of illite and montmorillonite suspensions: *Clays & Clay Minerals* **38**, 493-500.
- Hamilton, D. L. and Henderson, C. M. B. (1968) The preparation of silicate compositions by a gelling method: *Mineral. Mag.* **36**, 832-838.
- Johansson, G. (1960) On the crystal structure of some basic aluminum salts: *Acta Chem. Scand.* **14**, 771-773.
- Johansson, G. (1962) The crystal structures of $[\text{Al}_2(\text{OH})_2(\text{H}_2\text{O})_8](\text{SO}_4)_2 \cdot 2\text{H}_2\text{O}$ and $[\text{Al}_2(\text{OH})_2(\text{H}_2\text{O})_8](\text{SeO}_4)_2 \cdot 2\text{H}_2\text{O}$: *Acta Chem. Scand.* **16**, 403-420.
- Johansson, G. (1963) On the crystal structure of basic aluminum sulfate $13\text{Al}_2\text{O}_3 \cdot 6\text{SO}_3 \cdot x\text{H}_2\text{O}$: *Ark. Kemi* **20**, 321-342.
- Keren, R. (1986) Reduction of the cation-exchange capacity of montmorillonite by take-up of hydroxy-Al polymers: *Clays & Clay Minerals* **34**, 534-538.
- Kloprogge, J. T., van der Eerden, A. M. J., Jansen, J. B. H. and Geus, J. W. (1990) Hydrothermal synthesis of Na-beidellite: *Geologie & Mijnbouw* **69**, 351-357.
- Kloprogge, J. T., Jansen, J. B. H. and Geus, J. W. (1990) Characterization of synthetic Na-beidellite: *Clays & Clay Minerals* **38**, 409-414.
- Kloprogge, J. T., Seykens, D., Jansen, J. B. H. and Geus, J. W. (1992) An ^{27}Al nuclear magnetic resonance study on the optimalization of the development of the Al₁₃ polymer: *J. Non-Cryst. Solids* **142**, 94-102.
- Occelli, M. L. and Rennard, R. J. (1987) Hydrotreating catalysts containing pillared clays: *Catal. Today* **2**, 309-320.

- Occelli, M. L., Senders, J. V. and Lynch, J. (1987) TEM analysis of pillared and delaminated hectorite catalysts: *J. Catal.* **107**, 557-565.
- van Olphen, H. (1977) *An introduction to clay colloid chemistry*, Wiley, New York, 43.
- van Olphen, H. and Fripiat, J. J. (1979) *Data handbook for clay minerals and other non-metallic minerals*, Pergamon Press, Oxford.
- Plee, D., Gatineau, L. and Fripiat, J. J. (1987) Pillaring processes of smectites with and without tetrahedral substitution: *Clays & Clay Minerals* **35**, 81-88.
- Prins, R., de Beer, V. H. J. and Somorjai, G. A. (1989) Structure and function of the catalyst and the promotor in Co-Mo hydrodesulfurization catalysts: *Catal. Rev. - Sci. Eng.* **31**, 1-41.
- Rausch, W. V. and Bale, H. D. (1964) Small-angle X-ray scattering from hydrolyzed aluminum nitrate solutions: *J. Chem. Phys.* **40**, 3391-3394.
- Schoonheydt, R. A. (1991) Clays: from two to three dimensions. In: *Introduction to zeolite science and practice*, H. van Bekkum, E. M. Flanigan and J. C. Jansen (eds.). Studies in surface science and catalysis **58**, Elsevier, Amsterdam.
- Schutz, A., Stone, W. E. E., Poncelet, G. and Fripiat, J. J. (1987) Preparation and characterization of bidimensional zeolitic structures obtained from synthetic beidellite and hydroxy-aluminum solutions: *Clays & Clay Minerals* **35**, 251-261.
- Tennakoon, D. T. B., Jones, W., Thomas, J. M. (1986), Structural aspects of metal-oxide pillared sheet silicates: *J. Chem. Soc., Farad. Trans. I* **82**, 3081-3090.
- Tuttle, O. F. (1949) Two pressure vessels for silicate-water studies: *Geol. Soc. Amer. Bull.* **60**, 1727-1729.

- Vissers, J. P. R., Groot, C. K., van Oers, E. M., de Beer, V. H. J. and Prins, R. (1984) Carbon supported transition metal sulfides: *Bull. Soc. Chim. Belg.* **93**, 813-821.
- Vissers, J. P. R., Scheffer, B., de Beer, V. H. J., Moulijn, J. A. and Prins, R. (1987) Effect of the support on the structure of Mo-based hydrodesulfurization catalysts: activated carbon versus alumina: *J. Catal.* **105**, 277-284.
- Warburton, C. I. (1988) Preparation and catalytic properties of iron oxide and iron sulfide pillared clays: *Catal. Today* **2**, 271-280.
- Welters, W. J. J., Koranyi, T. I., de Beer, W. H. J. and van Santen, R. A. (1992) Hydrodesulfurization activity of zeolite supported nickel- and cobalt- sulfide catalysts: *Proc. 10th Int. Congr. Catal., Budapest, July 1992*, in press.
- Yamanaka, S. and Brindley, G. W. (1979) High surface area solids obtained by reaction of montmorillonite with zirconylchloride: *Clays & Clay Minerals* **27**, 119-124.

Chapter XIX

CONCLUDING REMARKS

The industry producing organic chemicals uses liquid acids in many catalytic reactions. With reactions in liquids, transport of the reacting molecules to the active sites is often highly important. Transport within liquids proceeds more slowly than in gases, which can lead to problems with the use of solid acid catalysts. To present a sufficiently large number of active sites per unit volume, solid catalysts should exhibit a high specific surface area. To separate the solid catalyst after completion of the reaction readily from the liquid reaction products, catalyst bodies of at least one micron are required. Since the surface area and, hence, the number of active sites per unit volume of non-porous bodies of at least one micron is not sufficiently large, porous bodies must generally be used as catalysts. Since the transport of reactants and reaction products through the often narrow pores proceeds generally slowly, utilization of solid acid catalysts in liquid phase reaction can lead to unsatisfactory results. An instance is alkylation of *i*-butane with *i*-butene in the production of branched hydrocarbons of a high octane number. A requirement is that the aliphatic hydrocarbon molecules can approach the active sites as rapidly as the olefines. If the olefines are concentrated in the pores of the solid catalyst, the desired reaction of one olefine with one *i*-alkane does not proceed. Therefore acids as sulfuric acid or hydrofluoric acid are being used for alkylation, in spite of the fact that hydrofluoric acid is highly poisonous and that it is difficult to prevent environmental problems with the heavily contaminated sulfuric acid remaining after the reaction.

To replace homogeneous acid catalysts by solid catalysts the physical structure of the catalyst is therefore highly important. The size of the catalyst bodies must allow one to separate the catalyst easily from the liquid, while the porous system must provide a rapid transport of the reacting molecules. Since it is difficult to characterize adequately the porous structure of solid bodies suspended in liquids, the development of catalysts based on clay minerals to be used in liquid phase

reactions calls for much research. Development of clay minerals requires adjustment of the porous structure of the bodies, and more particularly of the stacking of the clay layers.

Utilization of solid acid catalysts is required at high temperatures where liquid acids have volatilized. Since catalytic cracking calls for high temperatures, solid acids are employed with catalytic cracking. As mentioned above, Houdry, who developed the first catalytic cracking process, used activated clays as catalysts. When fluidized beds were introduced for catalytic cracking, activated clays were replaced by amorphous silica-alumina catalysts. Spray-drying provided catalysts of the desired particle size distribution and the required mechanical strength. Catalytic cracking actually involves redistribution of hydrogen over the carbon atoms of the reacting molecules. A fraction of the molecules is deprived from hydrogen and deposited as carbon on the catalyst, while the hydrogen released is distributed over other molecules and thus leads to fractions of a lower molecular weight. The thermal energy required to perform the endothermic cracking reaction is provided by combustion of the carbon deposited on the catalyst. During the combustion the temperature of the catalyst bodies rises to 800°C or more. The thermal stability of the catalyst bodies consequently has to be very elevated. The thermal stability of natural clay minerals, that usually are contaminated, is often not sufficient.

A new item has been introduced by the use of zeolites in catalytic cracking, viz., shape selectivity. With zeolites, that produce less gas and gasoline of a higher octane number, catalytically active sites are present within interstices of a limited size. A different diffusivity of the reacting molecules, but, more probably, limitation of the size of the reaction products by the size of the zeolite pores provides the shape selectivity. To deal with heavier crude oil fractions containing larger molecules, zeolites of a larger pore size are required. Since preparation of zeolites of a large pore size still has to be developed, producing shape-selective catalysts based on clay mineral has been considered. As discussed extensively in this thesis pillaring of suitable clay minerals can provide interstices of molecular dimensions.

Though pillaring of clay minerals has been studied for a considerable period of time, the application of cracking catalysts based on pillared clays in industrial units has not been achieved. The thermal stability of pillared clays generally appears to

be insufficient and the catalytic properties are not outstanding. Difficulties involved in controlling the chemical composition and the physical properties may lead to the relatively low thermal stability. Therefore utilization of synthetic clay minerals may provide more thermostable catalysts. Since natural clays are very cheap, utilization of synthetic clay minerals can only be considered if the production does not involve long periods of time at elevated (hydrothermal) pressures. This thesis therefore deals with the synthesis of beidellite and saponite, clay minerals where the excess negative charge is brought about by substitution of Si^{4+} by Al^{3+} in the tetrahedral layer. The synthesis of beidellite calls for hydrothermal synthesis for extended periods of time at high temperatures and at high pressures. Although saponite can be synthesized at lower temperatures, problems with the expandability and the location of the aluminum ions in the structure on other than the tetrahedral sites cause catalytic application of this clay mineral to be less obvious. The simple chemistry involved with the preparation of beidellites and the interesting acid properties, on the other hand, bring about that beidellite is still an important catalytic clay mineral.

Besides the use of zeolites in catalytic cracking, zeolites are used increasingly in hydrocracking processes, where heavier oil fractions are being treated at elevated temperatures with hydrogen in the presence of acid sites. The demands on the thermal stability with hydrotreating catalysts are much lower than those with catalytic cracking catalysts, where combustion of the deposited carbon leads to relatively high temperatures. The catalytic properties of some of the pillared clays prepared in this work therefore have been studied with hydrocracking.

The pillaring agent and its preparation is extremely important for the properties of the pillared clay. It is essential to be able to produce the pillaring agent in large quantities not contaminated by other species that can be taken up at the interlayer positions of the clay minerals. In this thesis therefore, much attention has been given to the preparation and characterization of Al13 pillaring agents. First of all the results of Chapters VII to XVII show that the study of inorganic reactions in aqueous solutions and of the resulting solid products can profit very much from modern NMR techniques. The formation of the Al13 complex and its subsequent reaction to hexamers and boehmite has been elucidated mainly by NMR results.

Chapter XVII deals with the thermal treatment of montmorillonite and beidellite before and after pillaring with Al¹³ complexes. The stability of Ga¹³ pillared montmorillonite appeared to be low, which impeded NMR analysis of the Ga¹³ pillars, which can be performed more readily than that of Al¹³ pillars in view of the presence of aluminum in the octahedral and tetrahedral layers, as well as at interlayer positions. The intrinsic thermal stability of the layers as well as migration into the octahedral layer of protons released during reaction of the Al¹³ pillars to alumina and subsequent reaction with the structural hydroxyl groups of the octahedral layer strongly affects the thermal stability. The results of Chapter XVII suggest that the use of modified Al¹³ pillars and of pillars of a different chemical composition may provide pillared clay minerals of a higher thermal stability.

Chapter XVIII finally showed that montmorillonite pillared by Al¹³ can provide hydrotreating catalysts with favorable catalytic properties. Application of a sulfur resistant hydrogenation component onto pillared montmorillonite provided an interesting hydrotreating catalyst. Modification of the Al¹³ pillars by application of nickel or cobalt may lead to even better hydrotreating catalysts.

Above we mentioned utilization of clays in liquid phase reaction to replace acids used as homogeneous catalysts. An important advantage of pillared clays in liquid phase catalytic reactions is the possibility to use shape selectivity. First of all the size of the bodies of pillared clay cannot be too large to prevent the rate of transport determining the catalytic activity. With large pillared clay bodies the activity therefore will be low. Furthermore the active sites at the external edge of the clay bodies have to be eliminated to ensure shape selectivity. Either deposition of a layer covering the sites present at the external edge of the clay bodies can be considered, or local extraction of the active sites. Highly interesting is application of chiral components at the interlayer position to endow the resulting catalysts with a chiral selectivity.

The research described in this thesis has combined work on the synthesis of clay minerals, the preparation of the pillaring agent, the pillaring of clay minerals, the thermal stability of (pillared) clay minerals, and the catalytic properties of catalysts in which pillared clays are used as a support and as an acid catalyst. The results have demonstrated that combination of the extensive range of analytical

procedures and characterization techniques presently available can adequately elucidate the many different processes proceeding during synthesis of clay minerals and pillaring agents, as well as during the pillaring process and the thermal treatment of (pillared) clay minerals.

SUMMARY

After an extensive introductory chapter (Chapter I), in which the background and the aim of the research is dealt with, the hydrothermal synthesis and the characterization of Na-beidellite is discussed in Chapter II and III. The conditions of temperature, water pressure, and sodium activity under which Na-beidellite can be synthesized in the chemical system $\text{Na}_2\text{O}-\text{Al}_2\text{O}_3-\text{SiO}_2-\text{H}_2\text{O}$ are investigated in Chapter IV. The stability field is limited at low temperatures by the formation of kaolinite and at high temperatures by that of paragonite and quartz. In Chapter V solid-state magic-angle spinning ^{23}Na NMR combined with XRD and TGA is used to study the interlayer collapse and the migration of sodium present at the interlayer during dehydration of synthetic Na-beidellite. It is shown that the Na^+ surrounded by two water molecules is relocated in the hexagonal cavities of the tetrahedral sheet.

The low-temperature synthesis of ammonium-saponites is considered in Chapter VI, while solid-state ^{27}Al NMR combined with ^{29}Si NMR provides evidence for the presence of Al at the octahedral and the interlayer sites as dealt with in Chapter VII. In Chapter VIII a model is developed for the crystallization of saponite based on the hydrothermal synthesis of ammonium-saponite at increasing periods of aging time. Chapter IX discusses the synthesis of Mg-saponites using gels containing different competing cations.

Since the preparation of Al pillaring agents is highly important in the preparation of pillared clays, much work has been devoted to the study of the forced hydrolysis of Al^{3+} . Chapter X to XV are dealing with NMR studies of the aqueous chemistry of Al^{3+} . Chapter X to XIII concentrate on the formation, thermal stability, and aging of monomeric, oligomeric, and tridecameric Al^{3+} species during forced hydrolysis. In Chapter XIII direct evidence based on NMR line broadening data for the existence of the $[\text{Al}(\text{OH})_2]^+$ species is provided. The aging of the tridecameric Al complex in partly hydrolyzed Al-sec-butoxide solutions and the reaction to fibrous boehmite are considered in Chapter XIV. Chapter XV and XVI deal with the characterization, thermal stability, and NMR properties of basic Al sulfate resulting

from addition of sodium sulfate solution to partly hydrolyzed Al solutions containing the tridecameric Al species, such as described in Chapter X to XIII.

Pillaring and thermal treatment of synthetic beidellite and natural montmorillonite is described in Chapter XVII and the catalytic conversion of thiophene over pillared clays into which nickel has been applied in Chapter XVIII. Finally in Chapter XIX some concluding remarks concerning the results obtained in this study and the implications for the applications of (synthetic) clay minerals in catalytic reactions are made.

SAMENVATTING

Na een uitgebreid inleidend hoofdstuk (Hoofdstuk I), waarin de achtergrond en het doel van het onderzoek wordt behandeld, worden in de hoofdstukken II en III de hydrothermal synthese en de karakterisering van Na-beidelliet besproken. De condities betreffende temperatuur, water druk en natrium activiteit waarbij Na-beidellite kan worden gesynthetiseerd in het chemische systeem $\text{Na}_2\text{O}-\text{Al}_2\text{O}_3-\text{SiO}_2-\text{H}_2\text{O}$ wordt onderzocht in hoofdstuk IV. Het stabiliteitsveld wordt aan de lage temperatuur kant begrensd door de vorming van kaoliniet en aan de hoge temperatuur kant door de vorming van paragoniet en kwarts. In hoofdstuk V wordt vaste stof magic-angle spinning ^{23}Na NMR, gecombineerd met XRD en TGA, gebruikt voor het bestuderen van het instorten van de tussenruimte en de migratie van natrium aanwezig in de tussenruimte gedurende dehydratie van synthetische Na-beidellite. Aangetoond wordt dat de Na^+ omringd door twee water moleculen wordt herplaatst in de hexagonale holten van de tetraedrische laag.

De lage temperatuur synthese van ammonium-saponieten wordt besproken in hoofdstuk VI, waarbij vaste stof ^{27}Al NMR gecombineerd met ^{29}Si NMR bewijs leveren voor aanwezigheid van Al in de octaeder en tussenruimte posities, zoals aangetoond in hoofdstuk VII. In hoofdstuk VIII wordt een model ontwikkeld voor de kristallisatie van saponiet gebaseerd op de hydrothermale synthese van ammonium-saponiet met toenemende verouderingstijd. Hoofdstuk IX behandelt de synthese van Mg-saponiet gebruik makende van gelen die verschillende competitieve kationen bevatten.

Aangezien de bereiding van Al pilaar oplossingen zeer belangrijk is voor de bereiding van gepilaarde kleïen, is veel werk gewijd aan het bestuderen van de geforceerde hydrolyse van Al^{3+} . De hoofdstukken X tot en met XV behandelen NMR studies over de aquatische chemie van Al^{3+} . De hoofdstukken X tot en met XIII concentreren zich op de vorming, thermische stabiliteit en veroudering van monomere, oligomere en tridecamere Al^{3+} vormen gedurende geforceerde hydrolyse. In hoofdstuk XIII wordt direct bewijs geleverd voor het bestaan van de $[\text{Al}(\text{OH})_2]^+$ vorm gebaseerd op NMR lijnverbreding gegevens. De veroudering van

het tridecamere Al complex in gedeeltelijk gehydrolyseerde Al-sec-butoxide oplossingen en de reactie tot fibervormige boehmiet wordt behandeld in hoofdstuk XIV. Hoofdstuk XV en XVI behandelen de karakterisering, thermische stabiliteit en NMR eigenschappen van het basische Al sulfaat. Deze verbinding ontstaat door de toevoeging van natriumsulfaat oplossing aan gedeeltelijk gehydrolyzeerde Al oplossingen welke de tridecamere Al vorm bevatten, zoals beschreven in de hoofdstukken X tot en met XIII.

Het pilaren van synthetische beidelliet en natuurlijke montmorilloniet wordt beschreven in hoofdstuk XVII en de katalytische conversie van thiofeen over nikkel bevattende gepilaarde kleïen is toegepast in hoofdstuk XVIII. Tenslotte worden in hoofdstuk XIX een aantal concluderende opmerkingen gemaakt ten aanzien van de resultaten van deze studie en de implicaties voor de toepassing van (synthetische) klei mineralen in katalytische reacties.

CURRICULUM VITAE

Jacob Teunis Kloprogge werd op 19 februari 1965 geboren te Zoetermeer. In juni 1983 behaalde hij het diploma Atheneum aan het Oranje Nassau College te Zoetermeer. In september van dat jaar begon hij met de studie Geologie aan de Rijksuniversiteit te Utrecht. In september 1984 werd het propedeutisch examen afgelegd en in januari 1988 het doctoraal examen met als hoofdvak Petrologie en als bijvak Mineralogie. Gedurende zijn studie vervulde hij diverse student-assistentschappen bij de vakgroep Petrologie. In de periode van februari 1988 tot en met augustus 1992 was hij werkzaam als assistent in opleiding bij de vakgroepen Anorganische Chemie, faculteit Scheikunde, en Geochemie/HPT, faculteit Geologie/Geofysica, binnen het samenwerkingsverband van het Debye Instituut. Gedurende de periode van februari 1990 tot en met mei 1990 deed hij een deel van zijn onderzoek bij het Koninklijke/Shell Laboratorium in Amsterdam.